

WIND CHARACTERISTICS OVER COMPLEX TERRAIN:
LABORATORY SIMULATION AND FIELD MEASUREMENTS
AT RAKAIA GORGE, NEW ZEALAND
FINAL REPORT: PART II

Robert N. Meroney *
Anthony J. Bowen **
David Lindley **
John R. Pearse **

Fluid Mechanics and Wind Engineering Program
Civil Engineering Department
Colorado State University
Fort Collins, Colorado 80523

May 1978

Prepared for the United States
Department of Energy
Division of Solar Technology
Federal Wind Energy Program

DOE Contract No. EY-76-S-06-2438, A001

NOTICE

This report was prepared as an account of work sponsored by an agency of the United States Government. Neither the United States nor any agency thereof, nor any of their employees, makes any warranty, expressed or implied, or assumes any legal liability or responsibility for any third party's use or the results of such use of any information, apparatus, product or process disclosed in this report, or represents that its use by such third party would not infringe privately owned rights.

* Civil Engineering Department
Colorado State University, U.S.A.

** Mechanical Engineering Department
University of Canterbury, New Zealand

CER77-78RNM29



U18401 0074904

TA17
CG
CER-77/78-29

50

EXECUTIVE SUMMARY

New Zealand and the United States have a common Wind Energy Conversion System (WECS) siting problem. They are both geographically complex, contain many potentially attractive wind power sites, and yet in many such areas of complex terrain there are "meteorological data" deserts. One such area is the Rakaia River Gorge region on the eastern slope of the Southern Alps in New Zealand. Climatological records obtained from stations somewhat removed from the area suggest moderate to very high wind energy. Local farmer and fishermen wisdom and folklore speak of incredible winds in the gorge canyon. Extended field measurement programs are invariably expensive and time consuming; hence, a survey program was proposed to utilize laboratory simulation of the relevant wind characteristics in a meteorological wind tunnel. To evaluate the validity of laboratory simulation methods and provide a confidence measurement bound for laboratory data, a simultaneous limited field measurement program was organized.

In this study both terraced and contoured models of the Rakaia River Gorge region were prepared to an undistorted geometric scale of 1:5000. The contoured model was examined for three separate surface roughness conditions--a surface textured to represent typical paddock grass roughness only, the same surface with zero-porosity shelterbelts added, and the same surface with porous shelterbelts added.

On two spring days, selected for strong neutral down valley wind flow, three teams of investigators surveyed up to 27 sites on either side and within the river gorge. Measurements consisted of wind speed at a 10 meter height and direction at a 2 meter height

on lightweight portable towers. All measurements were completed during the course of a 5 hour independent wind event and normalized against continuous records taken from a New Zealand Wind Energy Task Force anemometer near terrain center.

The laboratory simulation results were compared with the available field data by means of statistical correlation and scatter diagrams.

The model and field results were used to assess the value of the laboratory experiments for assisting WECS siting field programs.

Specific results and conclusions resulting from this research are:

1. Physical modeling can reproduce wind patterns produced by the near neutral atmospheric shear layer flowing over complex terrain to within the inherent variability of the atmosphere to produce stationary results;
2. Physical modeling reproduced the relative wind speeds found over complex terrain by rank to sample correlation coefficient levels equal to 0.78 to 0.95;
3. Physical modeling reproduced the individual day-to-day quantitative wind speeds found over complex terrain to sample correlation coefficient levels equal to 0.70 to 0.76;
4. Physical modeling reproduced the average of two field days quantitative wind speeds found over complex terrain to a sample correlation coefficient level equal to 0.81;
5. Physical modeling reproduced the individual day-to-day site wind directions found on complex terrain to sample correlation coefficient levels equal to 0.65 to 0.67;
6. Adequate physical modeling of neutral shear flow over complex terrain requires attention to surface roughness, terrain shape, and vegetation as well as upstream velocity profile, turbulence intensity, and turbulence eddy structure;
7. Terraced models are not as effective as contoured models that include surface texture when modeling flow over complex terrain;
8. Over complex terrain local wind speeds may vary by over 100% in a distance of a few hundred meters as a result of terrain shadowing, flow separation, or flow enhancement;

9. In the Rakaia River Gorge area preferred WECS locations are the surrounding hills and ridges, and not the gorge or river bottoms; and
10. Generic hill study results predicted the fractional speedup levels found over two pseudo-ridge areas; however, they did not predict the levels with impressive accuracy. Consideration of differences between the two studies such as three-dimensional effects as well as hill height to boundary layer thickness ratio may explain deviations.

Climatology statistics and simulation techniques are the "pick and shovel" of the modern wind prospector. Methods such as those described in this report will eventually coalesce into means to provide early selection of suitable locations for wind-powered electrical generation systems.

ACKNOWLEDGMENTS

Financial assistance for the senior author from Department of Energy Contracts EG-77-S-06-1043 and EY-76-S-06-2438, a Fulbright Hays Travel Grant, and an Erskine Lectureship appointment at the University of Canterbury are gratefully acknowledged.

The gracious and enthusiastic co-operation of Professor D. C. Stevenson, Chairman, Department of Mechanical Engineering, University of Canterbury, who provided laboratory and staff support for this research is appreciated. In particular our thanks go to the Workshop staff and the Laboratory Technicians for their diligence and who smilingly volunteered for field duty. Photographic reproduction and drafting were jointly shared by Mrs. J. Ritchie, University of Canterbury, and Ms. H. Akari, Colorado State University. A special thanks to Mrs. L. Warren for her willing co-operation and perseverance in typing this report.

TABLE OF CONTENTS

<u>Chapter</u>		<u>Page</u>
	EXECUTIVE SUMMARY	v
	LIST OF SYMBOLS	xii
	LIST OF FIGURES	xv
	LIST OF TABLES	xx
1.0	INTRODUCTION	1
	1.1 General Statement of Problem	1
	1.2 Objectives of Research	4
	1.3 Procedures for Completing Objectives	5
	1.4 Organization of This Report	6
2.0	WIND CHARACTERISTICS IN MOUNTAIN/VALLEY-GORGE TERRAIN	8
	2.1 Review of Effects of Terrain Structure on Airflow	8
	2.1.1 Neutral Airflow Over Mountainous Terrain	8
	2.1.2 Stratified Airflow Over Mountainous Terrain	9
	2.1.3 Winds Enhanced by Passes, Saddles, Gaps, Canyons or Gorges	12
	2.2 Laboratory Simulation of Wind Characteristics Over Irregular Terrain	14
3.0	TERRAIN AND WIND CHARACTERISTICS OF THE RAKAIA GORGE REGION, NEW ZEALAND	20
	3.1 Geology	20
	3.2 Meteorology of Southern Alps Region	22
	3.3 Wind Energy Resource Survey Results	25
	3.4 Micrometeorological Characteristics of the Rakaia River Gorge Region	27

TABLE OF CONTENTS (continued)

<u>Chapter</u>		<u>Page</u>
4.0	CRITERIA FOR LABORATORY SIMULATION OF WIND CHARACTERISTICS OVER IRREGULAR TERRAIN	31
4.1	Basic Equations and Assumptions	32
4.2	Laboratory Constraints for Neutral Air Flow Model	39
4.3	Summary of Similitude Criteria for Rakaia River Gorge Simulation	41
5.0	EXPERIMENTAL EQUIPMENT AND PROCEDURES FOR LABORATORY MEASUREMENTS	43
5.1	Atmospheric Boundary Layer Wind Tunnel	43
5.2	Topographic Models	44
	5.2.1 Terraced Model	45
	5.2.2 Contoured Model	46
	5.2.3 Shelterbelts	46
5.3	Flow Field Measurements	48
	5.3.1 Visualization Techniques	48
	5.3.2 Hot Wire Anemometry and Associated Equipment	49
	5.3.3 Pressure Probe Equipment	52
5.4	Experimental Program and Procedures	53
6.0	EXPERIMENTAL EQUIPMENT AND PROCEDURES FOR FIELD MEASUREMENTS	55
6.1	Rationale for Mobile Survey	55
6.2	Portable Towers and Cup Anemometers	58
6.3	Stationary Measurement Sites	59
6.4	Team Procedures and Field Text Matrix	60
6.5	Synoptic Meteorology on Field Test Days	61

TABLE OF CONTENTS (continued)

<u>Chapter</u>		<u>Page</u>
7.0	EXPERIMENTAL RESULTS	64
	7.1 Results of Wind Tunnel Measurements	64
	7.1.1 Approach Flow Field Characteristics	64
	7.1.2 Flow Visualization and Trajectory Results	66
	7.1.3 Flow-Field Results - Terraced Model Configuration	68
	7.1.4 Flow-Field Results - Contoured Model - Alternate Roughness Conditions	72
	7.1.5 Flow-Field Results - Contoured Model Configuration	73
	7.2 Results of Field Measurements	75
	7.2.1 Normalization Procedures	76
	7.2.2 Field Test Day - November 25, 1977.	77
	7.2.3 Field Test Day - December 28, 1977.	78
8.0	COMPARISON OF LABORATORY AND FIELD EXPERIMENT RESULTS	80
	8.1 Correlation of Wind Velocity Magnitudes	82
	8.2 Ranking Wind Stations by Wind Speed	86
	8.3 Comparison of Wind Directions	87
9.0	CONCLUSIONS AND RECOMMENDATIONS	89
	9.1 Implications of Experiment With Regard to WECS Siting Procedures	89
	9.2 Correlation of Laboratory and Field Experiments	90
	9.3 Character of Rakaia Gorge Flow	91
	REFERENCES	93
	APPENDIX	103
	FIGURES	112
	TABLES	196

LIST OF SYMBOLS

<u>Symbol</u>	<u>Definition</u>	<u>Dimensions</u>
a) b)	Coefficients of linear regression, Eq. 8.4	
c_p	Specific heat capacity	$L^2 T^{-1} \theta^{-2}$
C_f	Skin friction coefficient	
D_i	Rank difference for station i, Eq. 8.7	
Ek	Eckert Number, Eq. 4.5	
Eu	Euler Number, Eq. 4.6	
g	Gravitational Constant	LT^{-2}
h	Hill height - base to crest	L
H	Shelter belt height	L
I_{ij}	Turbulence intensities, Eq. 4.7	
k	von Karman constant	
K_H	Eddy diffusivity for heat	$L^2 T^{-1}$
K_m	Eddy diffusivity for momentum	$L^2 T^{-1}$
k	Thermal conductivity	$MLT\theta^{-3}$
L	Hill half width: distance from crest to half height	L
L_{mo}	Monin Obukhov scaling length, Eq. 4.11	L
L_o	Characteristic length	L
ℓ	Scorer parameter = $g\beta/U_o^2$	L
L_{u_x}	Longitudinal integral scale	L

LIST OF SYMBOLS (continued)

<u>Symbol</u>	<u>Definition</u>	<u>Dimensions</u>
n	Frequency	T^{-1}
P_{xy}	Spatial correlation (See Section 6.1)	
Pr	Prandtl Number, Eq. 4.4 or 4.9	
p	Pressure	$ML^{-1}T^{-2}$
Q_H	Heat flux	M/T^3
r	Sample correlation coefficient, Eq. 8.1	
$R(\tau)$	Autocorrelation function $\frac{\overline{u'u'}(\tau)}{\overline{u'^2}}$	
Re	Reynolds Number, Eq. 4.2 or 4.10	
Ri	Richardson Number, Eq. 4.3 or 4.12	
R_o	Rossby Number, Eq. 4.1	
Ri_B	Bulk Richardson Number, Eq. 4.13	
$S(n)$	Energy spectrum function	
T	Temperature	θ
T_E	Time when correlation drop to 1/e	T
u'_i	Velocity fluctuation	LT^{-1}
\overline{u}	Mean velocity	LT^{-1}
U	Characteristic velocity	LT^{-1}
u_*	Friction velocity	LT^{-1}
x, y	Variables in linear regression	
z_o	Roughness length	L

LIST OF SYMBOLS (continued)

<u>Symbol</u>	<u>Definition</u>	<u>Dimensions</u>
α	Velocity profile index	
β	Volumetric compressibility	θ^{-1}
δ	Boundary layer thickness	L
λ	Roughness scale	L
μ	Absolute viscosity	$ML^{-1}T^{-1}$
ν	Kinematic viscosity	L^2T^{-1}
ρ	Mass density	ML^{-3}
Ω	Coriolis parameter, rotational velocity	T^{-1}

Subscripts

h	Length scaled to hill height
G	Geostrophic level
o	Characteristic scale
δ	Length scaled to boundary layer depth
m	Model
p	Prototype

LIST OF FIGURES

<u>Figure</u>		<u>Page</u>
2-1.	Classification of types of airflow over mountainous terrain (Orgill 1971)	113
2-2.	Methods in which terrain features affect atmospheric motions (Drake et al. 1977)	116
2-3.	The diurnal sequence of mountain and valley winds (DeFant 1951)	117
2-4.	A schematic of the type of flow patterns that may be observed through gaps and gorges (Drake et al. 1977)	118
3-1.	Annual windflow characteristics over New Zealand (Ward 1976)	119
4-1.	Performance Envelope to simulate wind energy effects over complex terrain	120
5-1.	Boundary layer wind tunnel, Department of Mechanical Engineering, University of Canterbury	121
5-2.	Models of Rakaia River Gorge region looking northwest	122
5-3.	Comparison of horizontal u/u_0 profiles for yarn shelterbelts with data in the literature	124
5-4.	Comparison of horizontal u/u_0 profiles for pipe cleaner shelterbelts with data in the literature	125
5-5.	Isoturbs for yarn shelterbelts	126
5-6.	Isoturbs for pipe cleaner shelterbelts	127
5-7.	Correlation of turbulent intensity and relative velocity behind model shelterbelts	128
5-8.	Block diagram of velocity and turbulence measurement instrumentation	129
5-9.	Block diagram of pressure probe equipment and associated electronics	130
5-10.	Rakaia Gorge region terrain modeled and associated survey locations	131
5-11.	Rakaia Gorge sections	132

LIST OF FIGURES (continued)

<u>Figure</u>		<u>Page</u>
6-1.	Maximum spatial correlation for hourly and daily velocity (Corotis 1977)	133
6-2.	Portable tower and anemometer Rakaia River Gorge field experiment	134
6-3.	Synoptic forecast - November 24-25, 1977	135
6-4.	Synoptic forecast - December 28-29, 1977	136
7-1.	Energy spectra for longitudinal velocity component at forward section, $z_p = 10$ m	137
7-2.	Energy spectra for longitudinal velocity component at section D-3, terraced model, $z_p = 10$ m	138
7-3.	Energy spectra for longitudinal velocity component at section D-3, contoured model, $z_p = 10$ m	139
7-4.	Auto-correlation coefficients for longitudinal velocity component at forward section, $z_p = 10$ m	140
7-5.	Auto-correlation coefficients for longitudinal velocity component at section D-3, terraced model, $z_p = 10$ m	141
7-6.	Auto-correlation coefficients for longitudinal velocity component at section D-3, contoured model, $z_p = 10$ m	142
7-7.	Miniature flag direction behavior, terraced model	143
7-8.	Polystyrene bead trajectory and deposition diagram, terraced model	144
7-9.	Horizontal isotachs, terraced model, $z_p = 10$ m	145
7-10.	Horizontal isotachs, terraced model, $z_p = 25$ m	146
7-11.	Horizontal isotachs, terraced model, $z_p = 50$ m	147
7-12.	Vertical section B-B isotachs, terraced model	148
7-13.	Vertical section B-B isoturbs, terraced model	149
7-14.	Vertical section G-G isotachs, terraced model	150
7-15.	Vertical section G-G isoturbs, terraced model	151

LIST OF FIGURES (continued)

<u>Figure</u>		<u>Page</u>
7-16.	Vertical section C-C isotachs, terraced model	152
7-17.	Vertical section C-C isoturbs, terraced model	153
7-18.	Vertical section F-F isotachs, terraced model	154
7-19.	Vertical section F-F isoturbs, terraced model	155
7-20.	Vertical section D-D isotachs, terraced model	156
7-21.	Vertical section D-D isoturbs, terraced model	157
7-22.	Vertical section D-D isotachs, terraced model	158
7-23.	Vertical section D-D isoturbs, terraced model	159
7-24.	Vertical section E-E isotachs, terraced model	160
7-25.	Vertical section E-E isoturbs, terraced model	161
7-26.	Miniature flag direction behavior, contoured model . .	162
7-27.	Polystyrene bead trajectory and deposition diagram, contoured model	163
7-28.	Horizontal isotachs, contoured model, $z_p = 10$ m	164
7-29.	Horizontal isotachs, contoured model, $z_p = 50$ m	165
7-30.	Airflow pitch and yaw at section G-3, contoured model	166
7-31.	Airflow pitch and yaw at section between C and F Gorge, contoured model	167
7-32.	Airflow pitch and yaw Point A-A, contoured model . . .	168
7-33.	Airflow pitch and yaw, section D-3, contoured model	169
7-34.	Vertical section B-B isotachs, contoured model	170
7-35.	Vertical section B-B isoturbs, contoured model	171
7-36.	Vertical section G-G isotachs, contoured model	172
7-37.	Vertical section G-G isoturbs, contoured model	173

LIST OF FIGURES (continued)

<u>Figure</u>		<u>Page</u>
7-38.	Vertical section C-C isotachs, contoured model	174
7-39.	Vertical section C-C isoturbs, contoured model	175
7-40.	Vertical section F-F isotachs, contoured model with no shelterbelts	176
7-41.	Vertical section F-F isoturbs, contoured model with no shelterbelts	177
7-42.	Vertical section F-F isotachs, contoured model with yarn shelterbelts	178
7-43.	Vertical section F-F isoturbs, contoured model with yarn shelterbelts	179
7-44.	Vertical section F-F isotachs, contoured model	180
7-45.	Vertical section F-F isoturbs, contoured model	181
7-46.	Vertical section D-D isotachs, contoured model	182
7-47.	Vertical section D-D isoturbs, contoured model	183
7-48.	Vertical section E-E isotachs, contoured model	184
7-49.	Vertical section E-E isoturbs, contoured model	185
7-50.	Rakaia Gorge field data, November 25, 1977	186
7-51.	Rakaia Gorge field data, December 28, 1977	187
8-1.	Comparison of calculated and observed wind speeds (Fosberg et al. 1976)	188
8-2.	Comparison of calculated and observed wind direction (Fosberg et al. 1976)	188
8-3.	Scatter diagram field test data, December 28 versus field test data, November 25	189
8-4.	Scatter diagram field test data, November 25 versus terraced model data	190
8-5.	Scatter diagram field test data, November 25 versus contoured model data	191

LIST OF FIGURES (continued)

<u>Figure</u>		<u>Page</u>
8-6.	Scatter diagram field test data, December 28 versus terraced model data	192
8-7.	Scatter diagram field test data, December 28 versus contoured model data	193
8-8.	Terrain cross sections Rakaia Gorge at section B-2 and section G-6	194
8-9.	Fractional speedup factor results over crest of hills at sections B-2 and G-6	195

LIST OF TABLES

<u>Table</u>		<u>Page</u>
2-1	LABORATORY SIMULATION OF FLOW OVER IRREGULAR TERRAIN	197
3-1	RAKAIA RIVER GORGE CLIMATOLOGY	200
4-1	TYPICAL BOUNDARY LAYER WIND TUNNEL CHARACTERISTICS	201
4-2	TYPICAL FIELD CHARACTERISTICS	202
4-3	TYPICAL WIND TUNNEL AND FIELD PARAMETER RANGE	203
5-1	EQUIPMENT UTILIZED DURING RAKAIA GORGE EXPERIMENTS	204
6-1	FIELD SITE EXPOSURE NOTES	205
7-1	INTEGRAL SCALES - FLOW OVER RAKAIA GORGE MODEL	206
7-2	LABORATORY DATA - TERRACED MODEL	207
7-3	LABORATORY DATA - CONTOURED MODEL PIPE CLEANER SHELTERBELTS	209
7-4	LABORATORY DATA - CONTOURED MODEL	211
7-5	RAKAIA GORGE FIELD DATA - NOVEMBER 25, 1977	212
7-6	RAKAIA GORGE FIELD DATA - DECEMBER 28, 1977	214
8-1	COMPARATIVE WIND SPEED VALUES FIELD - LABORATORY	215
8-2	CORRELATION STATISTICS	216
8-3	WIND VELOCITY RANK TEST NOVEMBER 25, 1977, DATA	217
8-4	WIND VELOCITY RANK TEST DECEMBER 28, 1977, DATA	218
8-5	WIND DIRECTION AT GROUND LEVEL AT FIELD TEST SITES ¹⁾	219

1.0 INTRODUCTION

1.1 General Statement of Problem

Information on the general wind characteristics of a geographical region is a prerequisite for considering the utilization of wind power at a site. Climatological data gathered at area weather stations (usually located at flat open terrain near airports) will often provide information concerning wind speed, duration, return time, direction, etc., over a number of years. However, if the area in which wind power installations are to be made includes hilly country, an obvious desire is to choose sites on or near the top of hills or ridges to take advantage of the faster moving stream of air which results from compression of streamlines near the summit. Thus, it is important to be able to correlate wind behavior approaching a terrain feature and the terrain topography with the character of flow at a prospective site.

Recognition of site selection importance has led to a series of monographs and papers on this subject. Unfortunately, there is only a limited amount of field and laboratory information from which the authors could draw conclusions. Indeed, because of the variability of the atmosphere and the presence of many factors which exist simultaneously, it is difficult to isolate the independent influence on wind-speed of topography profile, surface roughness or stability. In the 1940's and early 1950's, laboratory studies in aeronautical wind tunnels were also completed; unfortunately, the investigators found little resemblance

between the field and wind tunnel results. P. C. Putnam, summing up wind investigation connected with the Grandpa's Knob aerogenerator, wrote, "...after five years of increasing familiarity with the problem of site selection, we can point to no analogy between the profiles of mountains and the profiles of airfoils by which one can predict mean wind velocities at hub height within limits which will be useful," and, again, "...we have found no criteria by which to make an economically useful quantitative prediction of the effects of topography upon wind flow." E. W. Golding seems to fully subscribe to Putnam's views, but he somewhat wistfully writes,

... it would be very convenient if it were possible to use a precise formulae relating the wind speed at a certain height over the summit of a hill of a given altitude and shape to the undisturbed wind speed at the same altitude but at a distance upwind from the hill. This would facilitate the choice of sites; one might almost choose them from close study of contoured maps, if sufficiently detailed, without being familiar with the actual localities. But no such method can be followed: it is not possible to work from the formulae. (Putnam, 1942) (Golding, 1955)

Early efforts to accomplish this goal were hindered by difficulties in determining the undisturbed wind at the level concerned (Petterssen, 1961), and incorrect laboratory simulation of the effects of the atmosphere surface shear layer and stratification (Putnam, 1942; Lange, 1961).

Prediction of upper level flows in the undisturbed atmosphere has improved substantially in the last twenty-five years (Haugen, 1973). Successful modeling of atmospheric phenomena in a wind tunnel has only been accomplished in the last fifteen years. The thin surface layers

developed in the short aeronautical tunnels failed to reproduce even the gross character of wind profile, stratification, turbulence, and spectra required. In addition, early attempts to produce thicker shear layers with grids produced flows which were not spatially stationary. By combining the best of present understanding of the atmospheric surface layer, laboratory simulation, and numerical extrapolation procedures, Golding's speculation may become a reality. At this juncture all three methods are necessary since no single method appears capable of providing a complete solution to the problem. Since laboratory simulation has promise of being a versatile and inexpensive tool, the laboratory approach is considered herein as a principal method.

New Zealand and the United States have a common Wind Energy Conversion System (WECS) siting problem. They are both geographically complex, contain many potentially attractive wind power sites, and yet in many such areas of complex terrain there are "meteorological data" deserts. One such area is the Rakaia River Gorge region on the eastern slope of the Southern Alps in New Zealand. Climatological records obtained from stations somewhat removed from the area suggest moderate to very high wind energy (Cherry, 1976). Local farmer and fishermen wisdom and folklore speak of incredible winds in the gorge canyon. Extended field measurement programs are invariably expensive and time consuming; hence, a survey program was proposed to utilize laboratory simulation of the relevant wind characteristics in a meteorological wind tunnel. To evaluate the validity of laboratory simulation methods and provide a confidence measurement bound for laboratory data, a simultaneous limited field measurement program was organized.

1.2 Objectives of Research

The overall purpose of this research is to develop laboratory physical models as a tool for modeling the atmospheric planetary boundary layer over mountainous terrain as a means to predict WECS performance on terrain enhanced sites. A second phase of this research involves obtaining limited field data concerning the advisability of utilizing river valley or gorge sites as WECS stations. The more specific objectives for the research were as follows:

- 1) To examine the full capability for laboratory simulation of airflow over complex terrain at large length scale ratios,
- 2) To establish modeling criteria for future operational programs,
- 3) To compare the physical model and field data through the principles of similarity and to determine how well the physical models can simulate actual atmospheric airflow and turbulence characteristics,
- 4) To evaluate the influence of surface roughness and shelterbelts on prospective WECS sites,
- 5) To evaluate the "folklore" that river gorges and valleys are prime WECS site candidates due to airflow acceleration during channeling,
- 6) To evaluate typical spatial inhomogeneity in wind fields over a complex terrain region, and
- 7) To compare speedup effects measured over individual ridge cross sections with the predicted behavior as determined from generic hill shape measurements.

1.3 Procedures for Completing Objectives

The laboratory method consists of obtaining velocity and turbulence measurements over a scale model of selected terrain placed in a simulated atmospheric flow. The wind characteristics of the simulated atmospheric flow are chosen to reproduce the wind profile shape and length scales of the equivalent prototype situation. Since field profiles are rarely available in advance, velocity profiles and turbulence characteristics are chosen to fit an equivalent class of conditions as recorded by earlier investigators over terrain of similar roughness.

In this study both terraced and contoured* models of the Rakaia River Gorge region were prepared to an undistorted geometric scale of 1:5000. The contoured model was examined for three separate surface roughness conditions--a surface textured to represent typical paddock grass roughness only, the same surface with zero-porosity shelterbelts added, and the same surface with porous shelterbelts added.

The field program first considered the results of climatological measurements correlated by Cherry (1977) as part of the New Zealand Wind Energy Task Force (NZWETF) survey of Wind Energy Resources in New Zealand. A phase II program is presently gathering data at a number of additional sites upwind, in, and downwind of the Rakaia Gorge area.

On two spring days, selected for strong neutral down valley wind flow, three teams of investigators surveyed up to 27 sites on either side and within the river gorge. Measurements consisted of wind speed and direction at a 10 meter height on lightweight portable towers. All measurements were completed during the course of a five-hour independent wind event and normalized against continuous records taken from a NZWETF anemometer near terrain center.

* For explanation of terms terraced and contoured, see Sections 5.2.1 and 5.2.2.

The laboratory simulation results were compared with the available field data by means of statistical correlation and scatter diagrams. The model and field results were used to assess the value of the laboratory experiments for assisting WECS siting field programs.

1.4 Organization of This Report

Since the problem is complex, a brief review of the various aspects of the problem, such as effects of terrain on wind structure, and laboratory simulation are presented in Chapter 2.0. In Chapter 3.0 the geology, geography, and meteorology of the Rakaia Gorge region as it is currently understood is discussed. The required assumptions, equations, and similitude parameters which govern the airflow over complex terrain are established in Chapter 4.0 by examining and reducing the basic equations governing the atmosphere in the planetary boundary layer. A performance envelope for a typical meteorological wind tunnel suggests operational constraints which will place bounds on the use of the laboratory model as a predictive tool.

The experimental equipment and the procedures followed during the laboratory and field measurements are described in Chapters 5.0 and 6.0, respectively. Chapter 6.0 also contains a rationale for the mobile survey based on recent results concerning the spatial and temporal correlation of wind fields.

A discussion of both laboratory and field results are found in Chapter 7.0. These include mean wind profiles, longitudinal turbulence intensities, spectra, correlations, wind veering angles around gorge hills and saddles, as well as shelterbelt aerodynamics. Measurements over the laboratory model have been prepared into isotach contours in

the vertical and horizontal. Field measurements of wind speed have been normalized to a common time of data and tabulated. A comparison of the laboratory and field data by means of magnitude rank, scatter diagrams, and correlations is found in Chapter 8.0.

Conclusions and recommendations concerning the program objectives are summarized in Chapter 9.0.

2.0 WIND CHARACTERISTICS IN MOUNTAIN/VALLEY-GORGE TERRAIN

2.1 Review of Effects of Terrain Structure on Air Flow

As noted by Meroney et al. (1976) winds in valleys and winds over hills and mountains may be the most important sources of wind power. Experience suggests that the wind is enhanced or reduced as the larger scale motions encounter mountains and valleys. Upwind of an abrupt, steep mountain chain such as the Southern Alps, New Zealand, the air is often blocked, the wind is reduced, and only a weak flow along the mountain base exists. Downwind of the main divide, winds are enhanced by convergence and channeling effects.

Extended reviews of the effects of orography on the atmospheric boundary layer or higher in the troposphere have been prepared by Queney et al. (1960), Orgill (1971), and Eagen (1975). These reviews suggest that mountains may alter atmospheric airflow characteristics and motion in a number of different ways. These effects can generally be grouped into those resulting from inertial-viscous interactions associated with a thick neutrally stratified shear layer and thermally induced interactions associated with stratification or surface heating.

2.1.1 Neutral Airflow Over Mountainous Terrain

When the static stability is neutral, airflow over mountains creates pressure gradients in the flow direction which together with surface friction will produce separation, flow reversal, and reattachment. Separation eddies at the windward or lee side of a mountain can alter the effective shape of the mountain resulting in a modified wind profile at the crest. Scorer (1978) describes eight different variations on the separation phenomenon. In addition to bolster, corner,

and lee eddies he notes that separation may be changed in character by insolation, blocking, diabatic changes, or three-dimensional effects. Meroney et al. (1976) summarized experimental data available from field and laboratory structures over hills, ridges, and escarpments (see Table 2-1). Orgill (1977) surveyed wind measurement programs that have used wind networks (2 to 60 measurements sites) to identify data suitable for calibrating WECS siting methodologies. Out of 139 field programs 3 relate to an isolated mountain, 7 to mountain-plain flows, and 20 are for complex topography.

Deep neutral/or adiabatic atmospheric boundary layers will exist over mountains during situations when winds are high due to intense synoptic pressure fields, continuous cloud banks impede surface heating, and sharp terrain features produce separation eddies which mix the flow field vigorously in the vertical. Such a case is shown schematically as case b, Figure 2-1, from Orgill (1971) or as case a, Figure 2-2.

2.1.2 Stratified Airflow Over Mountainous Terrain

Thermal stratification or surface heating or cooling can result in dynamic effects associated with:

- 1) Quasi-laminar airflow,
- 2) Blocking and stagnation airflows,
- 3) Gravity oscillations,
- 4) Slope and valley airflow, and
- 5) Large scale eddies associated with horizontal eddy or unstable convective cells.

Quasi-laminar airflow comprises a smooth shallow wave over a ridge, providing only feeble vertical currents and no downstream phenomena (Figure 2-1, class a).

Blocking and stagnation airflows (Figure 2-1, case c) may occur whenever the mountain or ridge height exceeds $2\pi/\ell$ where $\ell = g\beta/U_0^2$ is the Scorer parameter. Blocking occurs because there is no systematic displacement of the air above the ridge which can produce a low enough pressure for the upwind surface air to reach the ridge top. Blocking is thus the main cause of Föhn winds. (Figure 2-1, class i). Channel and gap winds may result through mountain passes as stably stratified air layers seek a release from shear and pressure forces (Figure 2-1, case d).

Gravity oscillations have been studied extensively and may be further subdivided into cases involving lee waves (Figure 2-1, case g) or lee vortices (rotors) (Figure 2-1, case h). Due to the complexity of these phenomena it is doubtful whether we will ever be fully satisfied with any analytical or numerical predictions. As Scorer (1978) notes

"There are many original papers using very sophisticated mathematics designed to resolve certain mathematical issues, but seldom do they take us any nearer to matching our theory to the observational (out of doors) and experimental (laboratory) facts known.... Moreover, the theory cannot be used to any discriminating way in practice to help understand observations, nor does it make any useful difference to predictions we might make of the flow over any actual mountain because other factors dominate any particular case.

If more complicated calculations for everyday use could be done we would still get very little further than we would without them. This is because the differences between reality and theory lie in the considerable unsteadiness of actual flows, and in the fact that the flow often separates from the surface, particularly in the lee of a steep obstacle where the predictions would be most useful if

they could be made. Buoyancy produced by clouds and changes in the wind and temperature structure during the day, together with a variety of mathematically quite intractable situations leading to turbulence of various kinds, all militate against quantitative precision. (pg. 154-155)

This somewhat pessimistic view is supported by a recent review by Klemp and Lilly (1978) who conclude there are major discrepancies between many existing gravitational wave calculations and observations. Nonetheless simple theories do exist which give qualitative guidance for stratified orographic flows. (See Queney et al. (1960), Scorer (1978), Yih (1965))

Slope and valley airflows when dominated by surface heating often result in quite complicated secondary flows (Figure 2-1, case f). According to Munn (1966) the important properties of valleys are:

1. Orientation of the geostrophic wind,
2. Orientation of the valley (a north-south valley has a different radiation balance from one lying in an east-west direction), and
3. The geometric dimensions of the valley, such as length, width, depth, side slopes, slope of the floor and the number of bends or constrictions.

When a strong geostrophic wind blows parallel to a valley a funneling effect occurs. If the valley narrows, the wind is speeded up as it passes through the valley. If the geostrophic wind is blowing at right angles to the valley a large cross valley circulation or "valley eddy" may be formed. The diurnal sequence of light valley and mountain winds is shown in Figure 2-3 prepared by Defant (1951). The wind is a combination of up and downslope winds and the background synoptic flow modified by the mountains. During high wind speed conditions ($U_{10} > 5$ m/sec) slope heating plays a minor role and the valley behaves as another perturbation on a natural adiabatic shear flow approximation.

Large scale eddies associated with horizontal meandering have been identified in satellite photography. These eddies form in the wake of islands or tall mountains which extend through layers of low-lying temperature inversion. The eddies are made visible by patterns in stratocumulus clouds (Figure 2-1, case e). Barnett (1972) has reproduced this phenomena in stratified shear layers in meteorological wind tunnels. Unstable stratification near mountains during light winds together with surface insolation often produces large vertical mixing cells resulting in thick turbulent shear layers capped by active thunderclouds (Figure 2-2, case c.)

2.1.3 Winds Enhanced by Passes, Saddles, Gaps, Canyons and Gorges

Certain terrain forms are more wind energy rich than others because they tend to channel and enhance wind speeds. Many of the locations that lay wisdom associates with high winds are related to such terrain features. Windy Gap, Wyoming (Marrs and Marwitz (1977)), Nuvanu Pali Pass, Oahu (Hardy (1977)), the Tehachapi Mountain saddle, California (Lindley (1977) or Traci et al. (1977)), or even Wind Whistle near the Rakaia Gorge, New Zealand, are pertinent examples.

Mountain passes, saddles, and gaps are the more accessible, and usually the lowest, notches across a mountain barrier or between two or more distinct mountains. Canyons or gorges refer to a longer opening in otherwise complex topography usually associated with a river or erosion channel and normally having high, steep side walls (See Figure 2-4).

These types of topographic configuration have been cited as good wind energy sites because they produce enhanced wind speeds. The increased wind speeds are the result of a venturi or jet effect as the air is forced around the sides of mountains or hills and through the opening. As Davidson et al. (1964) remark this speedup will occur both day and night provided the prevailing wind is large enough. There appears to be no special set of criteria to judge the efficacy of a given venturi shaped surface feature. In addition to height, width, or length of a saddle, gap, or pass one might expect its elevation, shape, approach condition, and roughness are significant. Scorer (1952) discusses some data from Gibraltar, Liu and Lin (1976) report on laboratory measurements in stratified flow near an idealized mountain saddle.

Valleys or canyons are generally V shaped as a result of vigorous stream erosion or U shaped because of glacial movement. Sometimes a steep sided gorge may exist through glacial moraine or lower hills which lie at the end of a broader U shaped valley. This is the case for the Rakaia River Gorge studied herein. A broad U shaped valley lies between the Mt. Hutt range and the Big Ben Range. This valley has an average breadth of 10,000 meters. The gorge, which is the dominant feature at the valley exit, has a typical width of 1500 meters (See Figure 5-10).

The airflow pattern in any particular valley will depend upon the large-scale airflow or gradient wind above the valley and its direction with respect to the valley. Atmospheric stability, geometry of the valley, surface roughness, and insolation are all critical to the general flow circulation. As mentioned earlier the physical

situation studied for the Rakaia Gorge was limited to time periods in which the gradient wind is moderate to strong and the direction is parallel to the valley.

Detailed wind information for gaps and gorges is lacking. Some information from studies by Clements and Barr (1976) for flow in Los Alamos Canyon suggests that in high gradient wind conditions canyon floor winds are even less than the surrounding mesa top wind levels. Davidson (1961) reported observations from eight valleys in New England. The valley locations exhibit, on the average, less wind speed than does a flat terrain site. Although recognizing the possibility of venturi effects for valleys whose axis are along the prevailing wind direction Davidson concludes wind speeds in most valley locations in the zone of the westerlies are less than they would be over flat terrain.

2.2 Laboratory Simulation of Wind Characteristics Over Irregular Terrain

In view of the extreme difficulties in obtaining practically useful results in this area of meteorology over complex terrain, whether by theoretical analysis or field investigation, it is natural that some researchers have explored the possibilities of simulating the flow over irregular terrain by means of physical model experiments on the laboratory scale.

Certain advantages or benefits of laboratory simulation may be realized when similarity conditions are partially or actually satisfied between field and model. These benefits are that:

1. The problem may be studied in the three space dimensions;
2. A certain latitude is available for controlling the essential variables in the problem;
3. There is the inherent possibility for defining and locating particular problems which might exist on proposed weather-sensitive field projects;

4. Determination of the location of sites for meteorological instruments and towers, wind energy conversion generators, etc., in the actual field for the purpose of obtaining representative observations and results pertinent to a particular project is possible;
5. One may obtain relevant data that may be used in guiding field programs toward their proposed goals; and
6. Time and expense of extensive field programs or studies may be reduced.

On the other hand, laboratory simulation of flow over irregular terrain such as the Rakaia River Gorge area presents many problems such as:

1. The specification of criteria for similitude between model and prototype,
2. The adoption of restrictive assumptions associated with physical limitations of the laboratory apparatus,
3. The accurate measurement of flow variables to construct pertinent parameters, and
4. The necessity of verifying the model approach with actual field measurements.

Chapter 4.0 considers the equations and assumptions required to define appropriate similitude criteria. Although not all investigators agree on details most would concur that the dominant forcing mechanisms can now be identified and are understandable. In the past, however, there has been doubt that a laboratory model, particularly a wind tunnel model, could reproduce the essential characteristics of the atmosphere in a planetary boundary layer. Queney et al. (1960) as they reviewed the airflow over mountains observed that:

.... Now, even if it were possible to maintain the very large temperature gradient of $1^{\circ}\text{C cm}^{-1}$ in the model, we should require a flow speed of only 9 cm sec^{-1} . For smaller temperature gradients, even slower flow speeds in the model would be necessary. Such flows with large temperature gradients and very low flow speeds cannot be accomplished, at

least in conventional wind tunnels....The above considerations indicate that model experiments in a wind tunnel using air as the streaming medium would be useless if it is desired to accomplish quantitative similarity.

The critical qualification of course is the restriction to "conventional wind tunnels." Subsequently, Lin and Binder (1967), Yamada and Meroney (1971), and Kitabayashi (1977) have reproduced gravity oscillations or blockage phenomena in specially constructed thermally stratified wind tunnels.

Nonetheless when using models for study, often only parts of a problem may be realistically simulated and many simplifying, but not necessarily invalidating, assumptions are made by necessity. In some cases these restrictions relate to current facility limitations. Section 4.2 considers a performance envelope for the typical large boundary layer wind tunnel and its ability to deal with the task of WECS siting over a range of terrain size and scaling ratio.

Finally, there exists the reasonable concern that quite often adequate field data are not available in order to check the model results. In this work, the second method of research, the field program, was incorporated into the test plan in order to provide pertinent observations that would assist in evaluating the laboratory simulation and the accuracy of laboratory measurements.

At the present time only four general types of airflow can be generated in a wind tunnel (Orgill et al. (1971a):

1. Neutral airflow, where static stability is assumed neutral and the pressure field is determined by the geometry of the terrain features. If the terrain features are sharp, the flow patterns are not influenced by viscous forces or by Reynolds number differences between the model and prototype. Irreversibility in the flow is usually due to the production of separation eddies, which appear on the lee side of obstacles.

2. Barostromatic* airflow, where the air is stably stratified because of density or temperature stratification. This type of airflow is generally quasi-laminar, and with proper density stratification gravity waves and hydraulic "jumps" occur. Large vertical temperature gradients and low flow velocities are required in order to produce this type of flow in the wind tunnel.
3. Unstable airflow, where the air is heated from below producing thermal convection cells throughout the flow medium.
4. The elevated inversion, where mixed air of near neutral or unstable character at ground level is capped by a stable air mass aloft. Meroney, Cermak, and Yang (1975) considered the spatially growing elevated inversion near coastal boundaries. Ludwig and Skinner (1976) examined an elevated inversion laying over a rolling Pennsylvania countryside.

Most topographic wind-tunnel model studies have been made with neutral flow whereas barostromatic airflow has only recently been simulated. However, an effort was made in 1941 by Abe to study flow over Mt. Fuji with an air stream stratified by solid carbon dioxide. Table 2-1 gives a listing of terrain models which have been studied and the type of flow used.

A neutral airflow, although the most convenient to simulate, may only apply to the actual field conditions in very special atmospheric conditions, i.e., during periods of neutral stability through deep layers of the atmosphere. A barostromatic airflow attempts to simulate the normal temperature stratification one observes in the atmosphere, i.e., an increase of potential temperature with height. This type of airflow is difficult to produce realistically because

* Word derived from Greek and adopted by R. S. Scorer as representing an airflow which exhibits density stratification. For the purpose of this study it represents airflow with stable thermal stability in the upper levels and near-neutral thermal stability in the lower levels.

of the required temperature or density stratification. Not all of the some forty laboratory cases identified in Table 2-1 were successful.

Putnam (1948) reports meteorological measurements made over eleven peaks and ridges, four of these were modeled in aerodynamical wind tunnels. Unfortunately, the observed speed up factors are much in doubt because of difficulties in determining the undisturbed wind at peak level (Petterssen (1961)); hence the 20,000 velocity measurements made over the wind tunnel models are of dubious value. Since the shear layer of the atmosphere was not pre-established, approach velocity profiles may have had power law coefficients near zero, in addition the absence of stratification modeling may result in either too high or too low values for speed up, S . Other investigators (Field and Warden (1929) and Zrajevsky et al. (1968)) have also failed to model approach wind profile during atmospheric simulation. Early attempts to simulate stratified flow in brine-filled towing tanks were also constrained by uniform approach profile or wave reflection from tank walls and bottom. The early wind tunnel simulation of shear layer turbulence was often crude. Boundary layer depth, integral scale, or turbulence intensities might not match their atmospheric counterpart.

Nonetheless most studies accomplished their prestated limited objectives. Few claim unreasonable correlation. For example, stratification can make a major difference in the dynamic and kinematic behavior of windflow over topography. In cases 12, 13, 18, 19, and 20 from Table 2-1, flow over topography is considered in the presence of stable stratification. In each case, quantitative field evidence

A number of field and laboratory investigations are recently available which specifically examine the influence of hill slope and profile. Plate and Lin (1965), Plate and Shieh (1965), and Chang (1965) report measurements of neutral and unstable shear flows downwind of triangular and sinusoidal ridges. De Bray (1973), Freeston (1974), and Bowen and Lindley (1974) considered shear flows over upwind facing escarpments. When the upstream wind profile and stratification were simulated, close agreement appears between laboratory and field measurements. Measurements made by Meroney et al. (1976, 1976, 1977) and Bowen and Lindley (1974) over idealized hill shapes for neutral and stable flows have been compared with frozen vorticity numerical programs by Derickson and Meroney (1977) and Astley (1977). Sacre (1975), Deaves (1975), and Traci et al. (1977) have compared inviscid and second-order-closure turbulence-model solutions against two-dimensional wind-tunnel data with good agreement.

3.0 TERRAIN AND WIND CHARACTERISTICS OF THE RAKAIA RIVER GORGE REGION, NEW ZEALAND

3.1 Geology*

The Rakaia River rises from the main divide of the Southern Alps where it is fed by waters from the Ramsay and Lyell Glaciers as well as runoff from the Arrowsmith, Ragged, and Rolleston Mountain Ranges. These mountain ranges, which form a portion of the central part of the Southern Alps, act as a major barrier both physically and culturally between the West Coast and Canterbury. Rising to 2644 meters at Mt. Whitcombe northwest of the Rakaia Gorge, these mountains play a major part in the local meteorology and terrain appearance.

The Southern Alps, with their spectacular glacial, lake-holding valley systems, and their deeply cut braided river valleys developed during the New Zealand Kaikoura Orogeny period beginning only 25 million years ago. The rocks of the Southern Alps may have risen as much as twenty kilometers, although their height has been constantly reduced by erosion during uplift; the greatest uplift occurring immediately east of the Alpine Fault.

The principal sedimentary rocks of which these mountains are formed were probably laid down in the Mesozoic era some 75 to 230 million years ago. Hence New Zealand's geologic age is relatively young compared to the oldest known rocks dated between 3600 to 3900 million years.

* Extracted in part from New Zealand Atlas (Ward, 1976)

The mountains drop steeply to the Rakaia River valley floor (~600-900 meters). The river then flows east and south in a broad flat, steep-walled river valley for approximately 65 kilometers before it enters the region south of Lake Coleridge, which precedes the Rakaia Gorge proper. This section of the river lies on a broad flat plateau lying between 300 and 600 m above sea level running in a northwest-southeast direction. The Mt. Hutt Range rises abruptly to 2188 m on the south valley wall. The north side of the river valley is bounded somewhat irregularly by the Big Ben Range and Round Hill, which rise to a maximum of 1657 m and 900 m respectively.

The river valley floor consists of rocks that underlie dunes, river terraces, alluvial plains, and glacial moraines. In the late Quaternary period (essentially the present time) four major cold periods occurred during which glaciers advanced and formed moraines mostly on the South Island. During these cold periods, rivers built up terraces in many valleys outside the glaciated area and spread thick deposits of gravel beyond the mountains to form the Canterbury plains. Then fine dust blown off gravel terraces, plains and hills devegitated by cold, was deposited as loess over large areas, especially over the eastern South Island.

South of the Rakaia Gorge the land falls imperceptibly from 300-400 meters to sea level. The agricultural landscape of the Canterbury plains is interrupted by three major rivers from the main divide: the Waimakariri, Rakaia, and Rangitata, which have highly variable flows. The major rivers all have broad beds with braided channels, which though liable to flood, are occupied for much of the year by only a few streams of water.

In the 20 km long fetch of the Rakaia River investigated during this study, the river flows southeast from a broad flat plain of 350 m average height. The valley abruptly narrows as it enters the river gorge itself. The gorge walls rise to 460 meters and the width varies irregularly from 500 m to 2600 m. The gorge persists for about 8 km in a northwest-southeast orientation.

3.2 Meteorology of Southern Alps Region

Between the latitudes of about 30° and 70° , mid-latitude westerly winds blow around both hemispheres. New Zealand, which falls between 34°S to 47°S , lies within the mid-latitude westerly zone, i.e., the "Roaring 40's." Since the country is surrounded by a large body of water, the air arriving is moisture laden and moderate in temperature. (The nearest continental land mass, Australia, is over 2000 kilometers to the west.)

Within this band of mid-latitude westerlies is a succession of anticyclones and depressions. Generally, these features lie to the south of the subtropical high in the Southern Hemisphere; and the average position in New Zealand of the subtropical high goes through an annual cycle from about latitude 26° South in the winter to latitude 36° South in the summer, though there is considerable variability in all seasons. This predominantly eastward-moving sequence of anticyclones and depressions, with their associated cold and warm fronts, produces much of the day-to-day weather over New Zealand.

* Extracted in part from New Zealand Atlas (Ward, 1976)

The interval of time between the successive troughs of low pressure passing over the country is very variable. On a seasonal basis, only about one season in two experiences a regular progression with a fairly constant interval between troughs of low pressure. When this occurs the interval is usually between five and eleven days, with a marked preference for eight to ten days. There is no apparent seasonal variation throughout the year.

While the country's location in the mid-latitude westerlies determines the general nature of the climate, its orography has a very dominant effect on the variation of the climate and windflow within the country. The main ranges of the North and South Islands extend in a north-east/south-west line and provide a barrier to the prevailing westerly winds. This is most noticeable in the South Island where the Southern Alps provide a barrier of greater height than 1000 meters for about 750 kilometers. As the maritime air from the Tasman Sea rises to cross this barrier, it often cools enough to produce clouds and rain to the west of the main divide. These western slopes of the main ranges receive very high annual rainfall totals, sometimes in excess of 6000 millimeters, while just to the east of the main divide there are some areas of very low rainfall and high sunshine duration.

Winds from a westerly quarter prevail in all seasons, with a general tendency to increase in strength from the north to the south of the country; at the same time, considerable local modifications to the general airflow occur during its passage across the mountainous terrain. A considerable number of south-westerlies in Westland and

a predominance of north-westerlies in inland districts of Otago and Canterbury result, often as strong gales, in spring and early summer. High wind gusts occur over exposed parts of the country. Instantaneous gusts of up to 130 knots (67 m/sec) have been measured in the Southern Alps and are probably not uncommon.

Since the main mountain chains of New Zealand lie athwart the prevailing winds the coast west of the mountains should receive more wind than the apparently sheltered eastern coasts. Generally this is the case in the North Island but not in the South Island where the mountains are very close to the west coast. During periods of strong west to northwest winds a 'cushion' of air close to the steep western slopes of the Southern Alps forms an additional 'block' to the airstream. While the wind speed increases over the ridges the coastal strip is not exposed to the full force of the winds.

However, there is strong local enhancement of the flow around the southern and northern extremities of the country, through Cook Strait and down mountain valleys and gorges that run approximately east-west. In Canterbury, the flow out of mountain gorges, such as the Waimakariri, Rakaia and Rangitata, results in high winds down the rivers and across the plains. There are often lee waves set up to the lee of the mountains with high winds under their troughs and lighter winds under their peaks.

The Rakaia River Gorge lies within a cool wet hill climate with rainfall from 750 mm to 1500 mm. Northwest winds prevail with occasional very strong gales, especially along river courses. As

noted in Figure 3-1 from Ward (1976), the Rakaia Gorge lies within a region noted for 50 to 100 annual days per year of wind gusts reaching 34 knots (17.50 m/sec) or more. As noted on the figure, strong winds over 15 knots from the northwest predominate over the Southern Alps while winds at all speeds also show a marked predominance from the same sector.

3.3 New Zealand Wind Energy Resource Survey Results

As indicated by Lindley and Chin (1977) the New Zealand Wind Energy Task Force was established in 1974. The Task Force has attempted to coordinate wind engineering, power systems, and meteorological expertise by drawing upon the membership of the New Zealand Electricity Department (NZED), the Ministry of Works, the Meteorological Service, and the Universities. It has concentrated its activities, however, on resource assessment. Its first report on a preliminary analysis of the existing Meteorological data (Cherry, 1976) indicates that most areas of New Zealand have moderate to very high wind energy fluxes in comparison to other published national surveys.

Fifty stations from the New Zealand Meteorological Science anemograph network were analyzed for average wind speed and mean wind energy flux. These anemometers were not specifically sited for a wind energy survey but have been installed to give airport runway conditions, shipping winds in harbors, or urban climatology. Hence they have a wide range of exposures, heights above ground, types of observations, and frequency of recording. An estimate of reliability was made for each data set when estimating the wind energy at the particular locality.

Annual winds were found to range from a maximum of 12.5 m/sec to 1.9 m/sec. The country-wide average annual wind speed was 4.9 m/sec. In general well exposed sites in the south had low diurnal ranges because of persistent westerlies. The annual mean wind energy flux (WEF) varies from 1447 W/m^2 to 36 W/m^2 . Individual sites have annual variations ranging from 30 to 100%. The average proportional range of monthly mean WEF's over all sites in New Zealand is about 77%.

Out of 50 preliminary sites 10 had annual WEF exceeding 400 W/m^2 , 9 additional sites exceeded 200 W/m^2 , and 17 more exceeded 100 W/m^2 . Reed (1974) ranked sites in the United States by their annual mean WEF as

Very High WEF	Over 400 W/m^2
Moderate WEF	Over 150 W/m^2
Low WEF	Less than 100 W/m^2

The greatest portion of the land area of the continental U.S. has a surface WEF between 50 and 150 W/m^2 at a 10 m height.

The potentially available wind energy in New Zealand is felt to be greater than these results (Cherry, 1976) would indicate because some of the observing sites were not in the most exposed places. If large scale generation of electricity from wind turbines is to be undertaken in New Zealand, areas where winds are enhanced by local topography would be selected. Likely places in this respect include the Rakaia Gorge west of Christchurch.

Phase II of the Wind Energy Task Force program involves the collection of data from approximately 75 cup anemometers placed at a height of 10 m above the ground. These stations are additional to the existing meteorological network and are all situated in the provinces of Canterbury and Otago in the South Island and in the Chatham Islands

and Stewart Island. Data loggers have been used at selected sites to yield mean wind speeds over 5 minutes and less while other anemometers are being read for wind run at weekly intervals.

Six towers have been installed in the vicinity of the Rakaia River Gorge as part of the Phase II effort. Stations at Mt. Hutt (Map coordinates S82 105/572) and Rakaia Gorge (S82 131/584) are within the modeled region. Lake Coleridge (S74 043/793) is located ~20 km upwind of the gorge entrance. Highbank (S82 190/521), Methven 1 (S82 140/481) and Te Pirita (S82 397/403) are located on NZED transmission towers which cross the Rakaia River downwind of the gorge 10 km out onto the Canterbury plain. A NZED continuous recording anemometer is also located on top of Round Hill just to the north of the region studied. Data from these recorders will be tabulated and published during the next year. Their results may provide a valuable climatological counterpart to this study. Preliminary results have been provided by N. Cherry for this report for several stations. This data is provided in Table 3-1.

3.4 Micrometeorological Characteristics of the Rakaia River Gorge Region

There is no local data available concerning the depth, profile shape, or turbulence character of the atmospheric surface layer in the Rakaia River Gorge region. No results from meteorological towers, balloon soundings, or airplane soundings were found for similar New Zealand topography in available records. Hence the approach flow characteristics selected to model the approach wind profile are based on available experience from other parts of the world.

A number of investigators have prepared data for adiabatic atmospheric boundary layers into a tabular format with the intent to isolate functional dependence of shear layer properties on pertinent

surface parameters. The results of Counihan (1975), Harris (1971), Panofsky (1977), Teunissen (1970), etc., although they differ in detail, are consistent in their major conclusions. Hence this report will appeal to the review paper by Counihan (1975) for guidance. Other authors, such as Cermak (1975), Robins (1977), and Cook (1977), discuss the determination of model scale factors in wind tunnel simulation as will be referred to in Chapter 4.0. Unfortunately this information was developed for flat homogeneous terrain of large extent, and parameters such as boundary-layer depth, integral scales, friction velocities, and profiles may not remain similar to their homogenous surface counterparts after wind flows over complex mountain-valley systems onto a broad river valley.

Nevertheless, Counihan provides a number of suggestive correlations which should guide modeling decisions. Correlations for velocity power law, turbulence intensity at 30 m, Reynolds stress, and integral length scale, are

$$\frac{1}{\alpha} = 0.096 \log_{10} z_0 + 0.016 (\log_{10} z_0)^2 + 0.24 \quad (3.1)$$

$$\frac{\sqrt{\overline{u'^2}}}{\bar{u}} = 0.096 \log_{10} z_0 + 0.016 (\log_{10} z_0)^2 + 0.24 \quad (3.2)$$

$$\frac{\overline{u'w'}}{\bar{u}_0^2} = 2.75 \times 10^{-3} + 6 \times 10^{-4} \log_{10} z_0 \quad (3.3)$$

$$L_{u_x} = C (z)^{1/n} \quad (3.4)$$

where

$$\log_{10} C \approx -0.3733 \log_{10} z_o + 1.3275 \quad (3.5)$$

$$\log_{10} \frac{1}{n} \approx 0.1946 \log_{10} z_o - 0.4164 \quad (3.6)$$

Boundary layer depth with no surface heating has been estimated to vary from 250 m to 800 m by various authors. It is generally expected to be a function of roughness, gradient wind speed, and Coriolis parameter. Since no consistent functional dependence exists Counihan recommends $\delta = 600$ m as an average height for rural and urban boundary layers. Most authors realize both boundary layer depth and integral scale may increase over or near complex terrain, values as large as 1000 m have been proposed as plausible for both parameters (Wooldridge, 1978; Panofsky, 1978).

The surface texture in the Rakaia Gorge region consists of an intermesh of sheep paddock (grass ~ 5-10 cm), shelterbelts (coniferous trees ~ 10-20 m), gravel covered river bed (stones ~ 5-10 cm), intermixed with scrub, gulleys, and river escarpments.

The riverbed surface and grass paddocks combined with local terrain undulations has a moderately rough texture typical of a roughness length circa $z_o \approx 5$ cm. Shelterbelts similar to those observed have been extensively studied on the Canterbury plain by Sturrock (1972). He examined horizontal velocity profiles behind 10 typical Canterbury shelterbelts mainly of medium density varying in height from 8.5 to 19.8 m. When the visual cross section of these shelterbelts were considered it was concluded that the typical Rakaia Gorge shelterbelt has probable permeabilities between 0 to 20%.

In conclusion, the local micrometeorology of the Rakaia Gorge upwind atmospheric surface layer is controlled for high wind speeds by an effective surface roughness of $z_0 \approx 5$ cm and an array of 20 m tall shelterbelts. These surface features result in values for

$$\frac{1}{\alpha} \approx 0.11 - 0.14,$$

$$\frac{\sqrt{\frac{u'^2}{2}}}{\bar{u}} \approx 0.11 - 0.14, \text{ and}$$

$$\frac{\overline{u'w'}}{u_0^2} \approx 0.0015 - 0.0018.$$

Boundary layer depth should be $\delta \approx 600 - 1000$ m, and longitudinal Velocity integral length scale may be $L_{u_x} \approx 300 - 1000$ m at $z = 50$ m.

4.0 CRITERIA FOR LABORATORY SIMULATION OF WIND CHARACTERISTICS OVER IRREGULAR TERRAIN

In order for the flow in any laboratory model to be of value in interpreting or predicting the observed flow in the atmosphere, it is essential that the two flow systems should be dynamically, thermally and kinematically similar. This means that the flow in the two systems must be described by the same equations after appropriate adjustments of the units of length, time and other variables.

A number of authors including Cermak (1966, 1970, 1975), McVehil et al. (1967), Bernstein (1965), and Snyder (1972) have derived the governing parameters for atmospheric heat, mass, or momentum transport by dimensional analysis, similarity theory, and inspectional analysis. Another group justify similitude by considerations of turbulence theory and recent reviews of full scale wind data which present the characteristics of the prototype atmospheric wind on a parametric basis (Nemoto (1961, 1962), Counihan (1969, 1973), Cook (1977), and Melbourne (1977)). Although all investigators do not agree concerning details, most would concur that the dominant mechanisms can now be identified and are understandable. The following sections review similitude criteria as they relate to adiabatic atmospheric shear flow over irregular terrain. Restrictive assumptions are discussed and a typical performance envelope for large wind tunnel facilities is provided to guide subsequent use of wind tunnels as a model tool for WECS siting in irregular terrain.

4.1 Basic Equations and Assumptions

The basic equations necessary for considering atmospheric motions are the following:

Equation of turbulent momentum transfer,
Continuity equation,
Equation of state,
Poissons equation,
Equation of turbulent heat transfer,
Equation of heat transfer from the surface boundary, and
Equation of turbulent scalar transfer.

These equations together with the appropriate boundary conditions have been summarized in Appendix A, which has been reproduced from Orgill, Cermak, and Grant (1971).

For complete flow similarity in two systems of different length scales, geometrical, kinematical, dynamical and thermal similarity must be achieved. In addition, boundary conditions upstream, in the upper atmosphere, and downstream should also be similar.

Geometrical similitude exists between model and prototype if the ratios of all corresponding dimensions in model and prototype are equal. This is realized by using an undistorted scale model of the prototype geometry. Kinematic similitude exists between model and prototype if the paths of homologous moving particles are geometrically similar and if the ratio of the velocities of homologous particles are equal. Dynamic similitude exists between geometrically and kinematically similar systems if the ratios of all homologous forces in model and prototype are the same. Thermal similitude exists if the temperature or density stratification are similar.

The proper similitude parameters governing the phenomena of interest may be established by dimensional analysis, similarity theory or inspectional analysis. No attempt will be made here to give a

comprehensive description of each of these methods since several good discussions are available in various textbooks and publications. As noted from Appendix A, a consensus of the pertinent parameters for steady, turbulent, near neutral airflows are:

$$R_o = \frac{U_o}{L_o \Omega_o}, \text{ Rossby Number,} \quad (4.1)$$

$$R_e = \frac{U_o L_o}{\nu}, \text{ Reynolds Number,} \quad (4.2)$$

$$R_i = \frac{\Delta T_o}{T_o} \frac{L_o}{U_o} \frac{g_o}{2}, \text{ Richardsons Number,} \quad (4.3)$$

$$Pr = \frac{\mu}{c_p k}, \text{ Prandtl Number,} \quad (4.4)$$

$$Ek = \frac{U_o^2}{c_p \Delta T_o}, \text{ Eckert Number, and} \quad (4.5)$$

$$Eu = \frac{\Delta p_o}{\rho U_o^2}, \text{ Euler Number} \quad (4.6)$$

The foregoing requirements must be supplemented by the stipulation that the surface-boundary conditions and the approach-flow characteristics be similar for the atmosphere and its model. Surface-boundary-condition similarity requires similarity of the following features:

- a. Surface-roughness distribution with "aerodynamically rough" behavior
- b. Topographic relief, and
- c. Surface-temperature distribution.

Similarity of the approach-flow characteristics requires similarity of the following flow features:

- a. Distributions of mean and turbulent velocities,
- b. Distributions of mean and fluctuating temperatures,
- c. The longitudinal pressure gradient (should be zero), and
- d. Equality of the ratio of inversion depths if the flow is thermally layered.

As a result of similitude in the relevant parameters from the above list plus similarity in boundary conditions, one may expect similarity in approach flow turbulence quantities such as:

$$I_{ij} = \frac{\sqrt{(U_i U_j)_o}}{U_o} \quad ; \quad \text{Turbulence intensities,} \quad (4.7)$$

$$\text{or } \sqrt{\frac{T'^2}{\Delta T_o}}$$

$$\frac{\bar{z}_o}{L_o}, \frac{L_{u_x o}}{L_o}, \frac{L_{mo}}{L_o}, \frac{\delta_o}{L_o} \quad , \quad \text{Turbulence Length Scales,} \quad (4.8)$$

$$Re_t = \frac{U_o L_o}{K_m} \quad , \quad \text{Turbulent Reynolds Number, and} \quad (4.9)$$

$$Pr_t = \frac{K_m}{K_H} \quad , \quad \text{Turbulent Prandtl Number.} \quad (4.10)$$

Sometimes investigators go directly to the resulting turbulent parameter to validate a simulating methodology. This philosophy tends to emphasize that only results are relevant and the "ends justify the means."

If all the foregoing requirements were met simultaneously, all scales of motion ranging from micro to mesoscale, 10^{-3} to 10^5 m, could be simulated within the same flow field for a given set of boundary conditions. However, all of the requirements cannot be satisfied simultaneously by existing laboratory facilities, and partial or approximate simulation must be used. This limitation requires that atmospheric simulation for a particular wind-engineering

application must be designed to simulate most accurately those scales of motion which are of greatest significance for the application. By considering each similarity requirement separately it is possible to determine for what flow features "exact" similarity between the laboratory and the atmospheric boundary layer is lacking.

The effects of equal Rossby numbers cannot be obtained in non-rotating wind tunnels. The Ekman spiral in the wind profile is attributed to the Coriolis forces considered in this parameter. The laboratory boundary layer is an adequate model for atmospheric flow when either wind veering is not significant for the application, or the turning is small. Boundary layer wind tunnels do not yet simulate wind veering as it may occur across inversions. The Rakaia Gorge area model has a characteristic length of 20 km, northwesterly winds are circa 20 m/sec at gradient wind height, and $\Omega_0 = 9 \times 10^{-5} \text{ sec}^{-1}$ at $\phi \approx 40$ degree latitude; hence, $R_0 \approx 11$, i.e., the inertial effects are an order of magnitude greater than the Coriolis term. Indeed, Hoxit (1973) and Scorer (1978) observe that most of the time flow is not in equilibrium with Coriolis forces because of thermal winds or other effects; hence, the Ekman spiral is normally only of academic interest.

Equal Reynolds numbers are also not attainable. However, this does not seriously limit capabilities for modeling the atmospheric boundary layer over irregular terrain at high wind speeds significant flow characteristics are but weakly dependent on Reynolds number. Since essentially all natural surfaces are "aerodynamically rough," flow structure will be similar if the scaled-down roughness has a sufficiently large size to prevent the formation of a laminar sublayer. Generally the requirement for fully rough flow is

$\frac{U_* \lambda}{\nu} > 100$ or $\frac{U_o L_o}{\nu} > 10^4$ to 10^6 . The Rakaia Gorge model considered herein satisfied both these criteria. Duplication of the main streamline features, regions of turbulent eddies, and structure of turbulence thus becomes dependent upon geometric similarity and equivalence of relevant length scale ratios--such as z_o/L_o , $\frac{L_{u_x o}}{L_o}$, etc.

Equal gross or local Richardson numbers can be obtained in specially designed wind tunnels. Batchelor (1953) has established that (a) if the flow fields are such that the pressure and density everywhere depart by small fractional amounts only from the values for an equivalent atmosphere in adiabatic equilibrium, and (b) if the vertical length scale of the velocity distribution is small compared with the scale height of the atmosphere, the Richardson number is the sole parameter governing dynamical similarity. Unfortunately, these conditions are only normally satisfied in the first 100 m of the planetary boundary layer.

Another widely used parameter to describe the state of the atmospheric surface layer under nonadiabatic conditions is the Monin-Obukhov length. Monin and Obukhov (1954) assumed that when buoyancy forces exist, the character of the flow no longer depends upon the Reynolds number but upon u_* , Q_H , ρ , c_p , g and T . These may be combined dimensionally to yield a length L_{mo} defined as,

$$L_{mo} = - \frac{U_*^3 T \rho c_p}{\kappa g Q_H}$$

The Monin-Obukhov similarity statement is valid only if several conditions are fulfilled. Among these are:

1. Fractional changes in the potential temperature must be small;
2. The ratio of the eddy transport coefficients of momentum and heat must be a constant independent of both height and stability;
3. A change in z_0 should not alter the detailed turbulent structure of the flow;
4. u_* and $Q_H / \rho c_p$ must be independent of height; and
5. The flow must be fully aerodynamically rough and have planar homogeneity.

The Monin-Obukhov stability length was derived for the surface layer and not for the entire planetary boundary layer. Its many restrictions do not permit application to the total boundary layer. Also, another disadvantage of the Monin-Obukhov length is that the flux of heat, Q_H , and the flux of momentum, u_* , are very seldom known in the atmosphere. Other stability parameters such as the flux Richardson number or Panofsky's length have the same difficulties.

The discussion indicates that although the gradient Richardson number may not be the only sole similarity parameter governing the flow it still remains a parameter for checking similitude between model and field. The Richardson number expressed as a local parameter is defined by,

$$Ri = \frac{g}{\theta} \frac{\overline{\left(\frac{\partial \theta}{\partial z}\right)}}{\overline{\left(\frac{\partial u}{\partial z}\right)}^2} . \quad (4.12)$$

Batchelor has emphasized that no local, variable quantity can be used as a similarity parameter. Similarity parameters can have meaning only when they characterize the gross features of the flow.

When a gross or bulk Richardson number is desired to describe the thermal influence over a layer of fractional thickness, Δz , the following form is convenient

$$Ri = \frac{g}{\bar{\theta}} \frac{\Delta \bar{\theta}}{(\Delta u)^2} \Delta z . \quad (4.13)$$

In the case of the model airflow the potential temperature may be replaced by temperature or density.

The atmosphere for purposes of simulation was assumed to be in a neutral state over the Rakaia Gorge for these cases investigated. This implies $Ri \equiv 0$ or $\frac{\partial \theta}{\partial z} \Big|_{\text{field}} \equiv \frac{\partial T}{\partial z} \Big|_{\text{model}} = 0$ for the temperature distribution in the field and wind tunnel. No measurements over the boundary layer depth were available at the gorge on the days examined. Orgill et al. (1971) report near-neutral stability conditions through a depth of 2400 meters for a similar type day when the sky was totally overcast with moderate to light precipitation and surface winds were strong and gusty at Camp Hale, Colorado. This depth exceeded the highest mountains in the area. Such a situation closely describes weather conditions during the Rakaia Gorge field experiments.

The Prandtl numbers and Euler numbers are essentially equal for flows in the laboratory and the atmosphere. The Eckert number is equivalent to a Mach number squared, which is small compared to unity for both laboratory and atmospheric flows.

4.2 Laboratory Constraints for Neutral Airflow Models

The viability of a given simulation scenario is not only a function of the governing flow physics but the availability of a suitable simulation facility and the measurement instrumentation to be employed. It would seem appropriate, therefore, to suggest bounds for the range of field situations which can reasonably be treated by physical modeling. With few exceptions, scientists seem to make rather poor prophets; there is always the danger of what Arthur Clarke (1958) calls "failures of nerve" or "failures of imagination." Nevertheless, let us propose limitations on simulation for complex terrain.

A number of boundary layer wind tunnels exist at various laboratories. Generally these tunnels range in size from facilities with cross sections of 0.5 m x 0.5 m to 3 m x 4 m. Several of these facilities are equipped with movable side walls or ceilings to adjust for model blockage. By utilizing a variety of devices such as vortex generators, fences, roughness, grids, screens, or jets, a fairly wide range of turbulence integral scales can be introduced into the shear layer. Varying surface roughness permits control of surface turbulence intensity, dimensionless wall shear, and velocity profile shape. Density stratification can be induced by heat exchangers, different molecular weight gases; or latent heat adsorption or release during phase changes. Table 4-1 suggests parameter values for typical wind tunnels familiar to the authors. The probable range of the equivalent parameters in the atmospheric surface layer are tabulated in Table 4-2. A comparison between field and laboratory parameter ratios are summarized in Table 4-3.

When one combines various operational constraints into a performance envelope a clear picture appears of the performance region for wind tunnel facilities. (Figure 4-1 is such a performance envelope prepared for a large facility such as the Environmental Wind Tunnel at Colorado State University.) The criteria selected to specify operational ranges are:

Maximum model height $h \leq 0.5 \text{ m}$

Minimum convenient model height $h \geq 0.02 \text{ m}$

Minimum Reynolds Number $Re_h = \frac{U_o h}{\nu} \geq 10,000$

Maximum model integral scale $L_{u_x} \leq 0.5 \text{ m}$

Minimum model integral scale $L_{u_x} \geq 0.05 \text{ m}$

Minimum model measurement resolution $\Delta z \geq 0.1 \text{ mm}$

Maximum model boundary depth $\delta \leq 2 \text{ m}$

Minimum model boundary depth $\delta \geq 0.1 \text{ m}$

Since field values for some parameters are uncertain the prototype values of δ and L_{u_x} are assumed to range as follows over complex

terrain:

$$300 \text{ m} < \delta < 1000 \text{ m, and}$$

$$100 \text{ m} < L_{u_x} < 1000 \text{ m.}$$

Not all previous laboratory studies meet such similitude restrictions, some experiments were performed to meet other objectives than similitude of turbulence or mean velocity profiles; nevertheless, a number of the studies listed in Table 2-1 are indicated on Figure 4-1 by number. Almost all cases noted fall within the indicated operational envelope or just outside the predicted region.

Based on Coriolis force considerations Snyder (1972) suggests a 5 km cut-off point for horizontal length scales for modeling diffusion under neutral or stable conditions in relatively flat terrain. Mery (1969) suggests a 15 km limit, Ukejurchi et al. (1967) suggest 40 to 50 km and Cermak et al. (1966) and Hidy (1967) recommend 150 km, but some authors are considering diffusion and some are not. A middle road would be that of Orgill et al. (1971a and 1971b) who suggest that a length scale of 50 km is not unreasonable for rugged terrain in high winds.

Assuming an upper value of length scale ratio of 10,000 and a tunnel length of 25 m a distance of 50 km is well within the capacity of existing facilities to contain in the windward direction. Assuming a lateral width restriction of 4 m suggests a 40 km lateral maximum for the field area modeled.

4.3 Summary of Similitude Criteria for Rakaia River Gorge Simulation

The Department of Mechanical Engineering, University of Canterbury, Boundary Layer Wind Tunnel has a test section 1.22 m x 1.22 m x 12.2 m. Boundary layer depth and integral scales are controlled by a combination of square rod grids, fences, and surface roughness. An examination of the surface topography and vegetation in the Rakaia River Gorge area (Section 3.4) and the physical and operational constraints previously discussed (Sections 4.1 and 4.2) suggest the following model simulation criteria:

1. For a modeled region 6 km wide by 18 km long a 1:5000 geometrically undistorted model is required.
2. For a field roughness of $z_0 \approx 5$ cm a model roughness of $z_0 \approx 0.01$ mm is necessary.
3. For a region of field shelterbelts $H \approx 20$ m a model shelterbelt complex $H \approx 4$ mm is desired. Porosity should range from 0 to 20%.

4. Approach flow velocity profiles should have a power law coefficient $1/\alpha$ between 0.11-0.14, local surface turbulence intensities u'/\bar{u} between 0.11-0.14, and surface friction coefficients u_*/u_δ between 0.039-0.042.
5. A neutral shear layer whose field depth is 500-1000 meters is probable downwind of a mountain range; thus the model shear layer depth $\delta = 0.10-0.20$ m. Integral scales in complex flow are expected to range between $L_{u_x} = 300$ to 1000 meters at a height of 100 meters over a surface roughness $z_o \approx 0.05$ m. Hence a modeled flow should provide $L_{u_x} = 0.06$ to 0.20 m.

Section 5.0 will discuss the means used to obtain this similitude equivalence and the success therein.

5.0 EXPERIMENTAL EQUIPMENT AND PROCEDURES FOR LABORATORY MEASUREMENT

5.1 Atmospheric Boundary Layer Wind Tunnel

The Atmospheric Boundary Layer Wind Tunnel in the Department of Mechanical Engineering at University of Canterbury, New Zealand, was constructed in 1971-1973 as an open circuit "blower" configuration (Raine (1974)). Between 1975-1976 the fans were relocated downwind of the working section resulting in a test section that operates at a negative gauge pressure. Nonetheless the complete description of the structure of the facility and its range of operating characteristics found in Raine (1974) is still pertinent.

As shown in Figure 5.1, air enters a streamlined entrance section through a series of wire meshes and cardboard tube honeycombs into a short settling chamber. After a 1.25 contraction the air passes through a flow straightening aluminum honeycomb to the tunnel inlet.

The working section of the wind tunnel is a 1.22 m x 1.22 m cross section 12.2 m long. The roof panels were suspended from threaded steel rods to permit adjustment of the longitudinal pressure gradient. Flush surface static pressure taps located half way up one side wall facilitated measurement of longitudinal static pressure variation. The alternate wall was constructed of 0.64 cm flexible glass mounted in 20 doors over its full length.

A motorized traversing gear traveled in a slot centered in the test section floor. The worm gear driven traverse trolley could move full length of the test section while pressure integrity was maintained by a heavy nylon zip seal. A vertical load screw using a sewing machine universal motor moved a horizontal arm vertically above the trolley. To steady the horizontal arm during measurements, air operating piston

pads were added to each end of the horizontal arm. Thus, measuring instruments mounted on the horizontal traverse bar could readily be moved to a given site and still provide a steady foundation during measurement.

Air passes from the working region through two corner sections up to a mezzanine floor. Here air is drawn through a two stage fan unit. The Woods 48J₂-2 arrangement, with the fans contra-rotating to avoid induced swirl in the test section, were regulated by varying the pitch of the fan blades. Test section velocities from 0 to 20 m/sec were possible depending upon the fan setting and the flow control devices inserted upwind of the working section. Finally air exhausted from the wind tunnel through a diffuser at the laboratory mezzanine level.

5.2 Topographic Models

The area studied by means of a laboratory model is located along the Rakaia River as it emerges from the Southern Alps, South Island, New Zealand (see Section 3.0). The primary terrain features consist of the Rakaia River Gorge which generally runs in a northwest-southeast direction. Gorge walls rise 180 meters, surrounding hills rise to 460 meters. To the South lies the Mount Hutt range which climbs to 2188 m. The range parallels the course of the Rakaia River in this area. To the north lies the Rugged Range but Fighting Hill and Round Hill are the largest local features. A model section 6100 m wide by 18,300 m long centered over the Rakaia River Gorge was constructed to a scale of 1:5000. The topographical features of the model were obtained from New Zealand Department of Land and Surveys Maps numbers 1-S82 and 1-S74 at a scale of 1:63360. These maps were enlarged to the correct scale photographically and prints were prepared by the Christchurch branch of the New Zealand Printing Office. Corner map co-ordinates are included on Figure 5-10 which details the modeled area.

The construction material was expanded polystyrene beadboard cut to 0.61 cm thickness to match 100 ft map contour intervals. This was mounted in layers on a particle board support sheet. The dimensions of the overall model are approximately 5 m long by 1.22 m wide which includes a 1.2 m terraced section upwind to transition the model to the tunnel floor. The model was divided into 4 major subsections which can be fitted together when in the wind tunnel. To provide a greater upwind fetch of equivalent surface roughness an additional 1.22 m x 2.44 m section of polystyrene beadboard was mounted immediately upwind of the transition subsection. The total model length was thus 7.3 meters. A 2.5 cm high trip fence and a square bar turbulence grid were placed upwind of the model to produce the desired similitude characteristics. Their influence are discussed in Section 7.1.1.

The final stages of model construction consisted of alternative combinations of surface filler, surface roughness, and paint. These configurations are discussed separately in the next three sections.

5.2.1 Terraced Model

Terraces resulting from the layers sandwiched together during model construction are often smoothed over with a filler compound, and then roughness is added to the surface to represent the field situation. Since this process appears to remove a roughness and then add it back, many investigators have followed a convenient alternative path which is to leave the model surface terraced. One then assumes separation over the terrace corners provides the drag normally contributed by distributed surface roughness. Whether the alternative terraced model is quantitatively adequate will depend upon the examined problem.

A terraced version of the Rakaia River Gorge model was constructed. Contour intervals were at 30 m (100 ft). Several colors of a latex paint were applied to protect and harden the surface. Roads, gravel, river areas, and shelter-belt regions were marked in contrasting colors. Figure 5-2a shows the topographic model during an experiment as installed in the wind tunnel.

5.2.2 Contoured Model

A contoured model was prepared from the terraced model after its measurement schedule was completed. Plaster was smoothed between terrace escarpments and was textured to provide an equivalent surface roughness. This surface roughness was such as to provide a $z_0 \approx 0.01$ mm equivalent to $z_0 = 0.05$ m at full scale. The model was repainted as before.

A series of measurements were made over the smooth contoured model. A second set was made over the contoured model but with shelterbelts modeled with 4 mm diameter wool yarn. Finally a third set of measurements was made over the contoured model but with shelterbelts modeled with 4 mm diameter pipe cleaners. The flow characteristics of the model shelterbelts are discussed in the next section.

5.2.3 Shelterbelts

The hillsides to either side of the Rakaia River are primarily devoted to sheep paddock. To protect flocks and paddock surface during high winds, farmers have planted shelterbelts around most fields. Most of these shelterbelts are stands of mature coniferous trees about 20 m high. The stands of trees often consist of several rows and appear quite dense. Aerodynamic studies of flow fields behind

shelterbelts in New Zealand have been performed by Sturrock (1972). Modeling of the wind shelter produced by such fences has been considered by Raine (1974) and Raine and Stevenson (1977).

Raine (1974) concludes that the comparison between the model and field shelterbelts is good when similar H/z_0 exists (i.e., within $\pm 10\%$). A single parameter suffices if turbulence in each case is at equilibrium. Greater surface roughness is found to decrease the shelter of a given belt wall. The optimum shelter exists for porosities between 0 to 20%. Lower turbulence intensities are generally found as permeability increases. A solid fence produces steeper streamline variation near the fence crest and may cause perturbations at higher levels. Raine's results are for $H/z_0 \approx 100$, Sturrock's measurements provide data for $H/z_0 \approx 500$, the Rakaia Gorge area appears to range between $H/z_0 = 400$ to 500.

A series of velocity and turbulence measurements were made over test shelterbelts in the simulated boundary layer. These measurements were made at heights $z/H = 0.5, 1.25, \text{ and } 2.5$ behind a large aspect ratio fence perpendicular to the flow. The ratio of winds found with and without the fence present versus location with respect to the fence are plotted in Figures 5-3 and 5-4. The yarn appears to behave as a 20% permeable fence, the solid pipe cleaners provide somewhat less shelter. Together the two materials bound the data provided by Sturrock (1972) and Raine (1974). Raine expected shelter to increase

as H/z_0 increases; hence it is reasonable that the yarn results lie at the bottom of Raine's measurements on Figure 5.3.

Isocontours of local turbulence intensity plotted in Figures 5.5 and 5.6 agree very well with Raine's measurements. Raine found only a minor effect on $\overline{u'}/\overline{u}$ distributions versus $\overline{u}/\overline{u}_0$ as the structure of the permeable fence changed. The turbulence intensity results for both the yarn and the pipe cleaner correlate to the same expression suggested by Raine (1974) as shown in Figure 5.7.

It is comforting indeed that the 4 mm model fences utilized herein modeled the character of 20 m tree shelterbelts so well. The results suggest inertial effects dominate because:

$$Re_{\text{field}} = \frac{\overline{U}_H H}{\nu} \approx 0 (3 \times 10^7)$$

whereas

$$Re_{\text{model}} \approx 0 (4 \times 10^3)$$

5.3 Flow-field Measurements

5.3.1 Visualization Techniques

In complex terrain, hills, ridges, gorges, and shelterbelts may produce regions where wind speed, turbulence, and flow direction are perturbed from that of an average background flow. Since most measurement techniques are sensitive to exaggerated variations in any of these quantities the flow field over each model was examined in advance by means of small flags and polystyrene micro-beads.

Small flags made of light balsa wood were carved to a size of 4 mm high x 8 mm long and mounted above a bead bearing on a drawing pin. These flags were inserted into the surface of the model as required. Observation of flag movement indicated surface flow direction and regions of high turbulence or recirculating flow. Surface flow directions were found to agree consistently with Cobra probe measurements made over the same locations.

Streaklines and regions of relatively low shear were visualized by the drifting of 2 mm polystyrene beads over the model surface. A pile of beads were placed well upwind of the model. The wind tunnel speed was slowly increased in a series of increments. At various times the tunnel was turned off and sketches made of zones where polystyrene beads collected or recirculated. Initially beads would deposit behind even the most insignificant prominence; however as the wind speed increased the most persistent drifts indicated those regions of maximum shelter.

5.3.2 Hot-Wire Anemometry and Associated Equipment

Detailed operating procedure and the hot-wire anemometer theory are not dealt with in this report. The former is amply described in the DISA equipment manuals, and the latter is described by Hinze (1975), Bradshaw (1971), and Sandborn (1972). Only concepts essential to meteorology and sources of error are discussed here. A list of equipment with associated manufacturers trade names, models, and pertinent specifications are provided in Table 5-1.

The DISA hot-wire anemometer, linearizers, and associated equipment were connected and calibrated according to the detailed instructions set down in the DISA manuals. The DISA TCA system, which was also used for autocorrelations was connected as instructed in the manual for the 55D70 Analogue Correlator. T-junctions were used at the output terminals of the auxiliary unit to duplicate signals for supply to the Brüel and Kjaer 1/3 Octave Bandwidth Spectrometer. The schematic connection diagram for the equipment is shown in Figure 5-8.

Hot wire anemometer probes were calibrated against the behavior of a Thermal Systems Incorporated Model 1125 Calibrator. Vertical position of the single wire probes were controlled to within 0.2 mm by a DISA Sweep Drive Unit Model 52B01 and a Model 55H01 Traversing Mechanism.

Vertical profiles were made at sites over the model where flow visualization suggested wind veering effects were small. Local turbulence intensities reached values as large as 60% in a few cases. The accuracy of hot wire anemometry in the presence of large turbulence intensities is of notable concern. Raine (1974) reviewed a range of opinions and analyses on this topic and concluded that effects of thermal drift, dirt, misalignment, and turbulence on indicated mean velocity do not exceed 5% when $\overline{u'}/\overline{u} \leq 0.4$. For the turbulence intensity readings he suggests that

at $\frac{\overline{u'}}{\overline{u}} = 0.2$, the error is less than 1%

at $\frac{\overline{u'}}{\overline{u}} = 0.4$, the error is less than 4%, and

at $\frac{\overline{u'}}{\overline{u}} = 0.7$, the error is about 15%, possibly much less.

The sign of the error is uncertain. Pending the availability of more accurate correction factors, intensity and velocity data were plotted and tabulated as recorded from the instruments. This problem was present only with the very high turbulence levels found within the Rakaia River Gorge itself. Even in the event errors are present, they would be systematic, so that regions where the apparent turbulent intensity is 0.6 are certainly more turbulent than regions where the apparent intensity is 0.5 or 0.4.

Probably more pertinent is the readable accuracy of the various equipment. Mean-velocity-related voltages (and those derived from the Schilknecht micromanometer) could only be judged to within ± 1 to 2%.

The root-mean-square (RMS) voltmeter was generally used with a 10 or 30 second averaging time. A certain variability in the RMS meter reading remained, however, because of the low frequency statistical variations in the turbulence structure. Readable accuracy was judged to be $\pm 2\%$.

The energy spectra from the spectrometer were recorded on a pen recorder. The readable accuracy is affected by the amount of fluctuation in the gear drive which related to averaging time used on the spectrometer. The accuracy on $S(n)$ was generally $\frac{\Delta n S(n)}{n S(n)} = \pm 5\%$ in the region of the peak. With flat peaked spectra, the spectral peak location was uncertain with $\pm 1\text{-}1/3$ octave bandwidth.

The DISA Analogue Correlator produced large reading uncertainties even with the maximum integrating time of 100 sec because of wander in the meter reading. Reading of the correlation coefficient directly off the correlation meter was accurate within $\pm 2\%$ at $R = 0.8$, this uncertainty increased to $\pm 20\%$ at $R = 0.15$, and up to $\pm 100\%$ at $R = 0.02$. Similar accuracies were expected for the X-Y recorder plots produced (Figures 7-4, 7-5 and 7-6).

5.3.3 Pressure-Probe Equipment

A standard Prandtl pitot-static pressure tube was used to set mean tunnel velocity as well as provide a number of vertical velocity profiles upwind of the model. The pressure difference provided by the probe was measured by means of a Schiltknecht Precision liquid micromanometer with $1/10$ mm H_2O divisions. The wind tunnel velocity pressures were always adjusted to within ± 0.2 mm H_2O steady reading before measurements were made. The mean velocity was monitored continuously and measurements were repeated if total head drifted more than 0.3 mm. A free stream mean velocity of $\bar{u} = 13.0$ m/sec was utilized throughout all laboratory velocity and turbulence measurements. To further reduce drift associated with day to day perturbations, all measurements were normalized by the free stream velocity as measured at the top of a given vertical traverse.

The longitudinal static pressure gradient was measured at the side wall flush static taps located approximately at half tunnel height. The variation found was less than ± 0.4 mm of H_2O or equivalent to a 2% variation in mean tunnel velocity. Hence no attempts was made to vary the ceiling height adjustment to remove these small perturbations.

A United Sensor 5 tube Cobra probe (see Figure 5.9) was used to measure pitch and yaw angles as the windflow passed over gorge terrain. This probe also measured mean velocity when adjusted by the appropriate calibration constant. The characteristics of this device are described in some detail in Section 6.3.4, Figure 52, of Bryer and Pankhurst (1971). Because Cobra-probe side tubes are fairly widely separated and sense pressure of only 0.5 dynamic velocity head below total pressure, the accuracy of the device in the presence of a steep velocity gradient is not high. Bryer and Pankhurst suggest accuracies of $\pm 3\%$ in wind speed when pitch and yaw are less than ± 25 degrees and ± 0.01 degrees in angle accuracies when the probe is used without rotation.

In the cases examined herein the probe was rotated around its vertical axis until the two lateral pressure taps indicated zero difference. Yaw angle was read from the pre-calibrated linear potentiometer. Pitch was determined by using the pressure difference between top and bottom tubes and a calibration chart provided by United Sensor with the probe.

Pressures from the Cobra probe were transmitted to a Setra linear pressure transducer via a Scanivalve. The Setra pressure transducer had been pre-calibrated against the Schiltknecht Precision Micromanometer.

5.4 Experimental Program and Procedures

Measurements were made over each of the four model surface textures: terraced, contoured, contoured with yarn shelterbelts, and contoured with pipe cleaner shelterbelts. To obtain the relevant values of mean velocity, longitudinal turbulence intensity, spectra,

or correlation with the hot wire equipment the following procedure was used:

1. Monitor barometric pressure and air temperature,
2. Check out hot wire anemometer circuitry and place wires in operating condition,
3. Calibrate the wire,
4. Place the wire probe on traversing mechanism and locate over the model,
5. Start tunnel and establish proper free stream velocity (13 m/sec),
6. Commence readings of voltmeter and rms meter at a given measurement height,
7. Take a series of measurements above the model until the free stream conditions are obtained,
8. Move to a different location and repeat the measurements, and
9. Recalibrate or re-linearize as necessary because of probe wire drift from thermal effects or contamination.

In the case of mean velocity and longitudinal turbulence intensity, measurements were made at 10 to 15 heights above some 40 sites above the model surface. Most sites were taken in sets of 5 to 6 positions placed on a straight line section perpendicular to the mean flow direction. There were seven measurement sections along the topographical model as well as an approach flow section approximately 2.2 m downwind of the trip fence. Survey points examined and the associated lateral cross sections are shown on Figure 5.10.

Spectra and correlation measurements were made at the upwind section, Section B-B, point 4, and Section D-D, point 3, at heights of $z = 5, 10,$ and 20 mm above the surface. These heights correspond to $z = 25, 50,$ and 100 meters at the field location.

Cobra probe profiles were made at Section G-G, point 3; Section F-F, point 3; point A-A; and Section D-D, point 3. Cobra probe measurements were only made over the contoured model including pipe cleaner shelterbelts.

6.0 EXPERIMENTAL EQUIPMENT AND PROCEDURES FOR FIELD MEASUREMENTS

Field tests required the joint cooperation of up to 13 staff, technicians, and student volunteers. In addition, the New Zealand Department of Fisheries loaned their Jet Boat, Lincoln College provided a 4-wheel drive vehicle, and various staff volunteered transport in private automobiles. When coordination of equipment and personnel is considered, it was extremely fortunate that two suitable testdays with northwesterly winds over the Southern Alps occurred when services were available. A great deal of credit must be given to the good nature and enthusiasm of all those involved.

6.1 Rationale for a Mobile Survey

Measurements of wind velocity and directions were desired over the Rakaia River Gorge test region to provide a basis for validation of laboratory methodology and physical modeling. Ideally a network of permanent meteorological instruments would be installed on multiple towers with data recording equipment versatile enough to intercept and record a northwesterly wind event. The cost of capitalization and maintenance of such a network was prohibitive. Even a small network of equipment such as the Portable Automated Mesonet (PAM) mobile network owned by National Center for Atmosphere Research (NCAR) and described by Cotton and George (1978) and Brock and Govind (1977) costs ~\$6,000 per unit.

An alternative proposal is to place a simple, lightweight cup anemometer on each of several collapsible pole towers and move the towers frequently during a wind event. The effectiveness of such a procedure depends upon spatial correlation of wind velocities over the same 100 square km region, the quasi-stationarity of the wind event

over a 3 to 6 hour period, and the statistical significance of a 15 minute sample at a given point taken once during a 3 to 6 hour recording period.

At first, such constraints might appear overwhelming; however recent statistical analysis of wind data taken simultaneously over separation distances up to 1947 km prepared by Corotis (1976, 1977) provides a good deal of optimism. Corotis (1976) examined hourly data from six towers in northern Illinois and Montana. The report utilized statistical methods and probability models to determine optimal procedures for survey data. Important conclusions for the purposes of this field study are:

- 1) At a given site there are only 2 to 4 statistically independent periods during a day. This suggests an autocorrelation time constant from 3.5 to 7 hours. Thus data taken from the same tower, or a set of towers, erected at a series of nearby stations within a given wind event period may be highly "dependent" or "correlatable" to the character of the wind event.
- 2) Spatial correlation of wind velocities taken from towers separated by various distances in rolling type terrain revealed in the following table.

SPATIAL SEPARATION (km)	MAXIMUM CORRELATION RANGE
	$P_{xy} = \frac{R_{xy}}{\sqrt{R_x} \sqrt{R_y}}$
0	0.780 - 0.923
22	0.757 - 0.832
42	0.712 - 0.816
105	0.632 - 0.745
1947	-0.024 - 0.079

That correlation remains as high as 0.7 over a distance of 100 km suggests that once anemometers are immersed in wind systems of this scale, or larger, wind patterns and velocities at nested sites must be strongly related. Since field sites within the Rakaia Gorge region were never separated by more than 12 km the behavior of the winds at different sites will be highly correlated at a given time or time lag.

- 3) Maximum spatial correlation occurred in almost all cases for zero time lag. This suggests that if wind data is available continuously at one site, data taken irregularly at other sites may be normalized by the reference site to a common measurement time.

Corotis (1977) analyzed data at additional sites in the United States chosen on the basis of their geographical diversity, topographical variation, and uniformly promising wind energy potential. Clusters of sites in northeast Kansas, southeast Wyoming, New England, and Texas were examined for cross correlation. The new sites reinforced conclusions arrived at in the earlier report.

Cross correlations remained high between most sites (See Figure 6.1). An additional separation category of 12-13 km revealed correlations between 0.75 to 0.85. The exception was correlations made between Cheyenne and Laramie, Wyoming. These two sites differ in height by 707 meters and in distance by 75 km. They are separated by the Laramie Mountains, which rise to 576 m between the two cities. Thus correlations remain high between sites in relatively smooth terrain, but care must be used when applying this procedure in mountainous terrain or over terrain where significant features affect the flow of air between locations.

6.2 Portable Towers and Cup Anemometers

The criteria for a field station were light weight, rapid erection, and low cost. Three masts were constructed of 5 cm diameter thin walled aluminum tube. The tubes were made in two 5 meter sections which could be connected via a simple sleeve joint. Three nylon rope ties were attached at 7.5 m to the upper section and when erected the ties attached to three steel stakes driven at convenient distances from the mast base. The three-cup RIMCO anemometers were attached to the top of the mast by a threaded fitting. A 3 lead supply and signal cable led from the anemometer to a power supply and counter module placed at the base of the mast.

The entire system was conveniently light and easy to handle. It could be carried on the luggage rack of a passenger car or in the back of a jet boat. Two or three men could erect the tower in 5 minutes and remove it in somewhat less time (Figure 6.2).

The features of the low torque RIMCO anemometer have been described by Sumner (1968). This three-cup, low-torque anemometer was fitted with a phototransistor electric pulse generator. The electric pulses were amplified and connected to a digital counter. The counter circuitry and portable battery power supply were contained in a water tight munitions box which was portable to the mast base. The box contained reset circuitry and a battery check switch. The cup design is such that starting wind speed is no more than 10 cm/sec, the instrument operates to 25 m/sec wind speed without damage. One pulse is generated for each rotation of the cups and a wind speed of 12 m/sec gives ~ 400 pulses/min. The pulse rate is linear within 1½% over its entire range.

All anemometer cup combinations used were calibrated before and after the field experiments in the University of Canterbury 1.22 x 0.91 meter aerodynamic wind tunnel. This tunnel maintained velocity uniformity within 0.5% over its center section. Each anemometer was mounted at test section center. The Prandtl pitot-static tube used to set the wind tunnel speed was located at the same tunnel section within 0.3 m of the cup anemometer. Each anemometer calibrated as linear within 1.4% over a wind speed range from 5 to 25 m/sec. The calibration constant variation between anemometers was less than 2%. Calibration change before and after the field experiments was not significant.

Wind directions, air temperature, and air pressure were also monitored at each station as necessary by noting wind compass heading, reading a glass thermometer, or reading a barograph respectively (See List of Instruments: Field).

6.3 Stationary Measurement Sites

The New Zealand Wind Energy Task Force (WETF) had erected two 10 m mast measurement sites within the test region. These masts were equipped with pulse counting cup anemometer systems. The count total was normally read once each day by local volunteers. During a test period two team members monitored the accumulated counts every 15 min. One team member also monitored air temperature and air pressure at 15-min intervals. Each installation was calibrated against the mobile masts by taking simultaneous measurements while the two masts were separated by distances less than 10 m.

The two sites were

- a. Rakaia Gorge Site - Map Coordinates S55/131/584/S93 or Site 15 this survey, and
- b. Mt. Hutt Site - Map Coordinates S55/105/572/S82 or Site 13 this survey.

The Mt. Hutt site stood on an exposed hill with no immediate vegetation, shelterbelts, or other topography in any direction. The Rakaia Gorge site had a clean view up the river gorge; however the terrain rose abruptly including tree vegetation some 100 m to the south.

During the two test days November 25, 1977, and December 29, 1977, continuous data was available from at least one site; however, equipment malfunctions resulted in only partial data from the alternate site. Fortunately, sufficient data are available to calibrate the sites against one another.

6.4 Team Procedures and Field Test Matrix

The Rakaia River Gorge Area was surveyed simultaneously by three teams, each equipped with portable mast, anemometer, compass, thermometer, etc. Team 1 dropped off the Mt. Hutt and Rakaia Gorge monitors and proceeded to survey sites on the south side of the gorge. The survey began at the east end of the area and proceeded west. Team 2 used a Hamilton Jet Boat to traverse the length of the River Gorge from east to west. Team 3 remained on the north side of the gorge and also moved westward from site to site. Twenty-seven separate sites were surveyed in a period of about 6 hours. Continuous measurements every 15 min were obtained at Rakaia Gorge and Mt. Hutt stations.

Sites were selected on the basis of distribution, exposure, ease of access, absence of severe shelterbelt or topographical sheltering, and time. If possible, sites were chosen at an equivalent model measurement section or station. Figures 7-50 and 7-51 summarize measurement stations for the two field dates. Sites 13, 17, and 36 required hand transportation of equipment to an elevated point; however the favorable exposure was worth extra effort in each case. Comments concerning exposure at each site are arranged in the accompanying Table 6-1.

Each team operated in the following manner:

1. Team traveled to pre-selected measurement site;
2. Portable mast and anemometer were erected at a spot with minimal upwind shelter;
3. A 15 minute count was taken from RIMCO anemometer, and time was noted before and after count;
4. Wind direction was noted by means of compass and map;
5. Temperature was recorded;
6. Site characteristics and comments were recorded;
7. Portable mast was taken down and stored on vehicle; and
8. Team proceeded to next site.

Including travel time, mast erection, measurement period, and mast removal, each site required an average period of 30-45 min.

6.5 Synoptic Meteorology on Field Test Dates

The geology and micrometeorology of the Rakaia River Gorge region has been described in Section 3.1, 3.2, and 3.4. Two days were finally selected to make field measurements: November 25 and December 29, 1977. In each case an extended period of high winds from the northwest were predicted by the New Zealand Meteorological Service based on weather data gathered from Australia, over the Tasman Sea, and satellite weather photographs.

November 25, 1977:

On November 24, an anticyclone present to the west of New Zealand was moving east and north. Northerlies and northwesterlies predominated over the west coast areas of the southern island. On November 25 a disturbed southwesterly was expected to move in to cover most of New Zealand; however, an early morning forecast suggested that northwesterlies would persist until late afternoon. The noon forecast provided by the New Zealand Meteorological Service appeared as shown in Figure 6.3.

In the Rakaia Gorge area, moderate northwesterlies existed from early morning until past noon with small variation. After noon a slow drop off in wind speed occurred. At 13:45 wind died. A half hour later southwesterlies appeared over the region. The sky was overcast most of the day.

December 28, 1977:

On December 28 an anticyclone existed over the Chatham Islands moving east. It drew after it a strong northerly flow over the Tasman Sea which also moved east. Northerlies predominated over the west coast areas turning to northwesterlies as they passed over the mountains. On December 29, a low developed between Australia and New Zealand which continued to draw northerlies onto the South Island. A ridge of high pressure extended onto the North Island from the southeast. A trough over the Tasman Sea was moving rather slowly eastward. The noon forecast provided by the New Zealand Meteorological Service appeared as shown in Figure 6.4.

In the Rakaia River Gorge area, strong northwesterlies existed from early morning until late afternoon with little variation. The sky was generally overcast with some rain on the mountain ridges. A large amount of dust was generated by winds blowing over the upwind, graveled, braided riverbed.

7.0 EXPERIMENTAL RESULTS

7.1 Results of Wind Tunnel Measurements

7.1.1 Approach Flow Field Characteristics

The wind tunnel entrance section was equipped with a square bar grid and a solid sharp edged fence 2.5 cm high. The first 3.66 m of the floor surface before the Rakaia Gorge model was covered with sheets of expanded bead polystyrene to provide a roughness texture.

The character of the approach flow shear layer was monitored at a distance 3.3 m downwind of the fence (0.36 m upwind of first topography). Velocity and turbulence profiles are obtained at eight lateral positions. The honeycomb grid fence combination provided extremely uniform flow with no noticeable lateral variations at this section.

The velocity profile had a power law exponent from 0.13-0.14 which fit the data to equivalent heights of 250 to 500 meters.

The semi log profile $\frac{\bar{u}}{u_*} = \frac{1}{k} \ln \frac{z}{z_0}$ fit the profile from equivalent heights of 10 m to 200 m when equivalent $z_0 = 0.045$ m, $\frac{u_*}{u_\delta} = 0.043$

and $k \equiv 0.40$. Resultant skin friction coefficients are $\frac{C_f}{2} = \left(\frac{u_*}{u_\delta}\right)^2 = 0.0019$

or $C_{f_{10}} = 2 \left(\frac{u_*}{u_{10m}}\right)^2 = 0.0108$. Local longitudinal turbulence intensities

at the surface were 0.14-0.15 at $z = 25$ m.

Point spectra (Figures 7.2 and 7.3) and correlations (Figures 7.4 to 7.6) were obtained at $z = 25$ and 100 m at tunnel centerline.

Integral scales were estimated from the spectral peak:

$$L_{u_x \text{ spec}} = \frac{0.146}{kp} = 0.146 \frac{\bar{u}}{n}, \quad (7.1)$$

from the area under the correlation curve:

$$L_{u_x \text{ corr}} = \bar{u} \int_0^{\infty} R(\tau) d\tau, \quad (7.2)$$

or from the integral time scale estimated from $T_E @ R = \frac{1}{e}$,

$$L_{u_x \frac{1}{e}} = T_E \left(R = \frac{1}{e} \right) \bar{u}. \quad (7.3)$$

Values range from 453 to 890 m depending upon the method selected (Table 7.1)*.

The spectral shape does not clearly indicate a single length scale ratio in Figure 7.1. Superimposed on the graph is the generalized spectra according to Harris (1971) for length scale ratios of 1000 and 5000 for flow over homogeneous flat terrain. Only a portion of the large-scale eddies injected by the bar grid have been redistributed to smaller scales by the fence and roughness. Between this roughness section and the majority of flow measurements lie 1.50 m of additional model topography. Spectra taken downwind above Section D-D Point 3 match the Harris spectra quite well, which suggests that local roughness dominates the spectra at that point (see Figures 7.2 and 7.3).

* Teunissen (1978) has observed that similar uncertainties exist in a given set of field data.

The values discussed above compare quite favorably with the range projected from the review provided by Counihan (1975) as noted in Section 3.4.

<u>Parameter</u>	<u>Section 3.4</u>	<u>Measured Approach Flow</u>
α	0.14	0.13-0.14
z_o	5 cm	4.5 cm
$\overline{u'}/\overline{u}$	0.14	0.14-0.15
$\overline{u'w'}/\overline{u}_\delta$	0.00197	0.0019
δ	600-1000 m	~ 500 m
L_{u_x} @ 50 m	300-1000 m	~ 600 m

7.1.2 Flow Visualization and Trajectory Results

Flow visualization using miniature flags and polystyrene beads was performed to determine flow direction at ground level, regions of turbulence, and regions of separation or low velocity. Procedures are discussed in Section 5.3.1. These results were used to select locations for laboratory and field measurements of velocity and turbulence.

Terraced Model

In general the flags aligned with the general contour lines of the topography as shown in Figure 7-7. As the river valley narrowed into the river gorge at Section B-B streamlines were deflected to the south as the ground level flow followed the river bed. There was extensive evidence in flag flapping just upwind of the cliffs at G-G 3 or downwind of the ridge at G-G 1 and 2 of flow separation, recirculation and turbulence. As the gorge narrowed further at Section C-C only a

small volume of the fluid entered the gorge while most of the airstream lifted up and over the terrain. Wind along the river gorge between Sections C-C and D-D follows the gorge centerline causing the air to zig and zag around the river bends while the air above the gorge cliffs is deflected only slightly from a northwest-southwest trajectory. At Section E-E there is evidence of separation and recirculation behind the cliffs on either side of the north and south banks of the Rakaia River gorge. Where no flags are shown in Figure 7-7, the small perturbations the along wind-tunnel axis were not considered significant enough to incorporate on the sketch.

Polystyrene beads drifted into low wind regions during the visualization experiment. The rapid accumulation of polystyrene beads in the narrow sections of the gorge strongly suggested that highest winds were not to be expected in these regions (Figure 7- 8). Despite "fisherman" lore to the contrary, the river gorge retained deposited beads until winds were increased to quite large values. Indeed given a large supply of beads the model gorge filled to its upper lip at lowest drift velocities. Beads also collected in separation regions downwind of ridges, hills, and in lateral stream gullies. Individual particles tended to stream along the gorge centerline at all wind speeds. For the terraced model the sharp change in elevation at the edge of each terrace produced a local quiescent area where beads would often catch or accumulate on the rough textured surface. Thus, flow in the terraced gorge was at a lower velocity and more turbulent than its contoured counterpart model.

Contoured Model: Pipe Cleaner Shelterbelts

The miniature flag behavior on the contoured model varied only to a slight degree from that for the terraced model (Figure 7-26).

Since the effective roughness on steep slopes was less over the smoothed contours, velocities were higher and turbulence was lower in the gorge. Nevertheless, wind direction down the gorge followed the gorge center line, veering around bends and cliffs as the gorge zigged or zagged. Regions of variant winds and high turbulence were similar to those noted over the terraced model.

Surprisingly bead deposition was more extensive in the gorge for the contoured model. As velocities increased, however, the gorge cleared quickly except for a few persistently sluggish regions between Sections D-D and F-F (Figure 7-27). Any accumulation of beads was absent behind individual terraces at the higher elevations noted initially over the terraced model.

7.1.3 Flow Field Results - Terraced Model Configuration

Vertical traverses of mean velocity and longitudinal turbulent intensity have been measured at seven cross wind sections or 40 stations. Measuring equipment and procedures used were discussed in Section 5.3.2. Data have been listed as \bar{u}/\bar{u}_g and \bar{u}'/\bar{u} in

Table 7- 2. Iso-contour lines of the vertical variation of constant velocity or turbulence intensity have been prepared for each section in Figure 7.12 through Figure 7.25. Iso-contour lines of the horizontal variation of velocity at 10 m, 25 m, and 50 m above the ground surface are displayed in Figures 7- 9, 7-10, and 7-11.

Upwind Section B-B displays the first region where significant perturbations of the uniform approach flow occurs. Velocities at riverbed level decrease while flow over the ridge at 1500 m north of the south model boundary increases to a magnitude of 0.80. Local

turbulent intensities over the ridge decrease in the same area as velocity increases. Turbulence intensities at gorge level are less than normal; consequently, turbulence increases as the wind moves down the gorge.

In Section G-G the riverbed develops a wide bend downwind of the ridge observed at Section B-B. In the separated region winds drop to 20% of the gradient velocity; whereas, turbulent intensity increases to 55% near the ground. On the top of Fighting Hill, wind speedup produced model maximum wind speeds of 99% gradient wind. Locally turbulent intensity falls to a minimum of 10%. This section developed the maximum range of wind conditions observed over the entire model; the values provide a demonstration of the importance and magnitude of terrain resistance as well as enhancement. In a distance of little more than two miles (3 km) the ratio of power available from the wind varies by a ratio of 100 to 1. Thus in complex terrain, climatological data from a single station may be clearly inadequate or misrepresentative.

Wind accelerates over the flat wide riverbed between Sections G-G and C-C while the turbulence associated with separation over the ridge dissipates. Between Section C-C and Section F-F the river enters the narrowest part of the Rakaia Gorge. Most of the air rises above the gorge; air velocities in the gorge drop to less than 30% while local turbulence intensity rises to 30%. The surface on either side of the gorge becomes relatively flat, sheep pasture only interrupted by occasional shelterbelt. Wind profiles approach shapes typical of homogeneous terrain.

At Section D-D velocity contours are plotted with reference to both the actual terrain shape as well as the model terraced configuration. Although slight variations appear in the iso-contours, there is no significant departure. Downwind of this Section the river broadens into a flat plain. Maximum turbulent intensity occurs above the ground as a result of separation and shear associated with upwind ridges. This elevated turbulence maximum also is evident at Section E-E downwind; however most turbulence excess has dissipated and only a small residue of the signature remains.

Longitudinal velocity turbulent spectra and correlation were measured at upwind locations and at Section D-D Number 3 as noted in earlier discussion (Section 5.3). Figure 7-2 compared the normalized spectral energy variation with wave number against the universal correlation suggested by Harris (1971). Clearly turbulent energy is distributed over different sizes in a manner consistent with previous atmospheric experience for equivalent roughness and stability conditions. The spectral peak suggests an integral scale $L_{u_x} \approx 150$ m which is also consistent with 25 m height values proposed by Counihan (1975) and Panofsky (1977). The complex gorge terrain has completed the energy redistribution begun by surface roughness as the wind moves downwind from the fence and bar grid representing the mountain range farther upwind.

Correlation measurements obtained at the same location displayed in Figure 7.5 indicate the expected exponential decay. Note, however,

that longitudinal integral scales evaluated by two different methods from the correlation exceed by a great deal spectral estimates by separate equipment. Teunissen (1978) comments such disparity is common during full scale atmospheric measurements; while Raine (1974) found a similar variation during laboratory measurements. Table 7-1 summarizes the values calculated by three different methods at vertical heights of 25, 50, and 100 m. Integral scale tends to increase with height as expected.

Horizontal iso-contours have been prepared from the vertical profile measurements at horizontal sections taken conformally at 10, 25 and 50 m above the ground surface. A sequential examination of Figures 7- 9, 7-10, and 7-11 emphasizes the shelter provided by the gorge and the speedup developed over Fighting Hill and the small knob at Section B-B Number 2. Complex terrain may produce very rapid horizontal variations in the flow structure. Neither the high wind speeds found above the small knob nor their rapid variation in the horizontal would have been obvious from a casual examination of a topographical map. On the other hand, high wind speeds above Fighting Hill were expected and low wind speeds within the Rakaia Gorge were suspected.

As one moves to the higher elevations above the ground at 50 or 100 m the influence of local surface irregularities become less significant. Windmill hub heights of 50 to 100 m may thus carry blades which are subjected to relatively small lateral wind shear when placed above moderately rough terrain.

7.1.4 Flow Field Results - Contoured Model - Alternate Roughness Configuration

A series of measurements were made over the contoured model of the Rakaia Gorge with and without the addition of shelterbelts (Table 7.4). Figures 7-40 through 7-45 provide a comparison of smooth, 20% permeable, and dense shelterbelt configurations. The contoured model without shelterbelt did not develop as much surface drag as the terraced model. Surface profiles of velocity had smaller, power law coefficients, and surface intensities were less. Velocities in the gorge were up to 100% greater than values found over the terraced model. Since shelterbelts in the prototype area were numerous and mature, this model configuration was not considered to be similar but was examined to evaluate the comparative effect of shelterbelt addition.

As noted in Section 5.2, two model shelterbelt designs were evaluated. The influence of 4 mm diameter yarn at Section F-F is displayed in Figures 7-42 and 7-43. Velocities are less than those measured over the terraced model; however, the influence of the yarn on wind profile is significant. Directly over the shelterbelts, intense shear gradients occur such as were observed by Sturrock (1972) and Raine (1974). The higher velocities found within the gorge are probably more realistic than those found over the terraced model which provided exaggerated roughness and separation at the gorge walls.

Finally, Figures 7-44 and 7-45 examine the effects of 4 mm pipe cleaner model shelterbelts. Velocities are somewhat less in the gorge whereas turbulence intensity increases above values developed by the yarn. There appeared to be little difference between the qualitative appearance of the two shelterbelt configurations. A decision was

made to develop a complete set of measurements over the pipe cleaner shelterbelt configuration.

7.1.5 Flow Field Results - Contoured Model Configuration - Pipe Cleaner Shelterbelts

While the model surface alone has an effective roughness of 4.5 cm, the shelterbelts represent 20 m mature tree stands. As noted in Section 5.2, the pipe cleaners appear to simulate the flow effects of large shelterbelts well. Indeed, hot-wire measurements at 10 m heights when taken near the model shelterbelts depict the confusing variation found in the field when measurements are made in the lee of obstacles (Table 7.3). To help interpret such measurements, sketches of upwind shelterbelt location are included on the vertical sections shown in Figures 7-34 to 7-49. Often the shelterbelts are some distance upwind but their influence on the iso-contours is obvious.

Considering the difference in model texture, the terraced model and contoured model results are quite similar. Scanning Figures 7-12 to 7-25 and comparing contours against Figures 7-34 to 7-49 indicates the following perturbations:

1. Wind velocities within the gorge are slightly greater over the contoured model;
2. Longitudinal turbulence intensities within the gorge are generally slightly less over the contoured model;
3. Wind velocities at shelterbelt height are generally slightly lower over the vegetated regions of the contoured model;
4. Longitudinal turbulent intensity above vegetated areas are about 20% over the contoured model as opposed to 15% above similar terraced model locations;
5. Shear layer depth is about the same over both models; and
6. Separation regions are not as large or intense over the contoured model.

Horizontal section velocity contours were also prepared for the contoured model as shown in Figures 7-28 and 7-29. At the 10 m height there are large regions associated with shelterbelt effects where local velocity variations resulted from shelterbelt shadow and not topographical distortion. These unshaded regions encountered winds varying from 0 to 50% of the gradient value. Again those regions where velocity was high or low over the terraced model are the same over the contoured model. Windspeed ratios, \bar{u}/\bar{u}_g , over Fighting Hill and the Section B-B knob exceed values of 1.0 and 0.85 respectively. Favorable sites for windmills are not at the base of a gorge or river channel where hypothetical venturi-like speedup occurs but on top of nearby hills or ridges where velocities approximate gradient wind values. At the 50 m level both shelterbelt and terrain influences blur so that similar velocity magnitudes exist over most of the region. Nonetheless, gorge low values and hill high values persist.

Longitudinal energy spectra and correlations were also examined at Section D-D Number 3 above the contoured model terrain. Although a spectral peak appears near that of the Harris algorithm not all large scale eddy energy has been redistributed to smaller scales by surface roughness. Thus, the net effect of a contoured surface with shelterbelts would be to produce less surface drag and separation than its terraced counterpart. Although the spectral peaks suggest integral scales a bit smaller for the contoured model, the auto-correlation results yield larger values which suggests that significant energy still resides at larger scales. Since almost no consistent field data exists concerning spectra and integral scale variation in complex terrain, the best conjecture is to project what eddy distribution is most

similar to the atmospheric case and appeal to other specific field measurements at the site for model verification.

Measurements of wind pitch and yaw around river bends and over gorge outcroppings or ridges were made at selected points along the Rakaia Gorge. The cobra probe concept is discussed in Section 5.3.3. Stations examined by the cobra probe are noted on Figure 7-26. A series of four figures have been prepared to display the tendency of surface winds to follow contour lines and terrain channeling. Figure 7-30 presents a profile measured immediately upwind on a steep gorge bluff at Section G-G, Number 3. At the surface, the cobra probe yaw angle agrees with that displayed by a miniature flag. Both yaw and pitch perturbations disappear at the elevation of the gorge lip. Winds align with the tunnel centerline above this height.

Figures 7-31 through 7-33 were each taken immediately downwind of a bluff or ridge. Again wind yaw agrees with flag angles, and wind perturbations are small above the gorge lip. Maximum yaw angles measured were near $+30^{\circ}$; maximum pitch angles did not exceed $+20^{\circ}$. At Section D-D, Number 3, pitch was essentially absent; however, yaw up to 15° existed as the wind blows out of the gorge.

7.2 Results of Field Measurements

Field measurements consisted of wind speed and direction measurements at as many as 27 sites distributed over a 100 square kilometer region on two separate test days. These days were one month apart and represented flows caused by completely separate weather systems; hence, results are statistically independent. The method chosen to normalize data taken from various sites during the time span of

several hours will be discussed in the following section, followed by a description of each day's measurements.

7.2.1 Normalization Procedures

During the time when mobile tower teams were examining sites in the Rakaia Gorge area, measurements were made every 15 min at two Wind Energy Task Force stations. The station with the most consistent data and regular performance was selected to normalize the mobile tower values to a common time.

The procedure chosen to prepare velocity magnitudes suitable for comparison with model results was:

1. Recorded count/minute values registered by the RIMCO cup anemometers were converted to meter/sec values via the prepared calibration curves;
2. Wind speeds were adjusted to equivalent 12:00 Noon values by the following algorithm:

$$\frac{\bar{u}_{\text{RIMCO}}}{12:00 \text{ Noon}} = \frac{\bar{u}_{\text{RIMCO}}}{@ \text{Time } t} \times \frac{\bar{u}_{\text{WETF TOWER @ 12:00 Noon}}}{\bar{u}_{\text{WETF TOWER @ Time } t}} ;$$

3. A gradient wind speed was estimated by assuming the \bar{u}/\bar{u}_δ value measured over the model was correct for the WETF tower site. Values used were:

Terraced Model:

$$\frac{\bar{u}}{\bar{u}_\delta} \Bigg|_{10 \text{ m}} = 0.50$$

Mt. Hutt

Contoured Model:

$$\frac{\bar{u}}{\bar{u}_\delta} \Bigg|_{10 \text{ m}} = 0.50$$

$$\frac{\bar{u}}{\bar{u}_\delta} \Bigg|_{10 \text{ m}} = 0.43$$

Rakaia
Gorge

$$= 0.61$$

Probable gradient wind speeds for

November 25, 1977, was $\bar{u}_\delta = 16.3$ m/sec and for

December 28, 1977, was $\bar{u}_\delta = 23.4$ m/sec; and

4. Wind speeds were converted to a velocity ratio by division of the time corrected RIMCO reading by the proposed gradient wind speed, i.e.,

$$\frac{\bar{u}}{\bar{u}_\delta} \Bigg|_{\substack{10 \text{ m} \\ \text{field} \\ \text{value}}} = \frac{\bar{u}_{\text{RIMCO @ Time T}}}{\bar{u}_\delta @ \text{Time T}} .$$

The empirical nature of this approach sacrifices one site to calibrate the model to field configuration, but it does permit an economically feasible field measurement program. Rationale for this approach to a mobile survey is discussed in Section 6.1.

7.2.2 Field Test Day - November 25, 1977

Synoptic conditions which existed on this day over the South Island, New Zealand, and the resultant wind flow over the Southern Alps is detailed in Section 6.5. Surface wind speeds to levels of 12 m/sec existed over the Rakaia Gorge area. Winds prevailed from the northwest until 1300 hours when the winds dropped abruptly and eventually swung around to the east. Because of this change, measurements made after 1300 hours have been discounted as to value. Wind speeds at the Rakaia Gorge Wind Energy Task Force (WETF) station did remain at levels near 8 to 10 m/sec for the four morning hours.

Table 7-5 presents RIMCO count rate, resultant wind speed, time adjusted wind speed, and gradient wind normalized speed fraction. They are tabulated versus their actual acquisition period and the normalization WETF station results. Over the four hour morning period wind speeds at the Rakaia Gorge were 82% of the Mt. Hutt values $\pm 20\%$. The Rakaia Gorge WETF anemometer developed speeds only 77% of the calibrated anemometer at the same site; whereas, the Mt. Hutt anemometer developed speeds near 84% of the calibrated RIMCO anemometer at the same site.

As the data indicates, the anemometer system used by the north bank team failed after only two stations; hence, most data are for the southern river bank drive and the river bottom. In addition the measurement series did not begin at the Mt. Hutt WETF site until 10:15 because of instrument irregularities. Nonetheless, the Rakaia Gorge WETF anemometer was sampled over the entire period required on this test date.

Wind directions at sites examined are superimposed on a topographical map as part of Figure 7-50.

7.2.3 Field Test Date - December 28, 1977

Synoptic conditions for December 28, 1977, are discussed in Section 6.5. Surface wind speeds to 23 m/sec were recorded near ground level. Winds prevailed from the northwest over the entire measurement period from 0930 until 1500. Wind speeds at the Mt. Hutt WETF station remained at levels between 9 and 18 m/sec over the entire time studied.

Table 7-6 presents RIMCO count rates, resultant wind speed, time adjusted wind speed, and gradient wind normalized speed fraction. They are tabulated versus their actual acquisition period and the normalization WETF station results. In this case the Rakaia Gorge WETF was not operational during the measurement series, whereas the Mt. Hutt WETF station operated without fault. All three mobile anemometer rigs operated successfully throughout the day; hence, all stations selected were sampled.

Wind directions measured at sites examined are superimposed on a topographical map as part of Figure 7-51.

8.0 COMPARISON OF LABORATORY AND FIELD EXPERIMENT RESULTS

Because physical modeling is intended for use in applied meteorology, actual data sets from a mountain valley mesoscale study were chosen to validate the wind field estimates. Field measurements of wind velocity at $z = 10\text{m}$ and direction at $z = 2\text{m}$ were made at 27 locations on two separate days involving strong northwesterlies over the Southern Alps. Laboratory measurements were made at the equivalent points over a 1/5000 scale model or they were extrapolated horizontally from nearby measurement locations. A summary has been prepared of the comparable wind velocity data in Table 8-1.

It is instructive to consider comparable numerical and physical model verification results by other researchers. A thorough search of the literature reveals that few authors have chosen to compare field and model results in other than qualitative terms. Indeed in many cases the accuracy of flow field replication is judged on the basis of the ability to predict the dispersion of some scalar such as silver iodide (Orgill et al. (1971b)) or different air pollution indicators such as Ozone, NO, CO, etc. (Duewer et al. (1978)).

Unfortunately, the prediction of scalar transport includes other uncertainties than those associated with errors in mean velocity, direction, or turbulence. These include photochemical effects, sinks, sources, deposition, etc. Indeed scatter diagrams such as are provided by Duewer et al. (1978) suggest correlations much less than 0.5 in several instances. Although a number of programs are now

underway to directly evaluate various mesoscale numerical models with exhaustive field data sets (Hardy (1978), Fosberg (1978), Cotton (1978)), none of these results are immediately available.

Recently Fosberg et al. (1976) developed a single layer model that includes terrain, thermally, and frictionally induced perturbations. This model is more complex than some simple mass consistent models; yet, it is less expensive to run than full primitive equation models. Seven data sets were used in the model validation. Six came from studies conducted in the Oregon Cascade Mountains. One data set came from central California. All seven depict daytime conditions: five for midafternoon, and two for morning. One morning case occurred under overcast skies and rain. The other six occurred with strong solar heating. Background winds ranged from 2 to 5 m/sec. The Oregon winds were calculated on a 6 km square grid, the California case on a 16 km square grid. Air temperatures were extrapolated to grid points from the field network weather stations.

Evaluation of the errors in both wind speed (Figure 8-1) and wind direction (Figure 8-2) demonstrates the utility of the model. The root mean square (rms) wind speed error was 2.0 m/sec. Forty-five percent of the calculated wind speeds fell within 1 m/sec of the observed wind, and 75 percent fell within 2 m/sec. These comparisons were made over an observed range of 0.5 to 10.5 m per second. For 51 data points the sample correlation coefficient is $r = 0.60$. Observed wind directions were reported on a 16-point compass basis. Therefore, the error analysis is presented as a compass-point error rather than a more precise evaluation of angle. The rms direction error was 1.9 points. Sixty percent of the calculated directions fell within 1 compass point of

the observed direction, and 92 percent fell within a 2-point envelope of the observed direction. Observed directions were from all compass points except for the east and northeast sections. For 43 data points the sample correlation coefficients among angles is $r = 0.62$.

The limited results discussed above may be used as a context within which to judge the efficacy of the present physical model. These results are not intended for criticism or to be used as a standard, but rather a statement of reasonably current alternative modeling capabilities.

8.1 Correlation of Wind Velocity Magnitudes

Each field data set has been compared separately against measurements made over the terraced model, the contoured model including pipe cleaner shelterbelts, and each other. Correlations and scatter diagrams have been prepared for each case.

If physical modeling is expected to be a useful means to predict wind speed, wind power, and airflow directions there must be a high linear causal relationship between measurements in the laboratory and field. The best estimate of the population correlation coefficient is the sample correlation coefficient commonly calculated as

$$r = \frac{n\sum xy - \sum x \sum y}{\left[[n\sum x^2 - (\sum x)^2] \right] \left[[n\sum y^2 - (\sum y)^2] \right]} \quad (8.1)$$

The correlation coefficient always lies between -1 and +1. If, and only if, all points lie on the regression line, then $r = \pm 1$. If $r = 0$, the regression line does not explain anything about the variation of y .

If it is assumed that there are only two variables of interest, an "independent" variable x , and a "dependent" variable y , then the equation of the sample regression line of y on x is:

$$y' = a + bx . \quad (8.2)$$

In a case where observations of x (laboratory measurements) also involve measurement error in addition to inherent variability, it is instructive to construct the equation of the sample regression line of x on y as:

$$x' = a + by . \quad (8.3)$$

When $r = \pm 1$ these lines will be co-linear; when $r = 0$ the lines will be perpendicular. Plotted on a scatter diagram, the lines provide visual evidence of the quality of correlation. Note that coefficients a and b are defined in the normal "least squares" manner for a two variable linear regression; that is;

$$\begin{aligned} b &= \frac{n\sum xy - \sum x \sum y}{n\sum x^2 - (\sum x)^2} \\ a &= \frac{\sum y - b\sum x}{n} . \end{aligned} \quad (8.4)$$

For each case, the null hypothesis that the slope of the true regression line has the value $B = 1.0$ was tested by considering

whether $|t|$ where

$$t = \frac{b-B}{s_b} , \quad (8.5)$$

when

$$s_b = \frac{sy/x}{sx\sqrt{n-1}} ,$$

$$s_x^2 = \frac{1}{(n-1)n} [n\sum x^2 - (\sum x)^2] ,$$

$$s_{y/x}^2 = \frac{n-1}{n-2} (s_y^2 - b^2 s_x^2) ,$$

exceeds the critical value $t_{\alpha/2, n-2}$ for $P(t) = \alpha/2$ and $f = n-2$ degrees of freedom (See Crow et al. (1960)).

The significance of the sample correlation coefficient r may be specified for each data set. If the computed $|r|$ exceeds the critical value, we reject at a 1% level of significance the null hypothesis that the population of x 's and y 's has zero correlation. We will also specify a confidence interval for the true (population) correlation coefficient ρ . In 95% of the experiments the interval so constructed contains ρ .

In practice, close prediction of an individual y (wind speed) is of more interest than the mean value of a regression line. The individual value of y corresponding to a given $x = x$ for a (100) $(1-\alpha)\%$ prediction interval for y is:

$$y' \pm t_{\alpha/2, n-2} s_{y/x} \sqrt{1 + \frac{1}{n} + \frac{(x-\bar{x})^2}{(n-1)s_x^2}} . \quad (8.6)$$

Example: Eighty percent prediction interval for a single observation y at $x = 0.5$ from Figure 8-7 (December 28, 1977, Field Test versus Contoured Model) is:

$$\begin{aligned} \left(\frac{\bar{u}'}{u_{\delta}'}\right)_{\text{Field}} &= -.013 + 1.20 (0.5) \pm 0.165 \\ &= 0.422 \text{ to } 0.752 , \end{aligned}$$

Figures 8-3 through 8-7 present scatter diagrams of field versus model measurements. The sample correlation coefficient, r , between the two field days--November 25 and December 25, 1977--is 0.68. Since these two days appeared to the authors to have similar boundary conditions, the same physical model or boundary driven numerical model was used to predict either date. The fact that measurements, nonetheless, vary to $r = 0.68$ suggest that inherent prediction limitations exist to any physical or numerical modeling approach. (Assuming, of course, the variations are not due to measurement or data reduction inaccuracies.)

Figures 8-4 to 8-7 present laboratory results. The terraced model to field-data correlation coefficients range from 0.70 to 0.78. Correlation coefficients for the contoured model to field data range from 0.68 to 0.76. The null hypothesis that correlation is actually zero may not be accepted even with a 1% level of confidence. The null hypothesis that the true slope is 1.0 can not be rejected without a 5%, 36%, 44%, or 36% chance of error in each case.

Other measures of the level of significance of such a comparison are summarized in Table 8-2. Calculations follow the earlier discussion of this section. It is felt that the contoured model with shelterbelts provides a more accurate picture of flow over the Rakaia area. Comparing this model with November 25 field data revealed that 43% of the model measurements for a measured wind speed range of 5 to 8.5 m/sec were within 1 m/sec of the field data, and 86% were within 2 m/sec of the field data. When considering the December 28 field data 38% of the model measurements for a measured wind speed range of 6 to 28 m/sec were within 1 m/sec of the field data, and 54% were within 2 m/sec of the field data.

8.2 Ranking Wind Stations by Wind Speed

Individual meteorological measurements are frequently characterized by extremes in magnitude about the actual mean as large eddies sweep across the terrain. Such large eddies are not modeled in a boundary layer wind tunnel. Hence, an alternative way to consider field data to physical model correlation would be to correlate station rank when both sets of data are ordered according to relative wind speed magnitude. Correlation by rank may be calculated by

$$r = 1 - \frac{6 \sum_{i=1}^n D_i^2}{n(n^2 - 1)} \quad (8.7)$$

where $D_i = \text{Rank}_{\text{field station}} - \text{Rank}_{\text{model station}}$.

Tables 8-3 and 8-4 provide a wind velocity rank test for the Rakaia Gorge data. As noted November 25 data correlates with the contoured model as $r = 0.95$; whereas the December 28 data correlates with the contoured model as $r = 0.78$. This improved correlation is gratifying and suggests that the addition of roughness elements such as shelterbelts may be critical to accurate local simulation.

One prospective role for physical modeling in the array of techniques used for WECS siting would be to rank sites considered as good or not so good. The high correlation found during the rank test discussed above should provide credibility when physical modeling is used to sort WECS sites.

8.3 Correlation of Wind Direction

Wind direction at each field site was estimated at eye level by a member of each team using a hand-held compass and the fluctuations of a small flag or the wind pressure variation on the team member's face. This crude wind vane indication has been compared with sketches of miniature wind vane deflection over each model. Table 8-5 considers the relative angle variations for each day and each model. As expected correlations are somewhat low, 0.65 to 0.67; however, one may still reject the null hypothesis that $r_{\text{field/model}} \equiv 0.0$.

Again the correlation of wind-speed angles between the two field days is strikingly low, $r = 0.47$. Can the physical model be expected to perform too much better than field data taken at the same sites under apparently identical situations?

8.4 Comparison Against Generic Hill Studies

Two sites in the Rakaia Gorge area are on the crest of ridges or hills which have a reasonably uninterrupted approach windflow. Site B-2 is on a knob topping a ridge of land which extends to the north causing a major bend in the Rakaia River before it enters the gorge. Site G-6 is on top of Fighting Hill, a large hill on the north side of the river which stands alone. Since both land features have only a small elevation change for at least 300 m perpendicular to the flow field, the width-to-height ratio is greater than 3.5 and the topography behaves as 2-dimensional ridges. Along the wind sections of each ridge are displayed on Figure 8-8 together with other scale ratios.

Figure 8-9 displays the vertical variation of the fractional speedup factor (ΔS), defined here as

$$\Delta S = \frac{\bar{u}(z)_{\text{crest}} - \bar{u}(z)_{\text{approach flow}}}{\bar{u}(z)_{\text{approach flow}}}$$

The 10 m value associated with December 28 data taken at B-2 varies depending on whether Site H-1 or H-2 is chosen as an upwind reference velocity.

Since the hill half-width to longitudinal integral scale ratio, L/L_{u_x} , is less than one for both cases, these results may be compared with generic hill studies performed by Meroney et al. (1976, 1977) or the numerical results of a "frozen vorticity" solution such as Derickson and Meroney (1977). Measurements from a comparable triangular hill case where $h/L = 0.33$ and 0.5 are overlaid on Figure 8-9.

Finally within an inner layer (ℓ), close to the hill surface, the perturbation solution of Jackson and Hunt (1975) suggests a simple approximation

$$\Delta S \approx 2.0 \frac{h}{L} \quad (8.9)$$

For these cases, $\ell \sim 20$ m; hence, a predicted value of ΔS has been associated with $z = 10$ m in each case.

All values plotted for Site G-6 appear consistent; this site would make an excellent WECS location. Field measurements at Site B-2 agree approximately with previous analytic and wind tunnel results; however, the pertinent Rakaia model results underpredict the field behavior. Perhaps some feature of the back slope has caused separation in the model case resulting in larger effective L than the topography suggests; nonetheless, Site B-2 would also make a good WECS location.

9.0 CONCLUSIONS AND RECOMMENDATIONS

Seven objectives of this research program were outlined in Section 1.2. Each of these will be discussed sequentially in order to draw final conclusions concerning the implications of this experiment for WECS siting procedures.

9.1 Implications of Experiment With Respect to WECS Siting Procedures

The first objective was to determine the full capacity for laboratory simulation of airflow over complex terrain at large scale ratios. A review of the literature revealed some 36 prior exercises in physical modeling of terrain-air field interaction over a period of fifty years. Sixteen previous studies included full scale comparative data. These studies generally are grouped by topography into idealized hill shapes and specific terrain and by meteorology into neutral or barostromatic stratification. The more sophisticated neutral air flow model efforts consider implications of surface roughness and boundary layer depth upon velocity profile, turbulence intensity, surface friction and turbulence integral scale. The barostromatic models generally emphasized the role of stability, mountain waves, and up or down slope winds to the exclusion of local turbulence characteristics.

When considering the results of this investigation in the context of prior experiment, a physical model reveals that:

1. Separation of flow occurs downwind of many topographical features which produces a turbulence and velocity field which is highly nonhomogeneous;
2. An undistorted model at scales as large as 1:5000 permits resolution of velocity and turbulence details adequate to discern preferable WECS sites; and

3. A wide range of scales and meteorological conditions may reasonably be simulated in existing boundary-layer wind-tunnel facilities. (See Performance Envelope Figure 4.1.)

The second objective was to establish (or affirm) modeling criteria for future operational programs. Current simulation criteria emphasize the importance of reproducing boundary conditions and inflow velocity and turbulence characteristics. The series of surface textures and flow devices studied herein determine that:

1. To produce equivalent wind speeds near ground level require accurate reproduction of surface roughness, shape, and vegetation. Hence terraced models, adequate for certain dispersion simulations, are not appropriate for WECS site analysis; and
2. Current meteorological data in complex terrain is not yet adequate to stipulate with confidence inflow conditions to either numerical or physical models. Hence an adequate approach flow length must be provided to allow the surface layer to come to an equilibrium with underlying terrain undulations.

9.2 Correlation of Laboratory and Field Experiments

The third objective was to compare the physical model and field data through the principles of similarity and to determine how well the physical models can simulate actual atmospheric airflow characteristics. Consideration of the correlation between the airflow during the two field test days as well as a comparison against the verification exercise carried out for numerical models implies that there exists an upper bound to the correlation which may reasonably be expected between any model and the atmosphere. Weighted in this context the experiments suggest that:

1. Wind velocities and directions for a given site and data will correlate with physical model predictions at $r \geq 0.70$. (An average taken over several days of equivalent conditions may be expected to have higher correlation, i.e., Nov. 25 + Dec.28/Model Contoured = 0.81.)

2. Wind velocities at a given set of sites when ordered according to speed magnitude may correlate with physical model predictions at $r = 0.78$ to 0.95 ; and
3. A physical model can locate regions of separation, high turbulence, and low wind speed caused by terrain inhomogeneities.

The fourth objective was to evaluate the influence of surface roughness and shelterbelts on prospective WECS sites. A comparison between measurements made behind full size tree shelterbelts and models constructed of yarn or pipe cleaners reveal that:

1. The height and extent of the sheltered zone behind a 1/5000 scale model are similar even when Reynold's numbers differ by three orders of magnitude;
2. The quantitative magnitudes of wind velocity and longitudinal turbulence are similar to field results even when Reynolds numbers differ by three orders of magnitude; and
3. Extended regions of fields protected by shelterbelts significantly alter the surface wind speed and turbulence levels. Such effects may be critical to the accurate evaluation of WECS site behavior in the bottom 50 meters of the surface layer.

9.3 Character of the Rakaia Gorge Flow Field

The fifth, sixth, and seventh objectives deal with the specific nature of wind flow over the Rakaia Gorge test area. Fisherman "folklore" suggested the gorge and gorge exit produced very high winds. Anemometers placed at Rakaia Gorge Station by the New Zealand Wind Energy Task Force measured annual average wind speeds of 6.4 m/sec and wind energy fluxes of 450 watts/m². Despite these indications the physical model and the field study suggest that:

1. The Rakaia River Gorge bottom and associated lower level terrain have low relative mean wind speeds and high turbulence levels when compared to nearby elevated terrain. Weighted by the climatological records taken at Rakaia Gorge sites B-2 and G-6 may have annual mean wind speeds near 8.6 m/sec and 11.02 m/sec respectively. While wind energy fluxes at sites B-2 and G-6 may reach 1093 watts/m² and 2295 watts/m² respectively. Hence one concludes the gorge proper is not the optimum location for WECS!

2. A gorge or canyon results in large horizontal inhomogeneities in airflow. Wind speeds may vary by more than 200% in horizontal distances of less than 2000 feet. Hence, WECS site location becomes very sensitive to geostrophic wind angle, and relation to other terrain features; and
3. Ridges and hills appear to be optimum locations for WECS; inhomogeneities make it difficult to use simple predictive formulae or generic hill results as accurate flow predictors. The comparators considered, however, did differ significantly in governing values of boundary-layer-to-hill-height ratio and surface-roughness-to-hill height ratio.

REFERENCES

- Abe, Masanao (1941), "Mountain Clouds, Their Forms and Connected Air Currents, Part II," Bull. Centr. Met. Obs., Japan 7 (3), pp. 93-145.
- Astley, J. (1977), "A Finite Element Frozen Vorticity Solution for Two-Dimensional Wind Flow over Hills," Proceedings of 6th Australian Hydraulics and Fluid Mechanics Conference, 1977, Adelaide, Australia, December 5-9, pp. 443-446.
- Barnett, K.M. (1972), "A Wind-Tunnel Experiment Concerning Atmospheric Vortex Streets," Boundary Layer Meteorology, Vol. 2, pp. 427-443.
- Batchelor, G.K. (1953), "The Conditions for Dynamic Similarity of Motions of a Frictionless Perfect-Gas Atmosphere," Quarterly Journal of Royal Meteorological Society, Vol. 79, pp. 224-235.
- Bernstein, A.B. (1965), "Dimensional Analysis Applied to the Wind Distribution in the Planetary Boundary Layer," Monthly Weather Review, Vol. 93, No. 10, pp. 579-585.
- Bowen, A.J. and Lindley, D. (1974), "Measurements of the Mean Wind Flow over Various Escarpment Shapes," 5th Australian Conference on Hydraulics and Fluid Mechanics, Christchurch, New Zealand, December 9-13, 9 p.
- Bowen, A.J. and Lindley, D. (1977), "A Wind Tunnel Investigation of the Wind Speed and Turbulence Characteristics Close to the Ground Over Various Escarpment Shapes," Boundary-Layer Meteorology, 12, pp. 259-271.
- Bradshaw, P. (1971), An Introduction to Turbulence and Its Measurement, Pergamon Press, London
- Briggs, J. (1963), "Airflow around a Model of the Rock of Gibraltar," Meteorological Office Scientific Paper No. 18, p. 20.
- Brock, F.V. and Govind, P.K., "Portable Automated Mesonet in Operation," Journal of Applied Meteorology, Vol. 16, No. 3, pp. 299-310.
- Bryer, D.W. and Pankhurst, R.C. (1971), Pressure-Probe Methods for Determining Wind Speed and Flow Direction, National Physical Laboratory, Her Majesty's Stationery Office, London, 125 pp.
- Cermak, J.E. et al. (1966), "Simulation of Atmospheric Motion by Wind-Tunnel Flows," Technical Report for DA-AMC-28-043-G20 Fluid Dynamics and Diffusion Laboratory, Colorado State University, Fort Collins, Colorado (CER66JEC-VAS-ESP-GJB-HC-RNM-SI17).
- Cermak, J.E. and Peterka, J. (1966), "Simulation of Wind Fields over Point Arguello, California, by Wind-Tunnel Flow over a Topographic Model," Colorado State University, Fort Collins, Colorado (CER65JEC-JAP64).
- Cermak, J.E. (1970), Proceedings, Symposium on Wind Effects on High-Rise Buildings, Northwestern University, Evanston, Illinois, March 23.

REFERENCES (continued)

- Cermak, J.E. (1975), "Applications of Fluid Mechanics to Wind Engineering," 1974 Freeman Scholar Lecture, ASME Journal of Fluids Engineering, Vol. 97, Series 1, No. 1, March, Colorado State University, Fort Collins, Colorado (CEP74-75JEC7).
- Cermak, J.E. and Mutter, D.G. (1978), "Physical Modeling of Atmospheric Transport of Stock Emissions at Kahe Electrical Generating Plant, Oahu, Hawaii," Fluid Dynamics and Diffusion Laboratory, Colorado State University, Research Report CER77-78JEC-DGM-28a, 55 pp.
- Chang, S.C. (1966), "Velocity Distributions in the Separated Flow behind a Wedge-Shaped Model Hill," Technical Report, Grant DA-AMC-28-043-G20, March, Colorado State University, Fort Collins, Colorado (CER65SCC66), 101 pp.
- Cherry, N.J. (1976), "Wind Energy Research Survey of New Zealand - Preliminary Analysis of Meteorological Data," New Zealand Energy Research and Development Committee, Report No. 8, Lincoln College, Christchurch, 31 pp.
- Clarke, A.C. (1958), Profiles of the Future, Bantam Science and Mathematics, New York, 235 pp.
- Clements, W.E. and Barr, S. (1976), "Atmospheric Transport and Dispersal at a Site Dominated by Complex Terrain," Proceedings of 3rd Symposium on Atmospheric Turbulence, Diffusion and Air Quality, Raleigh, North Carolina, October 19-22, 1976, pp. 430-435.
- Cook, N.J. (1977/1978), "Determination of the Model Scale Factor in Wind-Tunnel Simulations of the Adiabatic Atmospheric Boundary Layer," Journal of Industrial Aerodynamics, Vol. 2, pp. 311-321.
- Corotis, R.B. (1976), "Stochastic Modeling Site Wind Characteristics," Department of Civil Engineering, Final Report, ERDA/NSF/00357-76/1, Northwestern University, 297 pp.
- Corotis, R.B. (1977), "Stochastic Modeling of Site Wind Characteristics," Department of Civil Engineering, Final Report, ERDA/RLO/2342-77/2, Northwestern University, 143 pp.
- Cotton, W.R. and George, R.L. (1978), "A Summer with PAM," 4th Symposium on Meteorological Observations and Instrumentation, April 10-14, 1967, Denver, Colorado, American Meteorological Society, pp. 87-90.
- Cotton, W.R. (1978), Personal Communication.

REFERENCES (continued)

- Counihan, J. (1969), "An Improved Method for Simulating an Atmospheric Boundary Layer in a Wind Tunnel," Atmospheric Environment, Vol. 3, pp. 197-214.
- Counihan, J. (1973), "Simulation of an Adiabatic Urban Boundary Layer in a Wind Tunnel," Atmospheric Environment, Vol. 7, pp. 673-689.
- Counihan, J. (1973), "Flow over Two-Dimensional Hills and Plateau in Simulated Boundary Layer Flow," Central Electric Research Laboratories, Leatherhead, Surrey, Laboratory Note No. RD/L/N277/73, 17 pp.
- Counihan, J. (1975), "Review Paper: Adiabatic Atmospheric Boundary Layers: A Review and Analysis of Data from the Period 1880-1972," Atmospheric Environment, Vol. 9, pp. 871-905.
- Crow, E.L., Davis, F.A., and Maxfield, M.W. (1960), Statistics Manual, Dover Publications, New York, 288 pp.
- Davidson, B. (1961), "Valley Wind Phenomena and Air Pollution Problems," Journal of the Air Pollution Control Association, Vol. 11, No. 8, pp. 364-369.
- Davidson, Ben, Gerbier, N., Papagionakis, S.O. and Rijkvort, P.G. (1964), "Sites for Wind-Power Installations," W.M.O. Technical Note 63, WMO-NO156, TP76, 38 pp.
- Deaves, D.M. (1975), "Wind over Hills--A Numerical Approach," Environmental Sciences Research Unit, Cranfield Institute of Technology, United Kingdom, May, 30 pp.
- de Bray, B.G. (1973), "Atmospheric Shear Flows over Ramps and Escarpments," Industrial Aerodynamics Abstracts, 5, September-October, 4 p.
- DeFant, F. (1951), "Local Winds," Compendium of Meteorology, Ed. T.F. Malone, American Meteorological Society, Boston, pp. 655-672.
- Derickson, R.G. and Meroney, R.N. (1977), "A Simplified Physics Airflow Model for Evaluating Wind Power Sites in Complex Terrain," Proceedings of Summer Computer Simulation Conference, July 18-20, 1977, Chicago, Illinois, 14 pp.
- Drake, R.L., Orgill, M.M., and Huang, C. (1977), An Interim Handbook for Siting Small Wind Energy Conversion Systems, Draft Version, Battelle Pacific Northwest Laboratories, Richland, Washington, BNWL-2220, Wind-7, 326 pp.
- Duerver, W.H., MacCracken, M.C. and Walton, J.J. (1978), "The Livermore Regional Air Quality Model: II Verification and Sample Application in the San Francisco Bay Area," Journal of Applied Meteorology, Vol. 17, No. 3, pp. 273-311.

REFERENCES (continued)

- Eagan, B.A. (1975), "Turbulent Diffusion in Complex Terrain," Ch. 4 of Lectures on Air Pollution and Environmental Impact Analysis, American Meteorological Society, pp. 112-135.
- Field, J.H. and Warden, R. (1929), "A Survey of Air Currents in the Bay of Gibraltar, 1929-1930," Geophysics Memoirs, No. 59, Published by Her Majesty's Stationery Office, p. 84.
- Fosberg, M.A., Marlott, W.E., and Krupnak, L. (1976), "Estimating Airflow Patterns over Complex Terrain," USDA Forest Service Research Paper RM-162, Rocky Mountain Forest and Range Experiment Station, Fort Collins, Colorado, 16 pp.
- Fosberg, M.A. (1978), Personal Communication.
- Freeston, D.H. (1974), "Atmospheric Shear Flows over Ramps and Escarpments," 5th Australian Conference on Hydraulics and Fluid Mechanics, Christchurch, New Zealand, December 9-13, 8 p.
- Garrison, J.A. and Cermak, J.E. (1968), "San Bruno Mountain Wind Investigation--A Wind-Tunnel Model Study," Colorado State University, Fort Collins, Colorado (CER67-68JEC-JAG58).
- Golding, E.W. (1955), The Generation of Electricity by Wind Power, Philosophical Library, New York, 318 pp.
- Graham, N.E., Taylor, G.H., Hovind, E.L., Peterson, R.L., Cermak, J.E., and Sinclair, P.C. (1978), "An Analysis of Terrain Induced Aerodynamic Disturbances near the Kington Steam Plant, Tennessee," North American Weather Service, Draft Report AQ-78-22.
- Halitsky, L. Tolciss, J., and Kaplan, E.L. (1962), "Wind Tunnel Study of Turbulence in the Bear Mountain Wake," Quarterly Progress Reports No. 1, 2, 3, and 4, Contract No. DA 36-039 SC-89081, Department of Meteorology and Oceanography, New York University.
- Hardy, D.M. (1977), "Wind Studies in Complex Terrain," American Wind Energy Association Conference, Boulder, Colorado, May 11-14, 1977, 38 pp.
- Hardy, D.M. (1978), Personal Communication.
- Harris, R.I. (1971), "The Nature of the Wind," Paper 3 from The Modern Design of Wind-Sensitive Structures, Proceedings of a Seminar on June 18, 1970 at Institute of Civil Engineers, London. Published by Construction Industry Research and Information Association, pp. 29-55.
- Haugen, Duane A., ed., (1973), Workshop on Micrometeorology, American Meteorological Society, Boston, Massachusetts, 392 pp.

REFERENCES (continued)

- Hewson, E. Wendell, et al. (1973), "Wind Power Potential in Selected Areas of Oregon," Oregon State University (PUD73-1).
- Hidy, G.M. (1967), "Adventures in Atmospheric Simulation," Bulletin of American Meteorological Society, Vol. 48, pp. 143-161.
- Hinze, J.O. (1975), Turbulence, 2nd edition, McGraw-Hill Book Company, New York, 790 pp.
- Hoxit, L.R. (1973), "Variability of Planetary Boundary Layer Winds," Department of Atmospheric Science, Colorado State University, Paper No. 199, 157 pp.
- Hsi, G., Binder, G.J., and Cermak, J.E. (1968), "Topographic Influences on Wind near Green River, Utah," Technical Report, Grant DA-AMC-28-043-65-G20, for Atmospheric Science Laboratory, White Sands Missile Range, Colorado State University, Fort Collins, Colorado (CER67-68GH-GJB-JEC54).
- Jackson, P.S. and Hunt, J.C.R. (1975), "Turbulent Wind Flow over a Low Hill," Quarterly Journal of the Royal Meteorological Society, 101, pp. 292-955.
- Kitabayshi, K.K., Orgill, M.M., and Cermak, J.E. (1971), "Laboratory Simulation of Airflow in Atmospheric Transport-Dispersion over Elk Mountain, Wyoming." Technical Report prepared under Atmospheric Water Resources Research, Bureau of Reclamation, Contract No. 14-06-D-6455 and 14-06-6842, Colorado State University, Fort Collins, Colorado (CER70-71KKK-MMO-JEC65).
- Kitabayshi, K.K. (1977), "Wind Tunnel and Field Studies of Stagnant Flow Upwind of a Ridge," Journal of the Meteorological Society of Japan, Vol. 55, No. 2, pp. 193-204.
- Klemp, J.B. and Lilly, D.K. (1978), "Numerical Simulation of Hydrostatic Mountain Waves," Journal of the Atmospheric Sciences, Vol. 35, No. 7, pp. 78-107.
- Lange, K.O. (1961), "Some Aspects of Site Selection for Wind Power Plants on Mountainous Terrain," Proceedings of the UN Conference on New Sources of Energy Resources, 7, W/28, pp. 125-128, August 21-31.
- Lin, J.T. and Binder, G.J. (1967), "Simulation of Mountain Lee Waves in a Wind Tunnel," Technical Report, Grant No. DA-AMC-28-043-65-G20, Colorado State University, Fort Collins, Colorado (CER67-68JTL-GJB24, AD-664-172).
- Lindley, C.A. (1977), "Wind Machines for the California Aqueduct," 3rd Wind Energy Workshop, Vol. 1, September 1977, Washington, D.C., CONF-770921, pp. 262-272.

REFERENCES (continued)

- Lindley, D. and Chin, S.W. (1977), "Wind Energy Potential in New Zealand - Aspects of the Resource Assessment and Its Utilization," 3rd Wind Energy Workshop, Vol. 1, September 1977, Washington, D.C., CONF-770921, pp. 456-466.
- Liu, H.T. and Lin, J.T. (1976), "Plume Dispersion in Stably Stratified Flow over Complex Terrain," Flow Research, Inc., Report No. 57 or EPA-600/4-76-022, 54 pp.
- Long, R.R. (1954), "Some Aspects of the Flow of Stratified Fluids II, Experiments with a Two-Fluid System," Tellus, Vol. 6, pp. 97-115.
- Long, R.R. (1959), "A Laboratory Model of Airflow over the Sierra Nevada Mountains," The Atmosphere and the Sea in Motion - The Rossby Memorial Volume, pp. 372-380.
- Ludwig, G.R. and Skinner, G.T. (1976), "Wind Tunnel Modeling Study of the Dispersion of SO₂ in Southern Alleghany County, Pennsylvania," Calspan Corporation, EPA Report 903/75-019.
- McVehil, G.E., Ludwig, G.R. and Sundaram, T.R. (1967), "On the Feasibility of Modeling Small Scale Atmospheric Motions," Cornell AeroLab Report ZB-2328-P-1, Buffalo, New York, pp.
- Mari, Y., Miyata, K., and Mitsuta, Y. (1971), "A Case Study of Wind over a Hilly Terrain," Bulletin of the Disaster Prevention Research Institute, Kyata University, Vol. 21, pp. 179-189.
- Marrs, R.W. and Marwitz, J. (1977), "Locating Areas of High Wind Energy Potential by Remote Observation of Eolian Geomorphology and Topography," 3rd Wind Energy Workshop, Vol. 1, September 1977, Washington, D.C., CONF-770921, pp. 307-317.
- Melbourne, W.H. (1977), "Development of Natural Wind Models at Monash University," 6th Australian Hydraulics and Fluid Mechanics Conference, 1977, Adelaide, Australia, December 5-9, pp. 190-194.
- Meroney, R.N., Cermak, J.E. (1967), "Wind-Tunnel Modeling of Flow and Diffusion over San Nicolas Island, California," 97 pp., Colorado State University, Fort Collins, Colorado (CER66-67RNM-JEC44).
- Meroney, R.N. and Chaudhry, F.H. (1972), "Wind Tunnel Site Analysis of Dow Chemical Facility at Rocky Flats, Colorado," Colorado State University, Fort Collins, Colorado (CER71-72RNM-FC45).
- Meroney, R.N., Cermak, J.E., and Yang, B.T. (1975), "Modeling of Atmospheric Transport and Fumigation at Shorelines," Boundary Layer Meteorology, Vol. 9, No. 1, pp. 69-90.

REFERENCES (continued)

- Meroney, R.N., Cermak, J.E., and Garrison, J.A. (1975), "Wind Tunnel Study of Stock Gas Dispersal at Lansing Power Station, Units 1, 2, 3, and 4," Fluid Dynamics and Diffusion Laboratory, Colorado State University, Research Report CER74-75-RNM-JEC-JAG28, 199 pp.
- Meroney, R.N., Sandborn, V.A., Bouwmeester, R.J.B., and Rider, M.A. (1976), "Sites for Wind Power Installations: Wind Tunnel Simulation of the Influence of Two-Dimensional Ridges on Wind Speed and Turbulence," Annual Report: First Year, NSF/RANN Contract GAER75-00702, Report ERDA/NSF-00702/75/T1 (CSU CER76-77RNM-VAS-RB-MAR-5), 80 pp.
- Meroney, R.N., Sandborn, V.A., Bouwmeester, R.J.B., and Rider, M.A. (1976), "Sites for Wind Power Installations - Tabulated Experimental Data," Progress Report June-November 1976, ERDA Wind Energy Program Report ERDA/Y-76-S-06-2438/7611, (CSU CER76-76RNM-VAS-RB-MAR-29), 60 pp.
- Meroney, R.N., Sandborn, V.A., Bouwmeester, R.J.B., and Rider, M.A. (1977), "Sites for Wind Power Installations - Annual Report: Second Year," Department of Energy Report RLO/2438-77/1 (CSU CER77-78RNM-VAS-RB-MAR6), 186 pp.
- Meroney, R.N., Sandborn, V.A., Bouwmeester, R.J.B., and Chien, H. (1978), "Preliminary Measurements of Flow over Model, Three-Dimension Hills," Fluid Dynamics and Diffusion Laboratory, Colorado State University Research Memorandum No. 29, CEM-77-78HCC-VAS-RNM-RJBB29, 34 pp.
- Mery, P. (1969), "Reproduction en Similitude de la Diffusion dans la Cauche Limite Atmospherique," La Houille Blanche, No. 4 (Translation Air Poll. Tech. Inf. Cent. No. 1104).
- Monin, A.S. and Obukhov, A.M. (1954), "Basic Regularity in Turbulent Mixing in the Atmosphere," Trudy. Geophys. Inst. ANSSSR, No. 24.
- Munn, R.E. (1966), Descriptive Micrometeorology. Advances in Geophysics, Supplement 1, Academic Press, London, 245 pp.
- Nemoto, S. (1961/1962), "Similarity between Natural Wind in the Atmosphere and Model Wind in a Wind Tunnel," Papers in Meteorology and Geophysics, Tokyo:
 Vol. 12, No. 1, pp. 30-52,
 Vol. 12, No. 2, pp. 117-128,
 Vol. 12, No. 2, pp. 129-154,
 Vol. 13, No. 2, pp. 171-195 (1962).
- Orgill, M.M., Cermak, J.E., and Grant, L.O. (1971a), "Laboratory Simulation and Field Estimates of Atmospheric Transport-Dispersion over Mountainous Terrain," Technical Report, Colorado State University, Fort Collins, Colorado (CER70-71MMO-JEC-LOG40), 302 pp.

REFERENCES (continued)

- Orgill, M.M., Cermak, J.E. and Grant, L.O. (1971b), "Research and Development Technique for Estimating Airflow and Diffusion Parameters Related to the Atmospheric Water Resources Program," Final Report, Bureau of Reclamation Contract No. 14-06-D-6842, Colorado State University CER71-72MMO-JEC-LOG-20, 111 pp.
- Orgill, M.M. (1977), "Survey of Wind Measurement Field Programs," Battelle, Pacific Northwest Laboratories, Report BNWL-2220, Wind-3, 53 pp.
- Panofsky, H.A. (1977), "Wind Structure in Strong Winds Below 150m," Wind Engineering, Vol. 1, No. 2, pp. 91-103.
- Panofsky, H.A. (1978), Personal Communication.
- Petersen, R.L. and Cermak, J.E. (1977), "Atmospheric Transport of Hydrogen Sulfide from Proposed Geothermal Power Plants (Units 13, 14, 16, and 18) for the West Wind Direction," Fluid Dynamics and Diffusion Laboratory, Colorado State University, Research Report CER77-78RLP-JEC10, 57 pp.
- Petterssen, Sverre (1961), "Some Aspects of Wind Profiles," New Sources of Energy, Proceedings of the United Nations Conference in Rome, Vol. 7 (W/26), pp. 133-136.
- Plate, E.J. and Lin, C.W. (1965), "The Velocity Field Downstream from a Two-Dimensional Model Hill--Part 2," Colorado State University, Fort Collins, Colorado (CER65EJP-CWL41), 59 pp.
- Plate, E.J. and Sheih, C.M. (1965), "Diffusion from a Continuous Point Source into the Boundary Layer Downstream from a Model Hill," Colorado State University, Fort Collins, Colorado (CER65EJP-CMS60).
- Putnam, Palmer Cosslett (1948), Power from the Wind, Van Nostrand Reinhold Company, New York, 224 pp.
- Queney, P., et al. (1960), "The Airflow over Mountains," Technical Note No. 34, World Meteorological Organization, Geneva, 135 pp.
- Raine, J.K. (1974), Modeling the Natural Wind: Wind Protection by Fences, Ph.D. Dissertation, Department of Mechanical Engineering, University of Canterbury, Christchurch, New Zealand, Vol. 1 and 2, 558 pp.
- Raine, J.K. and Stevenson, P.C. (1977), "Wind Protection by Model Fences in a Simulated Atmospheric Boundary Layer," Journal of Industrial Aerodynamics, Vol. 2, pp. 159-180.
- Reed, J.W. (1974), "Wind Power Climatology," Weatherwise, December 1974, pp. 237-242.

REFERENCES (continued)

- Riley, J.J., Liu, H.T., and Geller, E.W. (1976), "A Numerical and Experimental Study of Stably Stratified Flow around Complex Terrain," Flow Research, Inc., Report EPA-600/4-76-021 for U.S. Environmental Protection Agency, 30 pp.
- Robins, A.G. (1977), "The Development and Structure of Simulated Neutrally Stable Atmospheric Boundary Layers," Central Electric Generating Board Report R/M/R246, Marchwood Engineering Laboratories, 44 pp.
- Sacre, C. (1975), "Numerical Method for near Calculation of the Excess Velocity of the Wind on a Hill," Centre Scientifique et Technique du Batiment, Nantes, France, 26 pp.
- Sandborn, V.A. (1972), Resistance Temperature Transducers, Metrology Press, Fort Collins, Colorado, 545 pp.
- Scorer, R.S. (1952), "Mountain-Gap Winds: A Study of Surface Wind at ,"
," Quarterly Journal of the Royal Meteorological Society, Imperial College, London, Vol. 78, pp. 53-61.
- Scorer, R.S. (1978), Environmental Aerodynamics, Ellis Horwood Limited, Chichester, 487 pp.
- Snyder, W.H. (1972), "Similarity Criteria for the Application of Fluid Models to the Study of Air Pollution Meteorology," Boundary Layer Meteorology, Vol. 3, pp. 113-134.
- Sturrock, J.W. (1972), "Aerodynamic Structures of Shelterbelts in New Zealand - 2: Medium-height to Tall Shelterbelts in Mid Canterbury," New Zealand Journal of Science, Vol. 15, No. 2, pp. 113-140.
- Sumner, C.J. (1968), "A Low Torque Cup Anemometer," Australian Journal of Instrumentation and Control, October 1968, pp. 39-40.
- Teunissen, H.W. (1970), "Characteristics of the Mean Wind and Turbulence in the Planetary Boundary Layer," University of Toronto Institute of Aerospace Studies, Review No. 32, 45 pp.
- Traci, R.M., Phillips, G.T., Patmaik, P.C., and Freeman, B.E. (1977), "The Utility of Mathematical Wind Field Models in a WECS Siting Methodology: A Case Study," 3rd Wind Energy Workshop, Vol. 2, September 1977, Washington, D.C., CONF-770921, pp. 677-688.
- Ukejurchi, N., Sakata, H., Okamoto, H., and Ide, Y. (1967), "Study on Stack Gas Diffusion," Mitsubishi Tech. Bull., No. 52, pp. 1-13.
- Ward, I., ed. (1976), New Zealand Atlas, A.R. Shearer Government Printer, Wellington, 292 pp.
- Wegley, H.L., Orgill, M.M., and Drake, R.L. (1978), "A Siting Handbook for Small Wind Energy Conversion Systems," Battelle, Pacific Northwest Laboratories, Report PNL-2521, 108 pp.

REFERENCES (continued)

Wooldridge, G. (1978), Personal Communication.

Yamada, Tetsuji and Meroney, Robert N. (1971), "Numerical and Wind Tunnel Simulation of Response of Stratified Shear Layers to Nonhomogeneous Surface Features," Project THEMIS TR No. 9, Fluid Dynamics and Diffusion Laboratory, Colorado State University, Fort Collins, Colorado (CER70-71TY-RNM62).

Yih, C.S. (1965), Dynamics of Nonhomogeneous Fluids, MacMillan, New York, 306 pp.

Zrajevsky, I.M., Doroshenko, V.N., and Chepik, N.G. (1968), "Investigation of the Effect of Various Types of Relief on the Characteristics of an Airstream in a Wind Tunnel," Trudi Glavnaya Geofizicheskoya Observatoriya, No. 207 (In Russian).

APPENDIX

REVIEW OF SIMILITUDE CRITERIA

(Orgill, Cermak, & Grant (1971b))

Basic Equations

The basic equations necessary for considering atmospheric motions and dispersion are the following:

equations of motion,
continuity equation,
equation of state,
Poisson's equation,
equation of turbulent heat transfer,
equation of heat transfer from the surface boundary, and
parabolic diffusion equation

In this study the continuity equation and equation of state are of little importance to the similarity analysis and will be omitted from further discussion. Therefore, the principal equations to be considered in determining similarity criteria for air motion and dispersion are:

1. Equation of motion

$$\frac{\partial \bar{U}_i}{\partial t} + \bar{U}_j \frac{\partial \bar{U}_i}{\partial x_j} + 2\epsilon_{ijk} \Omega_j \bar{U}_k = -\frac{1}{\rho} \frac{\partial \bar{p}}{\partial x_i} + \frac{1}{\rho} \frac{\partial \bar{\sigma}_{ij}}{\partial x_j} + \frac{1}{\rho} \frac{\partial \sigma_{ij}}{\partial x_j} - \frac{\Delta \bar{T}}{\bar{T}} g \delta_{i3} \quad A-1$$

2. Equation of Poisson

$$\theta = T \left(\frac{1000}{p} \right)^{R_d/C_p d} \quad A-2$$

3. Equation of turbulent heat transfer

$$\begin{aligned} \rho C_p \left(\frac{\partial \bar{T}}{\partial t} + \bar{U}_j \frac{\partial \bar{T}}{\partial x_j} \right) - \frac{\partial \bar{p}}{\partial t} - \bar{U}_j \frac{\partial \bar{p}}{\partial x_j} - \overline{U_j' \frac{\partial p'}{\partial x_j}} \\ = \frac{\partial}{\partial x_j} \left(k \frac{\partial \bar{T}}{\partial x_j} \right) - C_p \rho \frac{\partial}{\partial x_j} \left(\overline{T' u_j'} \right) + \bar{\phi} \end{aligned} \quad A-3$$

4. Equation of heat transfer from the surface boundary

$$Q_T - Q_R + Q_{L\downarrow} - Q_{L\uparrow} = \pm Q_G \pm Q_H \pm Q_E \quad A-4$$

5. Parabolic diffusion equation

$$\frac{\partial \bar{C}}{\partial t} = \frac{\partial}{\partial x_i} (\bar{C} \bar{U}_i) = \frac{\partial}{\partial x_i} K_{ii} \frac{\partial \bar{C}}{\partial x_i} + k_m \frac{\partial^2 \bar{C}}{\partial x_i \partial x_i} \quad A-5$$

This set of equations may be simplified further depending upon the type of airflow under investigation and the boundary conditions. The fourth equation, the equation of heat transfer from the surface boundary

has not been used in deriving similarity criteria before and, because of the similarity difficulties this equation presented to the study, it was neglected except as a general tool for analyzing the similarity problem in depth.

For the set of equations to be complete, equations dealing with the physics of clouds should be included, but this aspect of the study cannot be considered in a laboratory physical model at the present time.

Boundary Conditions

The general boundary conditions for a study of air motion and dispersion over irregular terrain can be expressed mathematically as the following (see Fig. 2-1 also):

1. $\lim_{z \rightarrow z_0} \vec{U} = 0$
2. $\lim_{z \rightarrow H} \vec{U} = \vec{U}_g$
3. $\lim_{z \rightarrow z_0} \vec{\tau} = \vec{\tau}_0$
4. $\lim_{z \rightarrow H} \vec{\tau} \rightarrow \vec{\tau}_{\min}$
5. $\lim_{x, y, z \rightarrow \infty} C \rightarrow 0$
6. $\lim_{x, y, z \rightarrow 0} C \rightarrow \infty$

A-6

The continuity condition

$$\int_{-\infty}^{\infty} \int_0^{\infty} \bar{U} C(x, y, z) dz dy = Q \quad \text{for all } x > 0 \quad \text{A-7}$$

will not be satisfied in the field because of the action of deposition and depletion variables.

Similitude Criteria

The similitude parameters governing the airflow and dispersion patterns may be derived by dimensional analysis, similarity theory and inspectional analysis. The purpose of this section is to give a review of the similarity criteria that several authors have derived that pertain to this particular problem and not to discuss the relative advantages and disadvantages of the similarity methods.

Sundaram (1967) derived the similitude requirements for the atmospheric boundary layer by applying similarity techniques to the differential equations governing the relevant flow processes. The

following mathematical expressions summarizes part of the similarity criteria derived by Sundaram for different airflow conditions:

1. Steady, turbulent, incompressible and neutral airflow:

$$\frac{u}{U_\infty} = f\left(\frac{z}{L_0}, \frac{U_\infty L_0}{\nu}, \frac{U_\infty L_0}{K_M}\right) \quad A-8$$

2. Steady, uniform, turbulent flow (aerodynamically rough):

$$\frac{u}{U_\infty} = f\left(\frac{z}{z_0}, \frac{U_\infty z_0}{K_{M_0}}\right) \quad A-9$$

3. Turbulent flow with temperature gradient (temperature gradient is sufficiently small so that deviation from neutral conditions are small; vertical gradients are more important than horizontal ones):

$$\left(\frac{u}{U_\infty}, \frac{\delta T}{\Delta T}\right) = f\left(\frac{z}{L_0}, \frac{U_\infty L_0}{\nu}, \frac{U_\infty L_0}{K_m}, \frac{U_\infty L_0}{K}, \frac{U_\infty L_0}{K_H}, g \frac{L_0}{U_\infty^2} \frac{\Delta T}{T_0}\right) \quad A-10$$

with modifications

$$\left(\frac{u}{U_\infty}, \frac{\delta T}{\Delta T}\right) = f\left(\frac{z}{z_0}, Pr_t, Re_t, B\right) \quad \text{where } B = g \frac{z_0}{U_\infty^2} \frac{\Delta T}{T_0} \quad A-11$$

4. Turbulent flow with temperature gradient (fractional changes in potential temperature are not small):

$$\left(\frac{u}{U_\infty}, \frac{\delta T}{\Delta T}\right) = f\left(\frac{z}{z_0}, Pr_t, Re_t, B, \frac{\Delta T}{T_0}\right) \quad A-12$$

5. Unsteady flows

$$\left(\frac{u}{U_\infty}, \frac{\delta T}{\Delta T}\right) = f\left(\frac{z}{L_0}, \frac{t}{t_0}, \frac{U_\infty t_0}{L_0}, \frac{U_\infty L_0}{\nu}, \frac{U_\infty L_0}{K_M}, \frac{U_\infty L_0}{K}, \frac{U_\infty L_0}{K_H}, g \frac{L_0}{U_\infty^2} \frac{\Delta T}{T_0}, \frac{u^*}{U_\infty}, -\frac{1}{ku^*} \frac{Q}{\rho C_p} \frac{1}{\Delta T}, \frac{\theta_0}{\Delta T}\right) \quad A-13$$

6. Similarity of turbulent fluctuations:

$$\frac{u_0}{\sqrt{u_0'^2}}, \frac{(\Delta T)_0}{\sqrt{T_0'^2}}, \frac{L_0}{z_0}, \frac{U_0 z_0}{K_{M_0}}, \frac{K_{M_0}}{K_{H_0}}, g \frac{z_0}{U_0^2} \frac{(\Delta T)_0}{T_0} \quad A-14$$

Nemoto (1961, 1962) derived the similitude requirements for the atmospheric boundary layer by using inspectional analysis and turbulence theory. A summary of his criteria are:

1. Turbulent and incompressible flow (neutral conditions)

$$\left[\frac{K_i}{L_o U_\infty} \right]_F \equiv \left[\frac{K_i}{L_o U_\infty} \right]_M \left[\frac{u_i'^2}{U_\infty^2} \right]_F \equiv \left[\frac{u_i'^2}{U_\infty^2} \right]_M \quad A-15$$

Nemoto modifies the eddy Reynolds number requirement by considering local isotropic turbulence theory and derives the following:

$$\frac{U_{\infty M}}{U_{\infty F}} = \left(\frac{\epsilon_M}{\epsilon_F} \right)^{1/3} \left(\frac{L_{M_o}}{L_{F_o}} \right)^{1/3} \quad A-16$$

2. Thermal stratification-similarity based on equation of turbulent energy change:

$$\frac{U_{\infty F}}{U_{\infty M}} = \left(\frac{L_{oF}}{L_{oM}} \right)^{1/2} \left(\frac{\theta_M / \Delta\theta_M}{\theta_F / \Delta\theta_F} \right)^{1/2} \quad A-17$$

3. Turbulent flow field with thermal stratification:

$$\left[\frac{K_i}{L_o U_\infty} \right]_F \equiv \left[\frac{K_i}{L_o U_\infty} \right]_M \left[\frac{u_i'^2}{U_\infty^2} \right]_F \equiv \left[\frac{u_i'^2}{U_\infty^2} \right]_M \left[g \frac{L_o}{U_\infty^2} \right]_M \equiv \left[g \frac{L_o}{U_\infty^2} \right]_F \quad A-18$$

Nemoto indicates that the above three conditions can be simultaneously satisfied if the following relation holds among the sizes and velocities of the apparent mean eddies in the *i*-direction of model and prototype flows:

$$\frac{U_{miM}}{U_{miF}} = \left(\frac{L_{M_o}}{L_{F_o}} \right)^{3/2} \left(\frac{\Lambda_{miM}}{\Lambda_{miF}} \right)^{-1} \quad A-19$$

Bernstein (1965) used the ordinary dimensional method and a generalized dimensional analysis to derive the similarity criteria for the atmospheric planetary layer. On the basis of the equations of motion and boundary conditions he indicates that the variables relevant to flow in the atmospheric planetary layer are \bar{U} , \bar{U}_g , ρ , f , τ , τ_o , z , H and z_o . In this analysis he represents vectors as complex variables and assumes that relevant vectors lie in the horizontal plane and, therefore, are two-dimensional.

Bernstein used ordinary dimensional analysis to find the following functional relationship for neutral conditions,

$$\frac{\vec{U}}{\vec{U}_*} = f\left[\frac{\vec{U}_{*o}}{\vec{U}_g}, \frac{\vec{U}_g}{fz_o}, \frac{H}{z_o}, \frac{z}{z_o}, \frac{\vec{U}_*}{\vec{U}_{*o}}\right] \quad \text{A-20}$$

and from his generalized dimensional analysis:

$$\frac{\vec{U}}{\vec{U}_g} = f\left[\frac{\vec{U}_{*o}^2}{fz_o \vec{U}_g}, \frac{H}{z_o}, \frac{z}{z_o}, \frac{\vec{U}_*}{\vec{U}_{*o}}\right] \quad \text{A-21}$$

Cermak et al. (1966) have used the inspectional method for deriving similarity criteria for atmospheric flows. These criteria are:

1. Turbulent and neutral airflow

$$\begin{aligned} \tau_{oF} &\equiv \tau_{oM} & \text{A-22} \\ C_{D_M} \rho_M \bar{U}_M^2 &\equiv C_{D_F} \rho_F \bar{U}_F^2 \end{aligned}$$

2. Turbulent flow with thermal stratification:

$$Re = \frac{U_o L_o}{\nu_o}$$

$$Ri = \frac{\Delta T_o}{\bar{T}_o} \frac{L_o}{U_o^2} g_o$$

$$Ro = \frac{U_c}{L_o \Omega_o} \quad \text{A-23}$$

$$Pr = \frac{\nu_o}{k_o / \rho_o C_{p_o}}$$

$$Ek = \frac{U_o^2}{C_{p_o} \Delta \bar{T}_o}$$

3. Comparison of laminar laboratory airflow model to a turbulent atmospheric prototype airflow:

<u>Model</u>	<u>Field</u>
$Re = \frac{U_o L_o}{\nu} \equiv R_{e_t}$	$= \frac{U_o L_o}{K_i}$
$Pr = \frac{\mu C_p}{k} \equiv P_{r_t}$	$= \frac{K_M}{K_H}$
$Ri \equiv \frac{g_o \Delta T_o L_o}{T_o U_o^2}$	
$Eu = \frac{\Delta p_o}{\rho U_o^2}$	
$Ek = \frac{U_o^2}{C_p \Delta T_o}$	

A-24

For dispersion similarity,

$$Pe = \frac{U_o L_o}{k_m} \equiv Pe_t = \frac{U_o L_o}{K_c}$$

Partial Simulation

One of the most important practical problems that arises in laboratory simulation is the effect of not satisfying exactly all the similarity requirements. The situation in which the modeling criteria are not completely fulfilled is called partial simulation. In practice partial simulation is unavoidable since many similarity criteria impose diametrically opposing requirements on the scaling parameters. Thus, it is well known that in fluids with the same kinematic viscosity, simultaneous modeling of both Reynolds and Froude number is nearly impossible.

Unfortunately, it is clear that in the flow problems of the type discussed above all the similarity criteria cannot be satisfied simultaneously and that partial simulation becomes unavoidable. When dealing with the simulation of the above class of flow problems on a different scale one has to decide which of the similarity parameters are more important for a satisfactory description of the physical processes governing the problems.

Sundaram (1967) listed the various questions that arise in connection with the practical application of laboratory modeling techniques. The ones important are:

- 1) "Of all the various similitude parameters occurring in a given problem which ones are the most important?"
- 2) "How accurately should the similarity parameters be reproduced in the laboratory and what are the effects of relaxing them?"

- 3) "What range of values of these similarity parameters should any facility be capable of reproducing?"
 4) "How accurately should quantities be measured in a facility?"

The area of modeling in which the greatest amount of experience is available and in which there is abundant evidence of successful partial simulation is in the modeling of flow about objects, buildings, and prominent features of terrain. The principal concern in these problems has been in the simulation of the streamlines of mean flow and the location of wakes and eddies.

In simulating the flow around sharp-edged terrain features, since Reynolds number is not expected to influence the gross flow features it has been possible to duplicate the mean streamline, the regions of turbulent eddies, and probably even the coarse structure of the turbulence by providing geometrical similarity in the models. Examples of successful modeling in this type of flow problem have been conducted by Field and Warden (1929), Garrison and Cermak (1968) and Halitsky *et al.*, (1965).

In the case of terrain features, such as hills and valleys, viscous effects may become important for gross flow features in a model and it is necessary to consider Reynolds number effects. In this case, the procedure in model experiments has been to match a model Reynolds number to a "turbulent" Reynolds number for the atmosphere, a number obtained by using a representative value of eddy viscosity. Studies in which this type of reasoning has been applied are Abe (1941) and Cermak and Peterka (1966).

Scale Distortion

Distorted geometric models are common in hydraulics and ocean engineering laboratory studies, but have not been used to any great extent in wind-tunnel modeling. A recent study by Chaudhry and Cermak (1971) has examined the problem in relation to modeling urban areas. A complete examination of the distorted similarity problem has not been considered, however, Nemoto (1961) has analyzed some aspects of the problem.

Nemoto examined the equations of motion of a turbulent atmosphere and found that in case of vertical exaggeration the degree of distortion is related to K_x and K_z , the eddy-diffusion (viscosity) coefficients in the longitudinal and vertical directions. He found that the relation,

$$\alpha = \left[\frac{\left(\frac{K_x}{K_z} \right) F}{\left(\frac{K_x}{K_z} \right) M} \right]^{1/2}$$

A-25

should be satisfied between α and the eddy-diffusion coefficients for the mean flow patterns to be similar for prototype and model. At the present time the difficulty of obtaining measurements of the eddy-diffusion coefficients in the field and model have hindered efforts to check this relation. However, the recent urban area study by Chaudhry and Cermak (1971) was an attempt to examine this relation in terms of a fully-rough flow in the wind tunnel.

GLOSSARY OF TERMS

Eckert No.	$Ek = \frac{U_o^2}{C_p (\Delta T)_o}$	-- Nondimensional ratio between inertia force and a compression force. Equivalent to the Mach number.
	$Ek = (\gamma - 1)M^2$	
	$\gamma = C_p / C_u$	
Euler No.	$Eu = \frac{\Delta P_o}{\rho_o U_o^2}$	-- Nondimensional ratio between the pressure force and the inertia force.
Froude No.	$Fr = \frac{U_o}{\sqrt{g_o L_o}}$	-- Nondimensional ratio between the inertia force and force of gravity.
Péclet No.	$Pe = \frac{U_o L_o}{K_c}$	-- Nondimensional ratio between inertial force and mass diffusivity.
Prandtl No.	$Pr = \frac{C_p \mu}{k}$	-- Nondimensional ratio between the product of heat advection and viscous forces and the product of heat diffusion and inertia forces.
	$Pr_t = \frac{K_M}{K_H}$	
Reynolds No.	$Re = \frac{U_o}{L_o \nu_o}$	-- Nondimensional ratio of the inertial force to the viscous force.
	$Re_t = \frac{U_o}{L_o K_M}$	
Richardson No.	$Ri = g_o \frac{1}{\theta_o} \frac{(\partial\theta/\partial z)_o}{(\partial U/\partial z)_o^2}$	-- Nondimensional number arising in the study of shearing flows of a stratified fluid. Number expresses a characteristic ratio of work done against gravitational stability to energy transferred from mean to turbulent motion.

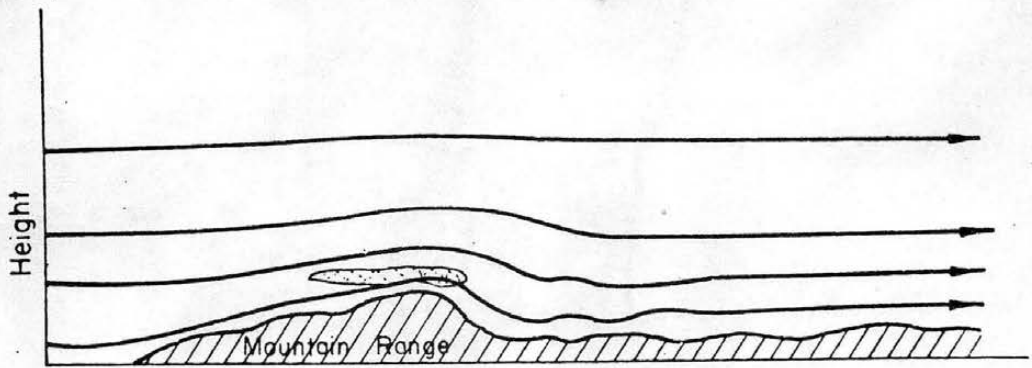
GLOSSARY OF TERMS - (Continued)

Rossby No.

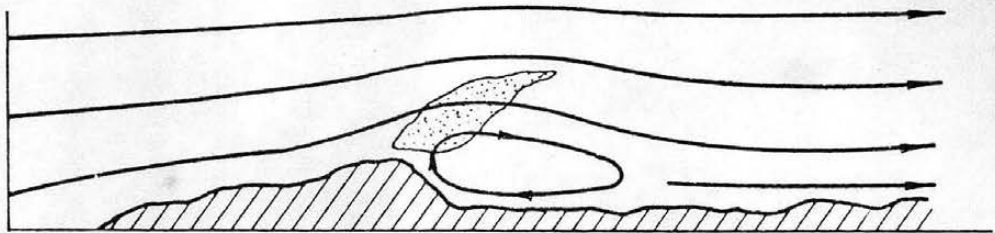
$$Ro = \frac{U_o}{f_o L_o}$$

-- Nondimensional ratio of the inertial force to the Coriolis force.

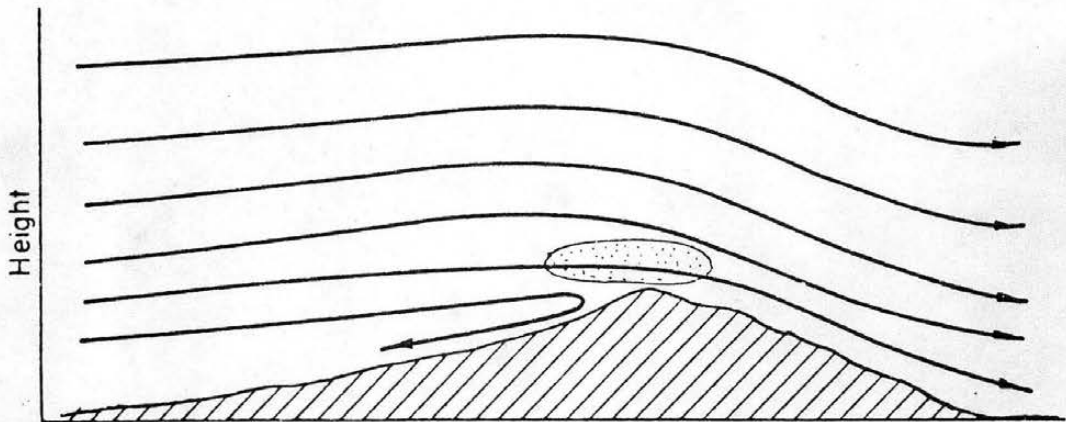
FIGURES



a. Quasi-Laminar Flow

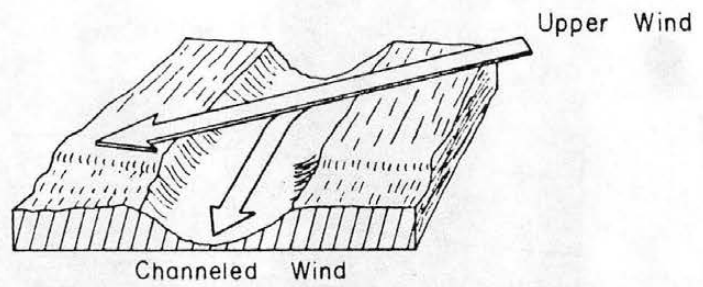
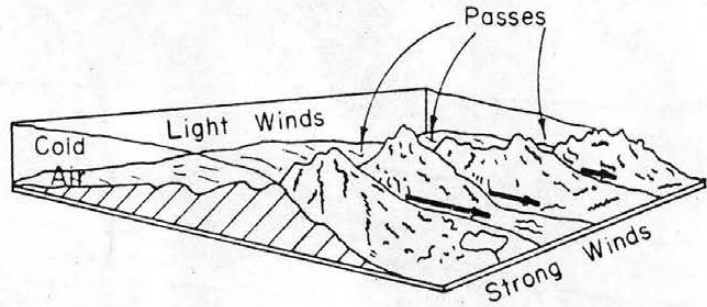


b. Separation Flow



c. Blocking and Stagnation

Figure 2-1. Classification of types of airflow over mountainous terrain (Orgill 1971).

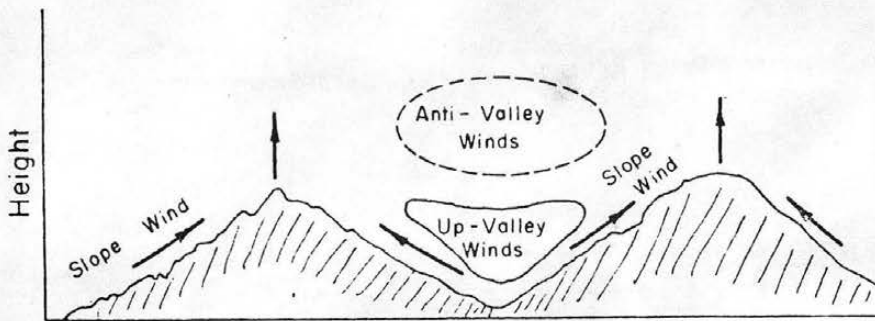


d. Channel and Gap Winds

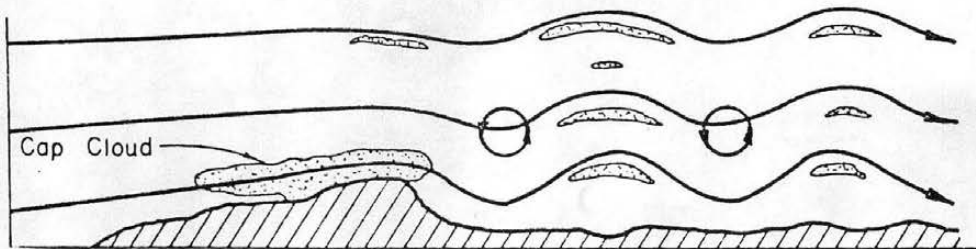


e. Horizontal Eddying

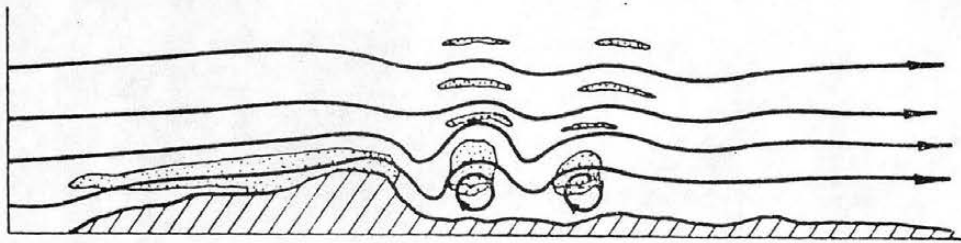
Figure 2-1. Classification of types of airflow over mountain terrain (continued).



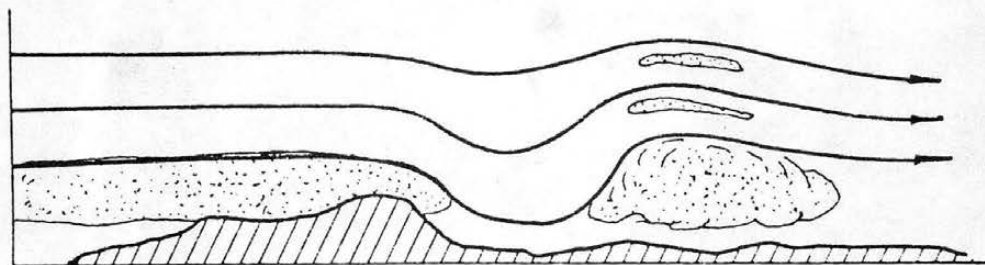
f. Slope and valley winds during daytime (reversed flow for night time)



g. Lee Waves



h. Rotors



i. Hydraulic (analog) Air Flow

Figure 2-1. Classification of types of airflow over mountainous terrain (continued).

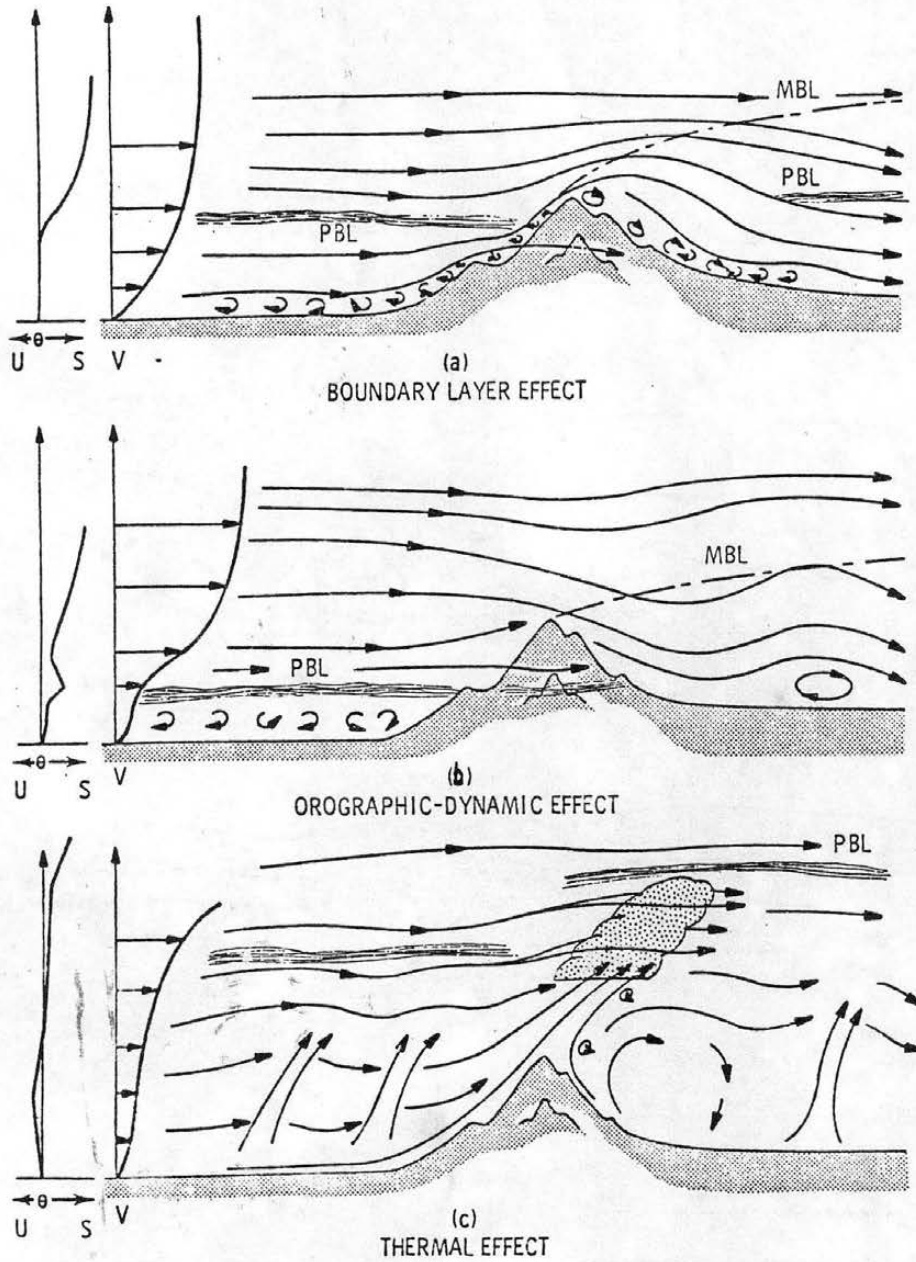


Figure 2-2. Methods in which terrain features affect atmospheric motions (Drake et al. 1977).

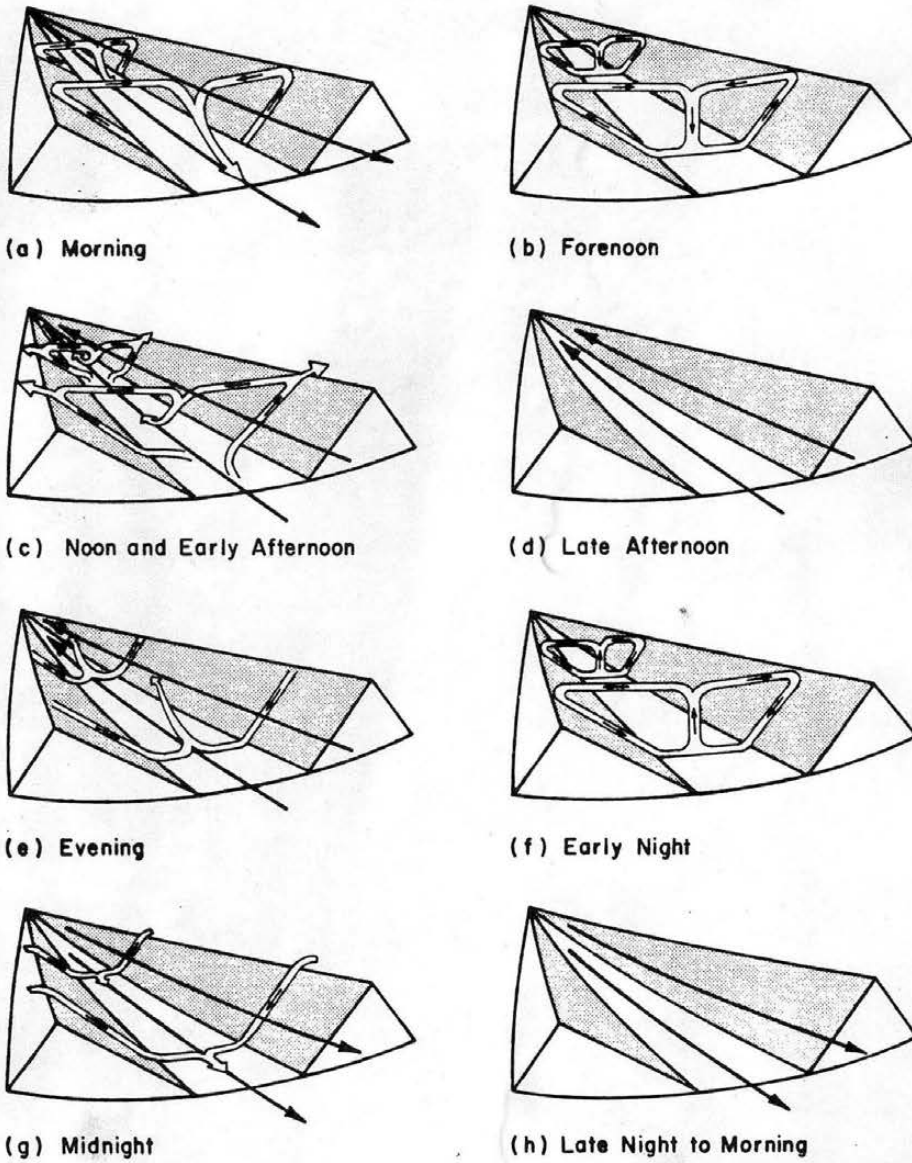


Figure 2-3. The diurnal sequence of mountain and valley winds (DeFant 1951).

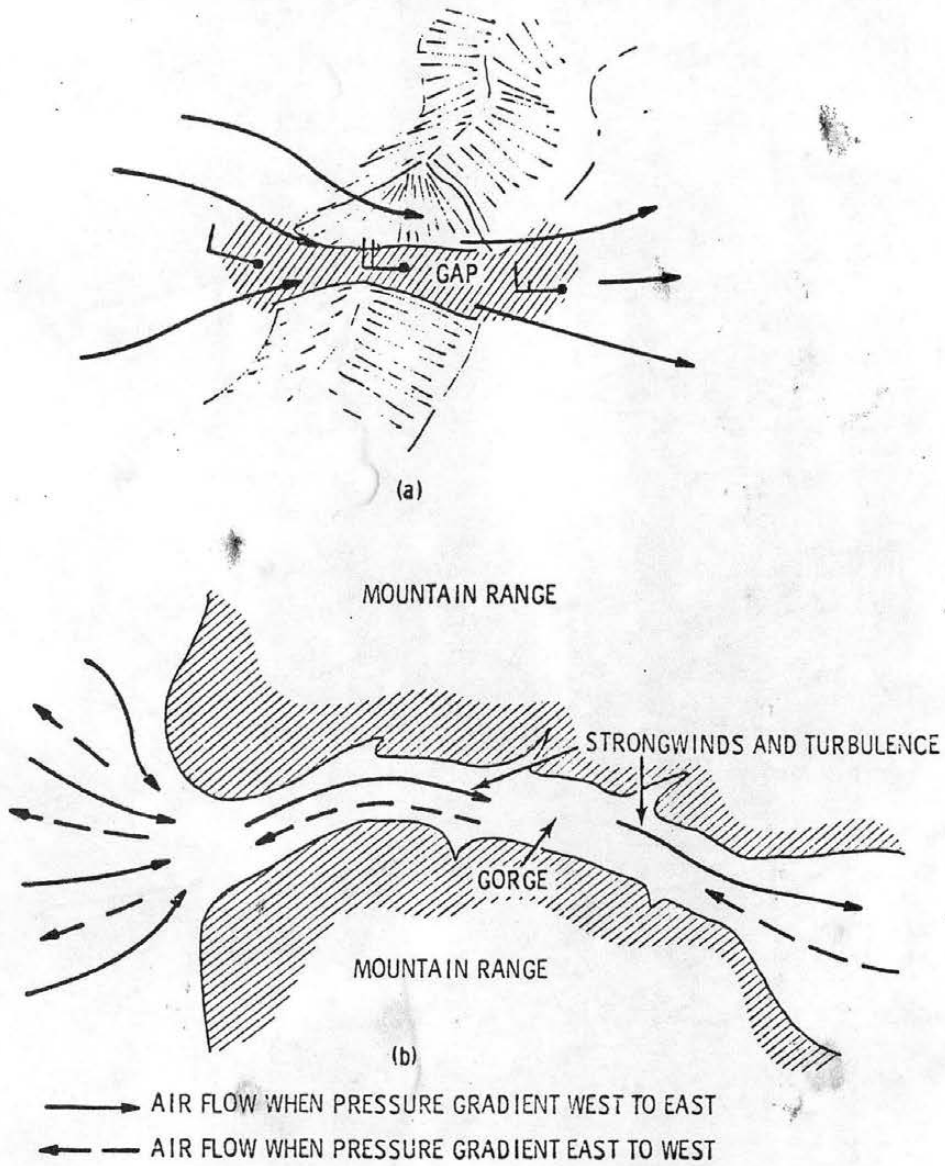


Figure 2-4. A schematic of the type of flow patterns that may be observed through gaps and gorges (Wegley et al. 1978)

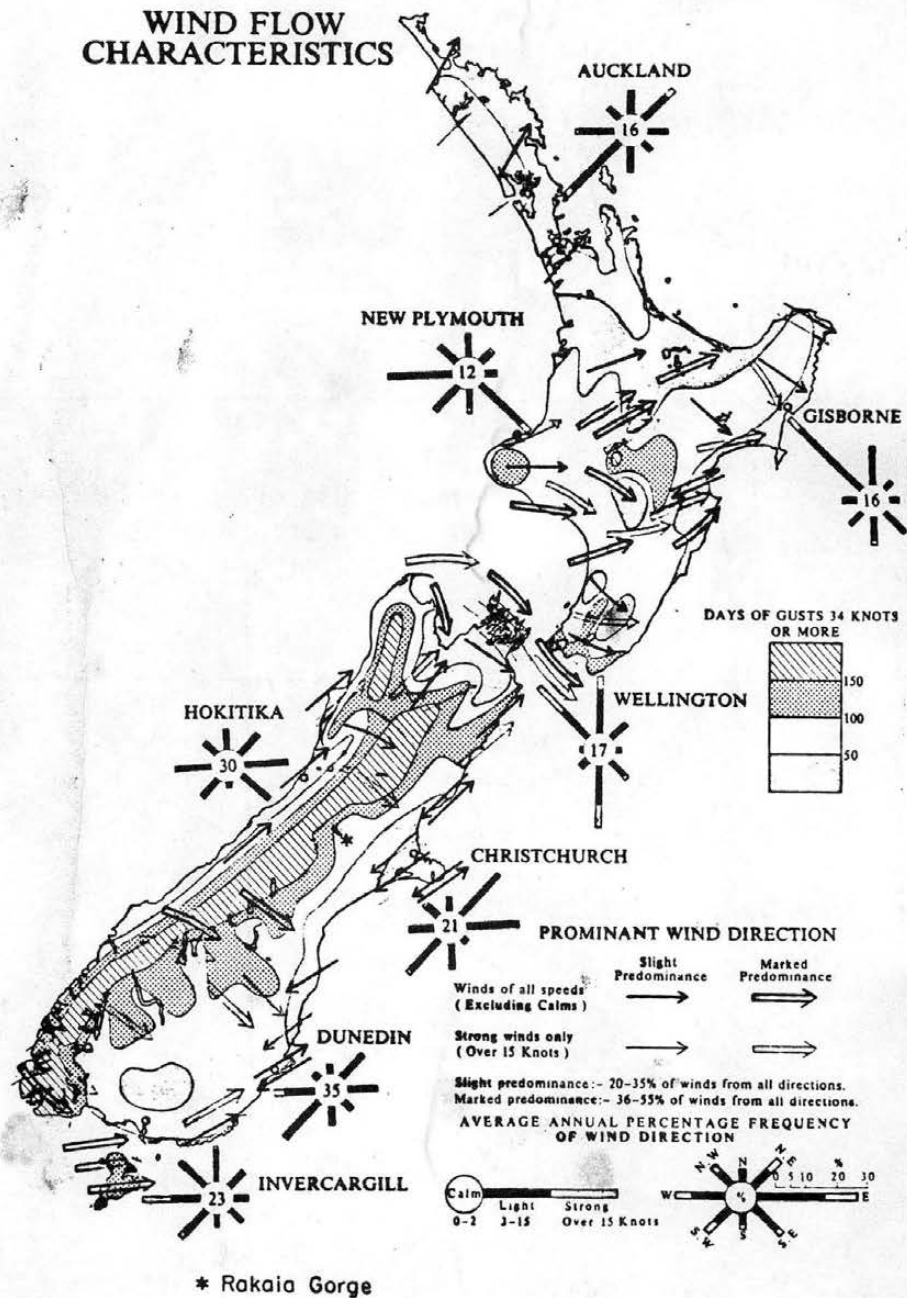


Figure 3-1. Annual windflow characteristics over New Zealand (Ward 1976).

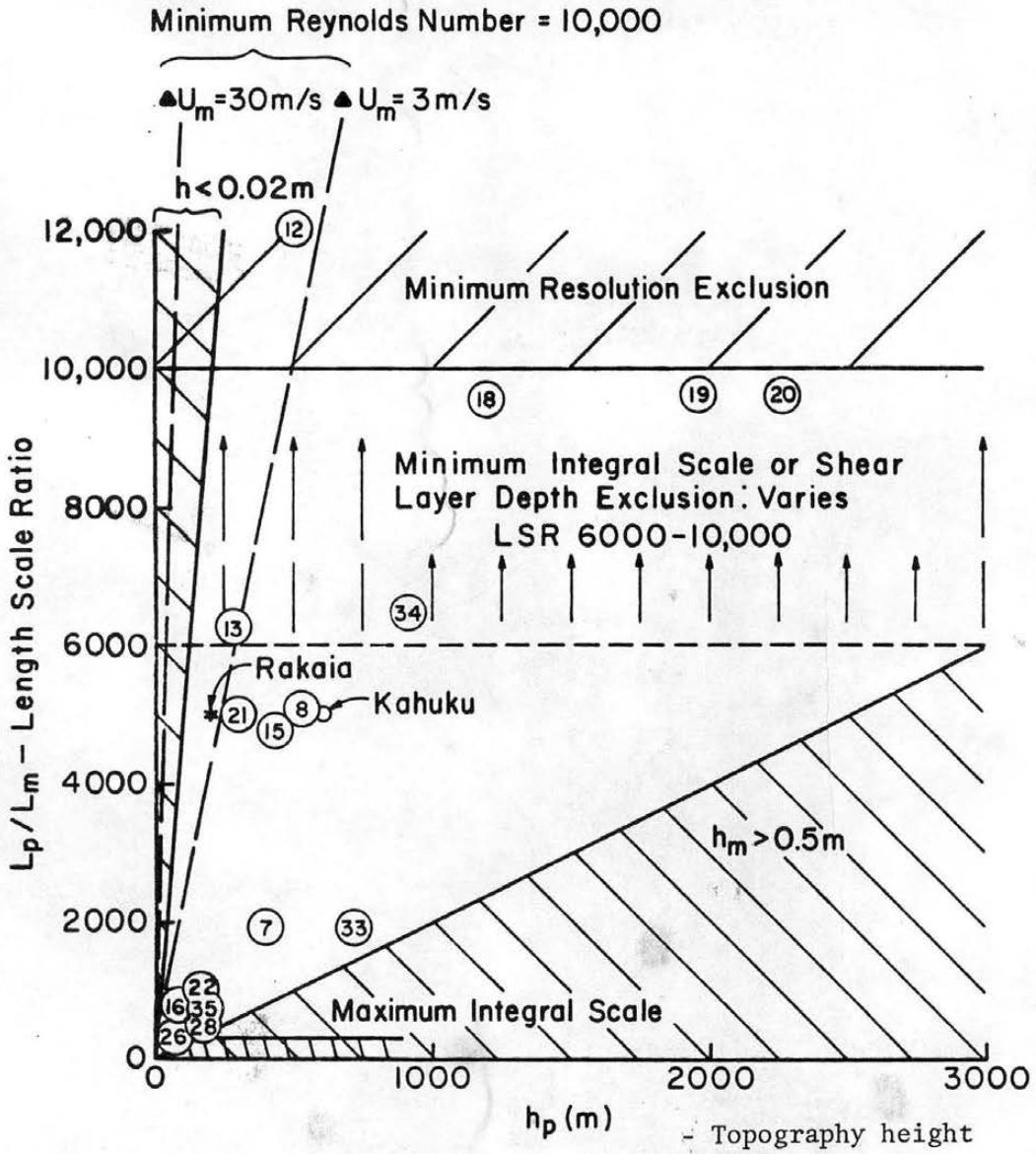


Figure 4-1. Performance envelope to simulate wind energy effects over complex terrain.

- F: FENCE
- I: 2.5 ENTRANCE CONTRACTION
- S: SCREENS
- H1: HONEYCOMB 6 cm D. x 25 cm
- H2: HONEYCOMB 1 cm D. x 7.5 cm
- G: GRID 4 cm x 2 cm BARS SPACED ~13 cm x 17 cm

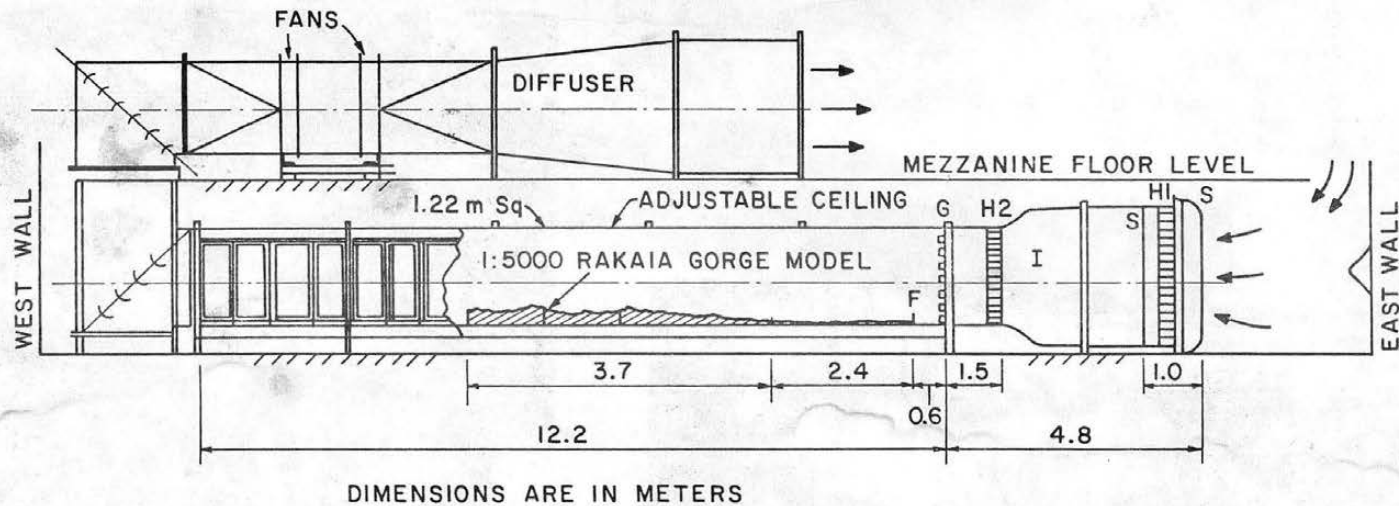
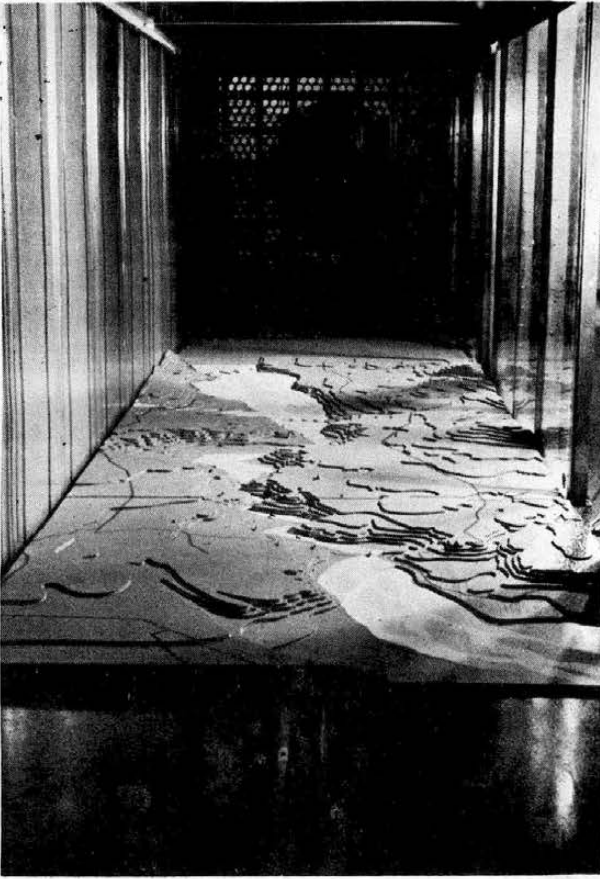


Figure 5-1. Boundary layer wind tunnel, Department of Mechanical Engineering, University of Canterbury.



Rakaia Gorge -
Terraced Model



Rakaia Gorge -
Contoured Model With
Pipe Cleaner Shelterbelts
(Polystyrene bead drifts)



Figure 5-2a Models of Rakaia River Gorge region looking northwest.





Rakaia Gorge Outlet - Mt. Hutt Range in background.



Aerial photo Rakaia River Gorge region.

Figure 5-2b Models of Rakaia River Gorge region looking northwest. (continued)

SYMBOL	z/H	H/z_0	H/Lu_x	H/δ	SHELTERBELT
□	2.50	450	0.05	0.04	YARN
○	1.25	450	0.05	0.04	$H \approx 4 \text{ mm}$
△	0.50	0.05	0.04	—————	
	0.50	40~100	0.17	—————	RAINE (1977) (WIND TUNNEL -20%)
	0.07~0.125	500	0.10~0.13	—————	STURROCK (1971) (FIELD)

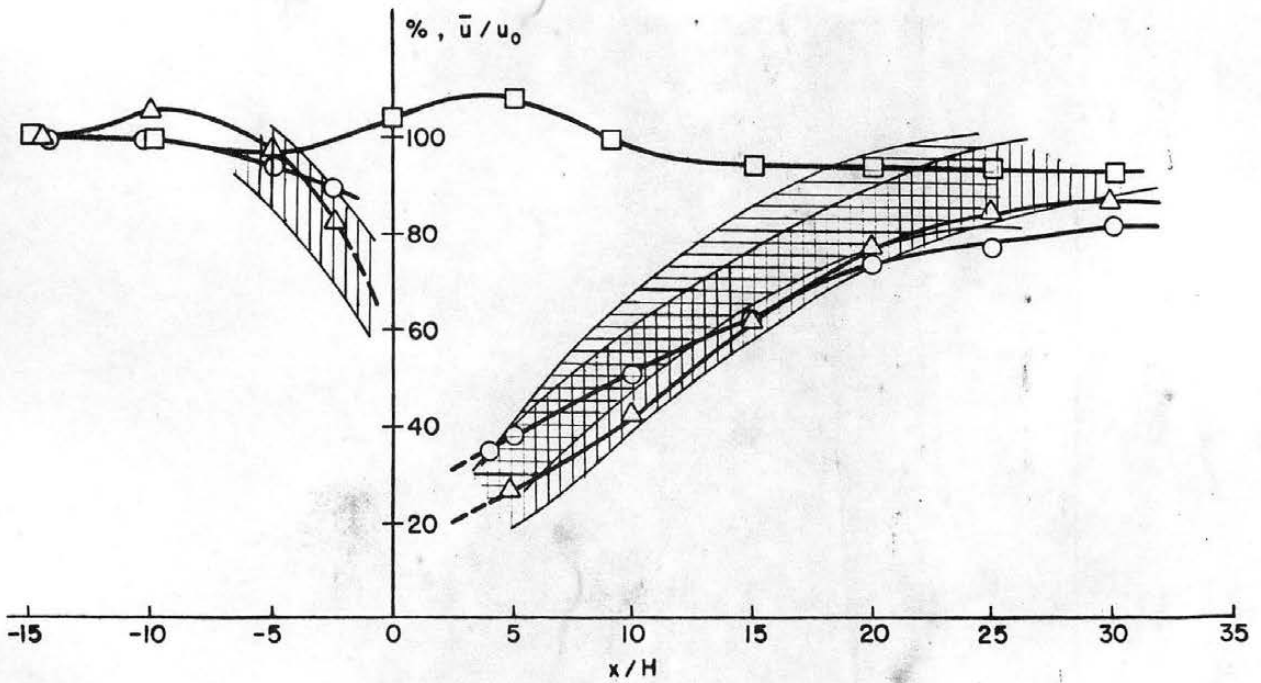




Figure 5-3. Comparison of horizontal u/u_0 profiles for yarn shelterbelts with data in the literature.

SYMBOL	z/H	H/z_0	H/Lu_x	H/δ	SHELTERBELT
□	2.50	450	0.05	0.04	PIPE CLEANERS
○	1.25	450	0.05	0.04	$H \approx 4\text{mm}$
△	0.50	0.05	0.04	—————	
	0.50	75 → 500	0.17	—————	RAINE (1977) (WIND TUNNEL -0%)
	0.07 → 0.125	500	0.10 → 0.13	—————	STURROCK (1971) (FIELD)

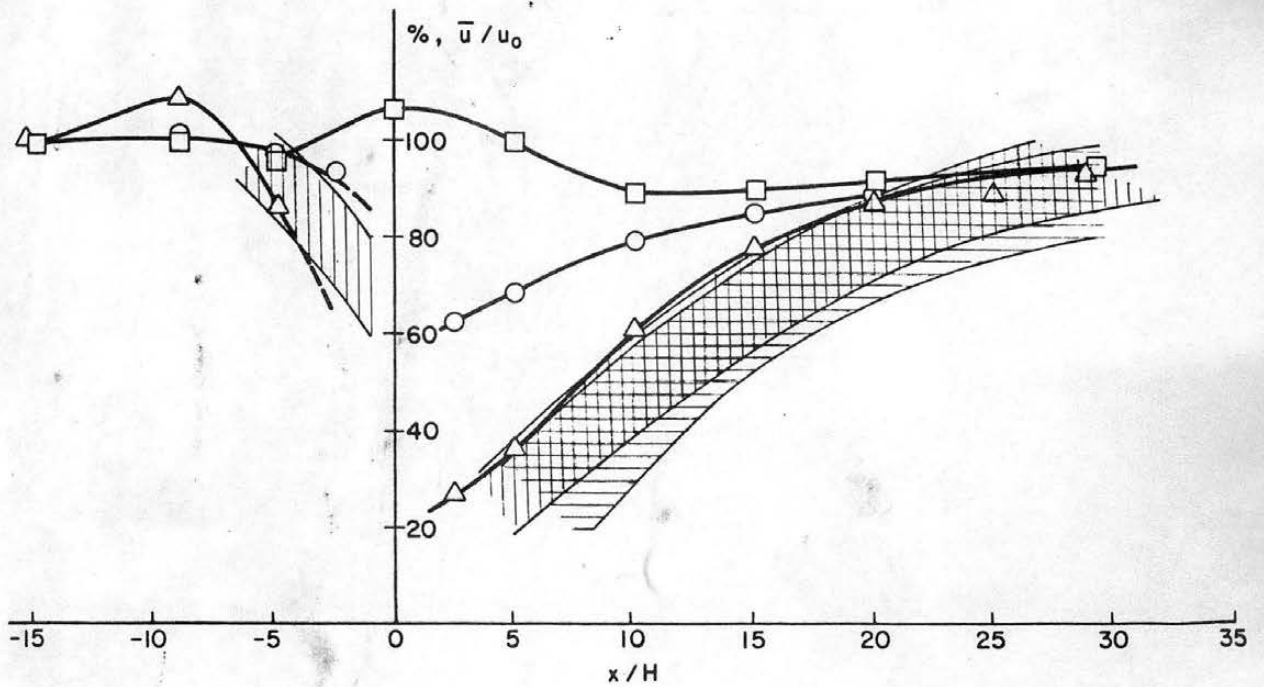


Figure 5-4. Comparison of horizontal u/u_0 profiles for pipe cleaner shelterbelts with data in the literature.

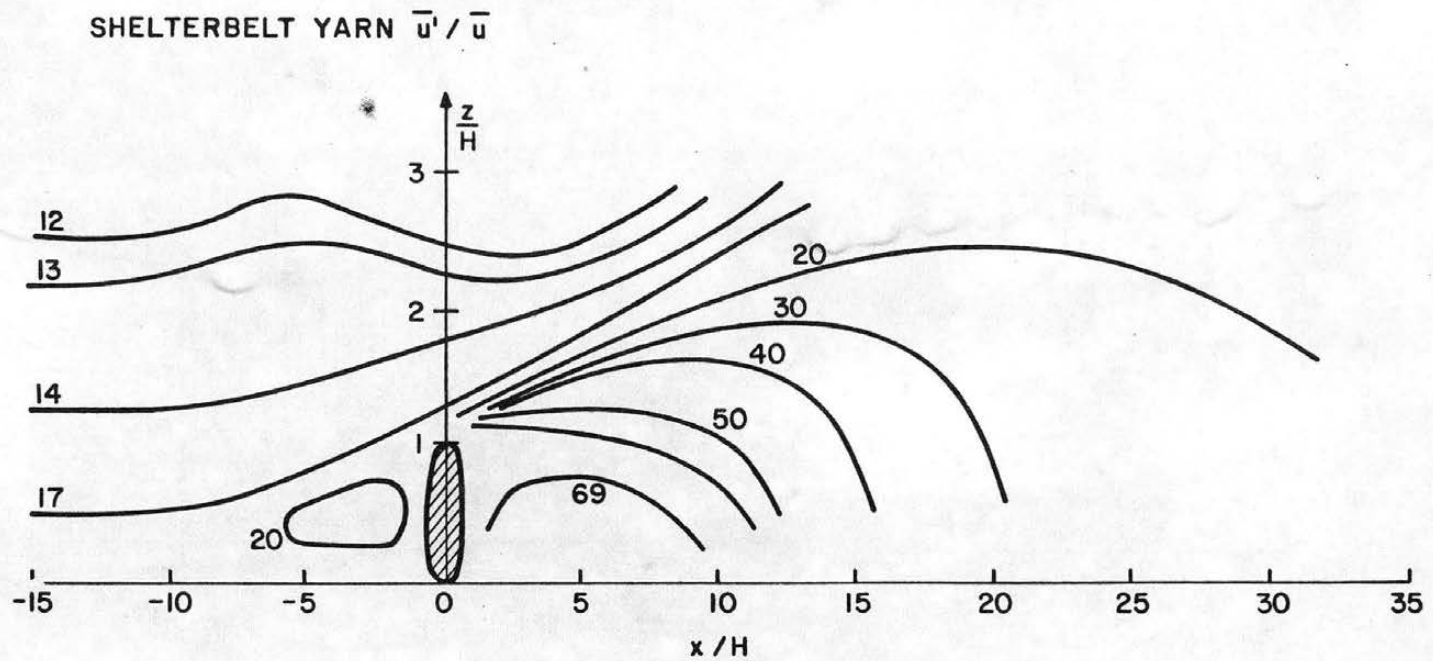


Figure 5-5. Isoturbs for yarn shelterbelts.

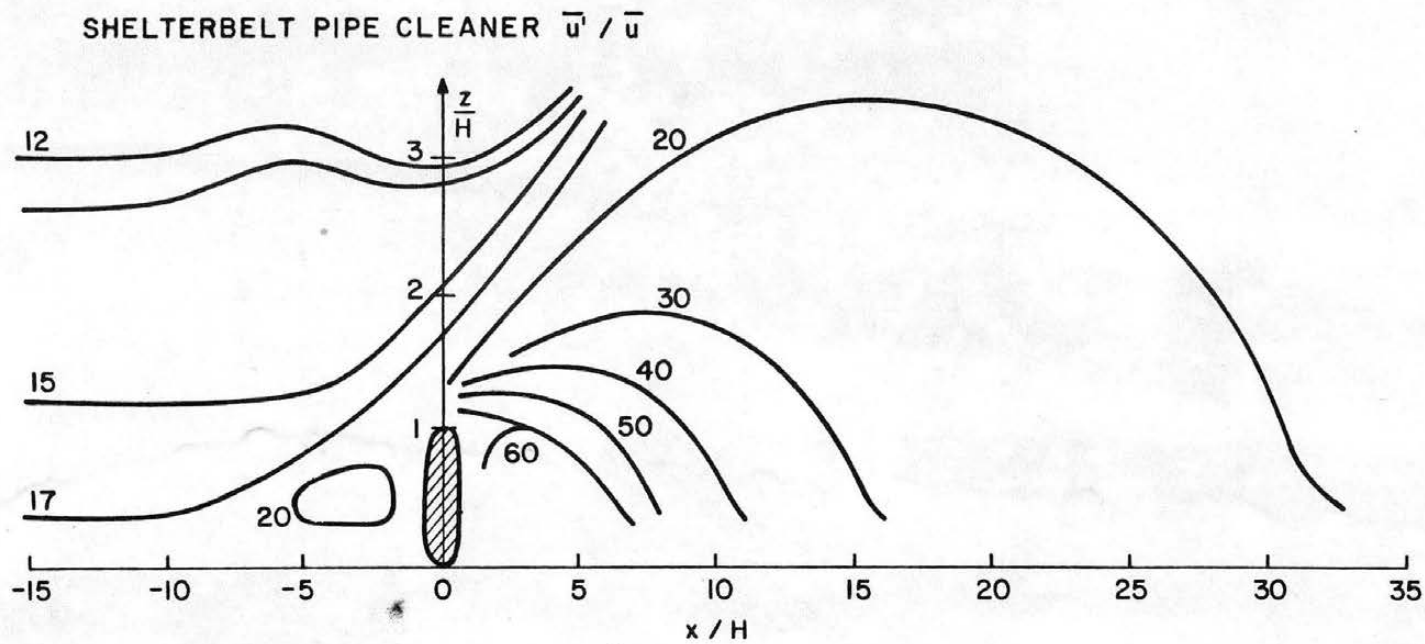


Figure 5-6. Isotherms for pipe cleaner shelterbelts.

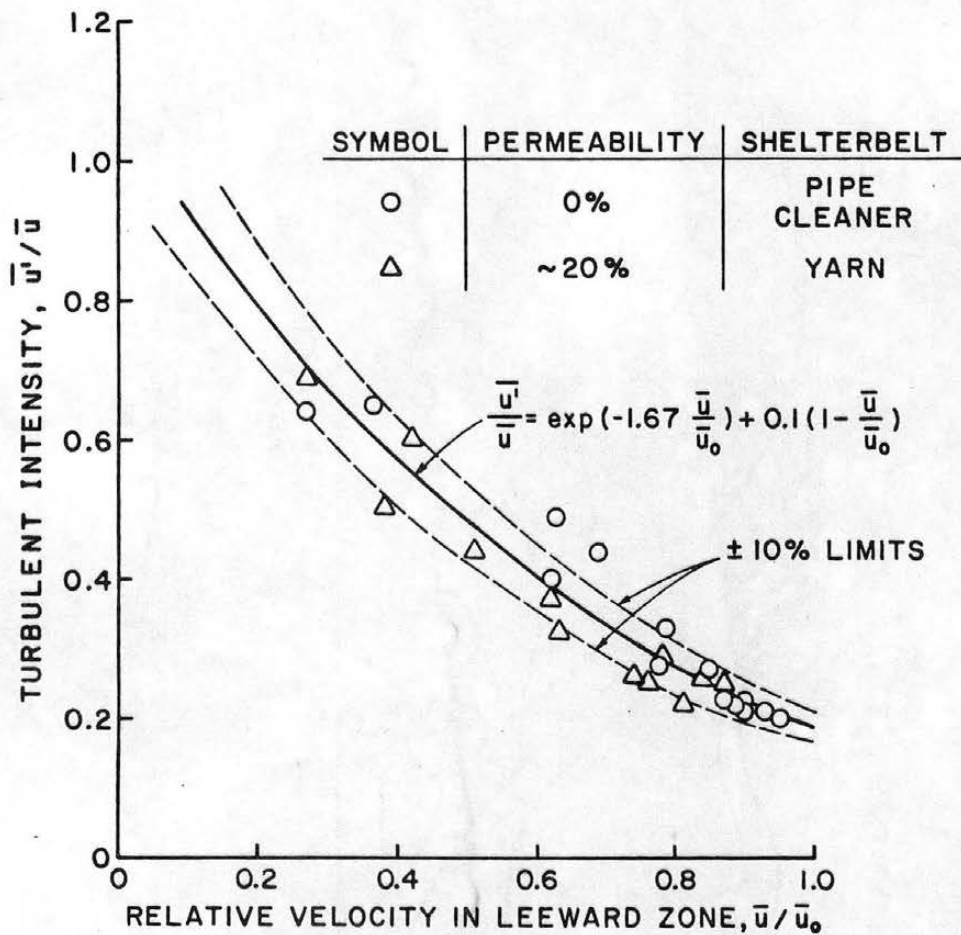


Figure 5-7. Correlation of turbulent intensity and relative velocity behind model shelterbelts.

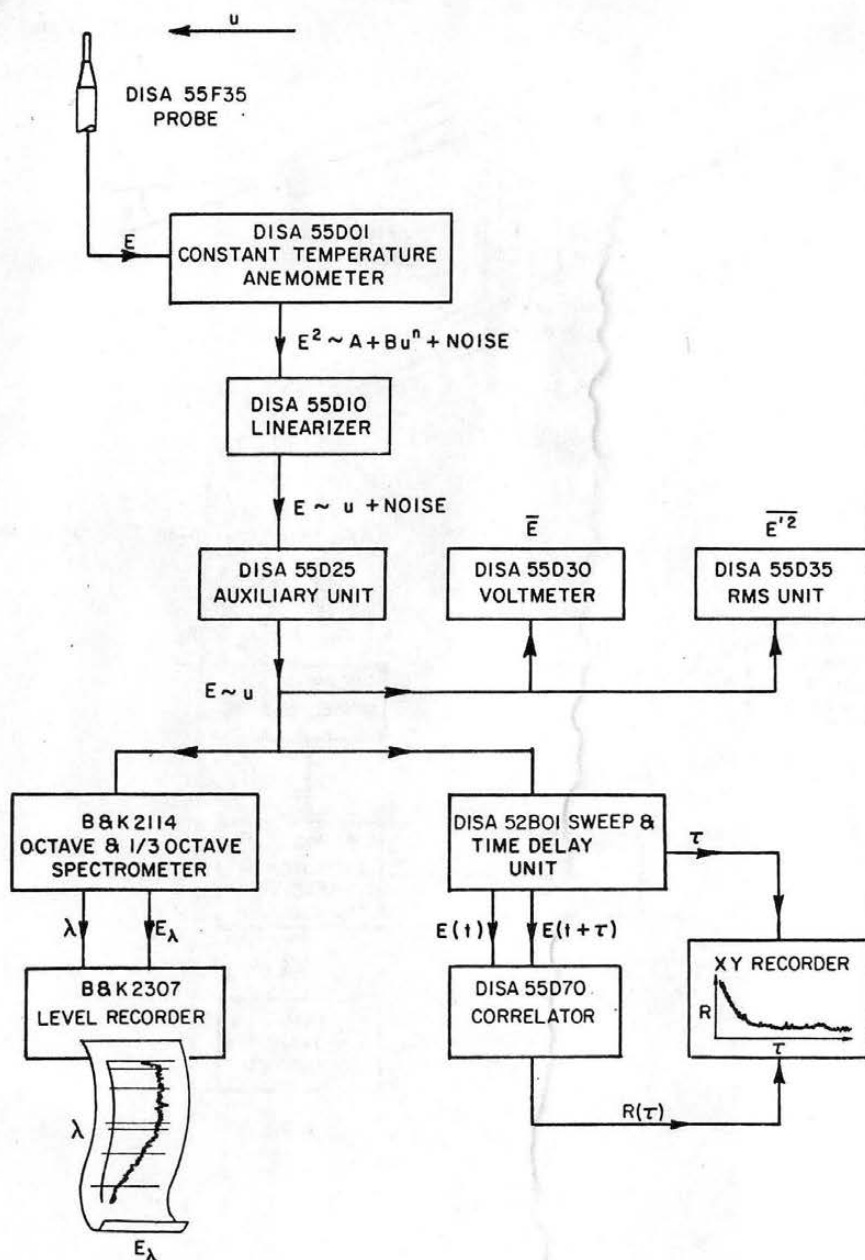


Figure 5-8. Block diagram of velocity and turbulence measurement instrumentation.

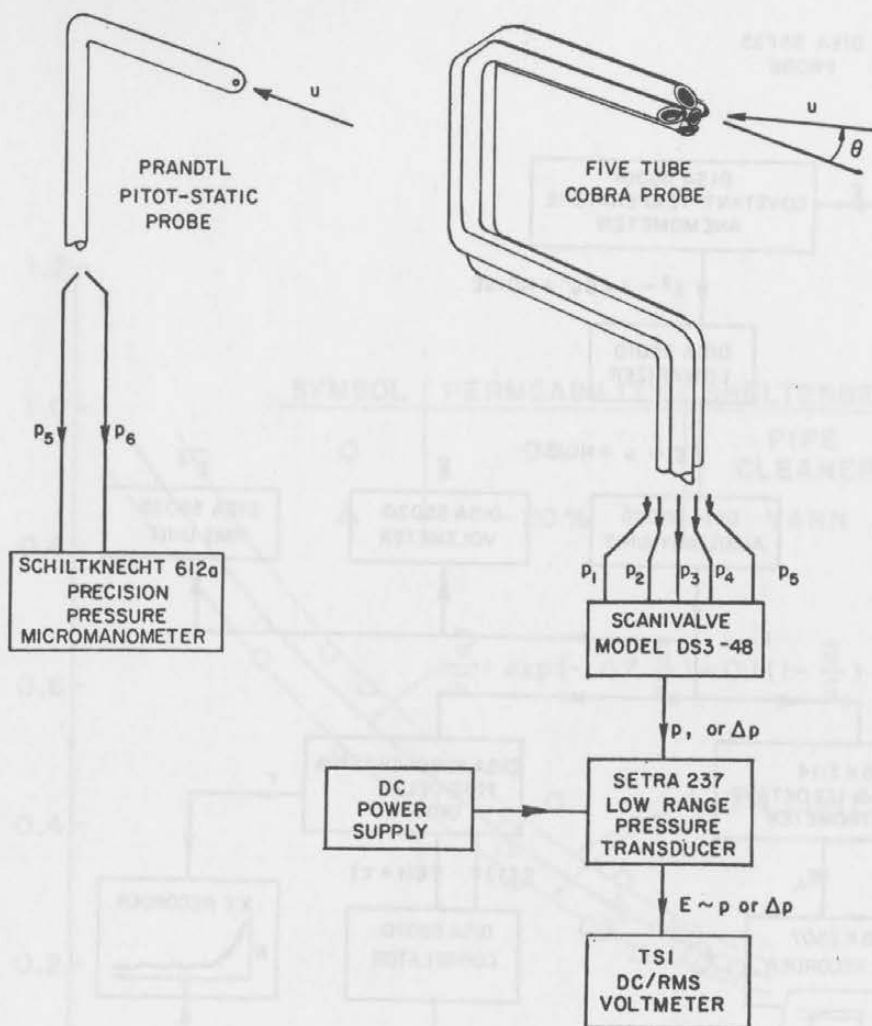


Figure 5-9. Block diagram of pressure probe equipment and associated electronics.

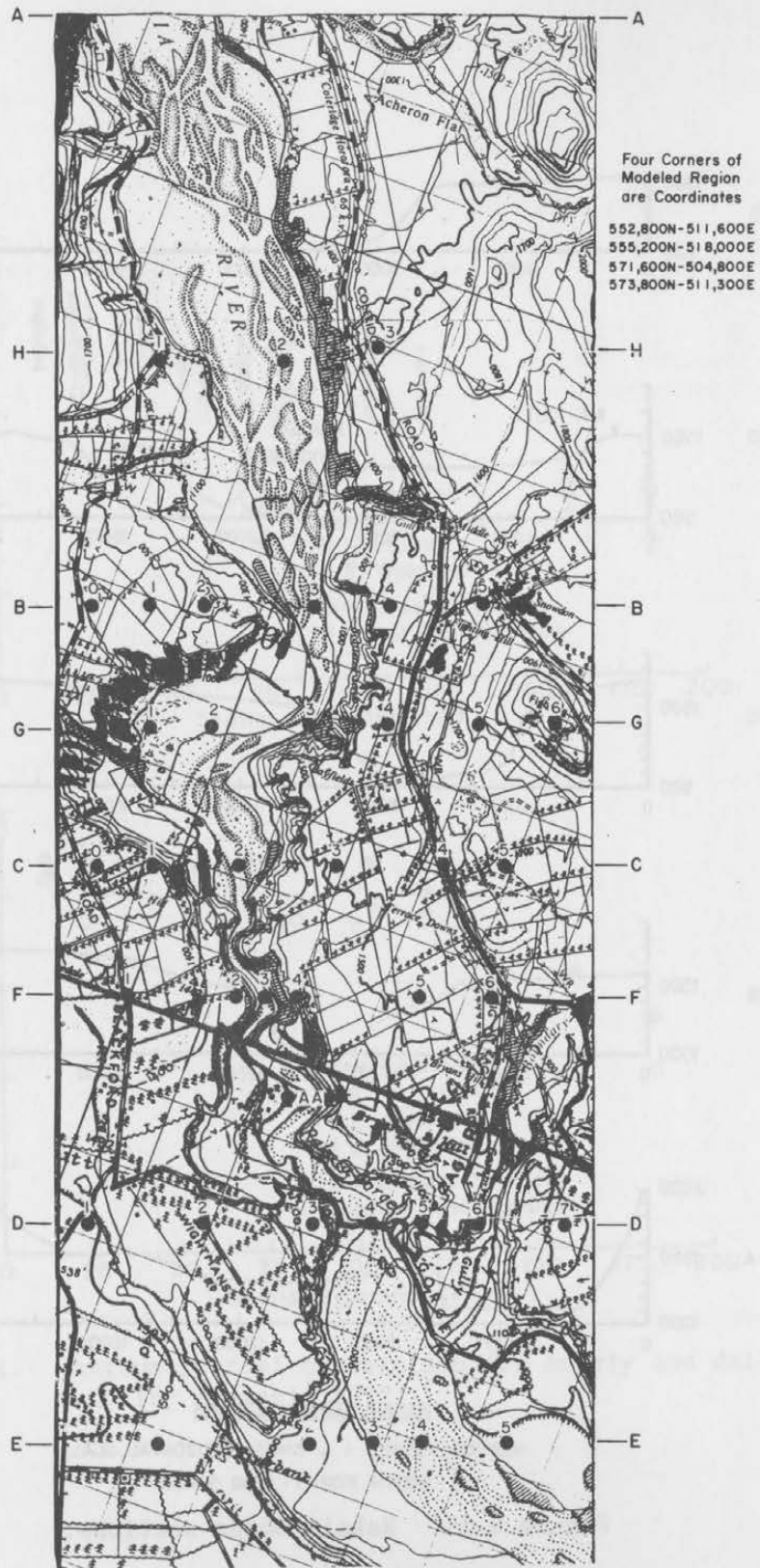
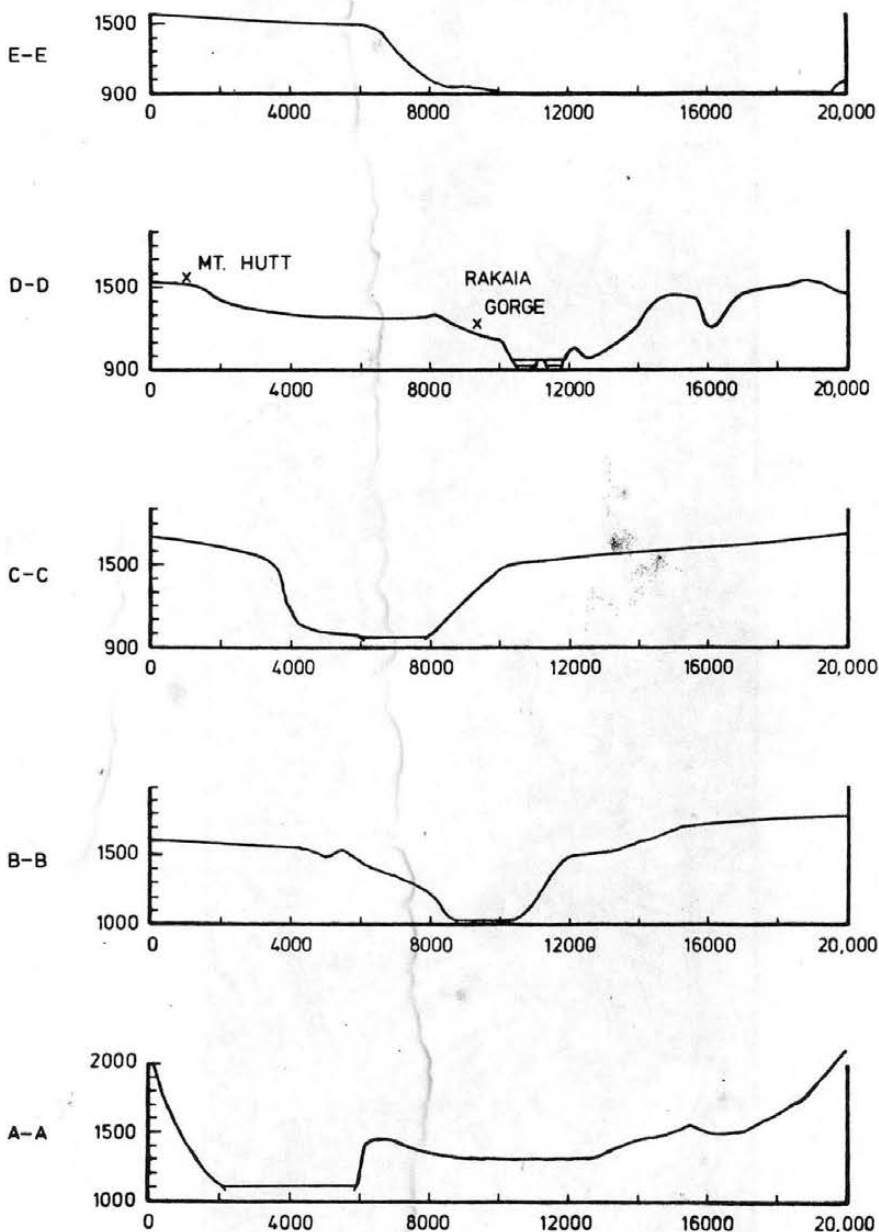


Figure 5-10. Rakaia Gorge region terrain modeled and associated survey locations.



RAKAIA GORGE SECTIONS

VERTICAL SCALE = 4 TIMES HORIZONTAL SCALE

WIDTH FOR 1:5000 SCALE

Figure 5-11. Rakaia Gorge sections.

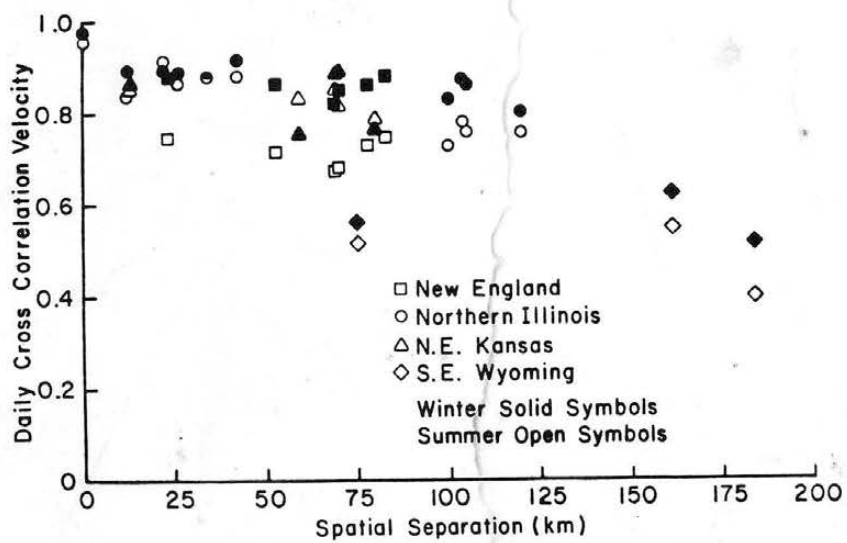
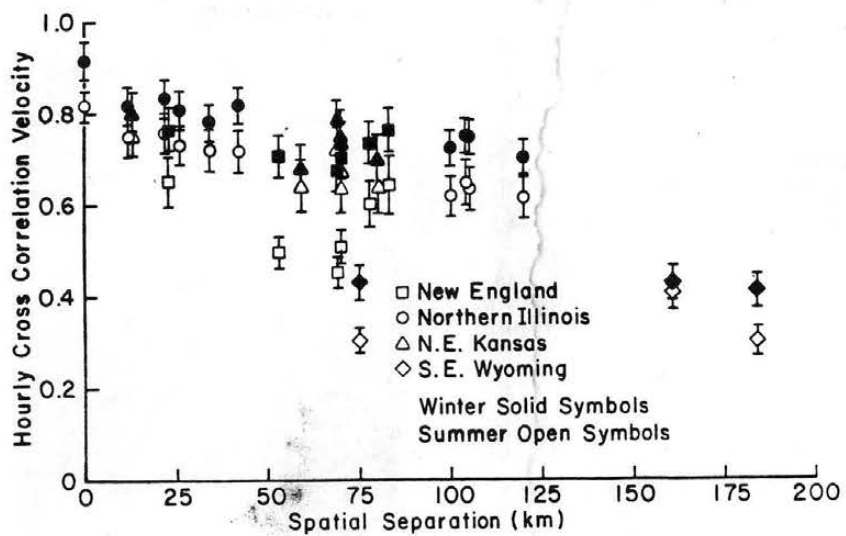


Figure 6-1. Maximum spatial correlation for hourly and daily velocity (Corotis 1977).

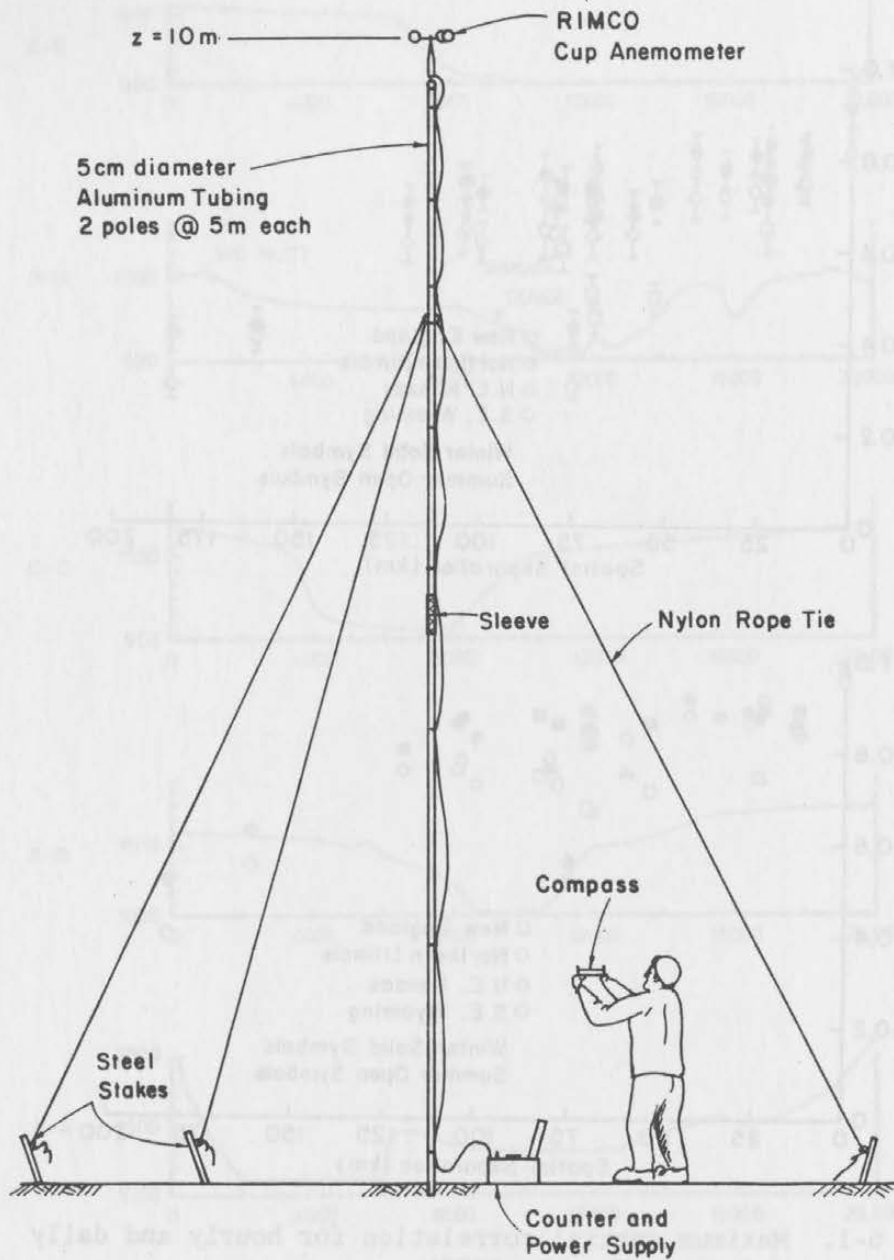
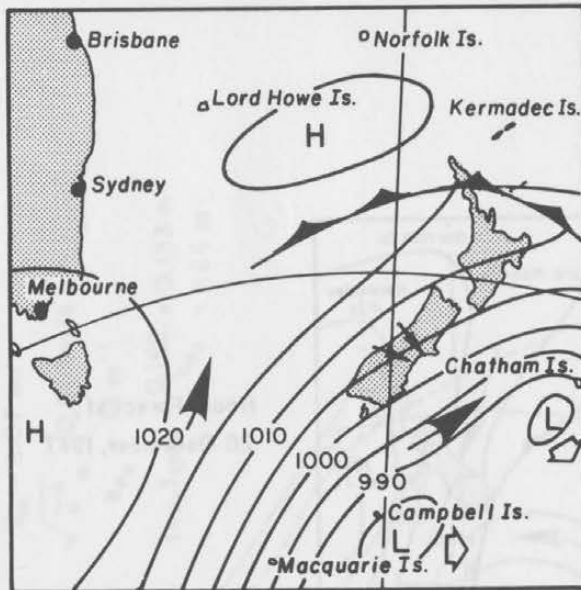
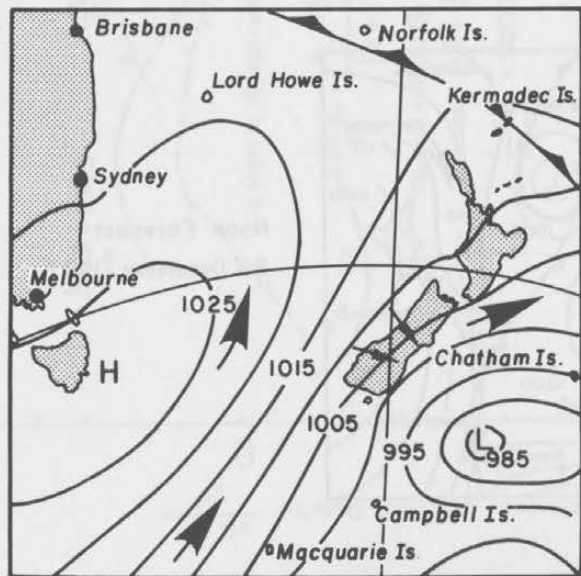


Figure 6-2. Portable tower and anemometer
Rakaia River Gorge field experiment.

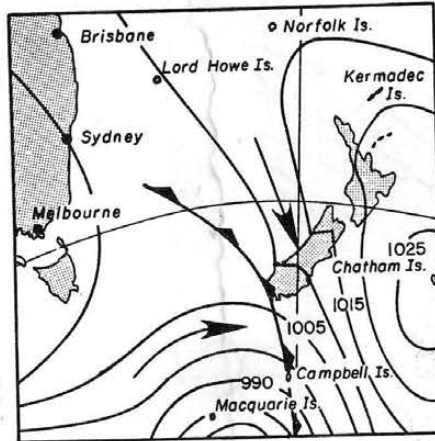


Noon Forecast
24 November, 1977

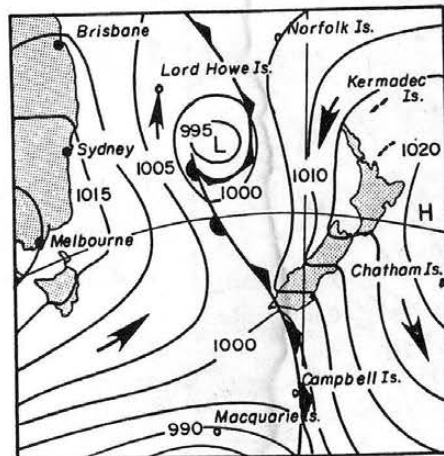


Noon Forecast
25 November, 1977

Figure 6-3. Synoptic forecast - November 24-25, 1977.
(Full arrows are winds aloft.)



Noon Forecast,
28 December, 1977



Noon Forecast
29 December, 1977

Figure 6-4. Synoptic forecast - December 28-29, 1977.
(Full arrows are winds aloft.)

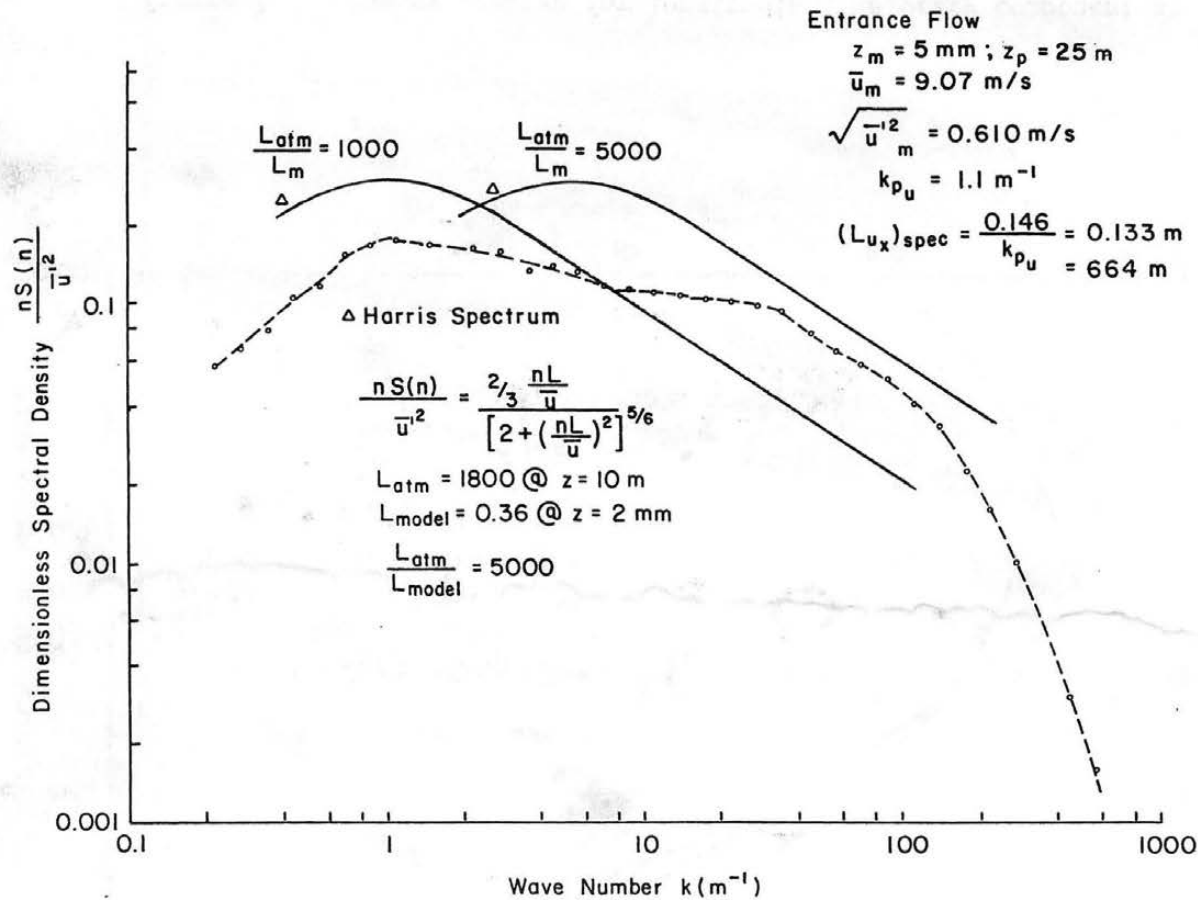


Figure 7-1. Energy spectra for longitudinal velocity component at forward section, $z_p = 10 \text{ m}$.

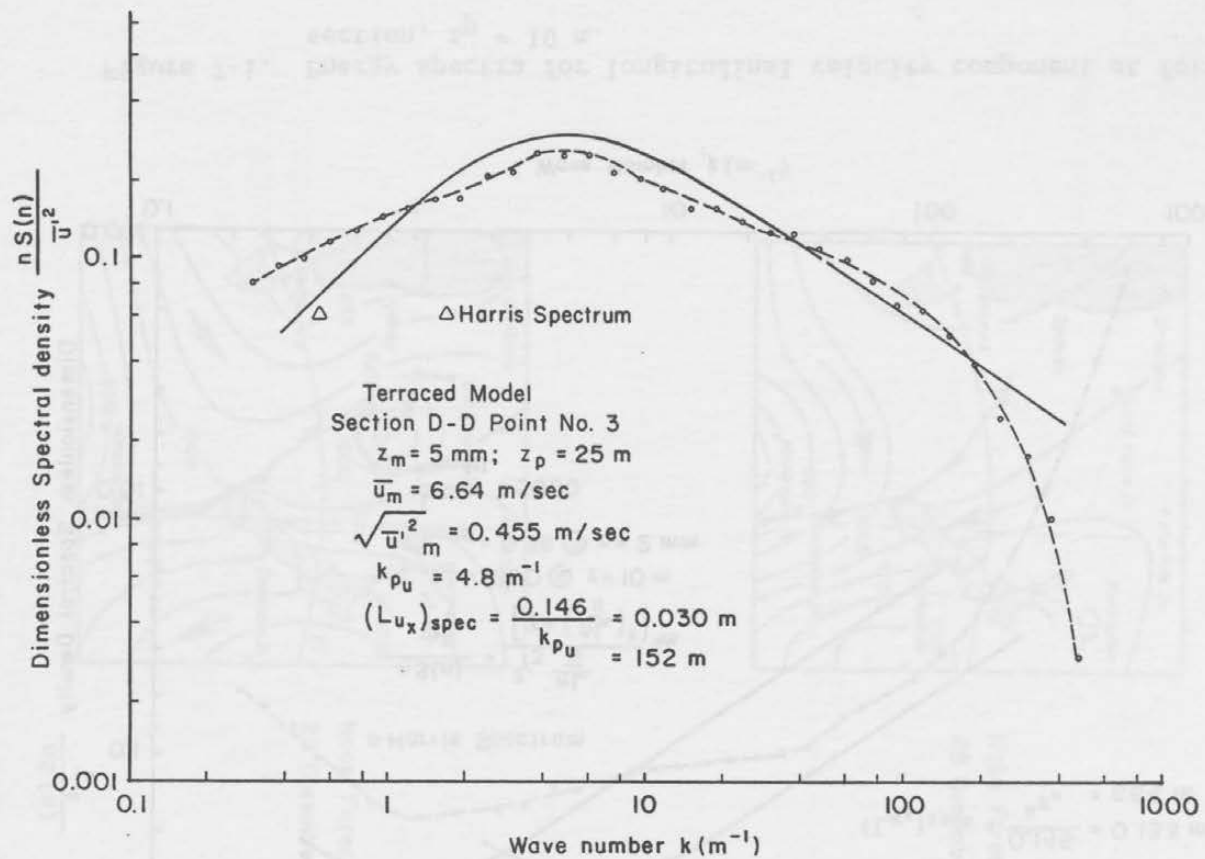


Figure 7-2. Energy spectra for longitudinal velocity component at section D-3, terraced model, $z_p = 10 \text{ m}$.

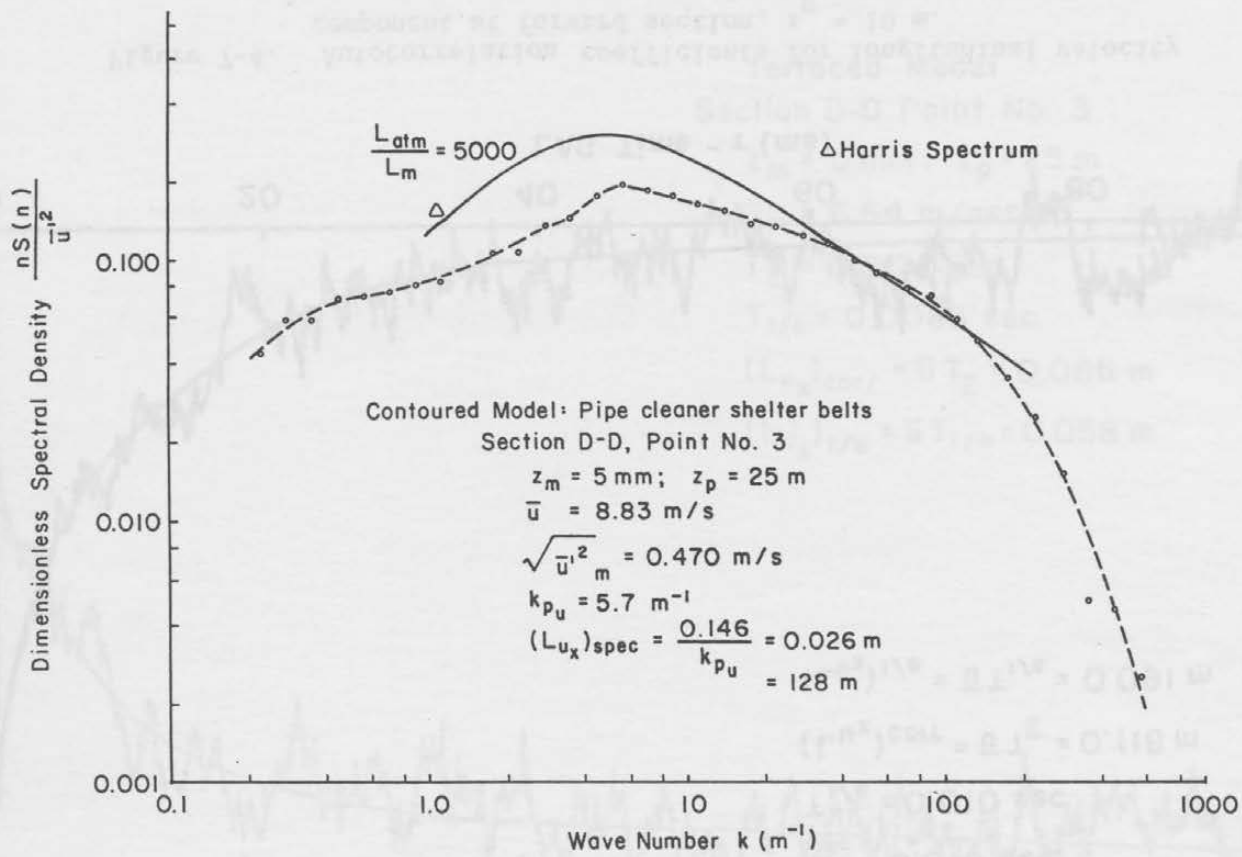


Figure 7-3. Energy spectra for longitudinal velocity component at section D-3, contoured model, $z_p = 10 \text{ m}$.

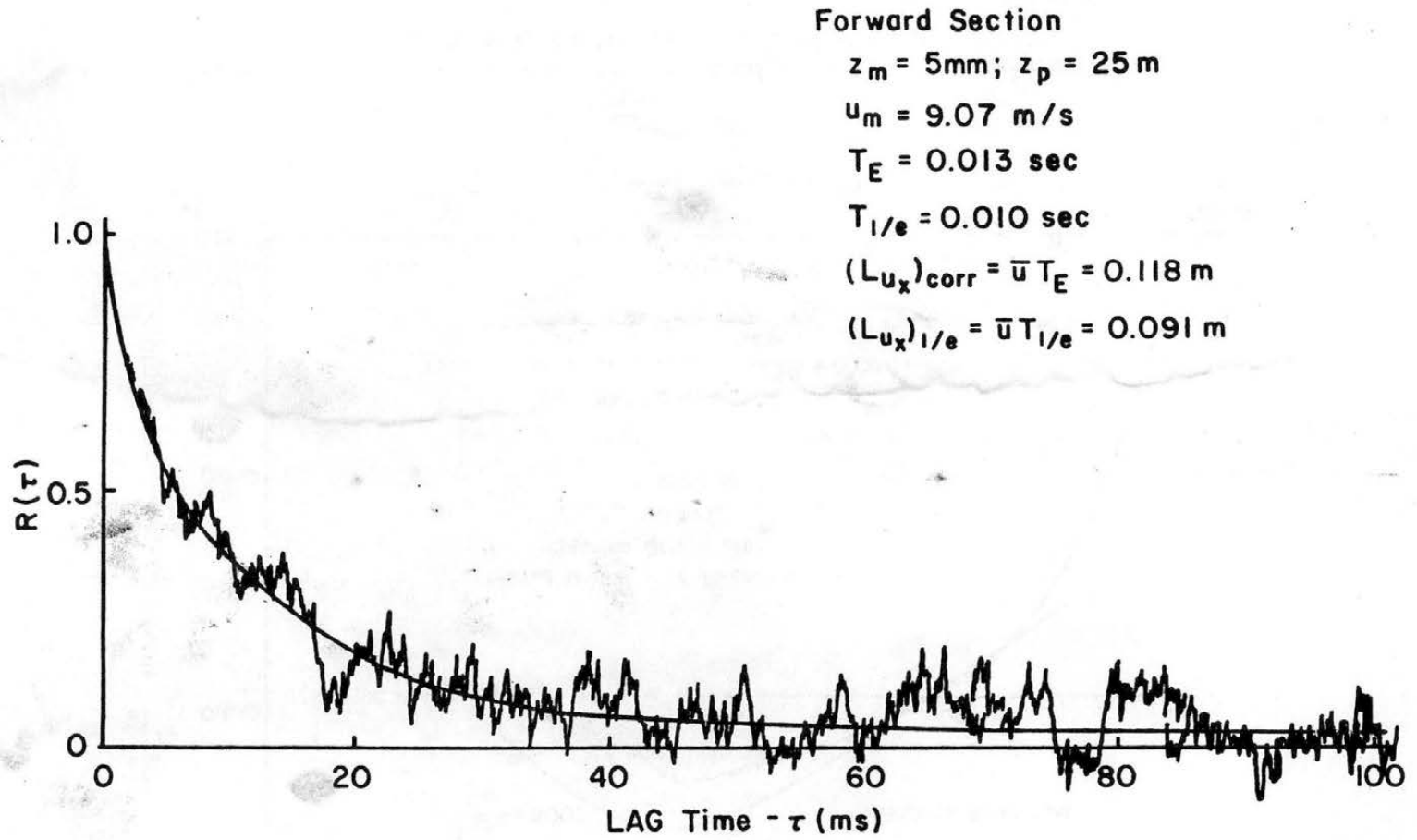


Figure 7-4. Autocorrelation coefficients for longitudinal velocity component at forward section, $z_p = 10\text{ m}$.

Terraced Model
Section D-D Point No. 3

$$z_m = 5 \text{ mm}, z_p = 25 \text{ m}$$

$$\bar{u}_m = 6.64 \text{ m/sec}$$

$$T_E = 0.0130 \text{ sec}$$

$$T_{1/e} = 0.0088 \text{ sec}$$

$$(L_{u_x})_{\text{corr}} = \bar{u} T_E = 0.086 \text{ m}$$

$$(L_{u_x})_{1/e} = \bar{u} T_{1/e} = 0.058 \text{ m}$$

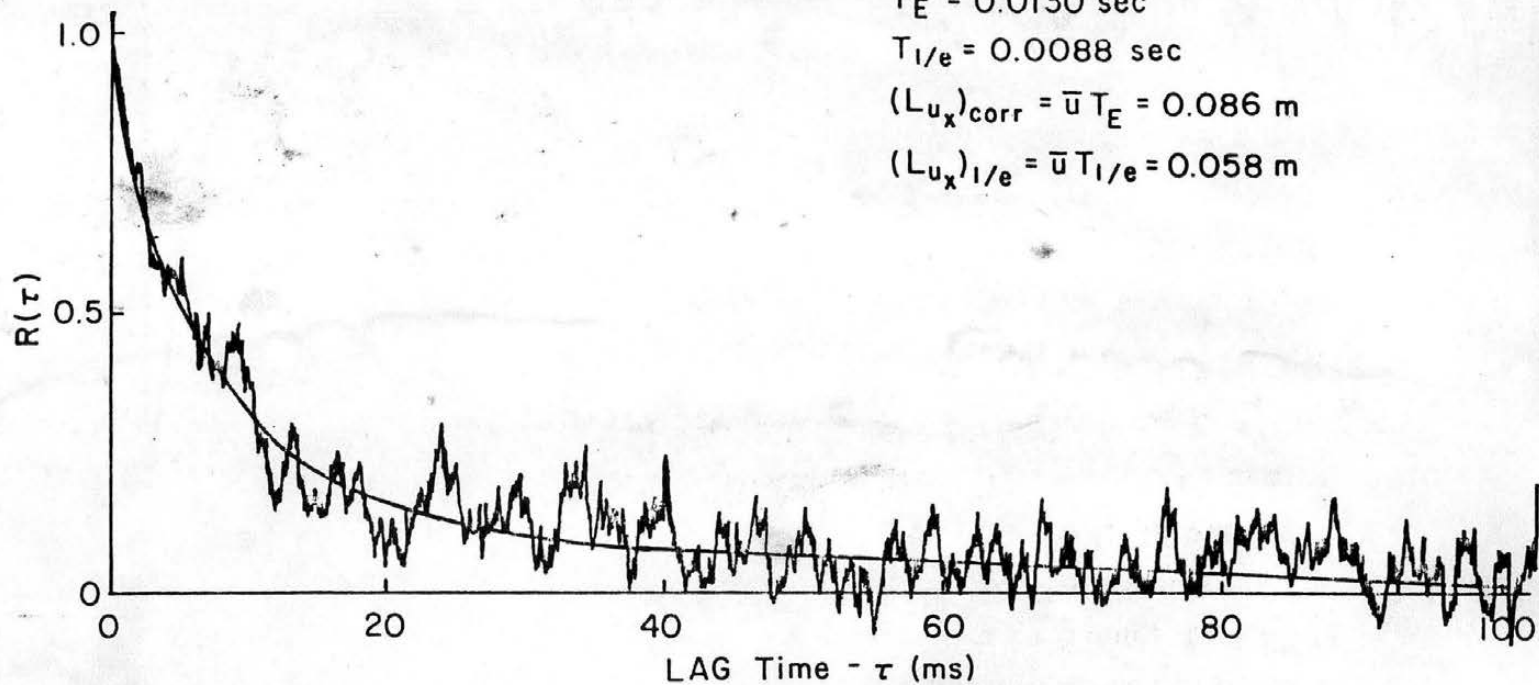


Figure 7-5. Autocorrelation coefficients for longitudinal velocity component at section D-3, terraced model, $z_p = 10 \text{ m}$.

Contoured Model: Pipe cleaner shelter belts

Section D-D Point No. 3

$$z_m = 5 \text{ m} ; z_p = 25 \text{ m}$$

$$\bar{u}_m = 8.83 \text{ m/s}$$

$$T_E = 0.0146 \text{ sec}$$

$$T_{1/e} = 0.0043 \text{ sec}$$

$$(L_{u_x})_{\text{corr}} = \bar{u} T_E = 0.129 \text{ m}$$

$$(L_{u_x})_{1/e} = \bar{u} T_{1/e} = 0.038 \text{ m}$$

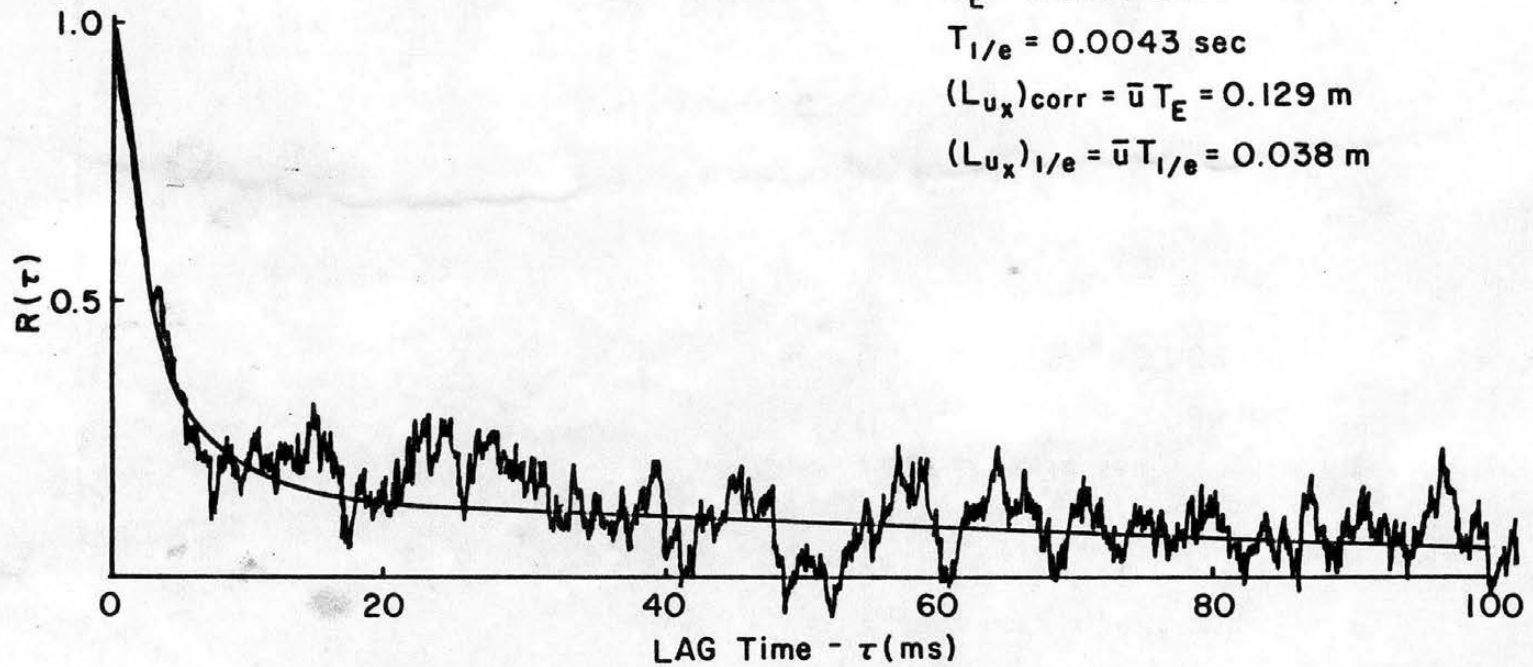


Figure 7-6. Autocorrelation coefficients for longitudinal velocity component at section D-3, contoured model, $z_p = 10 \text{ m}$.

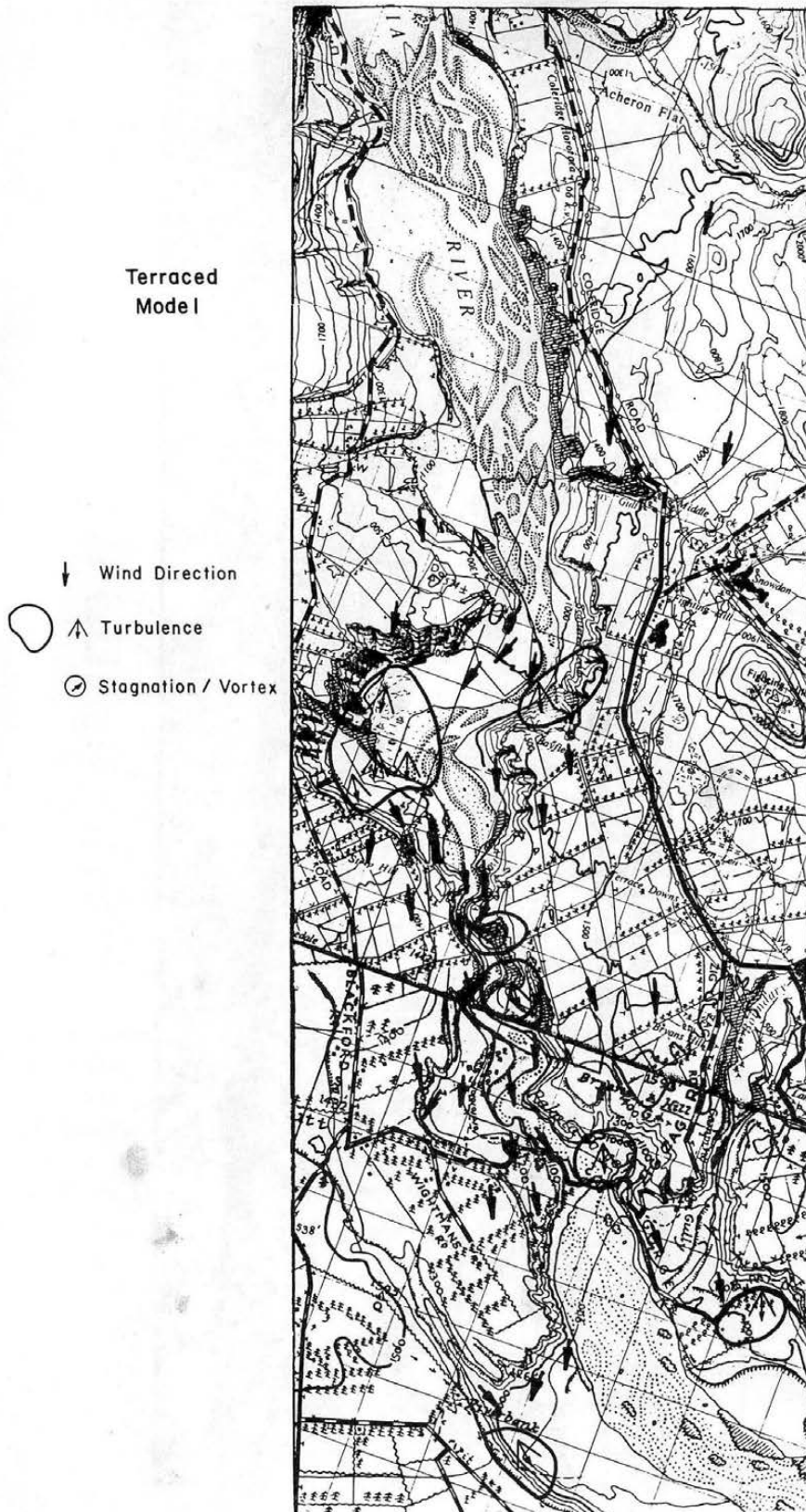


Figure 7-7. Miniature flag direction behavior, terraced model.

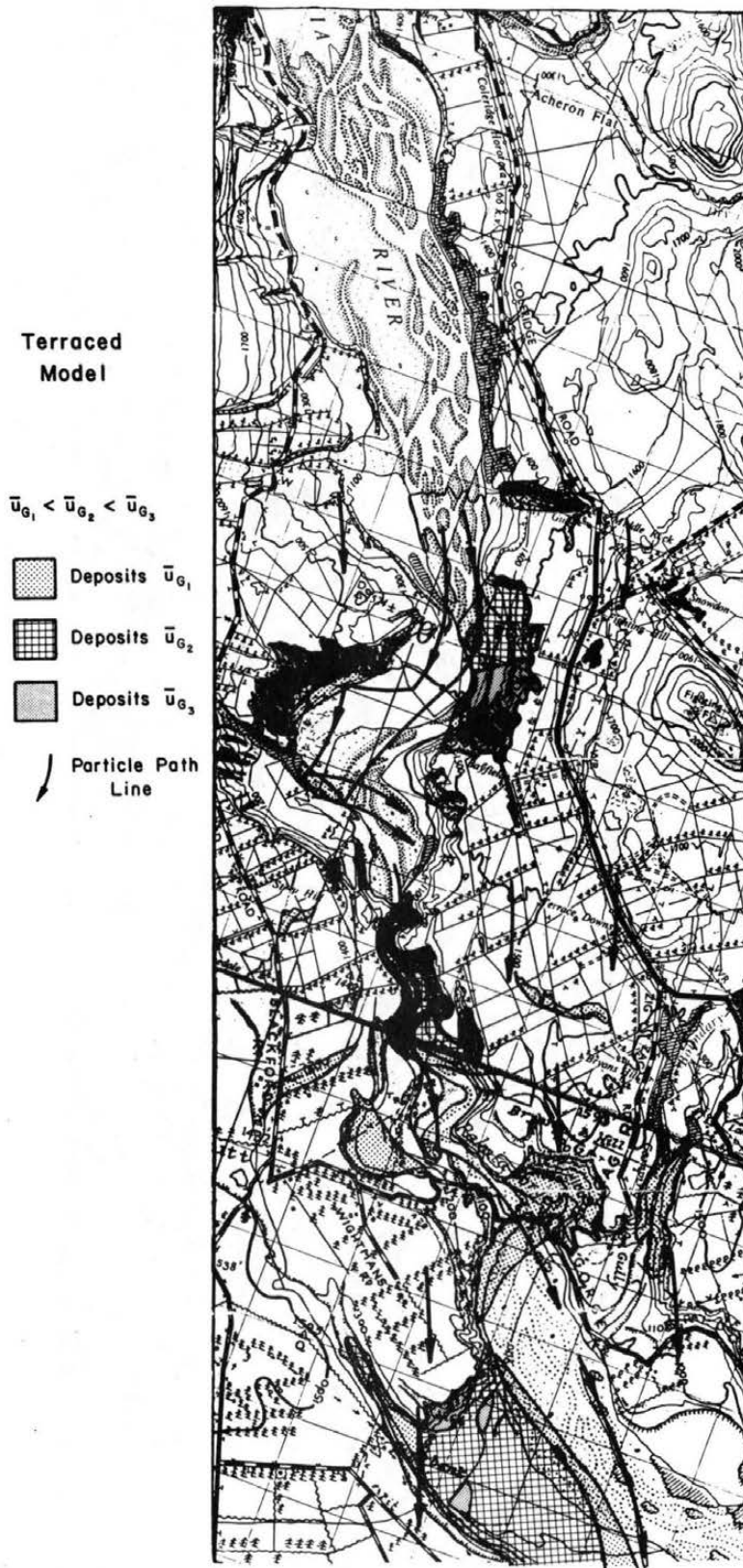
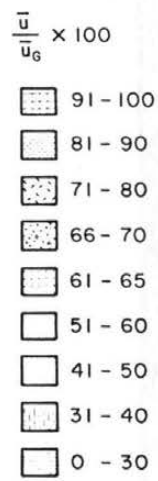


Figure 7-8. Polystyrene bead trajectory and deposition diagram, terraced model.

Terraced Model
z = 10 m



Values Calculated
Via Power Law
and Log Law
Extrapolation
from z = 25 and
50 m Heights



Figure 7-9. Horizontal isotachs, terraced model, $z_p = 10$ m.

Terraced
Model

$z = 50 \text{ m}$

$\frac{u}{u_0} \times 100$

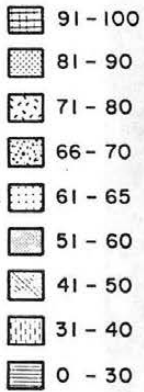


Figure 7-10. Horizontal isotachs, terraced model, $z_p = 25 \text{ m}$.

Terraced
Model
 $z = 25 \text{ m}$

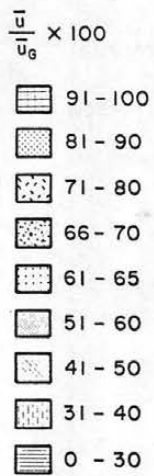


Figure 7-11. Horizontal isotachs, terraced model, $z_p = 50 \text{ m}$.

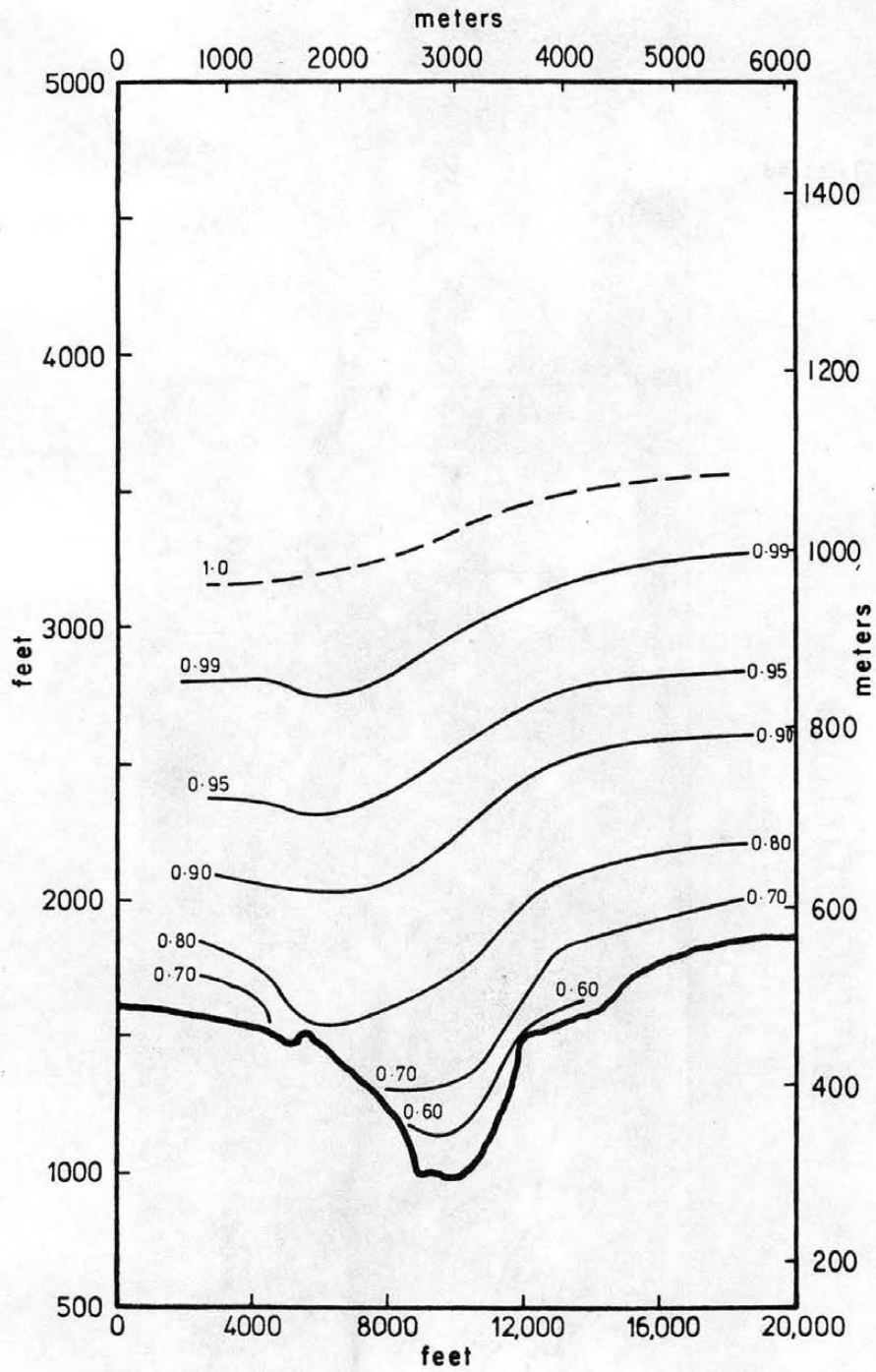


Figure 7-12. Vertical section B-B isotachs, terraced model.

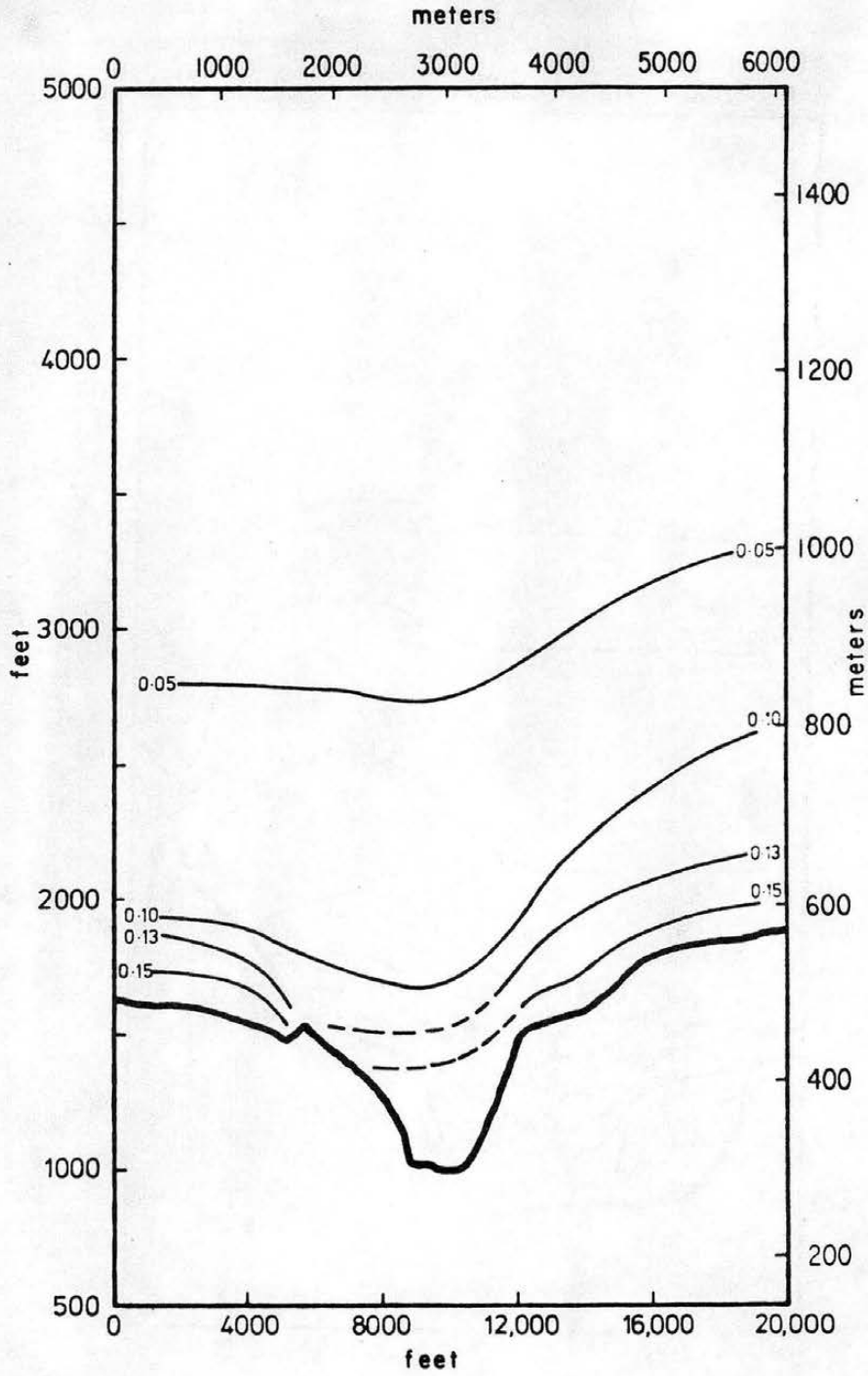


Figure 7-13. Vertical section B-B isoturbs, terraced model.

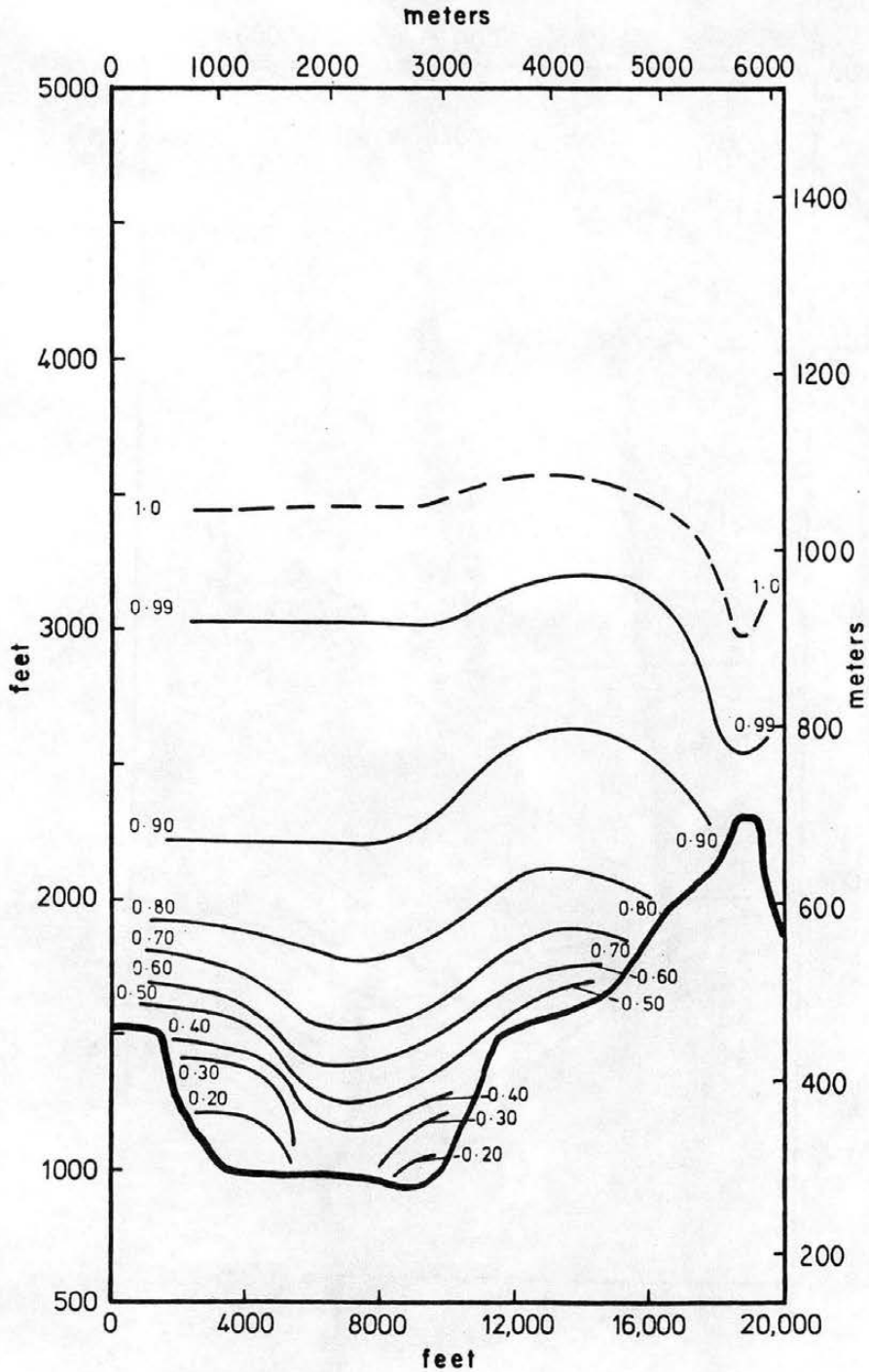


Figure 7-14. Vertical section G-G isotachs, terraced model.

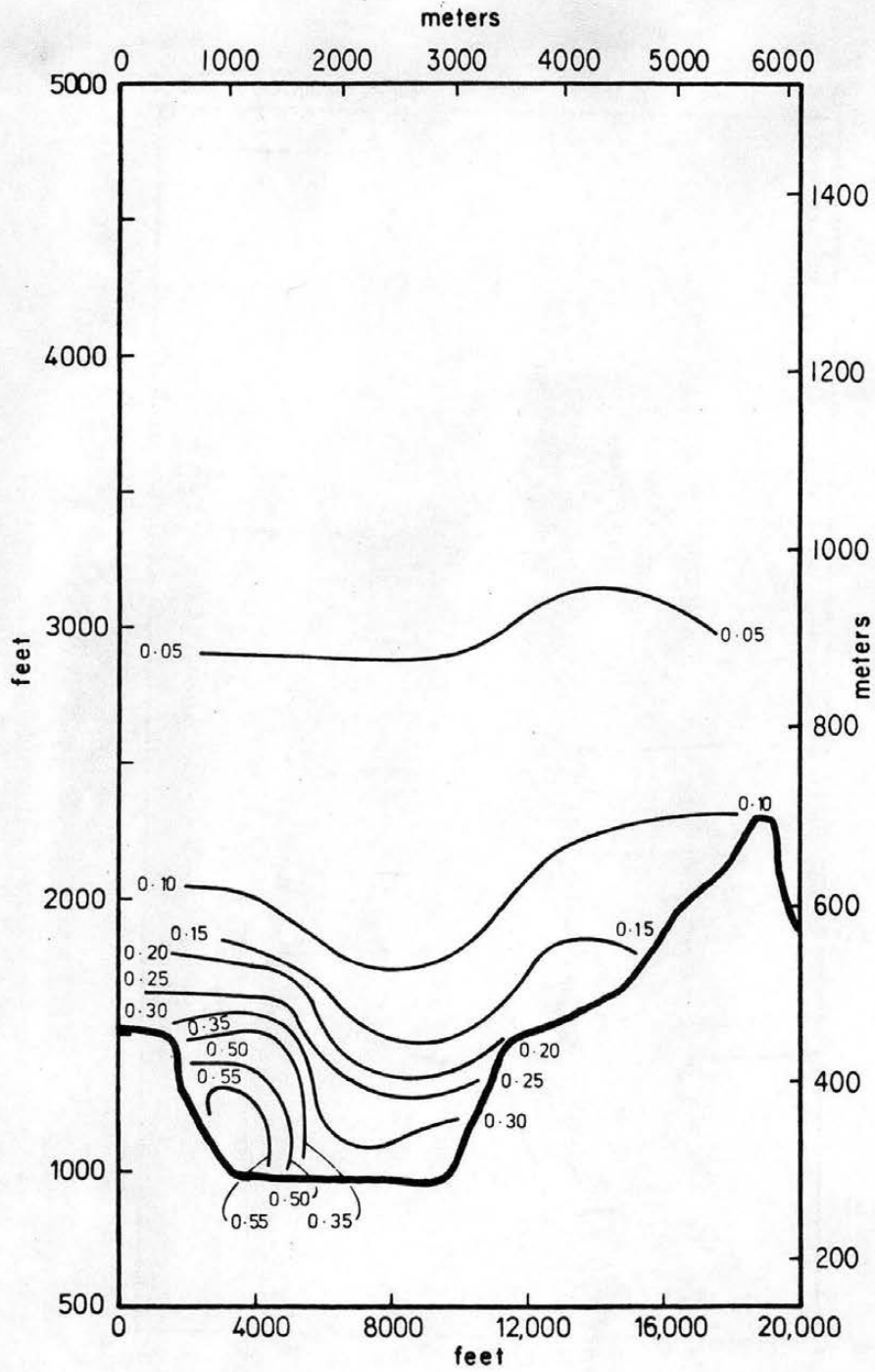


Figure 7-15. Vertical section G-G isoturbs, terraced model.

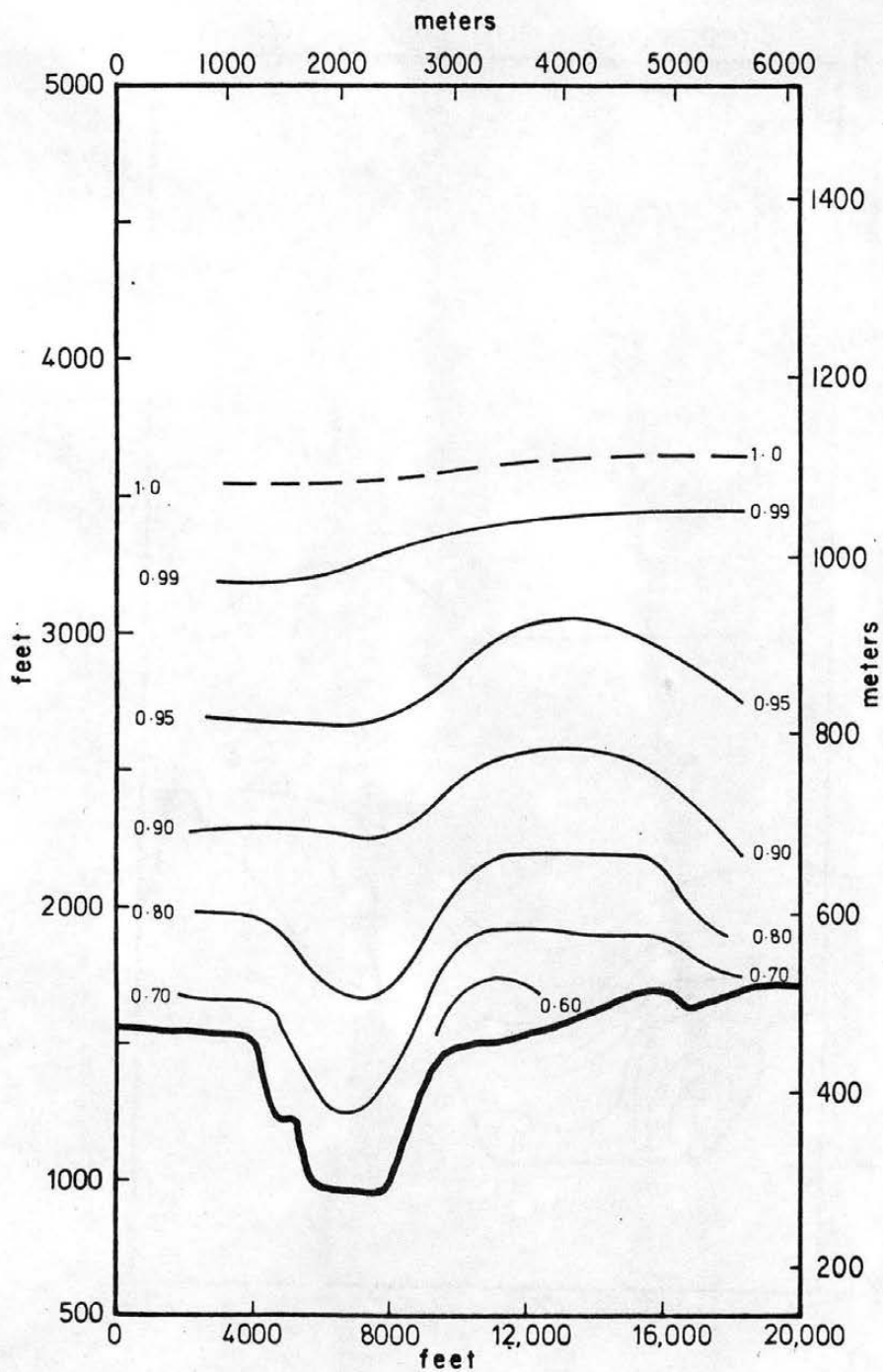


Figure 7-16. Vertical section C-C isotachs, terraced model.

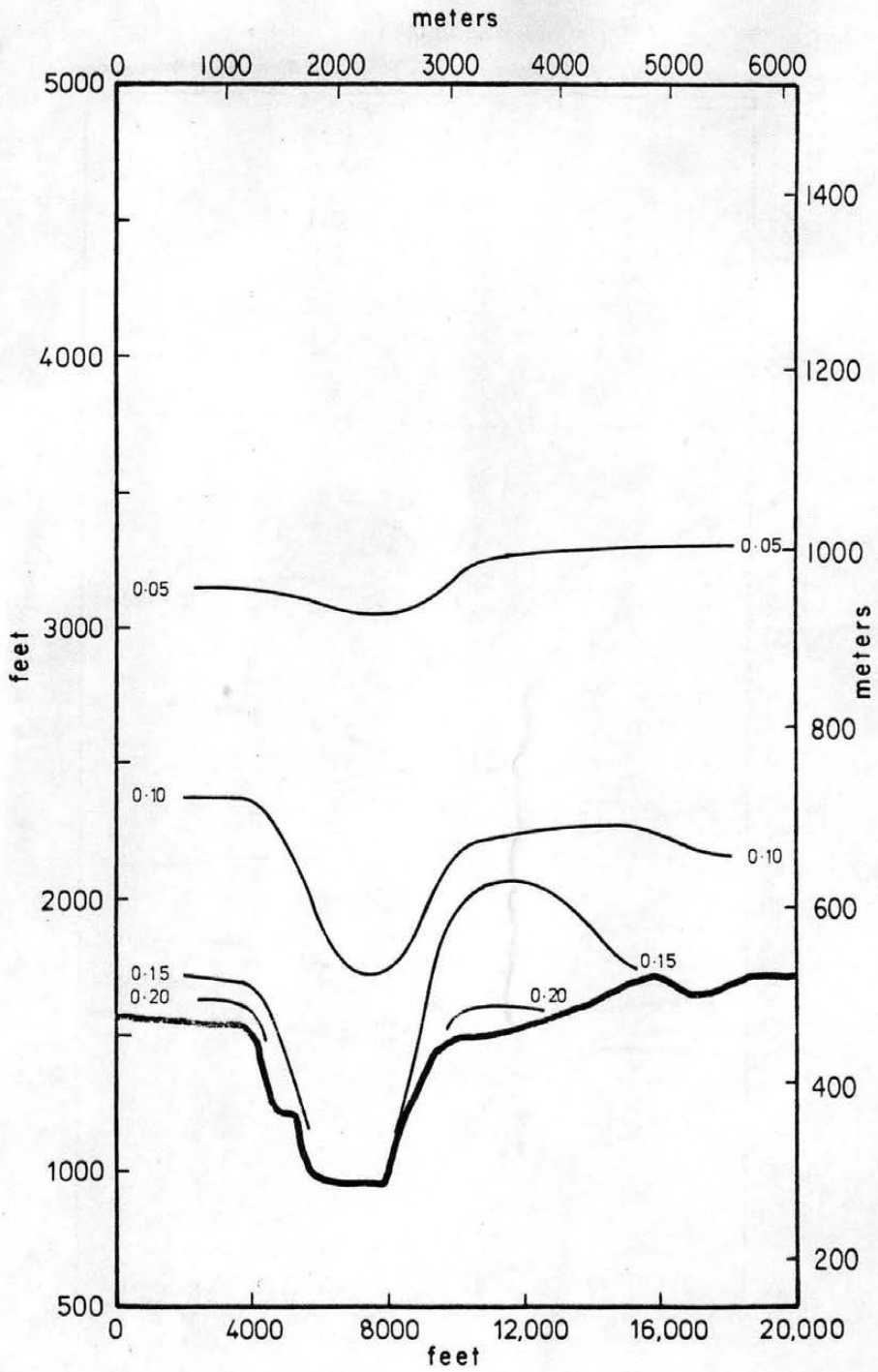


Figure 7-17. Vertical section C-C isoturbs, terraced model.

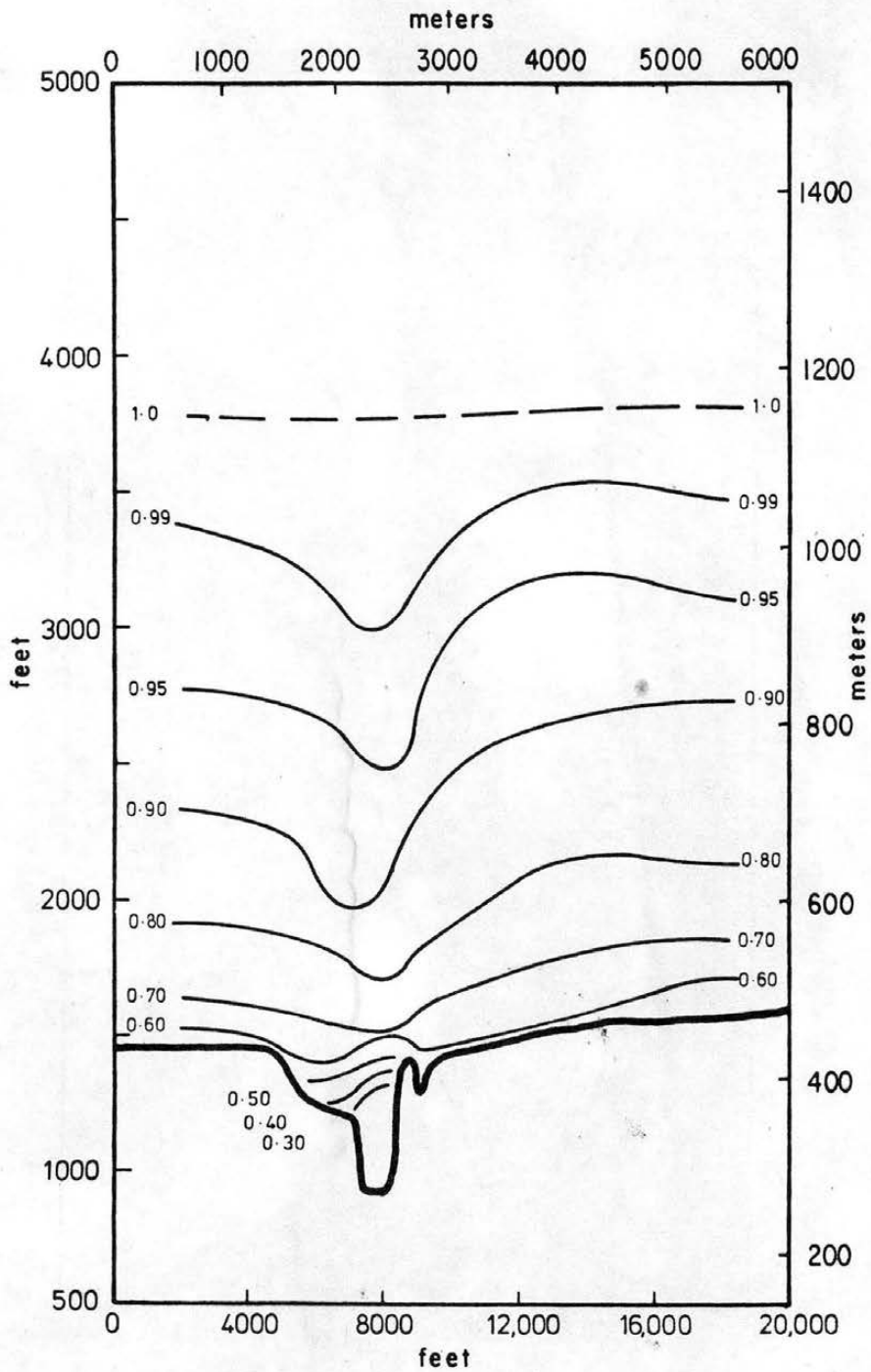


Figure 7-18. Vertical section F-F isotachs, terraced model.

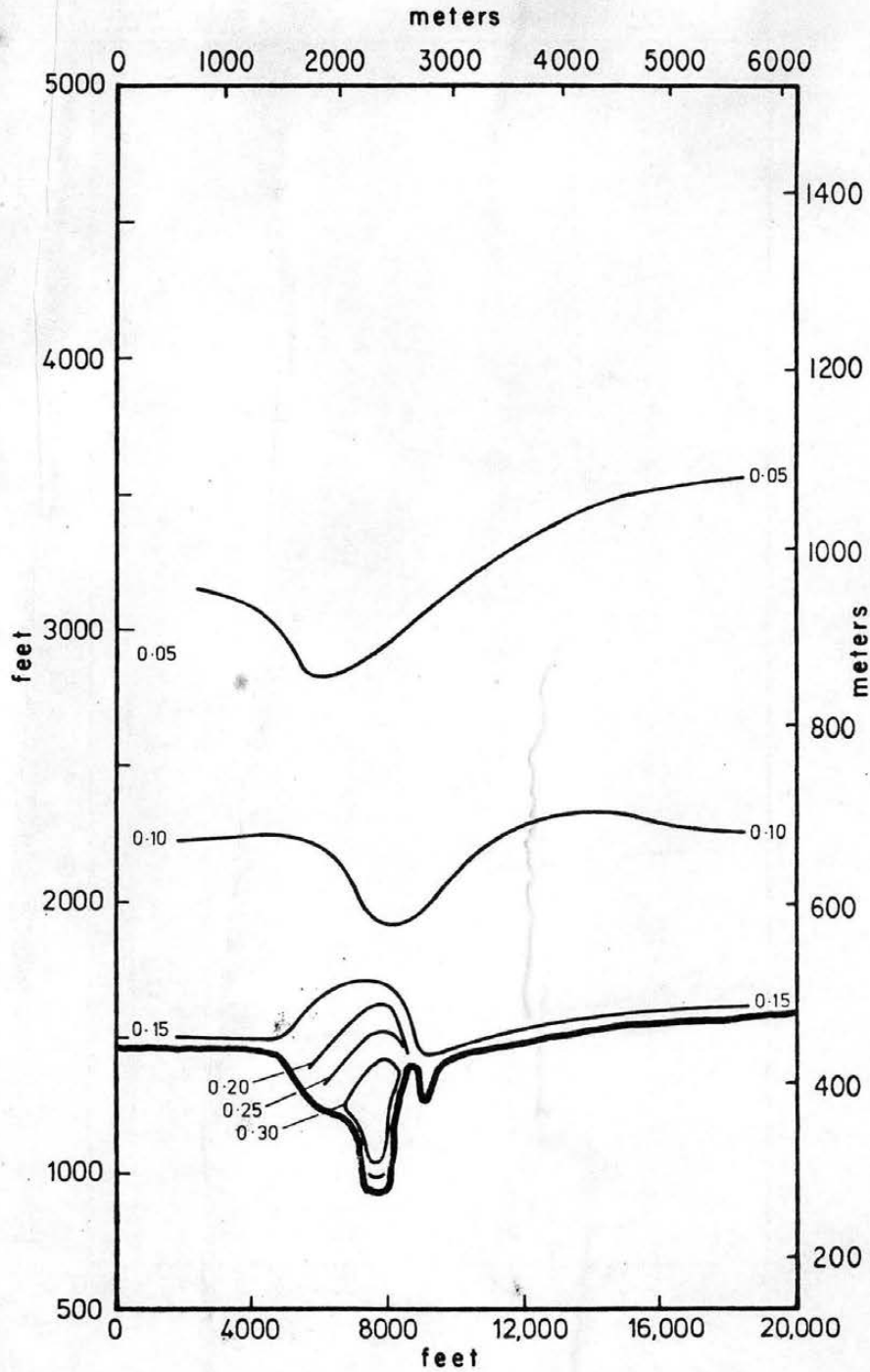


Figure 7-19. Vertical section F-F isoturbs, terraced model.

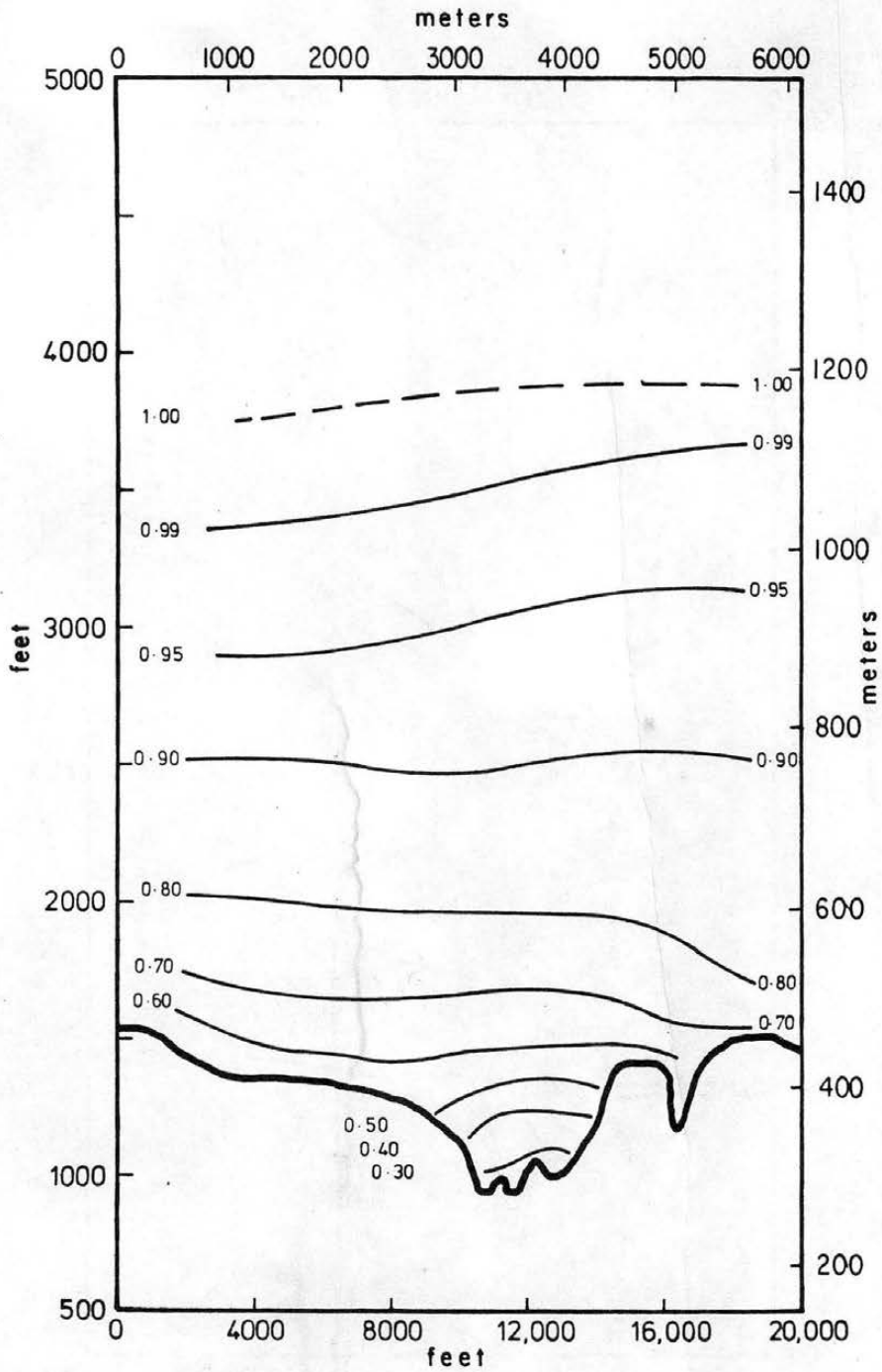


Figure 7-20. Vertical section D-D isotachs, terraced model.

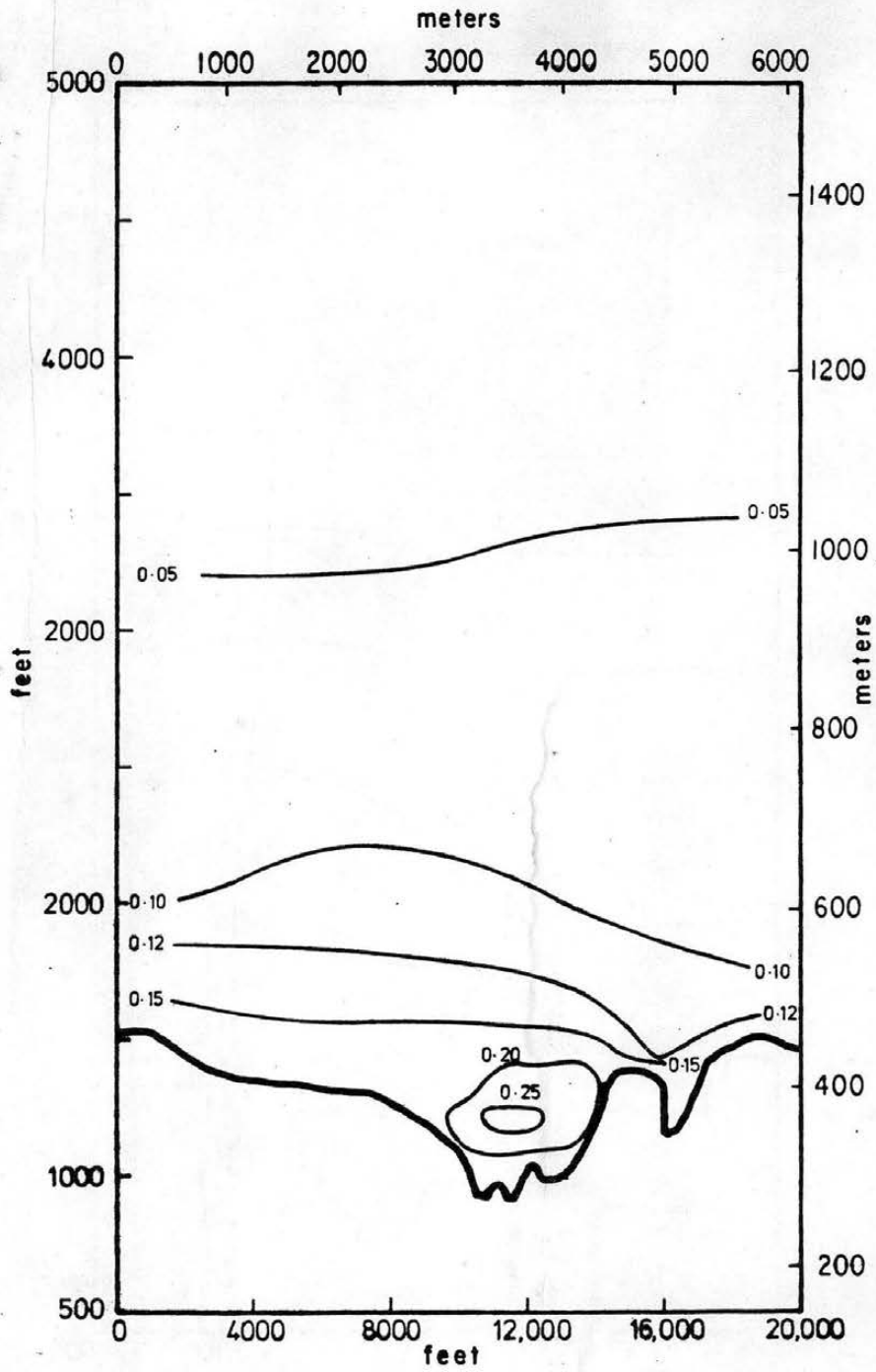


Figure 7-21. Vertical section D-D isoturbs, terraced model.

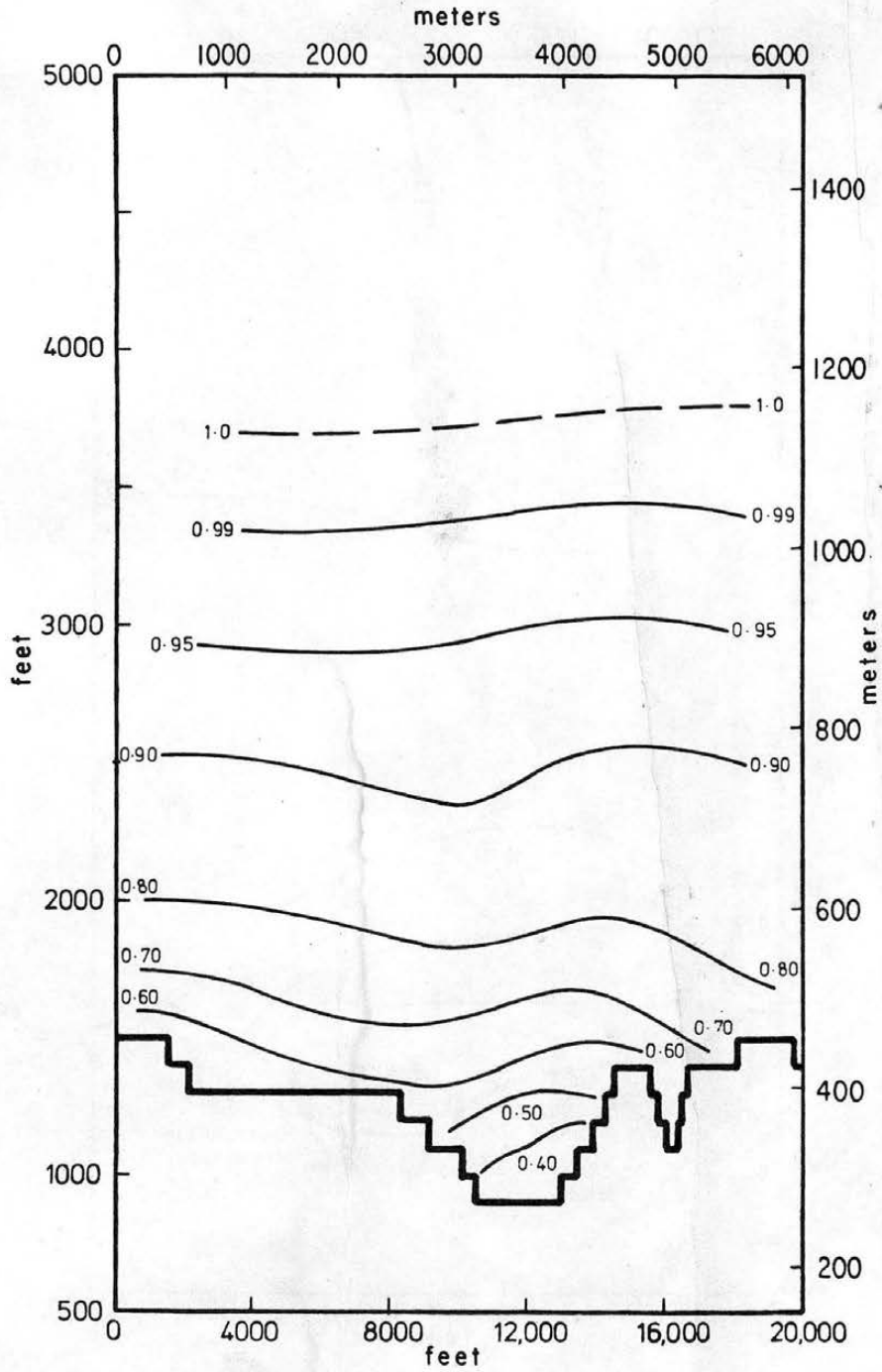


Figure 7-22. Vertical section D-D isotachs, terraced model.

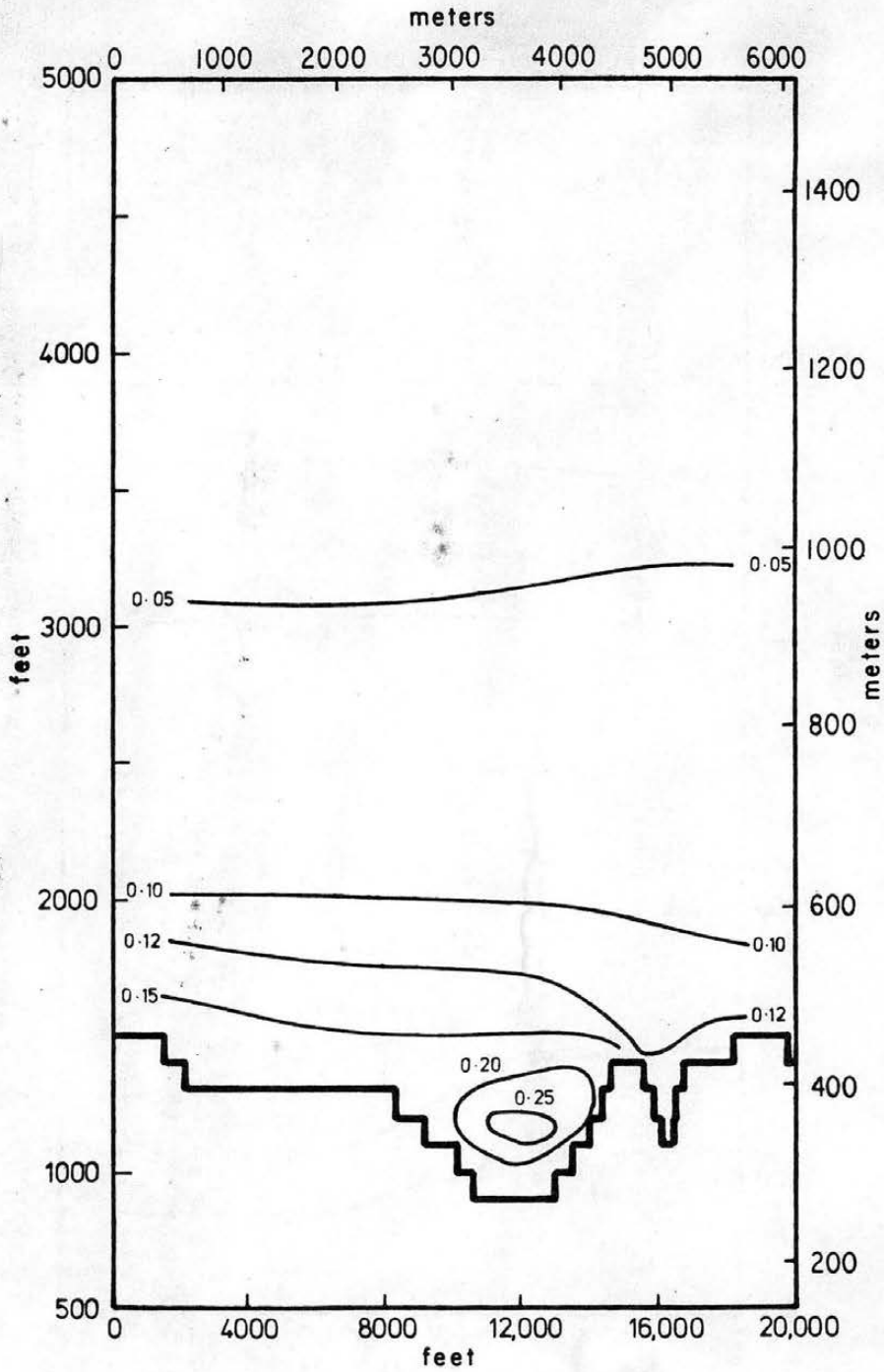


Figure 7-23. Vertical section D-D isoturbs, terraced model.

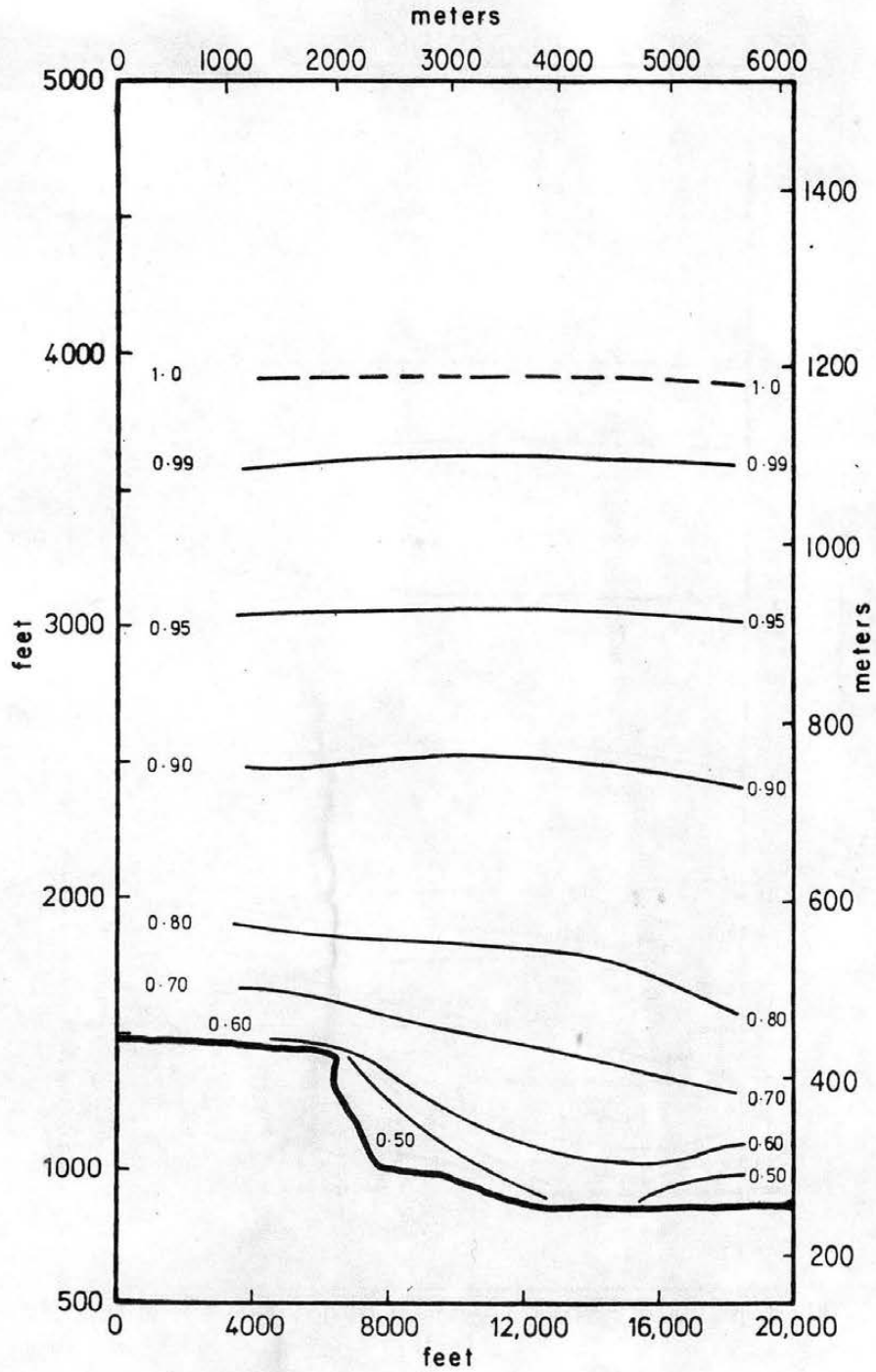


Figure 7-24. Vertical section E-E isotachs, terraced model.

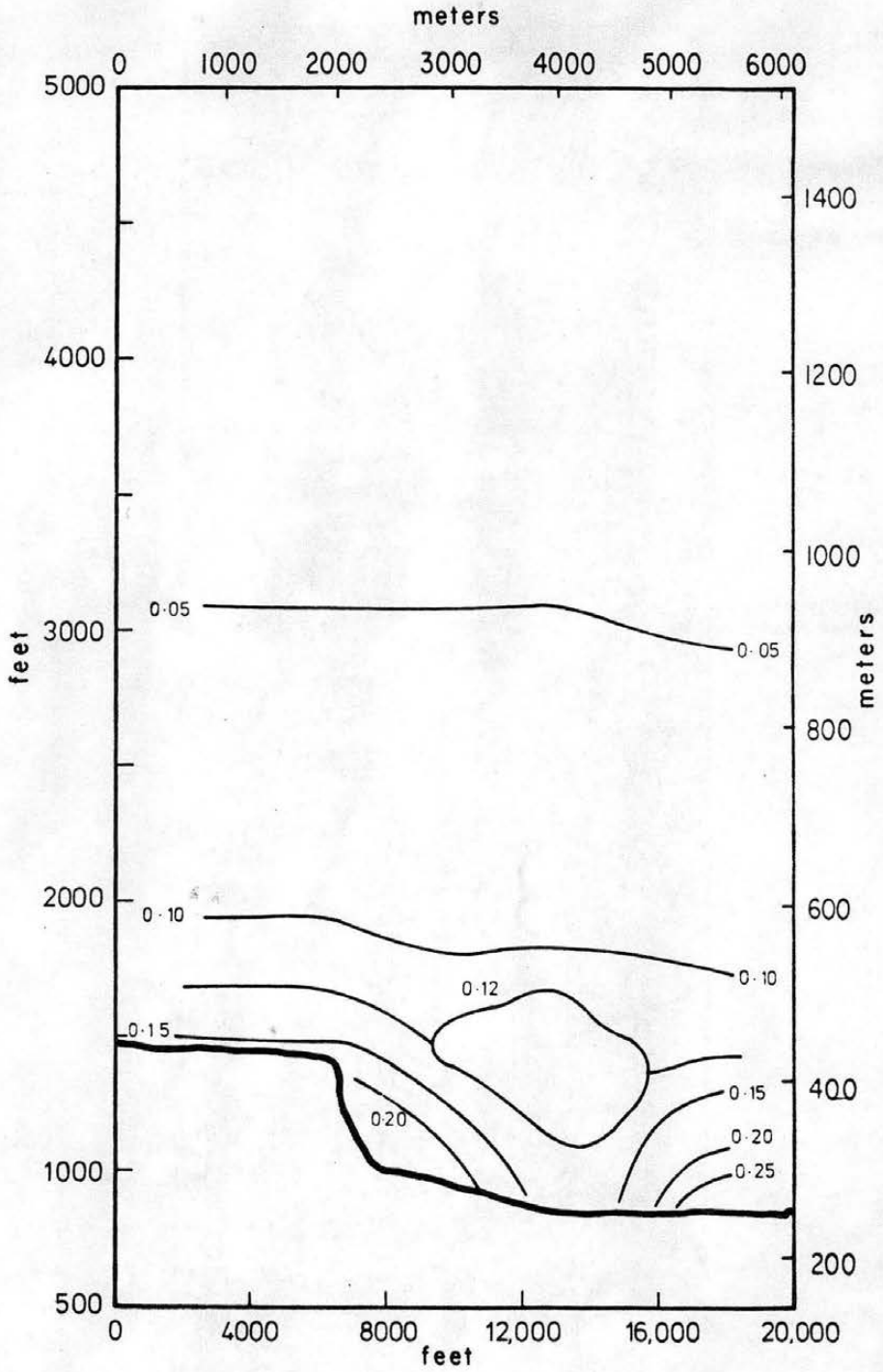


Figure 7-25. Vertical section E-E isoturbs, terraced model.

Contoured
Model

- ↓ Wind Direction
- ↗ Turbulence
- Vortex
- Cobra Probe Measurement



Figure 7-26. Miniature flag direction behavior, contoured model.

Contoured
Model

$$\bar{u}_{G_1} < \bar{u}_{G_2} < \bar{u}_{G_3}$$


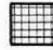


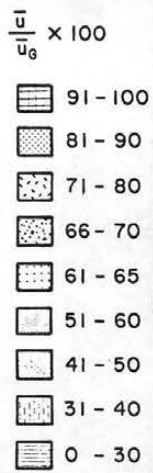
-  Deposits \bar{u}_{G_1}
-  Deposits \bar{u}_{G_2}
-  Deposits \bar{u}_{G_3}
-  Particle Path Line



Figure 7-27. Polystyrene bead trajectory and deposition diagram, contoured model.

Contoured
Pipe Cleaner
Shelterbelts

$z = 10 \text{ m}$



Unshaded Areas
Affected by
Shelterbelts
are between
0-50



Figure 7-28. Horizontal isotachs, contoured model, $z_p = 10 \text{ m}$.

Contoured
Pipe Cleaner
Shelterbelts
 $z = 50$ m

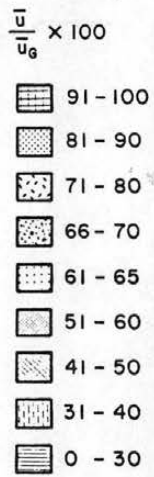


Figure 7-29. Horizontal isotachs, contoured model, $z_p = 50$ m.

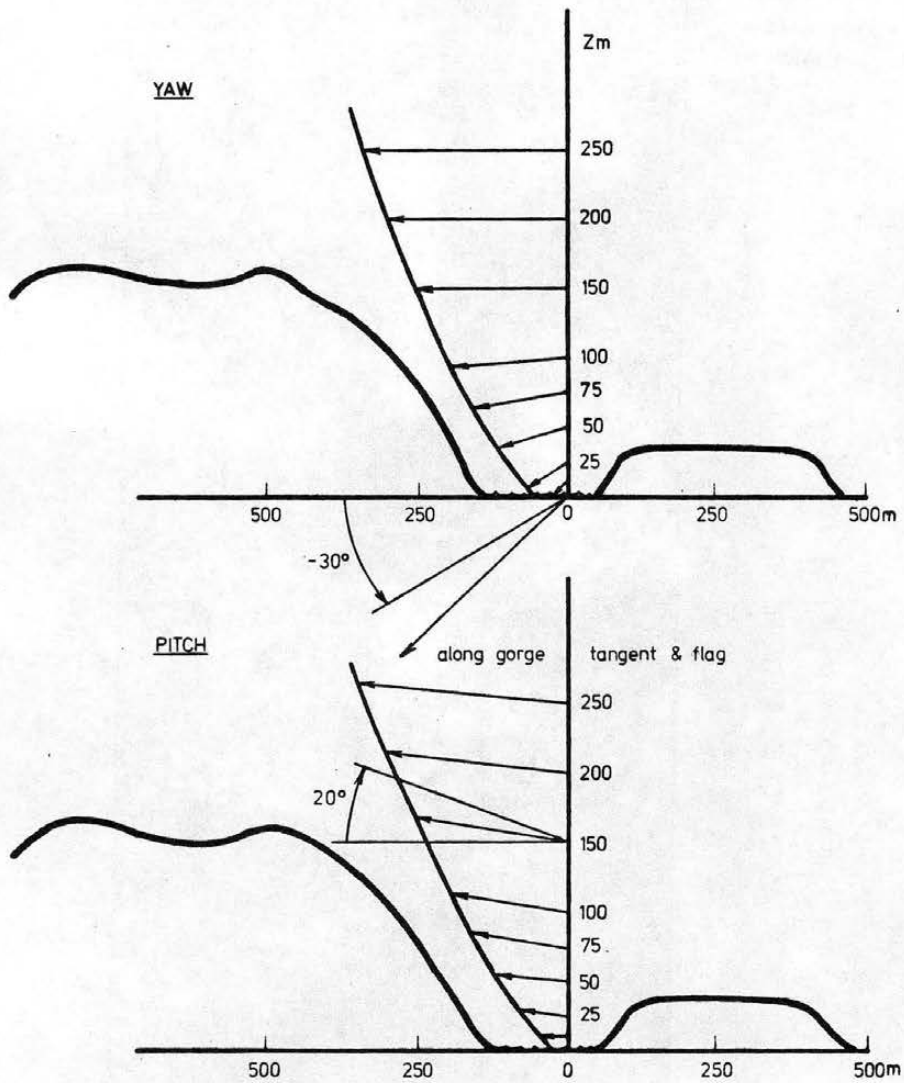


Figure 7-30. Airflow pitch and yaw at section G-3, contoured model.

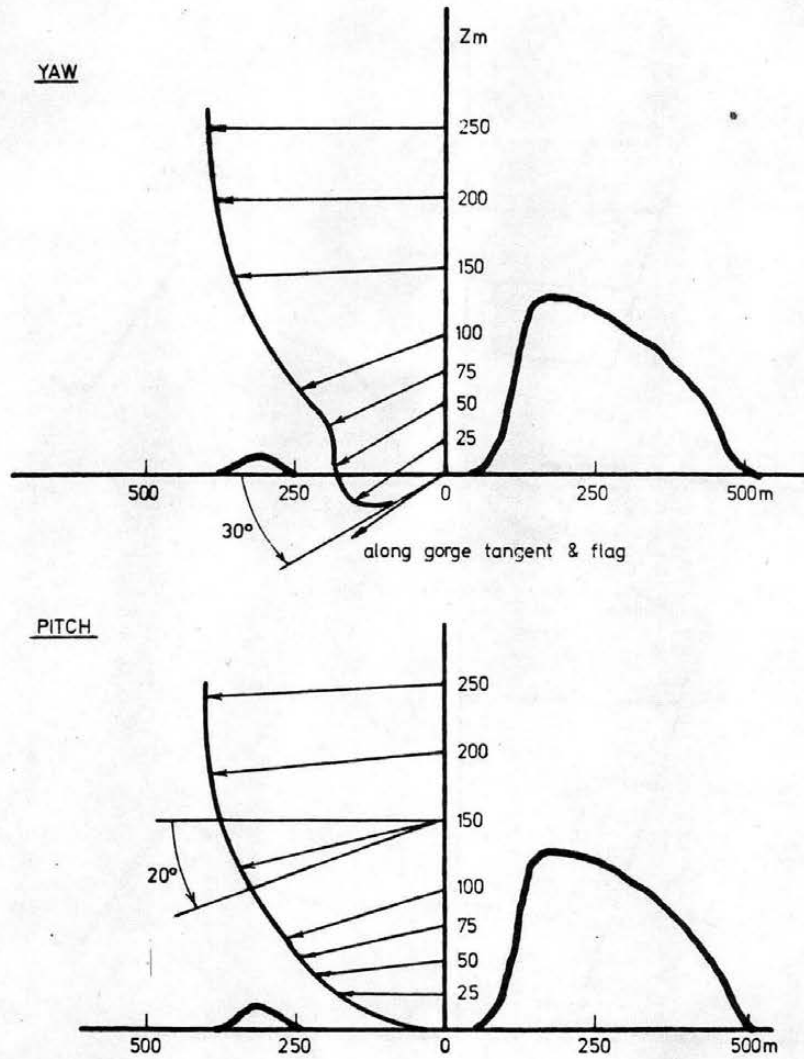


Figure 7-31. Airflow pitch and yaw at section between C and F gorge, contoured model.

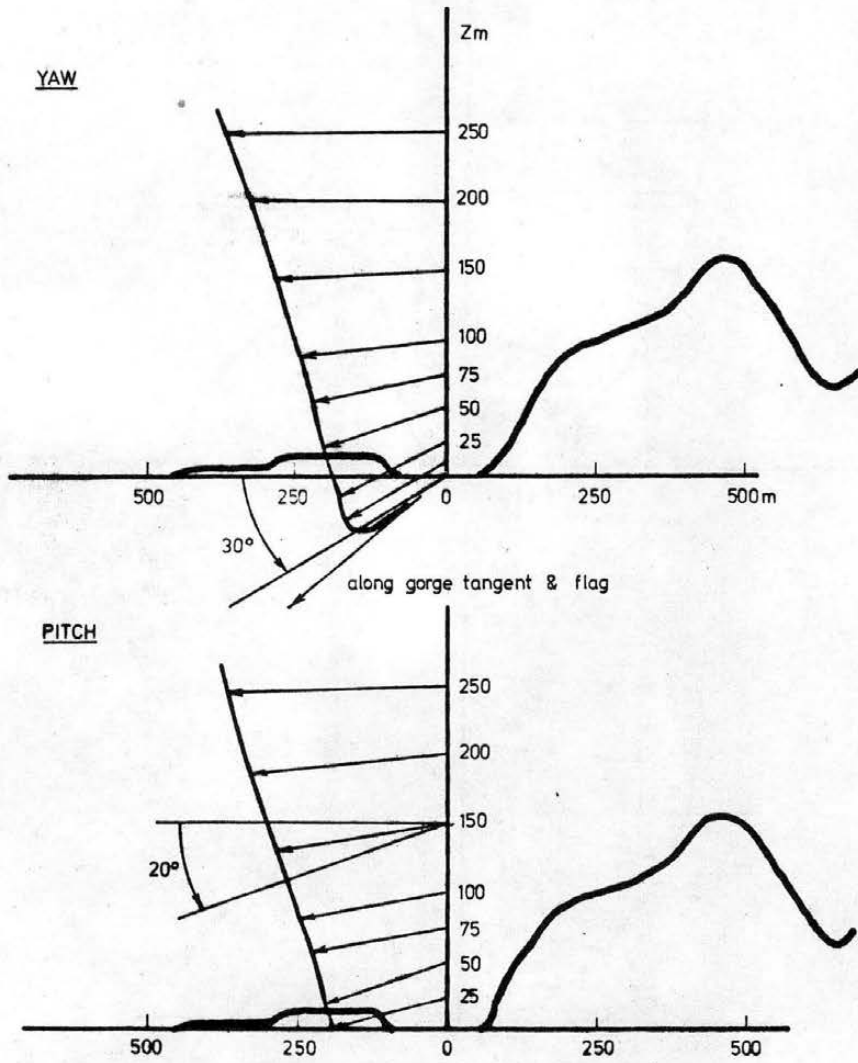


Figure 7-32. Airflow pitch and yaw Point A-A, contoured model.

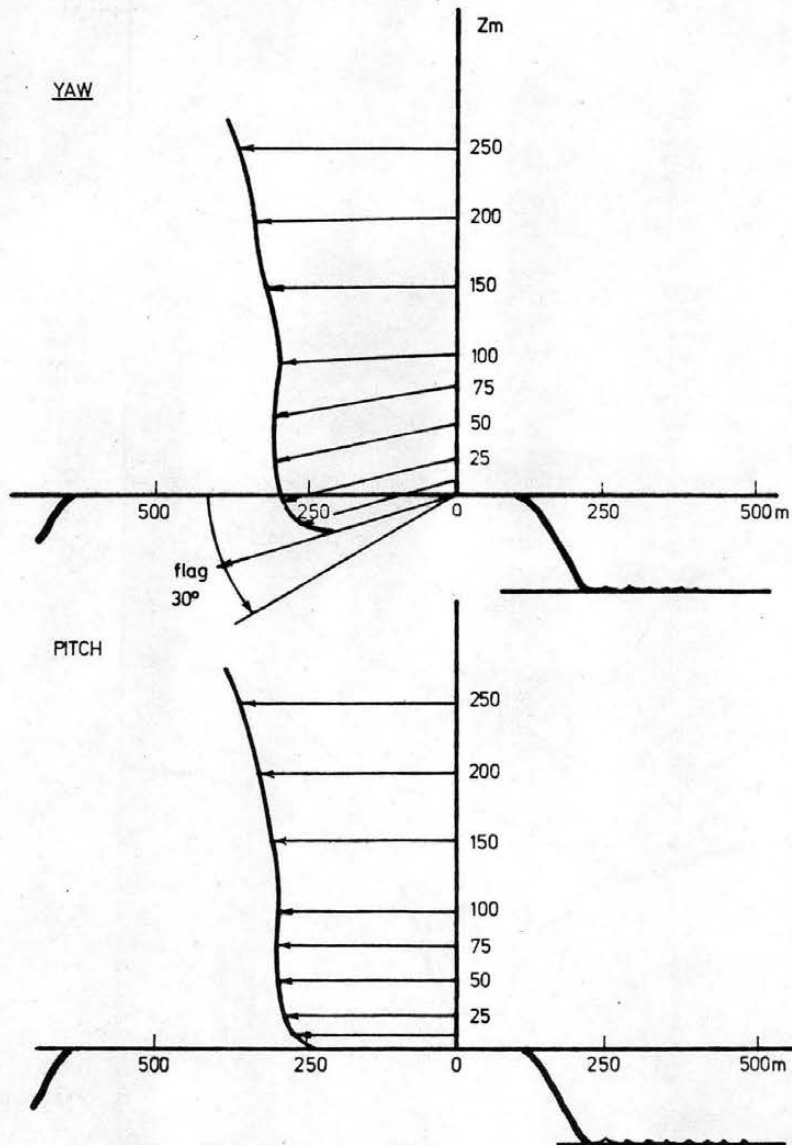


Figure 7-33. Airflow pitch and yaw, section D-3, contoured model.

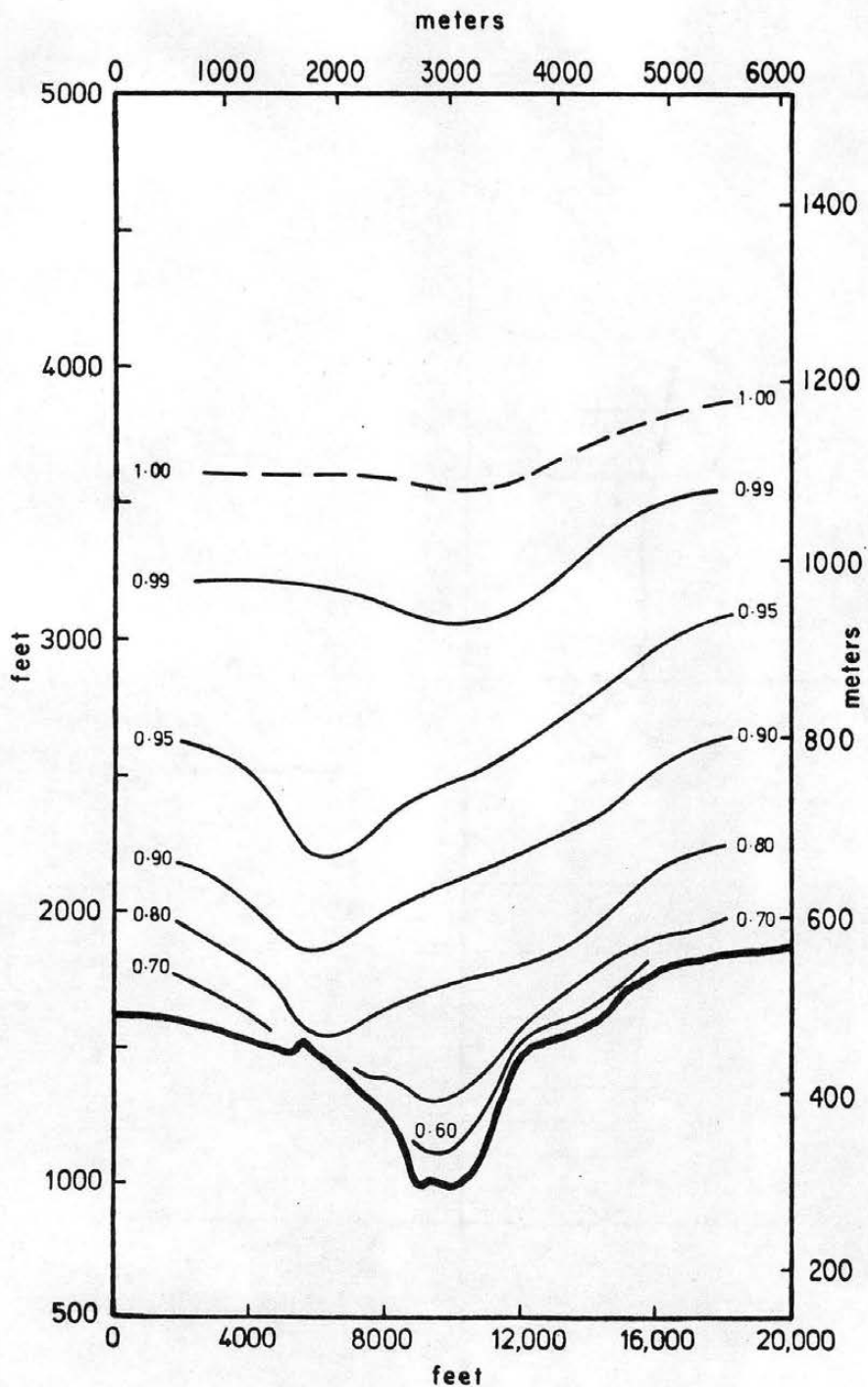


Figure 7-34. Vertical section B-B isotachs, contoured model.

Note: models include 4 mm pipe cleaner shelterbelts unless otherwise noted

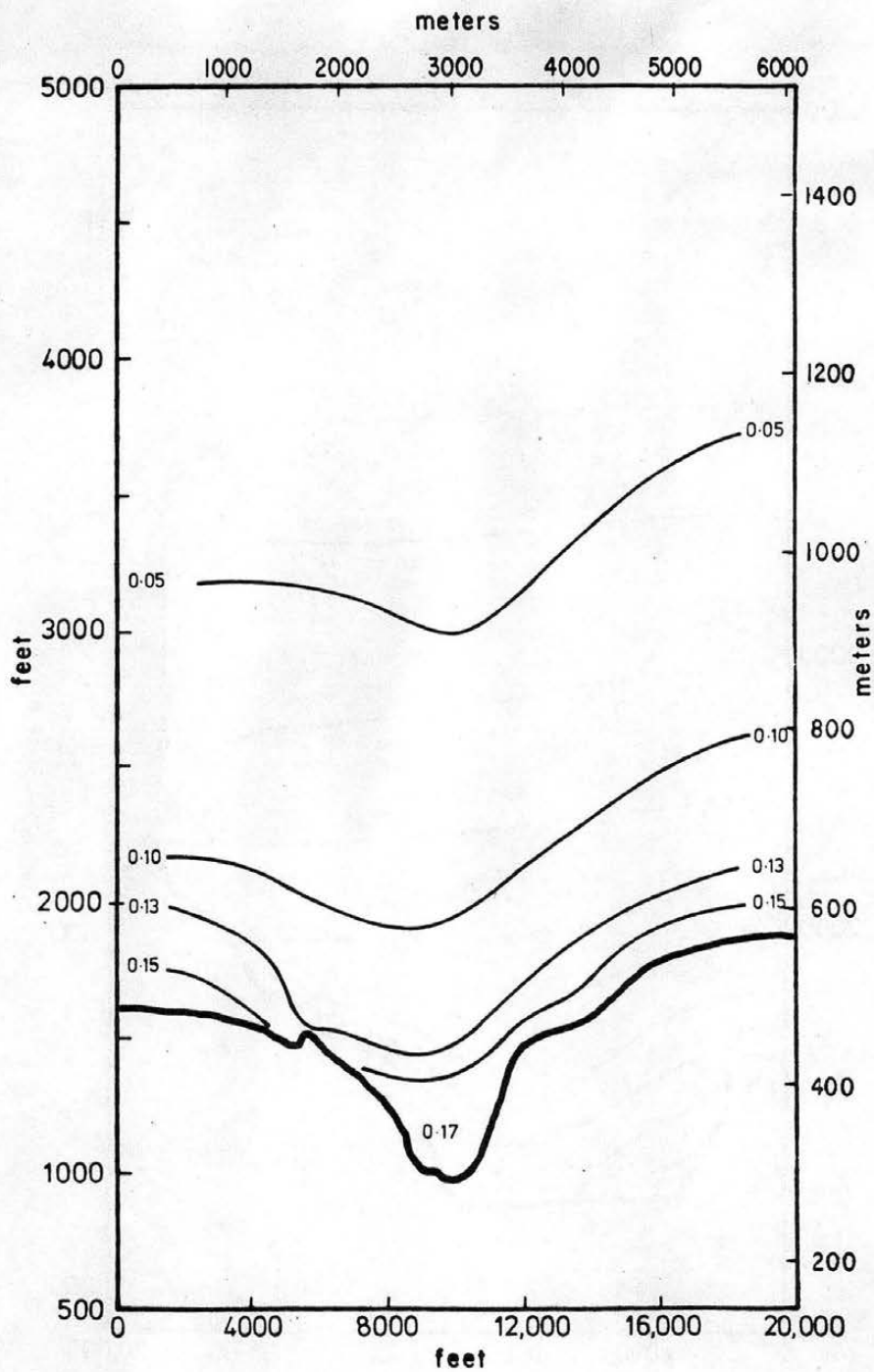


Figure 7-35. Vertical section B-B isoturbs, contoured model.

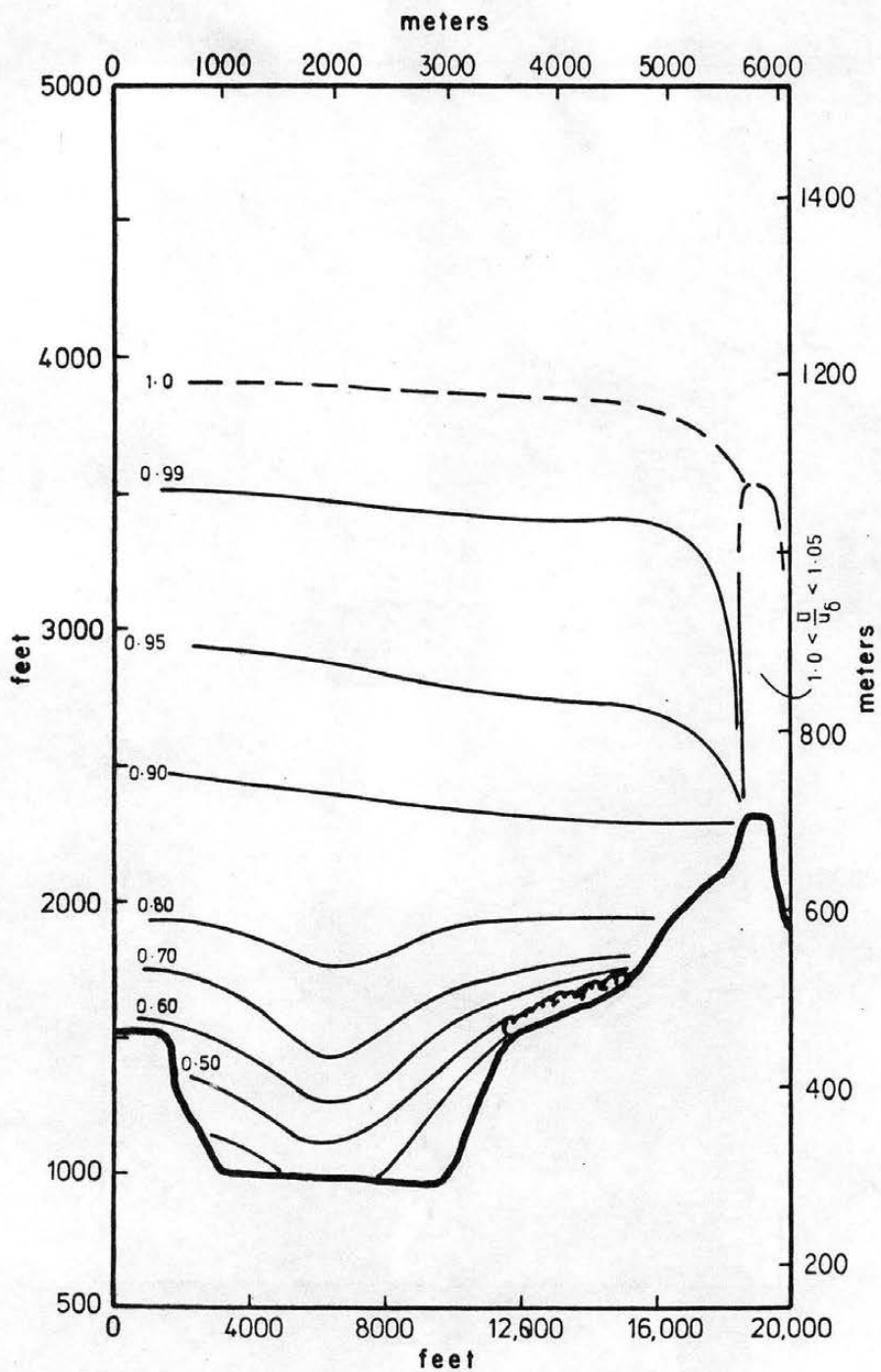


Figure 7-36. Vertical section G-G isotachs, contoured model.

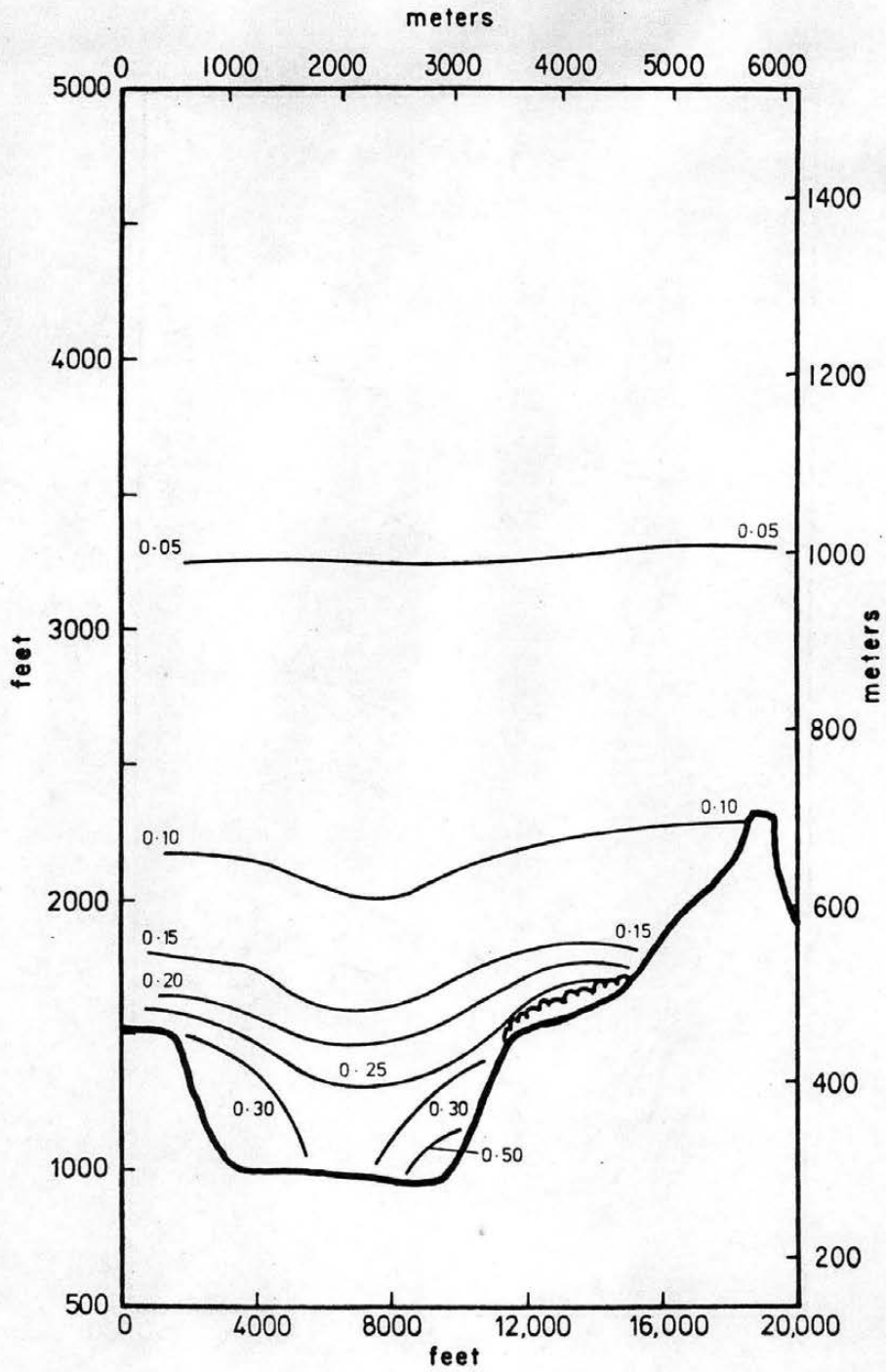


Figure 7-37. Vertical section G-G isoturbs, contoured model.

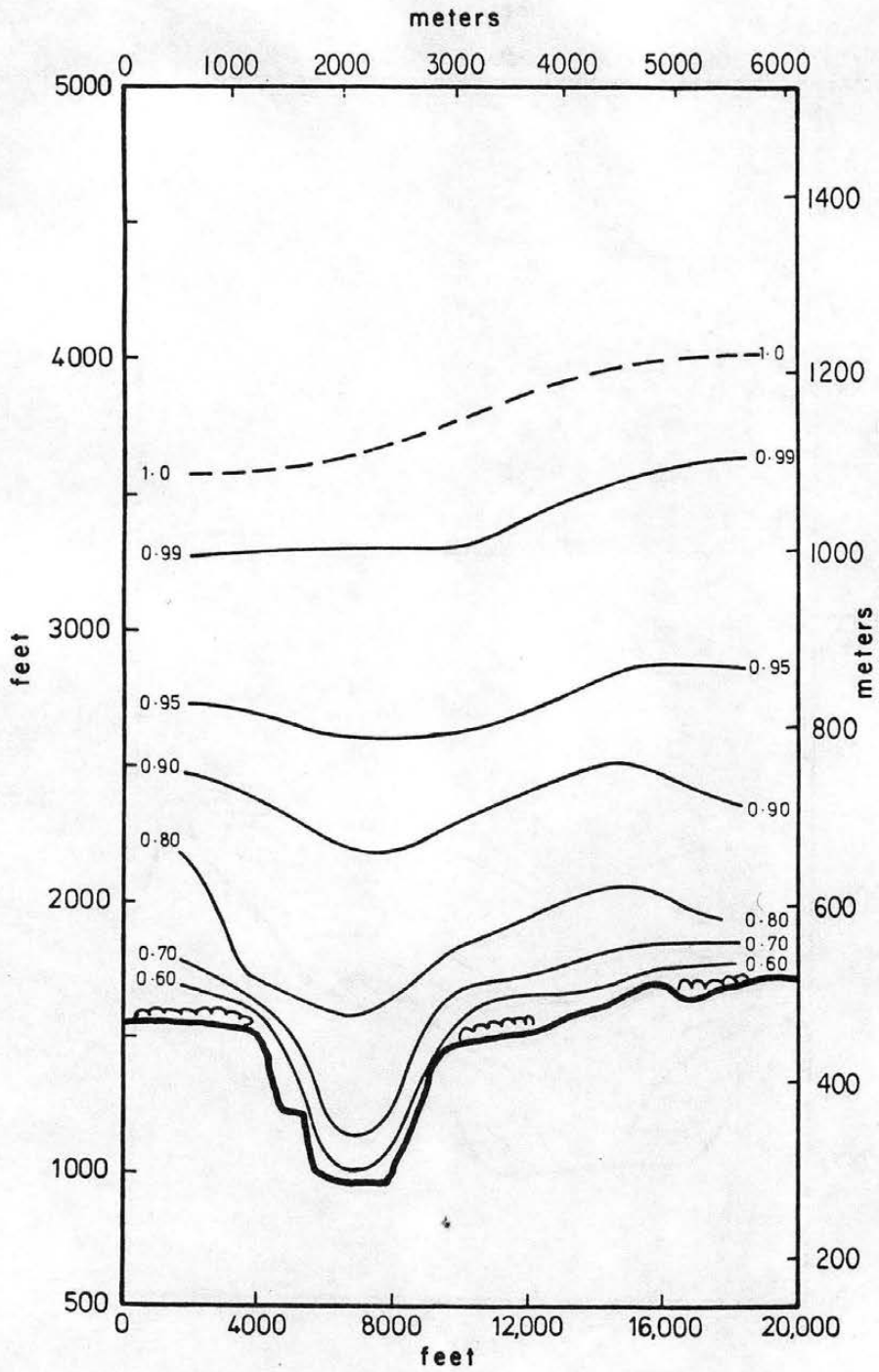


Figure 7-38. Vertical section C-C isotachs, contoured model.

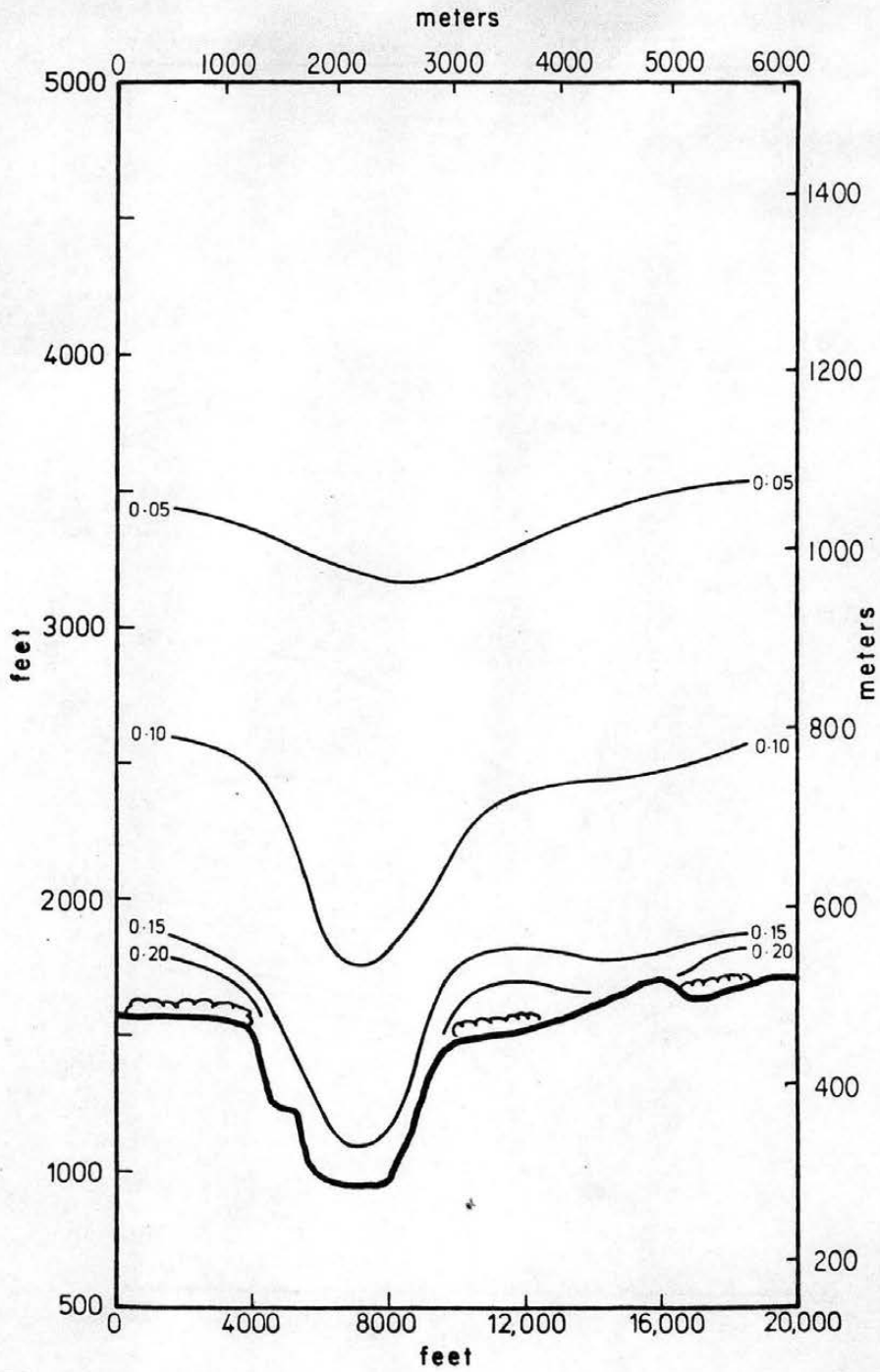


Figure 7-39. Vertical section C-C isoturbs, contoured model.

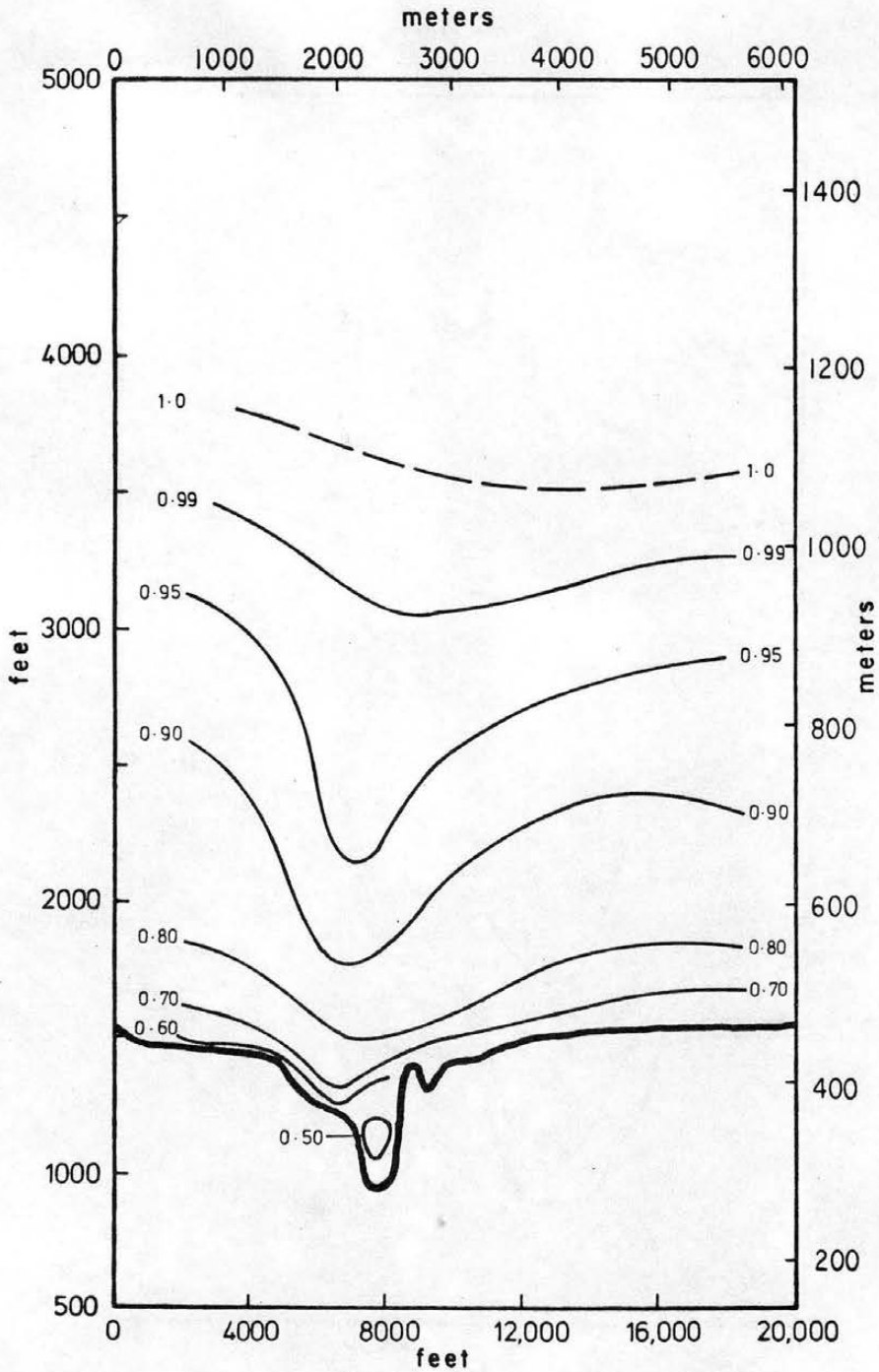


Figure 7-40. Vertical section F-F isotachs, contoured model with no shelterbelts.

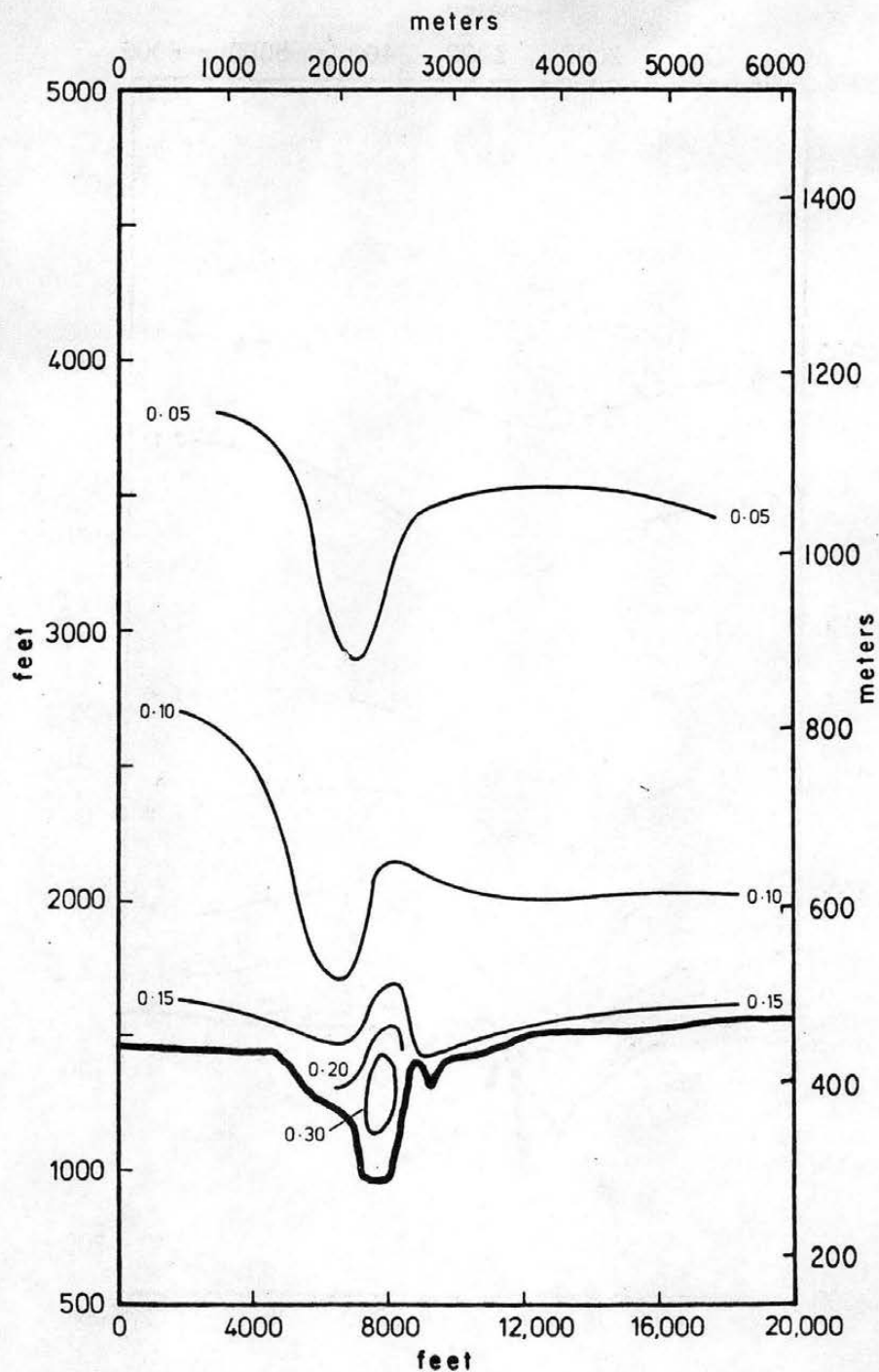


Figure 7-41. Vertical section F-F isoturbs, contoured model with no shelterbelts.

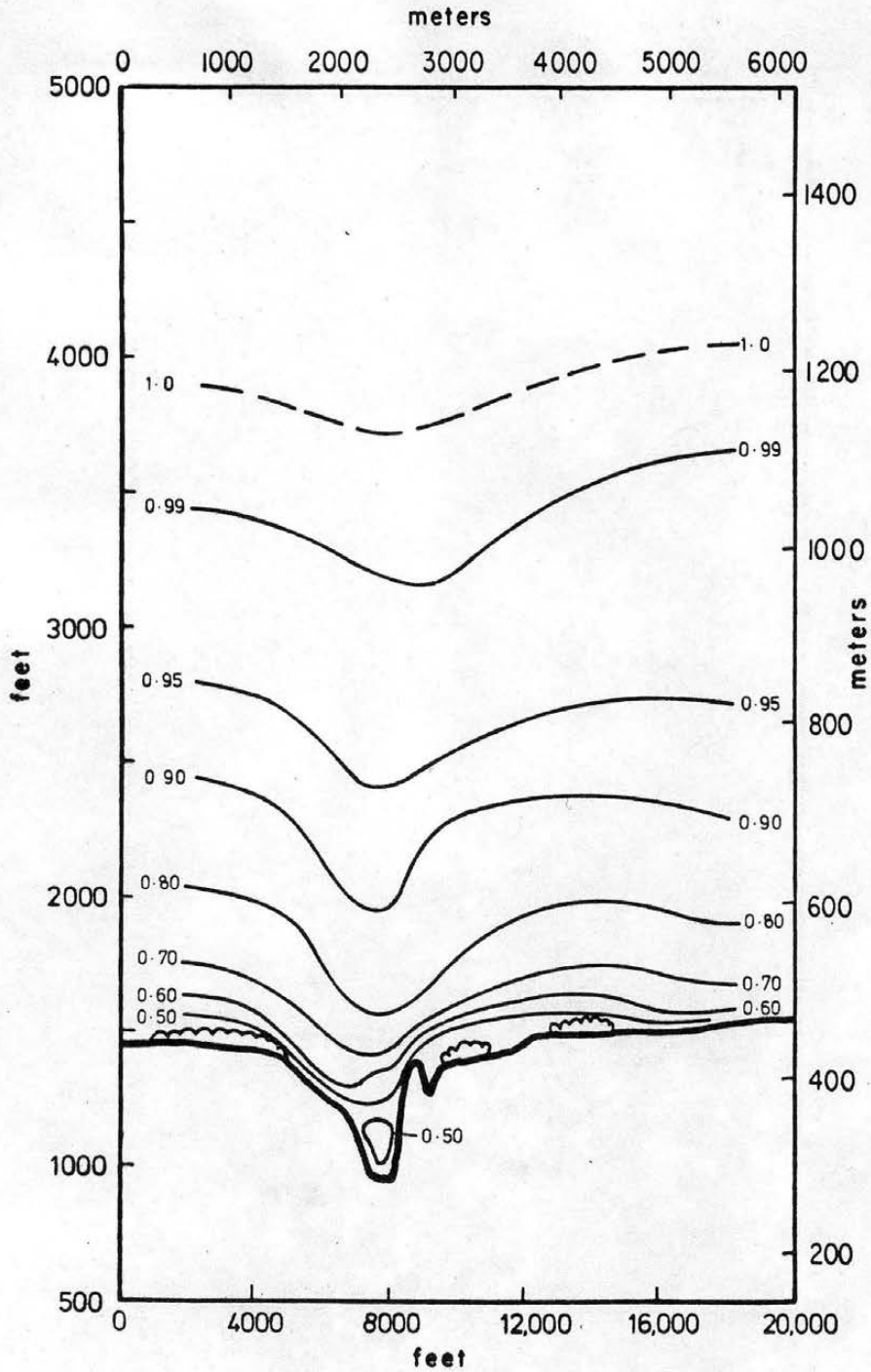


Figure 7-42. Vertical section F-F isotachs, contoured model with yarn shelterbelts.

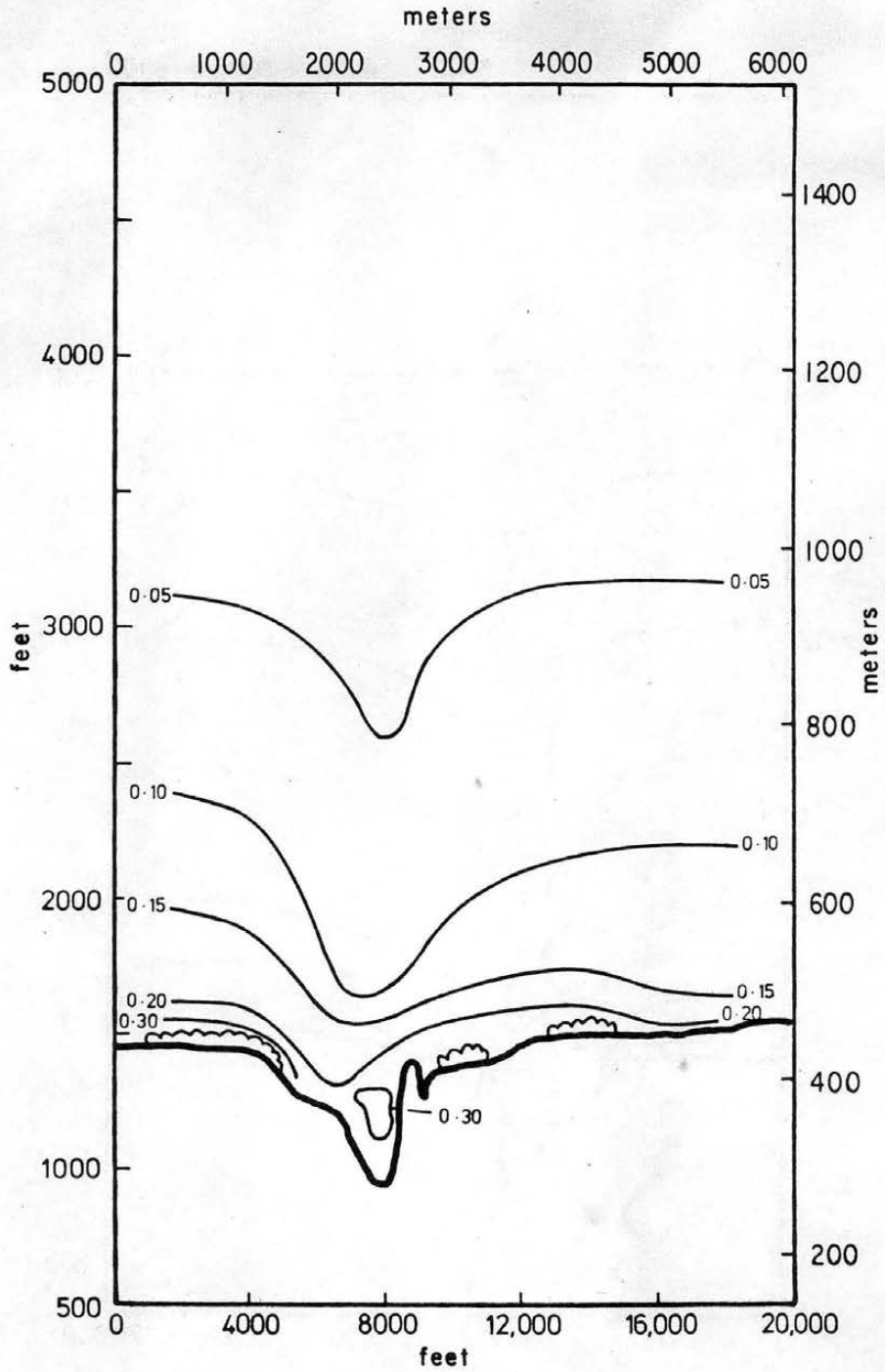


Figure 7-43. Vertical section F-F isoturbs, contoured model with yarn shelterbelts.

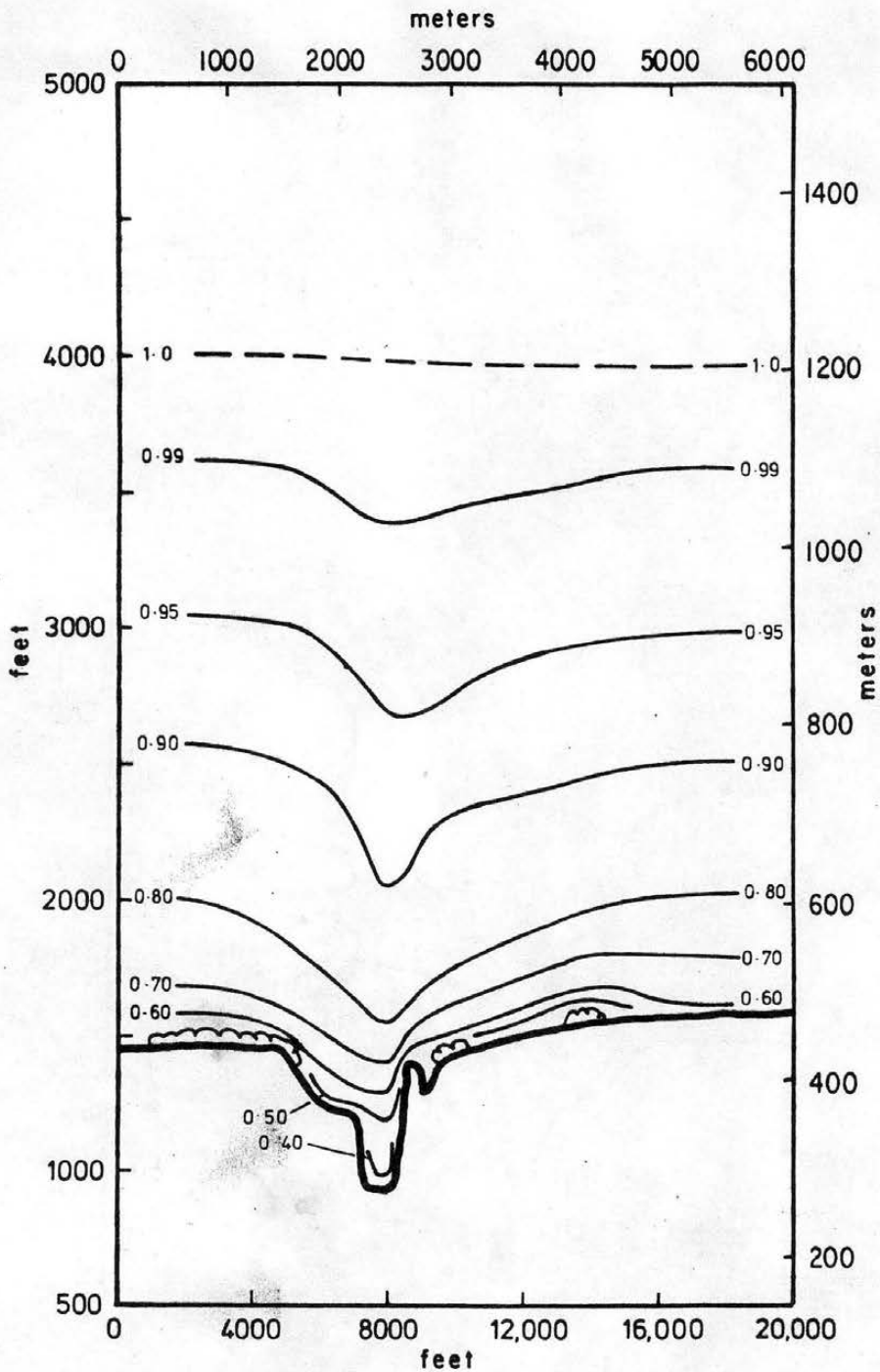


Figure 7-44. Vertical section F-F isotachs, contoured model.

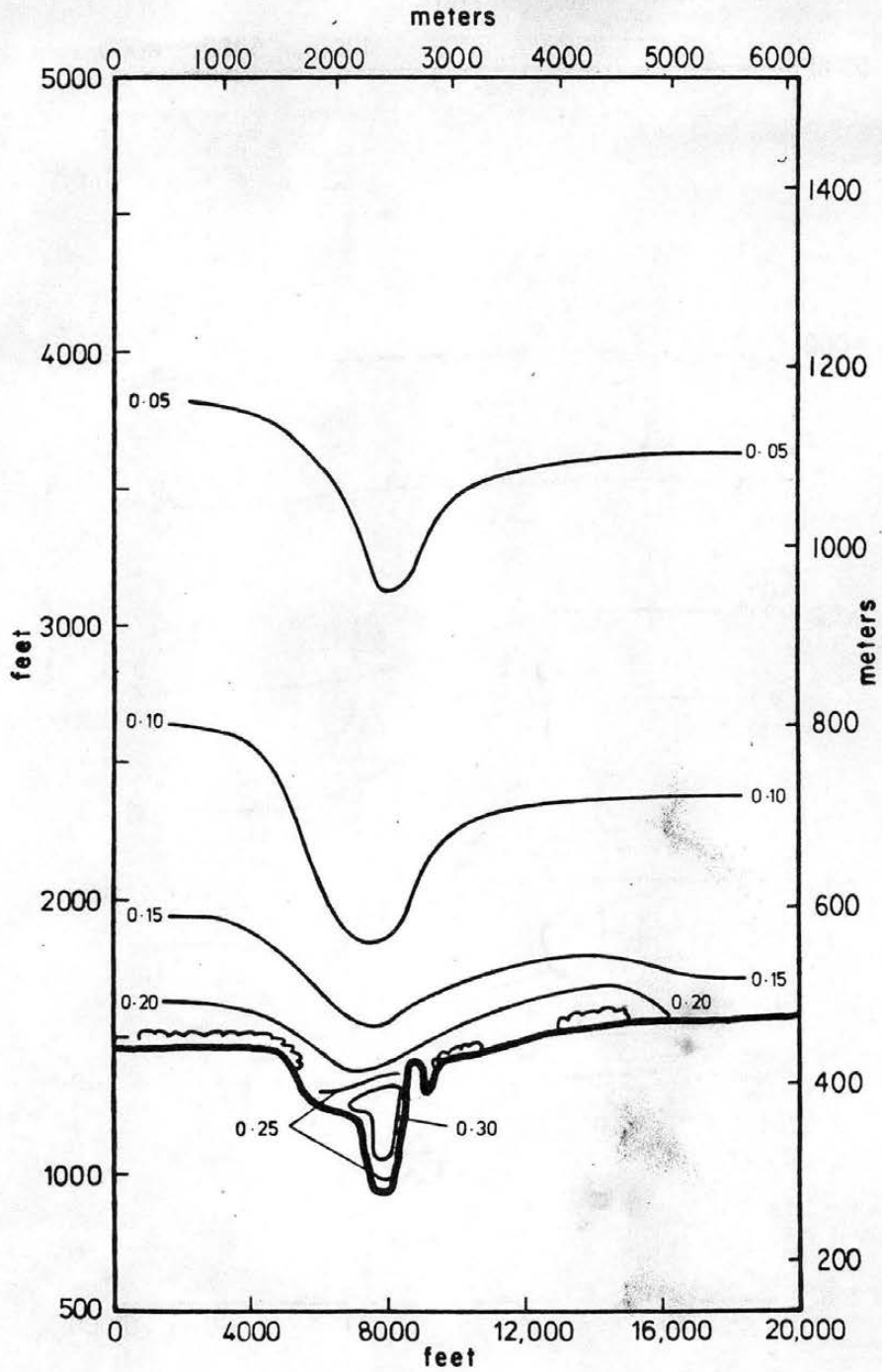


Figure 7-45. Vertical section F-F isoturbs, contoured model.

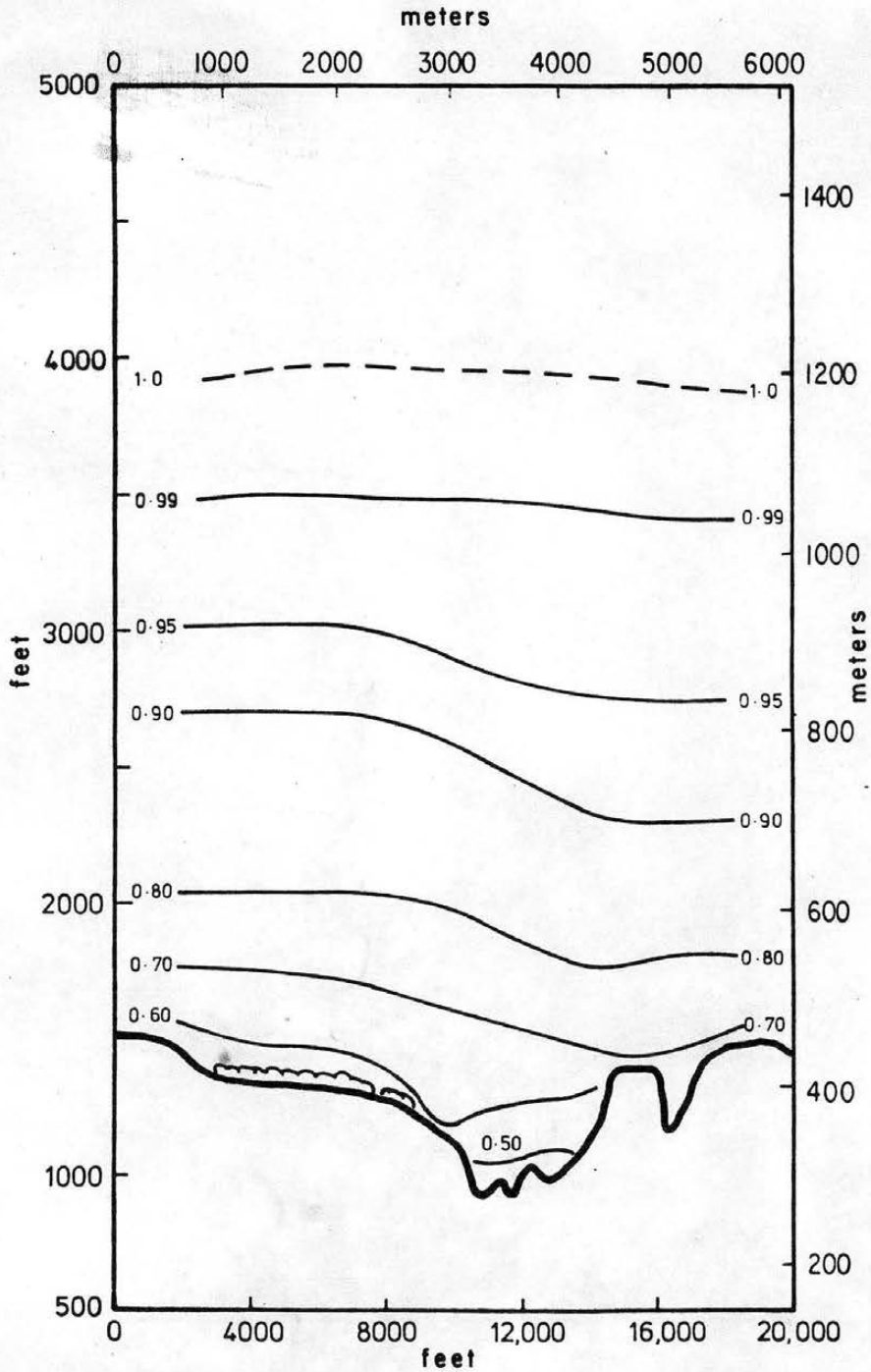


Figure 7-46. Vertical section D-D isotachs, contoured model.

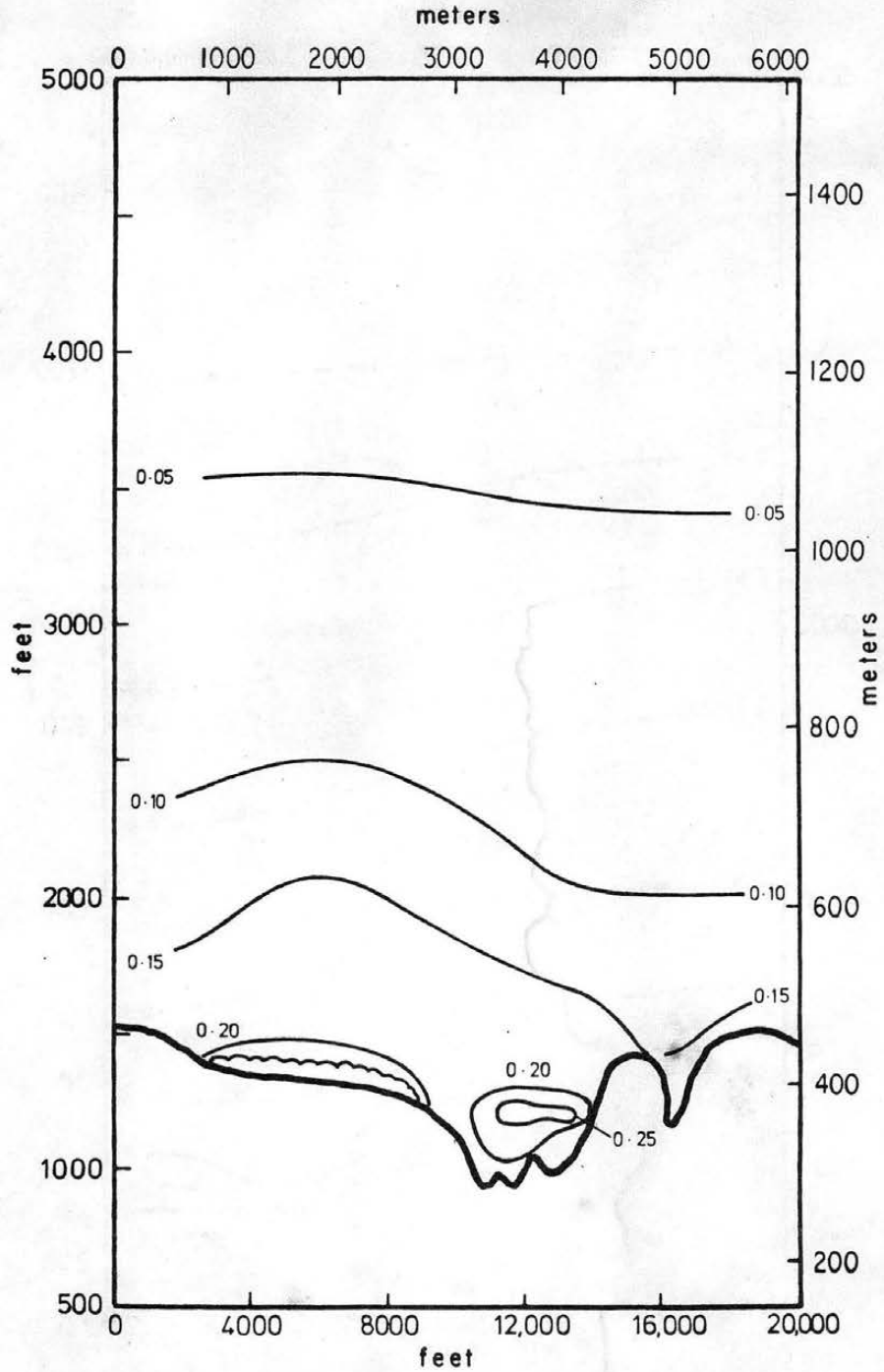


Figure 7-47. Vertical section D-D isoturbs, contoured model.

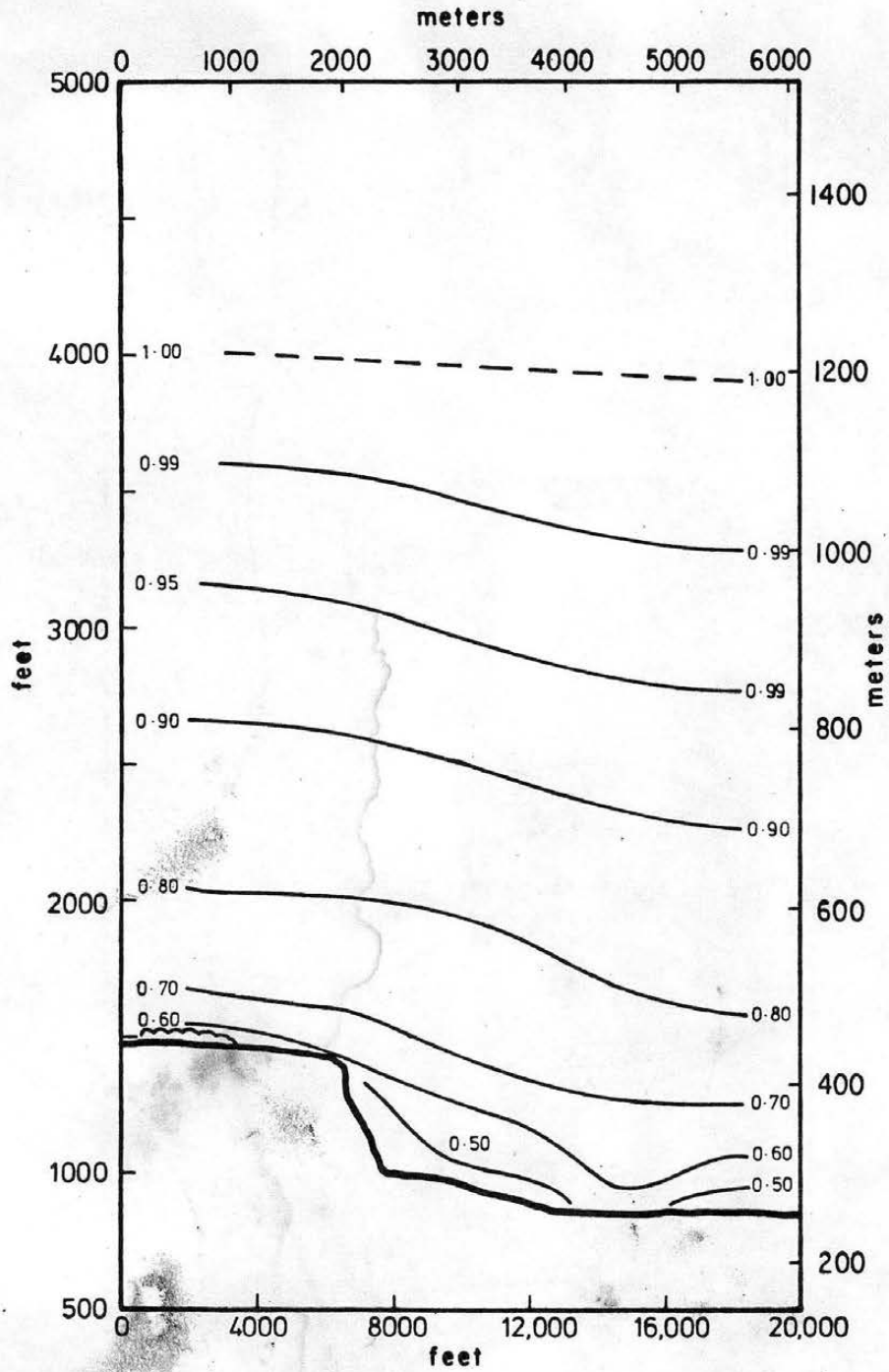


Figure 7-48. Vertical section E-E isotachs, contoured model.

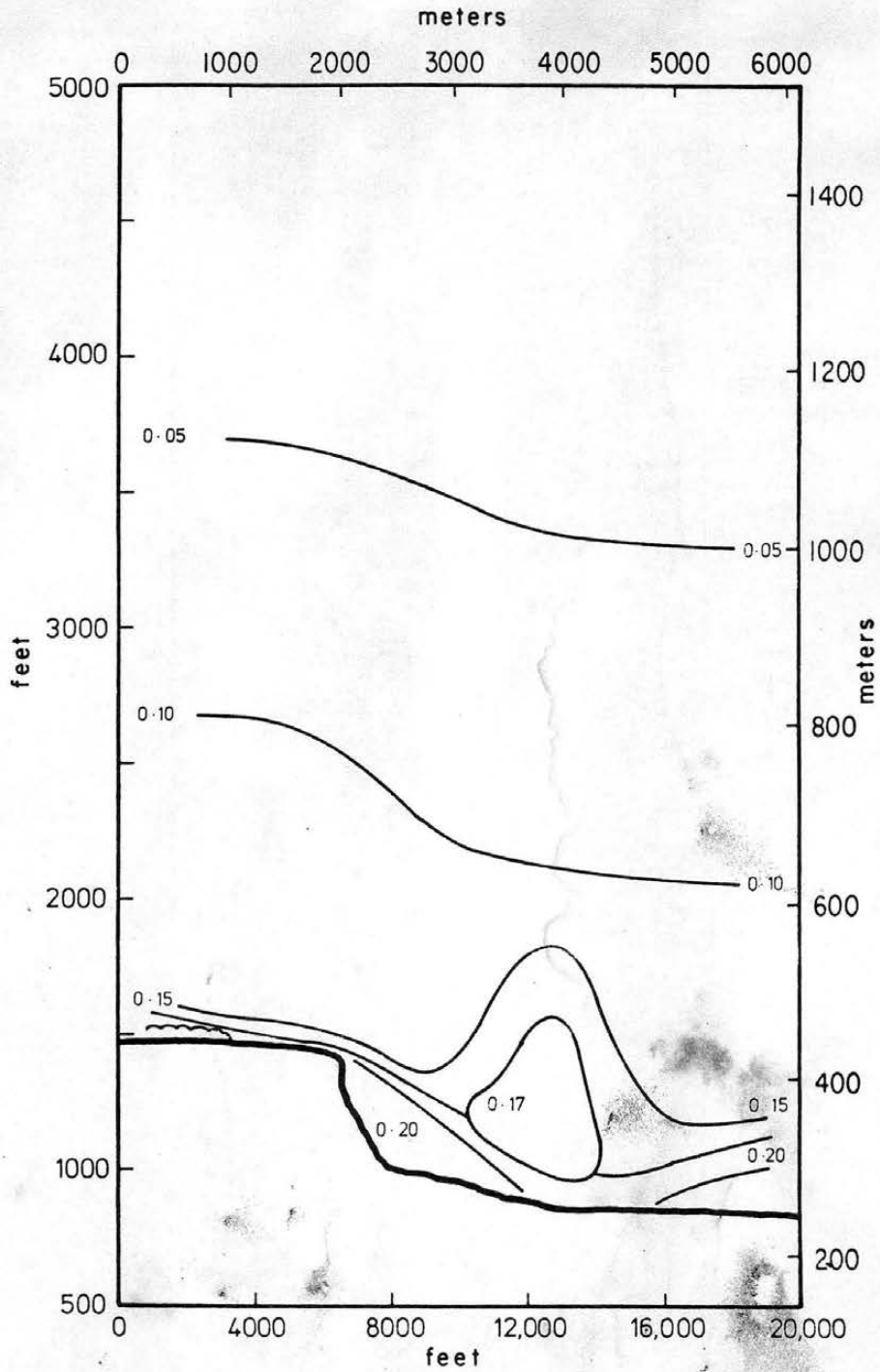


Figure 7-49. Vertical section E-E isoturbs, contoured model.

Field Data
November 25, 1977
z = 10 meters

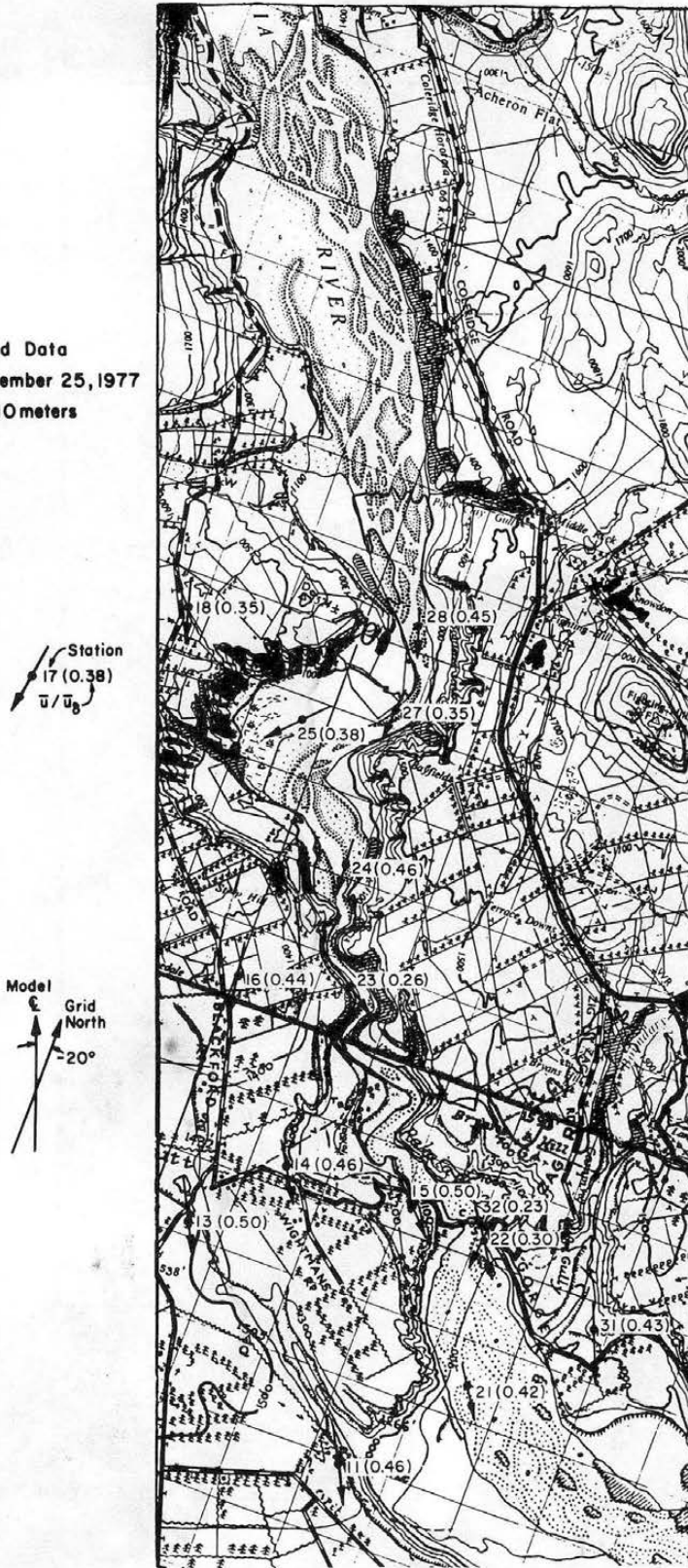


Figure 7-50. Rakaia Gorge field data, November 25, 1977.

Field Data
December 28, 1977
z = 10 meters

Station
17 (0.38)
 \bar{u} / \bar{u}_b

Model
Grid North
-20°



Figure 7-51. Rakaia Gorge field data, December 28, 1977.

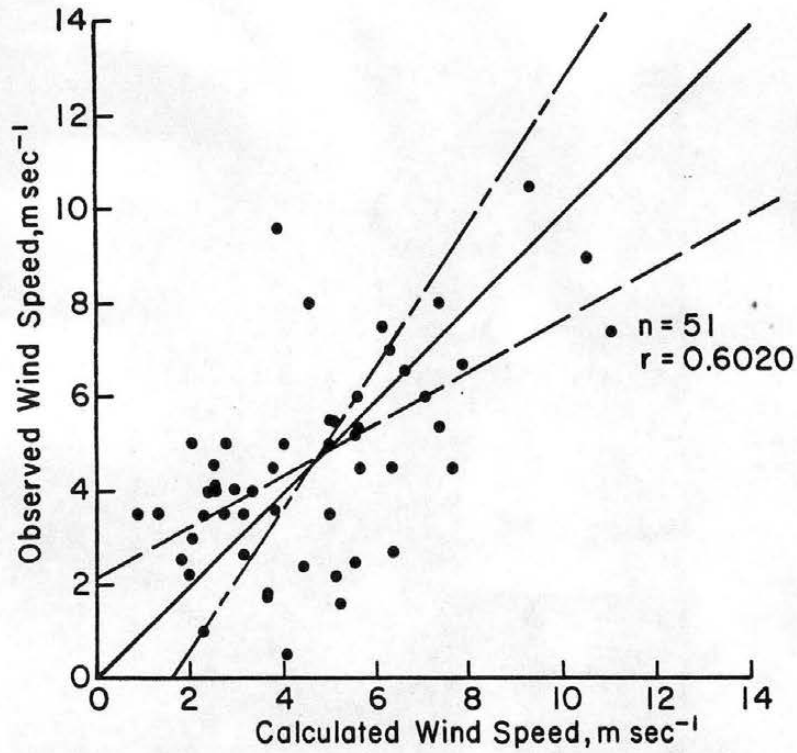


Figure 8-1. Comparison of calculated and observed wind speeds (Fosberg et al. 1976).

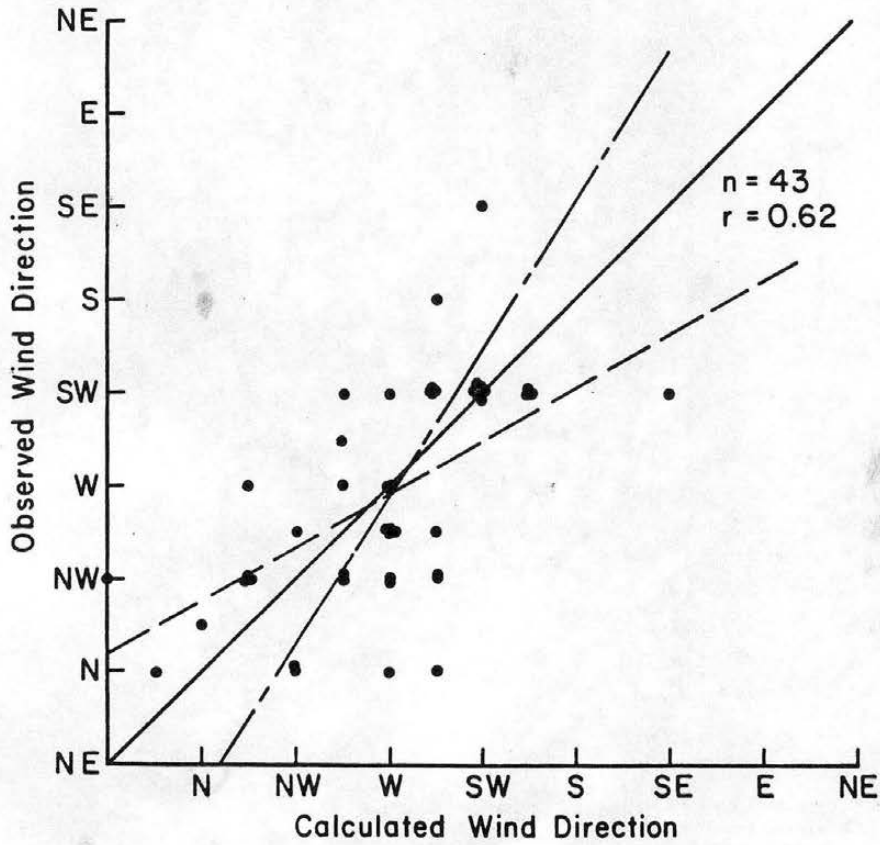


Figure 8-2. Comparison of calculated and observed wind direction (Fosberg et al. 1976).

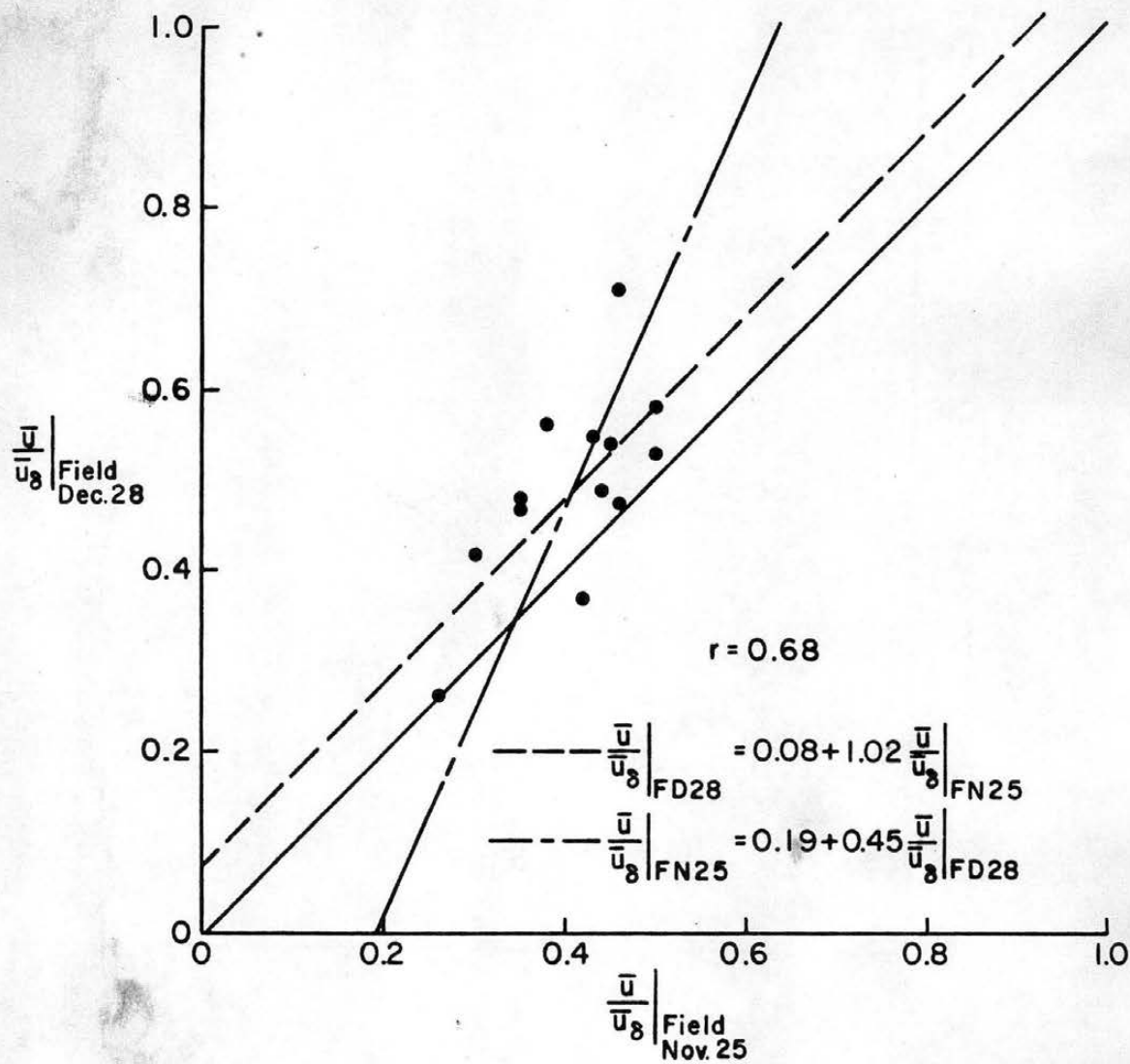


Figure 8-3. Scatter diagram field test data, December 28 versus field test data, November 25.

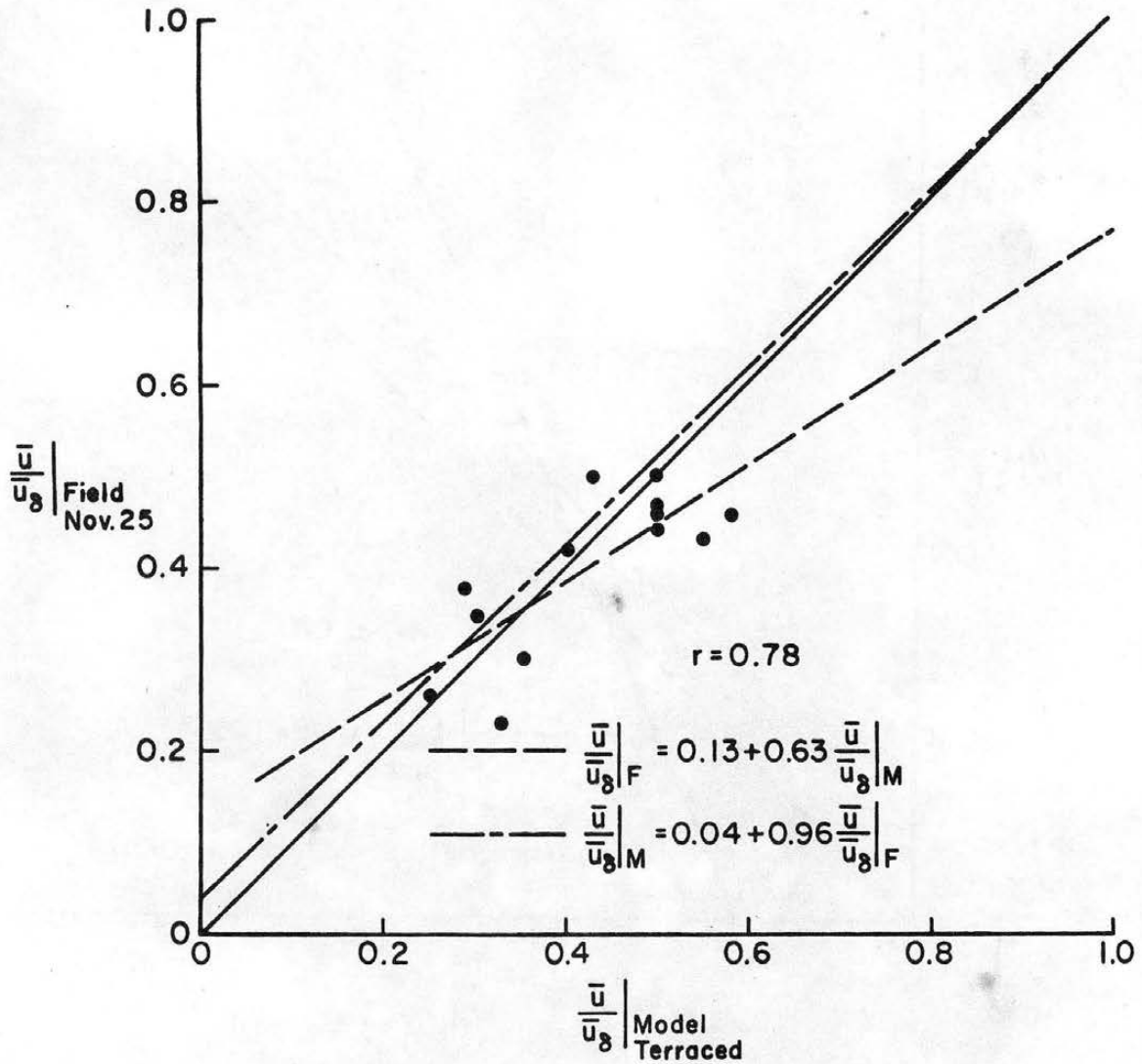


Figure 8-4. Scatter diagram field test data, November 25 versus terraced model data.

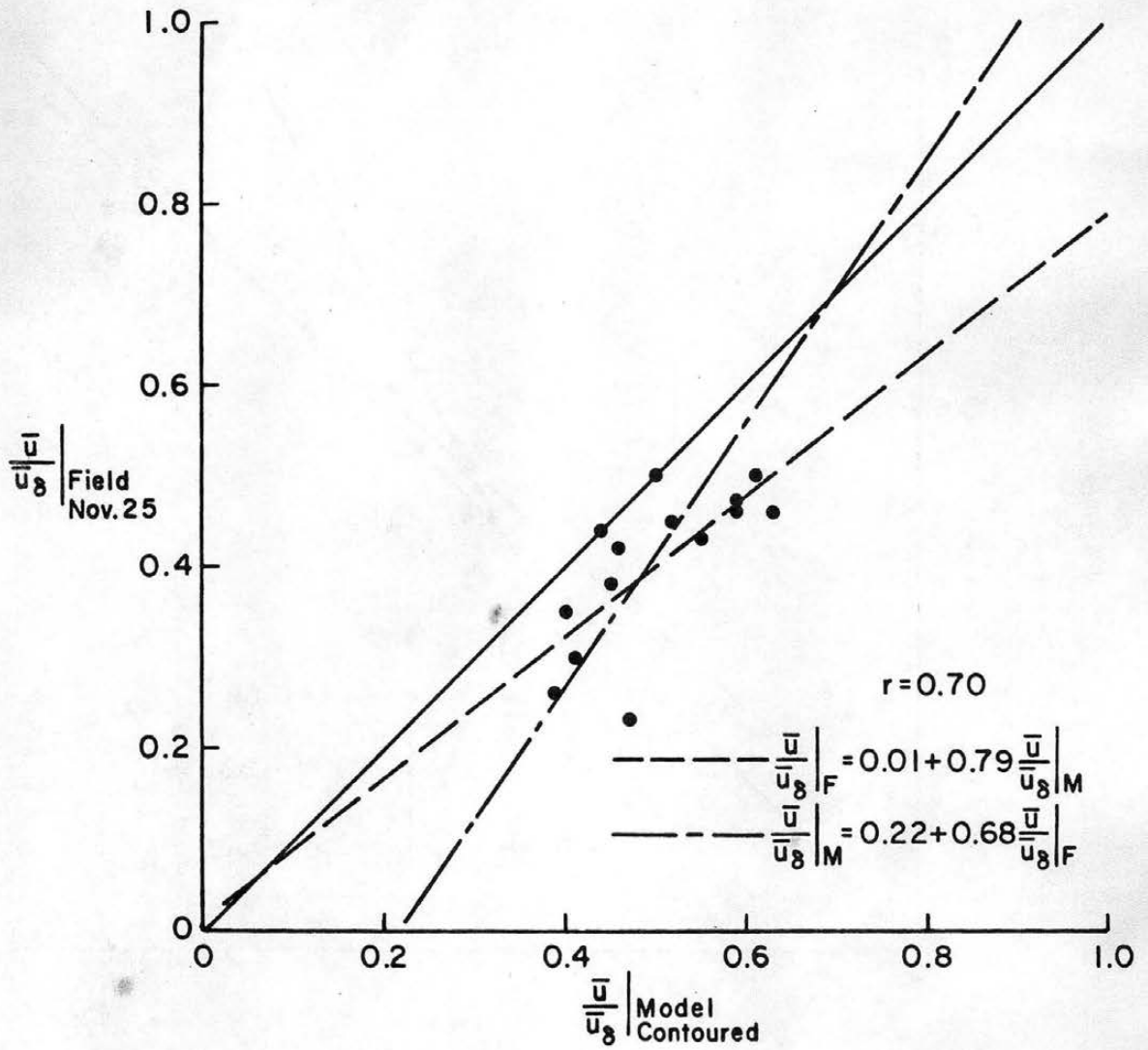


Figure 8-5. Scatter diagram field test data, November 25 versus contoured model data.

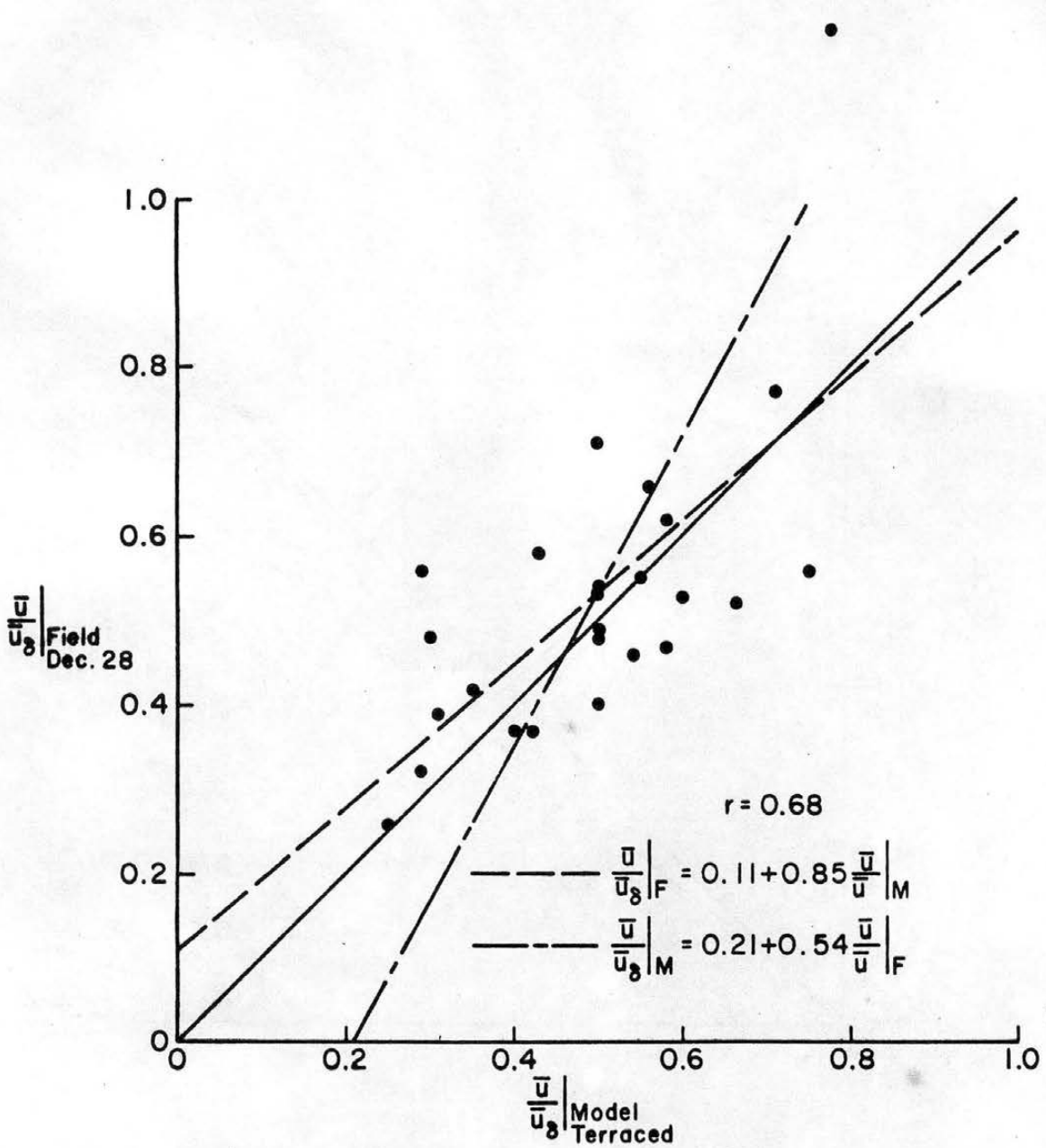


Figure 8-6. Scatter diagram field test data, December 28 versus terraced model data.

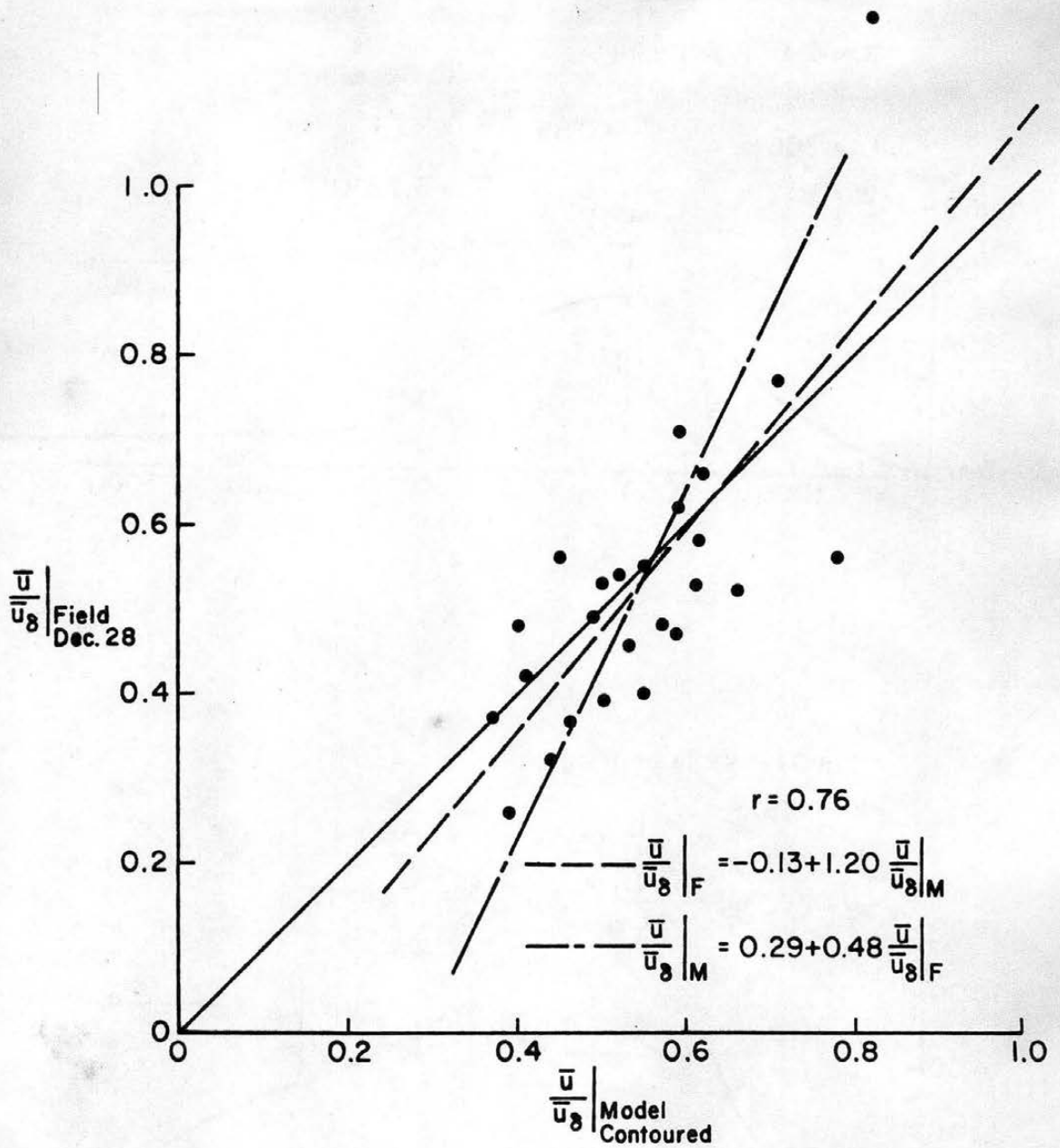


Figure 8-7. Scatter diagram field test data, December 28 versus contoured model data.

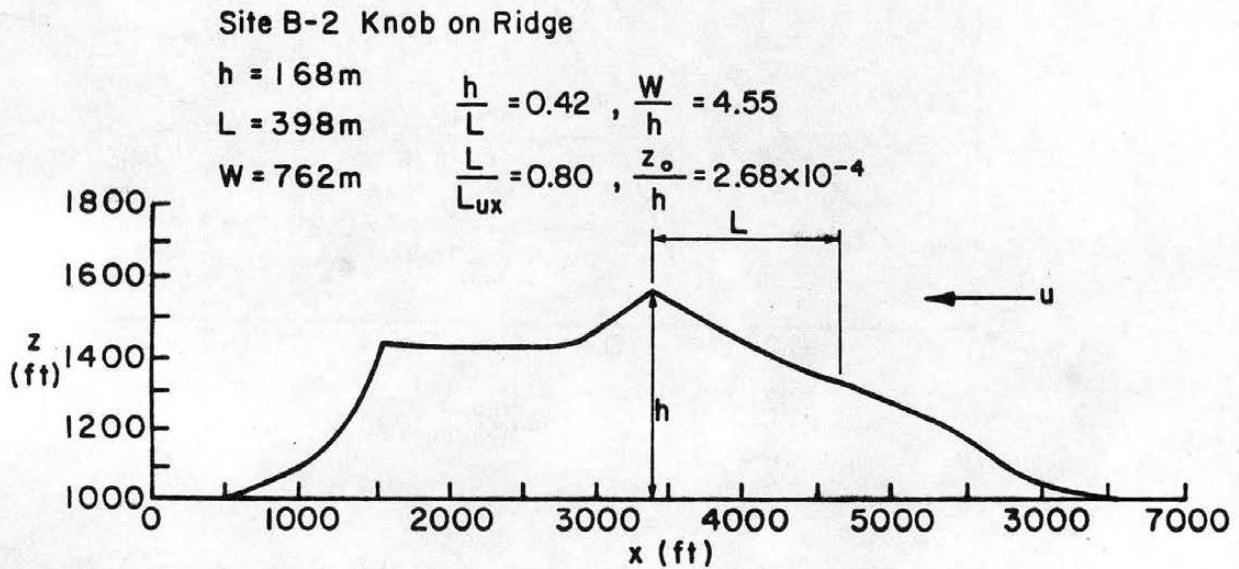
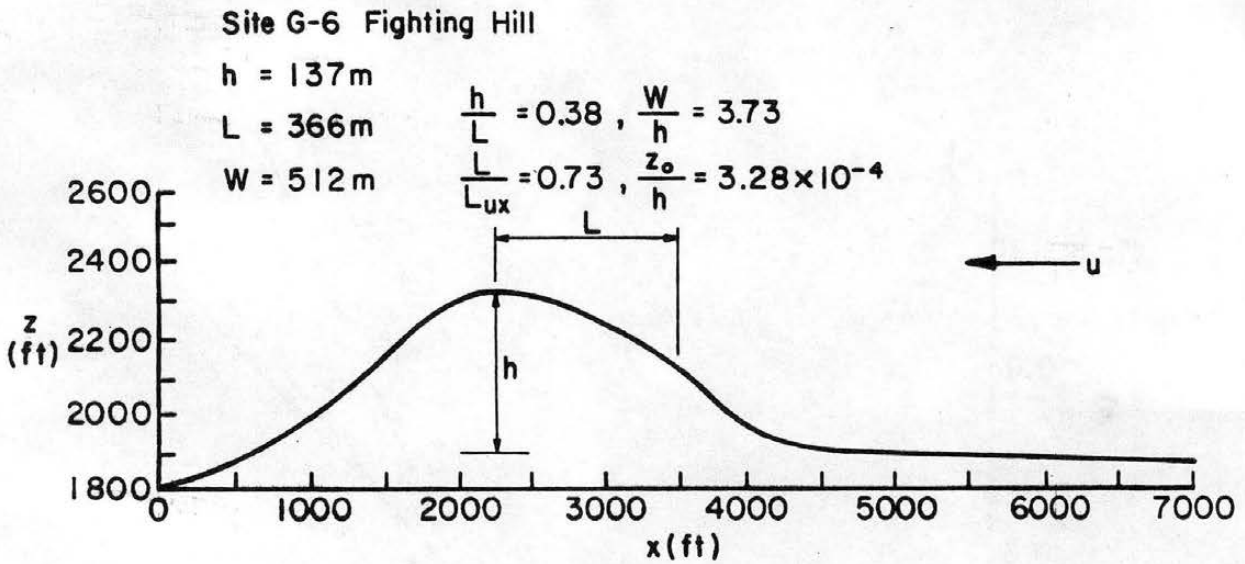


Figure 8-8. Terrain cross sections Rakaia Gorge at section B-2 and section G-6.

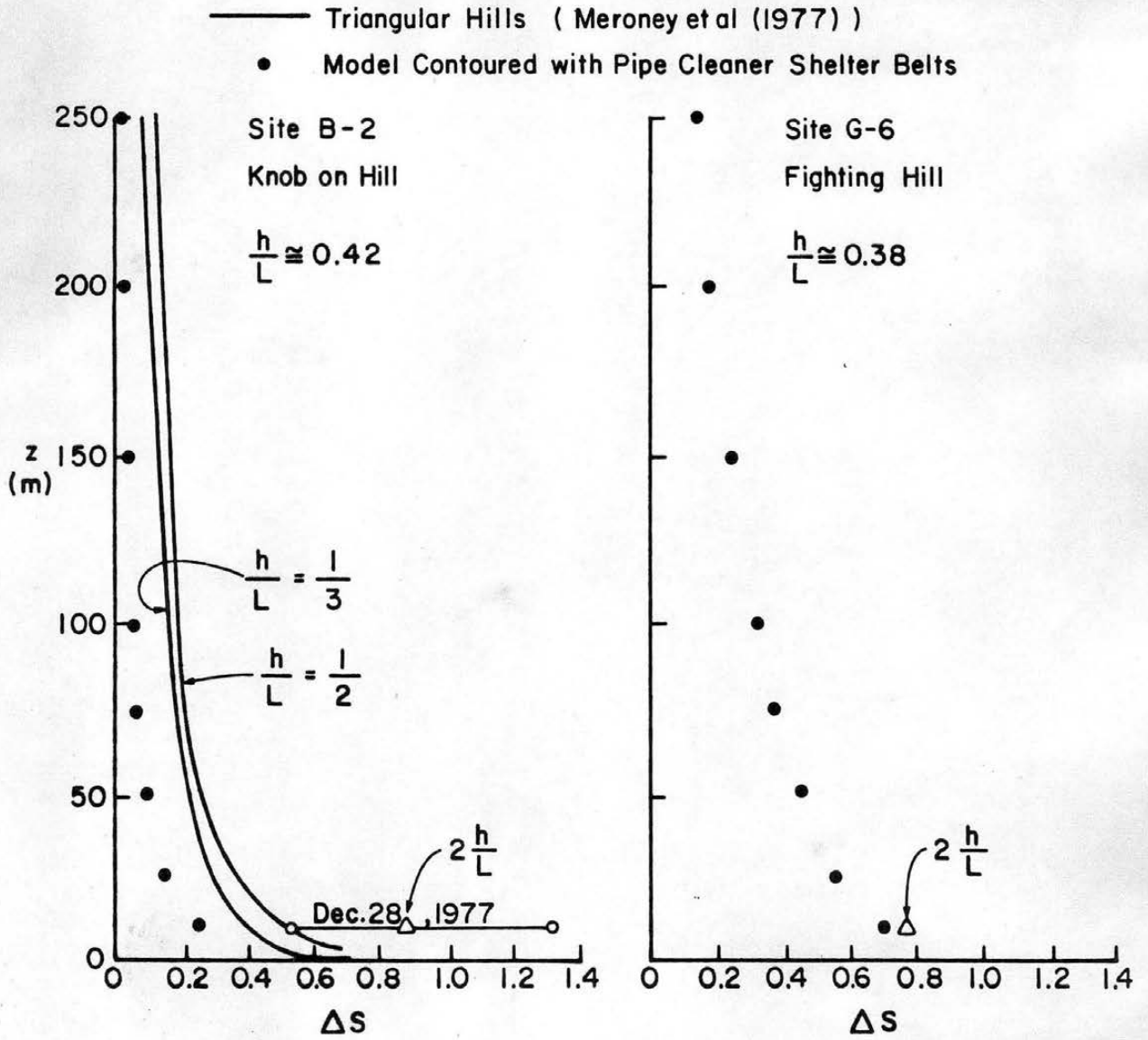


Figure 8-9. Fractional speedup factor results over crest of hills at sections B-2 and G-6.

TABLES

TABLE 2-1 LABORATORY SIMULATION OF FLOW OVER IRREGULAR TERRAIN

AUTHOR/(DATE)	TOPOGRAPHIC SITE	PROBLEM STUDIED	TYPE OF AIR FLOW	MAXIMUM HEIGHT OF RISE (m)	LENGTH SCALE RATIO	SIMILITUDE CRITERIA						
						$\delta/\Delta H$	$\frac{1}{\alpha}$	$\frac{z_0}{\Delta H} \times 10^4$	$\frac{\bar{U}^2}{U_0}$	$\frac{U_w}{U_0}$	$\frac{L_u}{\Delta H}$	Ri
▲1. Field & Warden (1929-1930)	Rock of Gibraltar	Topographic effects & turbulence	Neutral	520	5,000	0	0					
▲2 Abe (1941)	Mt. Fuji, Japan	Mountain clouds and topographic effects	Barostromatic (dry ice)	4,000	50,000							not accurate
▲3 Putnam (1948)	Pond Glastenberg, Mt. Washington	Topographic effects	Neutral	300 850 1,154	5,280 8,280 5,280							
4 Suzuki & Yabuki (1956)	Idealized hills	Mountain lee waves	Barostromatic (brine solution)			0	0					
5 Long (1953, 1954, 1955)	Idealized hills	Mountain lee waves	Barostromatic (brine solution)			0	0					13-94.0
▲ Long (1959)	Sierra Nevada Mountains, Calif.	Mountain lee waves	Barostromatic (brine solution)	2,750	75,000	0	0					12-300
6 Nemoto (1961)	Enoshima & Akashi Channel, Japan	Turbulence & Velocity Profiles	Neutral	60	600 3,300/ 10,000		1.0		0.20		1.33	
▲7 Halitsky, Toleiss, Kaplin & Magony (1962-63)	Bear Mountain, New York	Turbulence & wake patterns	Neutral	390	1,920	1.25			0.16			
8 Briggs (1963)	Rock of Gibraltar	Turbulence Patterns	Neutral	520	5,000	0	0					
9 Halitsky, Magony & Halpern (1964-65)	Mountains near Manchester, Vermont	Topographic effects	Neutral									
10 Plate & Lin (1965)	Idealized hill	Velocity & turbulence in wake	Neutral Unstable			3-9 3-5	0.15 0.19	1.5 1.5	0.14	0.032 0.032		0.02
11 Chang (1966)	Idealized hill	Velocity & turbulence in wake	Neutral			2	0.15	1.5				
▲2 Cermak & Peterka (1966)	Pt. Arguello, California	Topographic effects & diffusion	Barostromatic Neutral	500 500	12,000 12,000	9.0 9.0	0.25 0.25					0.31
▲3 Meroney & Cermak (1967)	San Nicolas Island, California	Topographic effects & diffusion	Neutral & Barostromatic	275 275	6,200 6,200	12.6 12.6	0.14 0.20	0.20		0.032		0.30
14 Lin & Binder (1967)	Idealized mountain	Mountain lee waves	Barostromatic									4-25

▲Field observations available.

TABLE 2-1 LABORATORY SIMULATION OF FLOW OVER IRREGULAR TERRAIN (continued)

AUTHOR/(DATE)	TOPOGRAPHIC SITE	PROBLEM STUDIED	TYPE OF AIR FLOW	MAXIMUM HEIGHT OF RISE (m)	LENGTH SCALE RATIO	SIMILITUDE CRITERIA						
						$\delta/\Delta H$	$\frac{1}{\delta}$	$\frac{z_o}{\Delta H} \times 10^4$	$\frac{\bar{U}^*}{U_o}$	$\frac{U_x}{U_o}$	$\frac{L_x}{\Delta H}$	Ri
15 Garrison & Cermak (1968)	San Bruno Mountain, California	Topographic effects	Neutral Barostromatic (dry ice)	400	6000/4800	3.7	0.16	25		0.125		0.32
				400	6000/4800	3.7	0.16	25				
				400	5000/2400	1.9						
16 Hsi, Binder & Cermak (1968)	Green River, Utah	Topographic effects	Neutral	65	800	6.0	0.14	2				
17 Zrajevsky, Doroshenko & Chepik (1968)	Idealized hill	Topographic effects	Neutral									
18 Kitabayashi, Orgill & Cermak (1971)	Elk Mountain, Wyoming	Topographic effects, diffusion	Neutral Barostromatic (dry ice)	1200	9600	2.0	0.21	70		0.149		1.70
				1200	9600	2.0	0.32					
19 Orgill, Cermak & Grant (1971)a	Eagle River, Chalk Mountain Area, Colorado	Topographic effects, diffusion	Neutral Barostromatic (dry ice)	1950	9600	4.0	0.25	3	0.28			6.0
				1950	9600	2.0		0.50				
20 (1971)b	San Juan Mountains, Colorado	Topographic effects, diffusion	Neutral Barostromatic	2250	14,000 hor.	2.0	0.35		0.15			
				2250	9,600 ver.	2.0						
21 Mori, Miyata, & Mitsuta (1971)	Mt. Takakura, Japan	Topographical effects	Neutral	300	5000							
22 Meroney, Chaudhry (1971-72)	Rocky Flats, Colorado	Topographic effects & diffusion	Neutral	140	1000	3.0	0.14	2	0.13			
23 de Bray (1973)	Idealized ramps & escarpments	Speedup	Neutral	-		3.0	0.14		0.12			
				-		3.0	0.11	0.15				
24 Sacre (1973)	Idealized ramps & hills	Speedup	Neutral	-		0.05			0.15			
				-		3.0	0.15					
25 Counihan (1973)	Idealized ramps & hills		Neutral			8, 12			0.10			
26 Hewson, et al (1973-75)	Yaquina Head, Oregon	Speedup for WECS	Neutral	15	300	1.7						
27 Freeston (1974)	Idealized hill escarpments	Speedup	Neutral				0.14					
28 Meroney & Cermak (1974-1975)	Mississippi River, Lansing, Iowa	Topographic effects & diffusion	Neutral Barostromatic	150	400	2.0	0.27	60				1.0
				150	400	2.0	0.70	60				
29 Bowen & Lindley (1974)	River banks & coastal beach, New Zealand	Speedup	Neutral	10,13	200-250	4.5	0.18	0.5	0.18	0.16		
30 Liu & Lin (1976)	Idealized Saddle Mountain Garfield, Utah	Topographic effects & diffusion	Barostromatic Barostromatic (brine solution)	1480	10,000							0-58 9-36

*Field observations available.

TABLE 2-1 LABORATORY SIMULATION OF FLOW OVER IRREGULAR TERRAIN (continued)

AUTHOR/(DATE)	TOPOGRAPHIC SITE	PROBLEM STUDIED	TYPE OF AIR FLOW	MAXIMUM HEIGHT OF RISE (m)	LENGTH SCALE RATIO	SIMILITUDE CRITERIA						
						$\delta/\Delta H$	$\frac{1}{\alpha}$	$\frac{z_o}{\Delta H} \times 10^4$	$\frac{U^*}{U_o}$	$\frac{U_*}{U_o}$	$\frac{L_u x}{\Delta H}$	Ri
31 Meroney, et al (1976) (1977) (1978)	Idealized hills Shapes: 2d 2d 3d	Topographic effects for WECS	Neutral			10.0	0.14	1.0	-0.15	0.032		
			Barostromatic			10.0		1.0				
			Neutral			10.0		1.0				
▲ 32 Kitabayashi (1977)	Idealized hills	Stagnant flows	Barostromatic			3.0						0.19-2.78
33 Petersen & Cermak (1977-78)	Geysers Area, California	Topographic effects of diffusion	Neutral	700	1920	2.5		7.0				
34 Cermak & Muttter (1977-78)	Kahe, Oahu	Topographic effects of diffusion	Neutral	900	6500							
▲ 35 Govind, et al. (1977-78)	Kingston, Tennessee	Topographic effects of diffusion	Neutral	150	800							
36 Riley, Liu & Geller (1976)	Idealized hill 3-d	Topographic effects of diffusion	Barostromatic (brine solution)	1480	10,000							5-288
▲ 37 This Report (1978)	Rakaia Gorge, New Zealand	Topographic effects for WECS	Neutral	200	5000	2.5	0.15	1.0	.13	0.03	0.75	

▲ Field observations available.

TABLE 3-1 RAKAIA RIVER GORGE CLIMATOLOGY

DATA*	WETF STATION			
	RAKAIA GORGE	MT. HUTT	METHVEN	HIGHBANK
<u>Wind Speed (m/s)</u>				
Average 1975	7.29 ^Δ	6.19 ^Δ	6.32 ^Δ	5.17 ^Δ
Average 1976	5.91	4.81 ^Δ	4.90 ^Δ	4.31
Average 1977	6.67	5.94	5.42 ^Δ	4.61
November 1977	8.74	7.94	-	5.88
December 1977	8.72	6.54	-	4.85
<u>Wind Energy Flux (w/m²)</u>				
Average 1975	485.7 ^Δ	301.0 ^Δ	126.5 ^Δ	150.4 ^Δ
Average 1976	299.9	121.4 ^Δ	59.6 ^Δ	93.7
Average 1977	403.7	269.7	65.5 ^Δ	110.9
November 1977	673.3	561.1	-	188.6
December 1977	795.4	270.3	-	136.7
<u>Energy Pattern Factor</u>				
Average 1975	2.047 ^Δ	2.067 ^Δ	1.615 ^Δ	1.780 ^Δ
Average 1976	2.369	1.783 ^Δ	1.709 ^Δ	1.908
Average 1977	2.220	1.574	1.410 ^Δ	1.849

* Corrected for instrument nonlinearities and scaled to 10 m AGL

^Δ Less than 6 months of data

Data made available courtesy N. Cherry, Lincoln College, Christchurch, New Zealand.

TABLE 4-1 TYPICAL BOUNDARY LAYER WIND TUNNEL CHARACTERISTICS

WIND TUNNEL PROPERTY	RANGE
Tunnel height H_T (m)	0.5 - 2.5
Tunnel width W_T (m)	0.5 - 4.0
Tunnel length L_T (m)	1.0 → 30.0
Boundary depth δ (m)	0.10 → 2.0
Roughness z_o (mm)	0.01 → 15.0
Velocity U_o (m/s)	0.0 → 36.0
Integral scale $L_{u_{x_o}}$ (m)	0.06 → 0.60
Temperature gradient $d\theta/dz$ ($^{\circ}\text{C}/\text{m}$)	0.0 → 200
Hill height h (m)	0.02 → 0.5
Hill half width L (m)	0 → 2
Resolution Δz (mm)	~ 0.1 mm
Surface friction $C_f/2$ (dimensionless)	0.0005 - 0.0040
Richardson number Ri_B (dimensionless)	0.0 → 1.0
Monin-Obukhov length L_{MO} (m)	0.065 → ∞
Turbulence intensity $\sqrt{U'^2}/U_o$	-2.0 - 3.0
Power law coefficient $1/\alpha$ (dimensionless)	0.05 - 0.80

TABLE 4-2 TYPICAL FIELD CHARACTERISTICS

FIELD PROPERTY	RANGE
Boundary depth δ_G (m)	300 - 600 - 1000+ ?
Roughness z_o (m)	0.001 → 1.5
Velocity U_G (m/s)	0.0 → 30
Integral scale (L_u) _o (m) @ 20 m @ 100 m	30 - 150 110 - 300 - 1000?
Hill height h (m)	10 → 3000
Hill half width L (m)	0 → 6 x 10 ⁴
Minimum resolution Δz (m)	~10 m
Turbulence intensity $\sqrt{U'^2}/U_*$ (dimensionless)	1.3 → 5.0
Surface friction $C_f/2$ (dimensionless)	0.001 → 0.004
Richardson number Ri_B (dimensionless)	+ - 1.0 → + 1.0 +
Monin-Obukhov length L_{MO} (m)	- ∞ → -8 & 12 → + ∞
Power law coefficient $1/\alpha$ (dimensionless)	0.05 - 0.70

TABLE 4-3 TYPICAL WIND TUNNEL AND FIELD PARAMETER RANGE

DIMENSIONLESS PARAMETER	WIND TUNNEL RANGE	FIELD RANGE
Reynolds number $Re_h = u_o h/\nu$	$0 \rightarrow 7.0 \times 10^5$	$0 \rightarrow 6.0 \times 10^6$
Richardson number $Ri_B = \frac{g(dT/dz) h}{T U_o^2}$	$-1.0 \rightarrow 1.0$	$-1.0 \rightarrow 1.0$
Prandtl number $Pr = \mu c_p/k$	~ 0.72	~ 0.72
Skin friction coefficient or Stanton number $\frac{C_f}{2} = \frac{\tau_w}{\rho U_o^2} = \left(\frac{u_*}{U_o}\right)^2$ $St = \frac{q}{\rho c_p (\Delta T)_o}$	$0.006 \rightarrow 0.004$	$0.001 \rightarrow 0.004$
Insolation parameter $Fr_I = \frac{U_o^2 T_w}{g(T_w - T_n)L}$	$0.002 \rightarrow \infty$	$2.5 \times 10^{-5} \rightarrow \infty$
Scaling lengths z_o/h	$2 \times 10^{-5} \rightarrow 0.25$	$3.0 \times 10^{-7} \rightarrow 0.15$
δ/h	$0.20 \rightarrow 50.0$	$0.10 \rightarrow 100$
h/L	$0.05 \rightarrow \infty$	$2 \times 10^{-4} \rightarrow \infty$
$(L_{u_x})_o/L$	$0.06 \rightarrow \infty$	$0.001 \rightarrow \infty$
h/H_T	$0.01 \rightarrow 0.15$	--
L_T/L	$0 \rightarrow 30 \rightarrow \infty$	--
h/L_{MO}	$0 \rightarrow 5.0$	$-360 \rightarrow 240$
Power law coefficient α	$0.05 \rightarrow 0.8$	$0.05 \rightarrow 0.7$

TABLE 5-1 EQUIPMENT UTILIZED DURING RAKAIA GORGE EXPERIMENTS

LABORATORY EQUIPMENT

1. DISA Type 55D01 CT Anemometer
55D25 Auxiliary Unit
55D10 Linearizer
55D35 RMS Unit
55D30 DC Voltmeter
2. DISA Type 52B01 Sweep Drive Unit
55H01 Traversing Mechanism and Guide Tubing
3. DISA Type 55D75 Time Delay Unit - 100 ms range delay
55D70 Correlator - integrating time 30 sec.
4. DISA Type 55F35 Probes
55F31 Right angle wire perpendicular to probe axis
5. Brüel & Kjaer Octave and Third Octave Spectrometer
Type 2114 Averaging times 1-100 sec
2 Hz - 160 kHz range
Rise time 20 μ sec

Brüel & Kjaer Level Reorder Type 2307

<u>Settings</u>	<u>Chart Speed</u>	<u>Averaging Times</u>
2-10 Hz	.01 mm/s	30
12.5-50	.03	10
63-200	.1	3
200-10,000	.1	1

6. E. Schiltknecht Precision Liquid Manometer
Type 612a 0-500 mm H₂O 1/10 mm H₂O division
7. Thermal Systems, Inc., Calibrator Model 1125
8. United Sensor Cobra Probe Type DC-125-24-F-22-CD
9. Setra Systems Low Range Pressure Transducer - Model 237 ± 0.1 psid full range
4 volt output, noise 1.2 mv RMS
10. Scanivalve 48 step Model DS3-48

FIELD EQUIPMENT

1. Thermometers 0 - 100°C 0.5°C increments
2. RIMCO CSIRO Cup Anemometers - Sensitive impulse anemometer
Rauchfuss Inst. & Staff Pty, Ltd.
Burwood, Victoria, Australia
3. Tower Poles 10 meters, 3 guyed at 7 m
2 inch diameter aluminum, 1/8 inch wall
4. Aneroid Barometer Type No. M1991
Mechanism Ltd., Croydon
Negretti & Zambra Ltd.
5. University of Canterbury
Anemometer Counter and Power Supply
6. Hamilton Jet Boat
New Zealand Fisheries

TABLE 6-1 FIELD SITE EXPOSURE NOTES

FIELD SITE NO.	COMMENTS BY TEAM CHIEF
11	Shelterbelt 100 m to W
13	Mt. Hutt WETF location
14	Shelterbelts 250 m to NWW and 500 m to S
15	Rakaia Gorge WETF location, shelterbelt 100 m to W
16	Center of sheep pasture, shelterbelts 500 m all directions
17	Top of knob open to N, S, E, W
18	Open to N, E & W, rise to S
19	Open to N, NW, E, rise to S & W
21	River embankment 100 m to W
22	50 m cliff 100 m to NE
23	170 m cliffs 200 m to N, cliffs 100 m to E, bush 50 m to W
24	
24A	Open to N & NW
25	Open to N, S, E, & W
27	200 m hills 50 m to E
28	10 m cliffs 150 m to W, 150 m hills 300 m to E
29	Open to N, S, E & W
AA	Gorge ~ 200 m wide, mast 40 m from W bank
31	Hills 100 m to N, shelterbelt 100 m SSW
32	Center of E bridge over Rakaia Gorge
33	Shelterbelt 150 m to W, 100 m to E
34	Gorse hedge 100 m to S
35	150 m downwind of shelterbelt
36	Open to N, S, E, W
37	Open to N, S, E, W
38	Open to N, S, E, W
39	Open to N, S, E, W

TABLE 7-1 INTEGRAL SCALES - FLOW OVER RAKAIA GORGE MODEL

Z _m (m)	APPROACH FLOW			SECTION D-3 TERRACED			SECTION D-3 CONTOURED & S.B.		
	(L _{u_x}) _{corr} (m)	(L _{u_x}) _{1/e} (m)	(L _{u_x}) _{spec} (m)	(L _{u_x}) _{corr} (m)	(L _{u_x}) _{1/e} (m)	(L _{u_x}) _{spec} (m)	(L _{u_x}) _{corr} (m)	(L _{u_x}) _{1/e} (m)	(L _{u_x}) _{spec} (m)
25	590	453	664	432	292	152	645	188	128
50	-	-	-	480	422	170	-	-	-
100	890	630	730	540	475	152	587	315	128

$$(L_{u_x})_{\text{corr}} = \bar{u}(z) \int_0^{\infty} R(\tau) d\tau$$

$$(L_{u_x})_{1/e} = (T_E)_R = \frac{1}{e} \bar{u}(z)$$

$$(L_{u_x})_{\text{spec}} = \frac{0.146}{(k_u)_{\text{peak}}} = \frac{0.146 \bar{u}(z)}{(n_u)_{\text{peak}}}$$

TABLE 7-2 LABORATORY DATA - TERRACED MODEL (continued)

SECTION F-F

SITE NO.	1		2		3		4		5		6	
	\bar{U}/\bar{U}_δ	U'/\bar{U}	\bar{U}/\bar{U}_δ	U'/\bar{U}	\bar{U}/\bar{U}_δ	U'/\bar{U}	\bar{U}/\bar{U}_δ	U'/\bar{U}	\bar{U}/\bar{U}_δ	U'/\bar{U}	\bar{U}/\bar{U}_δ	U'/\bar{U}
2	.55	-	.25	-	.26	-	.58	-	.55	-	.50	-
5	.63	.14	.45	.27	.30	.27	.66	.14	.62	.14	.58	.14
10	.69	.14	.60	.24	.26	.33	.72	.13	.67	.13	.64	.14
15	.72	.13	.68	.19	.26	.39	.76	.13	.70	.12	.70	.14
20	.75	.13	.72	.17	.30	.41	.79	.12	.73	.12	.74	.14
30	.81	.12	.79	.13	.53	.30	.84	.11	.77	.11	.80	.12
40	.86	.11	.83	.11	.77	.14	.88	.09	.80	.10	.84	.10
50	.91	.09	.86	.10	.84	.11	.91	.08	.83	.10	.89	.09
75	.98	.06	.91	.08	.93	.07	.95	.06	.89	.08	.93	.08
100	.99	.045	.97	.05	.97	.06	.97	.05	.94	.06	.96	.06
125	.995	.04	.99	.04	.99	.05	.97	.04	.99	.05	.98	.05
150	1.00	.04	1.00	.04	.996	.04	1.00	.04	1.00	.04	1.00	.04
175					1.00	.03						

SECTION D-D

SITE NO.	1		2		3		4		5		6		7	
	\bar{U}/\bar{U}_δ	U'/\bar{U}	\bar{U}/\bar{U}_δ	U'/\bar{U}	\bar{U}/\bar{U}_δ	U'/\bar{U}	\bar{U}/\bar{U}_δ	U'/\bar{U}	\bar{U}/\bar{U}_δ	U'/\bar{U}	\bar{U}/\bar{U}_δ	U'/\bar{U}	\bar{U}/\bar{U}_δ	U'/\bar{U}
2	.48	-	.52	-	.42	-	.33	-	.29	-	.57	-	.66	-
5	.59	.18	.59	.16	.51	.19	.37	.19	.38	.21	.65	.12	.74	.62
10	.67	.14	.64	.16	.58	.17	.40	.23	.45	.21	.70	.11	.79	.12
15	.71	.12	.68	.14	.61	.17	.42	.25	.51	.21	.74	.11	.83	.11
20	.74	.12	.72	.13	.66	.16	.47	.22	.58	.18	.76	.11	.86	.09
30	.80	.10	.77	.12	.72	.15	.59	.19	.58	.14	.81	.10	.88	.07
40	.84	.09	.81	.11	.78	.13	.68	.14	.74	.11	.84	.095	.88	-
50	.88	.075	.84	.10	.83	.10	.74	.12	.79	.10	.87	1.09		
75	.89	.07	.91	.08	.90	.08	.83	.10	.85	.09	.92	.07		
100			.96	.06	.94	.06	.90	.07	.90	.07	.96	.06		
125			.99	.04	.97	.05	.94	.06	.95	.06	.99	.05		
150			1.00	.03	1.00	.04	.97	.05	.98	.05	1.00	.03		
175							1.00	.04	1.00	.04				

SECTION E-E

SITE NO.	1		2		3		4		5	
	\bar{U}/\bar{U}_δ	U'/\bar{U}	\bar{U}/\bar{U}_δ	U'/\bar{U}	\bar{U}/\bar{U}_δ	U'/\bar{U}	\bar{U}/\bar{U}_δ	U'/\bar{U}	\bar{U}/\bar{U}_δ	U'/\bar{U}
2	.54	-	.38	-	.47	-	.48	-	.30	-
5	.62	.14	.47	.21	.54	.14	.56	.13	.46	.25
10	.68	.13	.54	.20	.59	.13	.60	.13	.58	.20
15	.73	.12	.61	.17	.63	.12	.63	.12	.64	.17
20	.76	.11	.66	.14	.63	.12	.64	.12	.69	.16
30	.81	.10	.73	.12	.67	.12	.68	.12	.76	.13
40	.84	.09	.77	.11	.70	.12	.71	.11	.80	.11
50	.87	.08	.81	.10	.74	.11	.75	.10	.84	.10
75	.93	.07	.85	.08	.81	.11	.82	.09	.90	.08
100	.97	.05	.92	.06	.88	.08	.88	.07	.94	.06
125	.99	.04	.95	.05	.93	.06	.92	.06	.96	.05
150	1.00	.03	.98	.04	.96	.05	.96	.05	.98	.05
175			1.00	.04	.99	.04	.99	.04	.99	.04
185					1.00	.04	1.00	.04	1.00	.04

TABLE 7-3 LABORATORY DATA - CONTOURED MODEL (continued)
PIPE CLEANER SHELTERBELTS

SECTION F-F

SITE NO.	1		2		3		4		5		6		7		
	$\frac{z}{(\text{mm})}$	\bar{u}/\bar{u}_δ	u'/\bar{u}	\bar{u}/\bar{u}_δ	u'/\bar{u}	\bar{u}/\bar{u}_δ	u'/\bar{u}	\bar{u}/\bar{u}_δ	u'/\bar{u}	\bar{u}/\bar{u}_δ	u'/\bar{u}	\bar{u}/\bar{u}_δ	u'/\bar{u}	\bar{u}/\bar{u}_δ	u'/\bar{u}
2		.14	.64	.50	.29	.39	.25	.55	.21	.39	.27	.59	.18		
5		.38	.45	.62	.23	.47	.23	.62	.18	.48	.27	.64	.17		
10		.66	.20	.67	.19	.47	.29	.71	.17	.62	.21	.69	.15		
15		.71	.18	.71	.17	.50	.34	.79	.14	.70	.15	.72	.15		
20		.74	.17	.76	.15	.57	.33	.82	.12	.74	.15	.76	.14		
30		.79	.15	.81	.12	.76	.19	.85	.11	.81	.13	.81	.12		
40		.83	.13	.85	.10	.84	.11	.87	.11	.86	.11	.85	.11		
50		.85	.13	.86	.10	.86	.10	.89	.10	.89	.10	.88	.10		
75		.91	.10	.91	.08	.92	.08	.94	.08	.94	.07	.93	.08		
100		.96	.07	.94	.07	.96	.07	.98	.06	.97	.06	.97	.06		
125		.98	.06	.96	.06	.98	.05	.99	.05	.99	.05	.99	.05		
150		.99	.05	.98	.06	.99	.05	1.00	.04	1.00	.04	.998	.04		
175		1.00	.04	.99	.05	1.00	.04					1.00	.04		
200				1.00	.05										

SECTION D-D

SITE NO.	1		2		3		4		5		6		7		
	$\frac{z}{(\text{mm})}$	\bar{u}/\bar{u}_δ	u'/\bar{u}	\bar{u}/\bar{u}_δ	u'/\bar{u}	\bar{u}/\bar{u}_δ	u'/\bar{u}	\bar{u}/\bar{u}_δ	u'/\bar{u}	\bar{u}/\bar{u}_δ	u'/\bar{u}	\bar{u}/\bar{u}_δ	u'/\bar{u}	\bar{u}/\bar{u}_δ	u'/\bar{u}
2		.50	-	.43	.30	.61	.16	.47	.21	.51	.19	.67	.14	.63	.17
5		.62	.16	.52	.26	.62	.15	.51	.21	.53	.20	.72	.13	.73	.15
10		.67	.15	.61	.19	.64	.15	.55	.22	.58	.20	.75	.12	.77	.14
15		.72	.15	.62	.18	.64	.16	.59	.20	.62	.19	.76	.12	.81	.13
20		.76	.14	.66	.18	.64	.17	.63	.18	.66	.19	.78	.13	.84	.12
30		.80	.12	.71	.17	.66	.19	.68	.16	.74	.16	.81	.13	.90	.10
40		.84	.11	.76	.16	.73	.18	.74	.15	.80	.13	.84	.12	.93	.08
50		.86	.10	.80	.15	.78	.15	.79	.13	.83	.11	.88	.11	.95	.07
75		.92	.08	.88	.11	.86	.11	.88	.10	.90	.09	.94	.08	.96	.06
100		.92	.08	.93	.08	.93	.08	.93	.07	.95	.07	.96	.06		
125				.97	.07	.95	.07	.97	.06	.97	.06	.98	.06		
150				1.00	.06	.99	.06	.99	.05	.99	.05	.99	.04		
175						1.00	.05	1.00	.04	1.00	.04	1.00	.04		

SECTION E-E

SITE NO.	1		2		3		4		5		SECTION A-A		
	$\frac{z}{(\text{mm})}$	\bar{u}/\bar{u}_δ	u'/\bar{u}	\bar{u}/\bar{u}_δ	u'/\bar{u}	\bar{u}/\bar{u}_δ	u'/\bar{u}	\bar{u}/\bar{u}_δ	u'/\bar{u}	\bar{u}/\bar{u}_δ	u'/\bar{u}	\bar{u}/\bar{u}_δ	u'/\bar{u}
2		.58	.17	.43	.23	.46	.20	.54	.18	.44	.21	.44	.21
5		.65	.15	.51	.21	.51	.19	.59	.16	.52	.20	.47	.20
10		.70	.14	.58	.20	.55	.17	.63	.16	.60	.18	.46	.23
15		.73	.13	.65	.17	.58	.17	.65	.15	.65	.16	.48	.25
20		.75	.13	.70	.15	.59	.17	.67	.15	.69	.15	.52	.27
30		.78	.12	.75	.13	.63	.17	.71	.15	.74	.12	.63	.23
40		.81	.12	.79	.12	.68	.18	.76	.14	.78	.12	.73	.18
50		.84	.12	.81	.11	.73	.17	.79	.13	.81	.11	.80	.12
75		.90	.10	.87	.10	.85	.13	.87	.10	.88	.09	.87	.09
100		.94	.07	.92	.08	.92	.09	.93	.08	.93	.08	.93	.08
125		.98	.06	.97	.06	.97	.06	.96	.06	.96	.06	.97	.06
150		.99	.04	.99	.05	.99	.05	.98	.05	.98	.05	.99	.05
175		1.00	.04	1.00	.04	1.00	.04	.99	.04	.99	.04	1.00	.04
200								1.00	.04	1.00	.04		

TABLE 7-4 LABORATORY DATA - CONTOURED MODEL

SECTION F-F (NO SHELTERBELTS)

SITE NO.	1		2		3		4		5		6	
z (mm)	\bar{U}/\bar{U}_δ	U'/\bar{U}	\bar{U}/\bar{U}_δ	U'/\bar{U}	\bar{U}/\bar{U}_δ	U'/\bar{U}	\bar{U}/\bar{U}_δ	U'/\bar{U}	\bar{U}/\bar{U}_δ	U'/\bar{U}	\bar{U}/\bar{U}_δ	U'/\bar{U}
2	.59	.19	.61	.22	.45	.23	.68	.14	.63	.15	.59	.16
5	.66	.16	.72	.19	.50	.22	.78	.12	.70	.13	.67	.14
10	.73	.15	.77	.16	.49	.28	.82	.11	.75	.12	.73	.13
15	.77	.14	.81	.14	.51	.33	.84	.10	.79	.11	.77	.12
20	.79	.13	.85	.12	.58	.31	.85	.10	.81	.11	.80	.11
30	.81	.12	.91	.09	.78	.17	.87	.10	.85	.10	.84	.10
40	.84	.12	.93	.08	.87	.10	.90	.09	.88	.09	.88	.09
50	.86	.12	.95	.07	.89	.09	.91	.09	.91	.08	.90	.08
75	.91	.10	.97	.06	.95	.06	.96	.06	.96	.06	.95	.07
100	.95	.07	.98	.05	.98	.05	.99	.05	.99	.05	.99	.05
125	.98	.06	.99	.05	.99	.05	1.00	.04	1.00	.05	1.00	.04
150	.99	.05	1.00	.05	1.00	.04						
175	1.00	.04										
200												

SECTION F-F (YARN SHELTERBELTS)

SITE NO.	1		2		3		4		5		6	
2	.22	.57	.53	.21	.44	.23	.44	.28	.45	.21	.52	.20
5	.45	.32	.62	.19	.51	.20	.57	.22	.53	.21	.61	.17
10	.59	.20	.68	.17	.50	.24	.75	.13	.63	.16	.68	.15
15	.66	.18	.72	.16	.49	.30	.81	.11	.69	.15	.72	.14
20	.70	.17	.78	.14	.54	.30	.84	.10	.74	.14	.76	.14
30	.77	.15	.86	.10	.73	.19	.85	.10	.80	.12	.83	.12
40	.83	.13	.88	.09	.84	.09	.88	.09	.85	.10	.86	.10
50	.87	.11	.91	.08	.87	.08	.90	.08	.89	.08	.90	.09
75	.94	.08	.95	.07	.93	.07	.96	.06	.95	.06	.95	.07
100	.97	.05	.98	.05	.97	.05	.99	.05	.97	.05	.98	.05
125	.99	.04	.99	.04	.98	.04	1.00	.04	.98	.05	.99	.04
150	1.00	.04	1.00	.04	1.00	.04			.99	.04	1.00	.04
175									1.00			

SECTION H-H

SITE NO.	1		2		3	
2	.71	.13	.66	.14	.78	.13
5	.75	.13	.75	.12	.84	.12
10	.79	.12	.80	.11	.86	.11
15	.82	.12	.83	.10	.89	.11
20	.83	.11	.85	.09	.90	.10
30	.88	.10	.88	.09	.93	.09
40	.91	.09	.90	.08	.95	.08
50	.94	.08	.93	.07	.97	.06
75	.97	.06	.97	.06	.99	.05
100	.99	.05	.99	.05	1.00	.05
125	1.00	.04	1.00	.05		
150						

TABLE 7-5 RAKAIA GORGE FIELD DATA - NOVEMBER 25, 1977

TIME Nov. 25, 1977	WETF STATION		MOBILE STATION														
	Rakaia* Gorge (m/sec)	Mt.* Hutt (m/sec)	11	13	14	15	16	18	21	22	23	24	25	27	28	31	32
0900	-	-															
0915	13.59	-															
0930	11.62	-				9:18- 9:28										9:24- 9:34	
0945	10.91	-							9:31- 9:41								
1000	9.66	-															
1015	10.73	9.30								10:06- 10:16						10:06- 10:16	
1030	8.58	10.01		10:26- 10:36							10:37- 10:47						
1045	7.69	9.48	T	-----T													
1100	9.30	9.12		10:55- 11:05													
1115	8.58	11.09											11:15 11:25				
1130	7.87	8.58															
1145	7.51	7.69				11:32- 11:42											

TABLE 7-5 RAKAIA GORGE FIELD DATA - NOVEMBER 25, 1977 (continued)

TIME Nov. 25, 1977	WETF STATION		MOBILE STATION															
	Rakaia* Gorge (m/sec)	Mt.* Hutt (m/sec)	11	13	14	15	16	18	21	22	23	24	25	27	28	31	32	
1200	6.62	11.09												11:56 12:06				
1215	8.05	8.76					12:06- 12:16											
1230	8.58	10.01												12:27- 12:37				
1245	5.37	5.37																
1300	3.93	5.54												12:58- 13:08				
1315	3.76	5.01						12:59- 13:09										
1330	3.76	4.65																
1345	2.68	-																
1400	1.97	-																
AVG COUNTS/MIN			261	283	226	385	231	82	303	212	131	238	185	124	111	326	162	
Velocity @ Time t **			7.18	7.78	6.21	10.58	6.35	2.25	8.33	5.85	3.60	6.54	5.09	3.41	3.05	8.96	4.45	
Velocity @ Time = T ***			6.44	7.00	6.36	7.00	6.07	4.86	5.87	4.18	3.60	6.39	5.34	4.88	6.24	5.93	3.19	
Velocity Fraction (\bar{U}/\bar{U}_δ) @ Time + T $^\Delta$			0.46	0.50	0.46	0.50	0.44	0.35	0.42	0.30	0.26	0.46	0.38	0.35	0.45	0.43	0.23	

** $\bar{U} \cong 0.0275 \times (\text{Pulses/minute}) \left[\frac{\text{m}}{\text{sec}} \right]$

* $\bar{U} \cong 0.17882 \times (\text{Pulses/15 minutes}) \left[\frac{\text{m}}{\text{sec}} \right]$

*** $\bar{U}_T = \bar{U}_t \times \frac{(\bar{U}RG)T}{(\bar{U}RG)t} \left[\frac{\text{m}}{\text{sec}} \right]$

$\Delta \left(\frac{\bar{U}}{\bar{U}_\delta} \right) T = \frac{\bar{U}_T}{\bar{U}_\delta T}$ where $\bar{U}_T = 13.90 \text{ m/sec}$
T = 10:45 a.m.

TABLE 7-6 RAKAIA GORGE FIELD DATA - DECEMBER 28, 1977

TIME Dec. 28, 1977	WETF STATION Rakaia* Gorge (m/sec)	Me.* Hutt (m/sec)	11	13	14	15	16	17	18	19	21	22	23	24	24A	25	27	28	29	31	33	34	35	36	37	38	39	AA
10:00	13:05																			9:43- 9:53								
10:15	14:13										10:00- 10:20																	10:15- 10:25
10:30	14:13		10:17- 10:52																									
10:45	12:88																				10:33- 10:43							
11:00	14:13		10:54- 11:09												10:50- 11:05													
11:15	11:09																											
11:30	11:62																											
11:45	10:37				11:32- 11:47										11:25- 11:40													
12:00	12:16		T -----																									
12:15	12:88				11:58- 12:13										12:02- 12:17													
12:30	10:55																											
12:45	9:84																											
13:00	9:84					12:47- 13:03																						
13:15	14:66																											
13:30	10:19																											
13:45	10:19										13:42- 13:57																	
14:00	9:84																											13:45- 13:55
14:15	13:77																											
14:30	13:77											14:20- 14:35																14:20- 14:30
14:45	12:52																											
15:00	11:27																											
AVG COUNTS/MIN			340	469	563	518	339	813	464	609	362	333	228	318	502	502	357	557	498	498	353	433	340	318	382	451	535	318
Velocity @ Time t **			9.35	12.90	15.48	14.25	9.32	22.66	12.76	16.75	9.96	9.16	6.27	10.78	13.81	13.81	9.82	15.32	13.70	13.70	9.71	11.91	9.35	8.75	10.51	12.40	14.71	8.75
Velocity @ Time T ***			8.05	12.44	16.71	13.45	11.52	28.00	11.27	18.07	8.57	9.88	6.05	11.02	14.45	15.04	11.32	12.71	12.10	12.77	9.17	12.46	9.35	10.81	8.72	15.32	12.99	7.53
Velocity Fraction ΔΔ			0.34	0.53	0.71	0.58	0.49	1.20	0.48	0.77	0.37	0.42	0.26	0.47	0.62	0.56	0.48	0.54	0.52	0.55	0.39	0.53	0.40	0.46	0.37	0.66	0.56	0.32
$\left(\frac{\bar{U}}{U_s}\right) @ \text{Time T}$			ΔΔ $\bar{U}_T = 23.36 \text{ m/sec}$ T = 12:00 Noon																									

TABLE 8-1 COMPARATIVE WIND SPEED VALUES
FIELD - LABORATORY

GRID POSITION	FIELD DATA		MODEL DATA 1/5000 SCALE			
	Nov. 25 10 m	Dec. 28 10 m	Terraced 10 m (XT)	Terraced 25 m	Contoured 10 m	Contoured 25 m
11	.46	.34	.50	.60	.63	.67
13	.50	.53	.50	.60	.50	.62
14	.46	.71	.50	.60	.59	.65
15	.50	.58	.43	.51	.61	.65
16	.44	.49	.50	.60	(0-.50)	(0-.50)
17	-	1.20	.78	.82	.82	.86
18	.35	.48	.50	.60	.57	.64
19	-	.77	.71	.75	.71	.75
21	.42	.37	.40	.54	.46	.51
22	.30	.42	.35	.40	.41	.50
23	.26	.26	.25	.30	.39	.47
24	.46	.47	.58	.63	.59	.65
24A	-	.62	.58	.63	.59	.65
25	.38	.56	.29	.36	.45	.48
27	.35	.48	.30	.30	.40	.45
28	.45	.54	.50	.59	.52	.58
29	-	.52	.66	.75	.66	.75
31	.43	.55	.55	.63	.55	.63
32	.23	-	.33	.37	.47	.51
33	-	.39	.31	.37	.50	.60
34	-	.53	.60	.65	.61	.65
35	-	.40	.50	.58	.55	.62
36	-	.46	.54	.65	.53	.60
37	-	.37	.42	.51	(0-.50)	(0-.50)
38	-	.66	.56	.65	.62	.68
39	-	.56	.75	.80	.78	.84
AA	-	.32	.29	.35	.44	.47

Note: 1) $r_{\text{Nov. 25/Dec. 28}} = 0.54$
n = 14

$r_{\text{Nov. 25/Dec. 28}} = 0.68$
w/o sites 11 & 18
n = 12

2) $r_{\text{Nov. 25/model terraced}} = 0.78$
w/o site 18
n = 13

$r_{\text{Nov. 25/model contoured}} = 0.70$
w/o site 18
n = 13

3) $r_{\text{Dec. 28/model terraced}} = 0.68$
w/o site 11
n = 25

$r_{\text{Dec. 28/model contoured}} = 0.76$
w/o site 11
n = 25

TABLE 8-2 CORRELATION STATISTICS

Comparison	Relevant Figure	n	a	b	r	r _{crit} @ 1%	Reject r=0 with 99% Conf	Sx ²	Sy ²	S ² y/x	S _b	t	t _{/.01/n-2}	Reject b=1.0
x = Field Case Nov. 25 to y = Field Case Dec. 28	8-3	12	.18	1.02	.68	.708	No	.006	.013	.008	.348	0.057	2.76	No
y = Field Case Nov. 25 to x = Model Terraced	8-4	14	.13	.63	.78	.661	Yes	.011	.007	.003	.145	2.53	2.68	No
y = Field Case Nov. 25 to x = Model Contoured	8-5	14	.01	.79	.70	.661	Yes	.007	.007	.004	.210	1.00	2.68	No
y = Field Case Dec. 28 to x = Model Terraced	8-6	25	.11	.85	.68	.505	Yes	.021	.033	.019	.194	0.75	2.50	No
y = Field Case Dec. 28 to x = Model Contoured	8-7	25	-.13	1.20	.76	.505	Yes	.013	.033	.015	.219	-.91	2.50	No

TABLE 8-3 WIND VELOCITY RANK TEST
NOVEMBER 25, 1977, DATA

WIND SPEED RANK HIGH TO LOW	MODEL (z = 10 m) Terraced Figure 7-9 Table 7-2	FIELD SITE (z = 10 m) Table 7-5	MODEL (z = 10 m) Contoured/sb Figure 7-28 Table 7-3
1	24	13	15
2	31	15	11
3	13	11	24
4	11	24	14
5	14	14	13
6	28	28	28
7	16	16	16
8	15	31	31
9	21	21	21
10	22	25	25
11	27	27	27
12	25	22	22
13	23	23	23

NOTE: 1) Point 18 field data removed since wind was dying when measured.

2) Point 32 field data removed since data was taken immediately before instrument ceased working.

$$\left. \begin{array}{l}
 3) \quad r_{\text{Nov. 25/ model contoured}} = 0.95 \\
 \quad \quad n = 13 \\
 \quad \quad r_{\text{Nov. 25/ model terraced}} = 0.74 \\
 \quad \quad n = 13
 \end{array} \right\} r = 1 - \frac{6 \sum_{i=1}^n D_i^2}{n(n^2-1)}$$

4) $r_{\text{model terraced/ model contoured}} = 0.73$

TABLE 8-4 WIND VELOCITY RANK TEST
DECEMBER 28, 1977, DATA

WIND SPEED RANK HIGH TO LOW	MODEL (z = 10 m) Terraced Figure 7- 9 Table 7- 2	FIELD SITE (z = 10 m) Table 7-6	MODEL (z = 10 m) Contoured/sb Figure 7-28 Table 7- 3
1	17	17	17
2	39	19	39
3	19	14	19
4	29	38	29
5	34	24A	38
6	24A	15	15
7	24	39	34
8	38	25	14
9	31	31	24A
10	36	28	24
11	16	34	18
12	14	13	31
13	28	29	35
14	13	16	36
15	18	18	28
16	35	27	13
17	15	24	33
18	37	36	16
19	21	22	21
20	22	35	25
21	33	33	AA
22	27	21	22
23	25	37	37
24	AA	AA	27
25	23	23	23

NOTE: 1) Point 11 field data eliminated, instrument erected too close to shelterbelts.

$$2) \quad r_{\text{Dec. 28/ model contoured}} = 0.78$$

$$n = 25$$

$$r_{\text{Dec. 28/ model terraced}} = 0.68$$

$$n = 25$$

$$\left. \begin{array}{l} \\ \\ \end{array} \right\} r = 1 - \frac{6 \sum_{i=1}^n D_i^2}{n(n^2-1)}$$

$$3) \quad r_{\text{model terraced/model contoured}} = 0.87$$

TABLE 8-5 WIND DIRECTION AT GROUND LEVEL AT FIELD TEST SITES¹⁾TABLE 8- WIND DIRECTION AT GROUND LEVEL
AT FIELD TEST SITES¹⁾

TEST SITE	Angle Nov. 25 (1)	Angle Dec. 28 (2)	Model Terraced (3)	Model Contoured (4)
11	-25	-5	-20	-22
13	-28	-13	-20	-20
14	-32	-17	-20	-20
15	-48	-15	-30	-24
16	-10	-10	-20	-13
17	-	-32	-20	-25
18	-9	-7	-20	-20
19	-	-14	-20	-20
21	-31	-36	-30	-36
22	+10→-36	-	-30	-36
23	-55	-55	-50	-52
24	0	-	0	-14
24A	-	-21	-30	-30
25	+45	-8	+35	-15
27	+7	-	0	+25→-15
28	-16	-41	-27	-20
29	-	-40	-20	-20
31	-22	-29	-30	-30
32	-	-	-27	-17→-35
33	-	-9	-	-
34	-	-6	0	-23
35	-	+5	-20	-20
36	-	-19	-20	-20
37	-	-19	-20	-20
38	-	-3	-15	-20
39	-	-20	-20	-20
AA	-	-35	-28	-25

1) Angle expressed in degrees from grid north.

2) Model topography oriented to -20° to grid north

3) Angle measurements for both field and laboratory may vary by $\pm 5^{\circ}$ due to turbulence and gusting.

4) $r_{(1)/(4)} = 0.67$

$r_{(2)/(4)} = 0.65$

$r_{(1)/(2)} = 0.47$